Main Group Metal Complexes Supported By *N,N′*-Bidentate Ligands

Synthetic and Catalytic Investigations

Ben Day

Submitted for the Degree of Doctor of Philosophy

University of Sussex

August, 2012

I hereby declare that this thesis has not been and will not be, submitted in whole or in part to another University for the award of any other degree.

Signature:……

UNIVERSITY OF SUSSEX

PhD Chemistry

Main Group Metal Complexes Supported by *N,N'*-Bidentate Ligands: Synthetic and Catalytic Investigations

Abstract

The work presented in this thesis is divided in to six chapters. Chapter 1 introduces the two main classes of ligands utilised in the research presented here and gives a brief account of the Tishchenko reaction. Chapter 2 describes the synthesis and characterisation of several new examples of amidinate, guanidinate and phosphaguanidinate complexes of magnesium. A number of these compounds are then examined for their activity as pre-catalysts for the Tishchenko reaction in Chapter 3. This chapter includes the screening of pre-catalysts for the synthesis of benzyl benzoate from benzaldehyde, preliminary mechanistic studies and examination of the scope of the reaction using examples of primary, secondary, tertiary and quaternary aliphatic aldehydes.

Chapter 4 is a deviation from the main theme of this thesis and reports the synthesis of the first true 'phospha-Grignard' reagent. Preliminary reactivity studies with group 4 metallocenes, MCp_2Cl_2 (M = Ti, Zr), are also described.

Chapter 5 explores the reactivity of the cyclic bis(amino)stannylene $Sn\{NAr^{iPr}\}_2SiMe_2$ with platinum-chloride species $PtCl_2(PPh_3)_2$, $PtCl_2(COD)$, $[PtCl(\mu\text{-}Cl)(PEt_3)]_2$ and $PtCl_2$. In addition, one of the resultant Pt-Sn complexes is examined for its activity as a catalyst for the hydroformylation of 1-hexene.

Finally, Chapter 6 describes the synthesis of the antimony and bismuth complexes supported by the dianionic bis(amido)silane ligand $[Me_2Si\{NAr^{iPr}\}_2]^{2-}$.

Contents

Contents 1

Acknowledgments 3

Abbreviations 4

Chapter 1: Introduction 5

1.1 – Amidinates, Guanidinates and Phosphaguanidinates 5
1.2 – Bis(amido)silane Ligands 28

Chapter 2: Synthesis of Amidinate, Guanidinate and Phosphaguanidinate Complexes of Magnesium 38

2.1 – Synthesis of Mg(mesC{NCy}$_2$)(N{SiMe$_3$}$_2$)(thf) (1) and Structure of Mg(mesC{NCy}$_2$)(O-2,6-^{t}Bu$_2$C$_6$H$_3$)(thf) (2) 39
2.2 – Synthesis of Mg(tbo)Br(thf)$_n$ (3) and Mg(tbo){N(SiMe$_3$)$_2$}(thf) (4) 44
2.3 – Crystal Structure of a Tetrametallic Product from the Hydrolysis of 4 50
2.4 – Synthesis of Mg(Cy$_2$PC{NCy}$_2$)Br(Et$_2$O) (6) and Mg(Cy$_2$PC{NCy}$_2$)(N{SiMe$_3$}$_2$)(thf) (7) 53
2.5 – Summary 57
2.6 – Experimental Procedures for Chapter 2 58

Chapter 3: Magnesium Amidinates, Guanidinates and Phosphguanidinates as Pre-catalysts for the Tischenko Reaction 62

3.1 – Magnesium Bicyclic Guanidinate Compounds as Pre-Catalysts 68
3.2 – Magnesium Amidinates and Phosphaguanidinates as Pre-Catalysts 73
3.3 – Preliminary Mechanistic Studies 76
3.4 – Scope of Reaction 80
3.5 – Summary and Comparison with Other Recent Catalysts 84
3.6 – Experimental Procedures for Chapter 3 88

Chapter 4: Synthesis and Reactivity of the Phospha-Grignard Reagent Mg(P{SiMe$_3$}$_2$)Br(thf) 90

4.1 – Introduction 90
4.2 – Synthesis of MgX(P{SiMe$_3$}$_2$)(thf) (X = Br or Me) (8/8') 93
4.3 – Reactivity with Group 4 Metallocenes 99
4.4 – Summary 104

4.5 – Experimental Procedures for Chapter 4 **105**

Chapter 5: Reactions of a Cyclic Bis(amino)stannylene With Platinum(II) Chlorido Complexes **108**

5.1 – Introduction **108**
5.2 – Reaction of Sn{NAr^{iPr}}$_2$SiMe$_2$ (XLIII) with *cis*-PtCl$_2$(PPh$_3$)$_2$, PtCl$_2$(COD) and [PtCl(μ-Cl)(PEt$_3$)]$_2$ **111**
5.3 – Reaction of Sn{NAr^{iPr}}$_2$SiMe$_2$ (XLIII) with PtCl$_2$ **117**
5.4 – Investigation of *cis*-PtCl(SnCl({NAr^{iPr}}$_2$SiMe$_2$))(PPh$_3$)$_2$ as a Hydroformylation Catalyst **121**
5.3 – Summary **123**
5.4 – Experimental Procedures for Chapter 5 **124**

Chapter 6: Bis(amido) Complexes of Antimony and Bismuth **127**

6.1 – Introduction **127**
6.2 – Synthesis of E({NAr^{iPr}}$_2$SiMe$_2$)Cl (E = Sb 14 or Bi 15) **133**
6.3 – Reaction of 15 with AlCl$_3$ **142**
6.4 – Synthesis of Bi({NAr^{iPr}}$_2$SiMe$_2$)(N{SiMe$_3$}$_2$) (17) **145**
6.5 – Synthesis of Cyclopentadienyl Derivatives of 14 and 15 **150**
6.6 – Summary **163**
6.7 – Experimental Procedures for Chapter 6 **164**

Appendix A: General Experimental Procedures **169**

Appendix B **171**

Appendix C **173**

References **174**

Acknowledgments

First I would like to thank my supervisor, Dr. Martyn Coles, for all his support and guidance. It was while working for Martyn during the final year of my MChem degree that my passion for research was ignited and the opportunity to carry on working with him for my PhD was one I could not pass up. Working for Martyn has been a huge amount of fun, in part due to the freedom given to me to explore and develop my own ideas. I guess the odd "meeting" in The Swan helped as well.

Thank you to all the faculty at Sussex, especially Dr. Iain Day, who was invaluable in helping with my NMR studies, and Dr. Ian Crossley, whose advice both in the lab and regarding academic life in general I am extremely grateful for.

A huge thank you to all the technical staff at Sussex, the unsung heroes of the academic world. Specifically I would like to thank Alex Burns and Barry Jackson for keeping our precious glove box alive, Chris Dadswell for teaching me how to use the GC-MS machine and our now retired glass blowers, Roger and Ken (I don't know how the next crop of students will cope without such a valuble service).

Thank you to everyone who has worked in Lab 14 over the past few years for making the lab such an enjoyable place to work, I can honestly say it's been a blast (no pun intended!). Working in a lab alongside the Cloke, Crossley and (for a relatively short time) Lawless groups has provided exposure to many different facets of inorganic chemistry and, perhaps more importantly, a steady stream of pub companions. Especially memorable have been the annual Inorganic Christmas parties, I never thought I'd wake up on a boat (thanks Dan!). A special thanks to the MChem students Fran, Nikki and Becky for being great fun to work with and for their contributions to the research of the Coles group.

Thank you to my family, I hope I've made you proud.

Finally, thank you to Jacquie. Her support, encouragement and steadfast resolve that I WAS going to finish this thesis are what kept me going when the end seemed so far away.

Here's to the future!

Abbreviations

Ar^{iPr}	2,6-di-iso-propylphenyl, 2,6-$^{i}Pr_2C_6H_3$
Ar^{Me}	2,6-Dimethylphenyl, 2,6-$Me_2C_6H_3$
Bu	Butyl, $CH_2CH_2CH_2CH_3$
CCDC	Cambridge Crystallographic Data Centre
Cp	Cyclopentadienyl, $[C_5H_5]^-$
Cp^*	Pentamethylcyclopentadienyl, $[C_5Me_5]^-$
Cy	Cyclohexyl, C_6H_{11}
d	Doublet
DCC	*N*,*N*′-dicyclohexylcarbodiimide
dcpe	Bis(dicyclohexylphosphino)ethane
dd	Doublet of doublets
dme	Dimethoxyethane
DP %	Degree of pyramidalisation
Et	Ethyl, CH_2CH_3
hpp-H	1,3,4,6,7,8-hexahydro-2*H*-pyrimido[1,2-a]pyrimidine
H-tbo	1,4,6-triaza-bicyclo-[3.3.0]oct-4-ene
i	Ipso
^{i}Pr	Isopropyl, $CH(CH_3)_2$
m	Meta
MAO	Methylaluminoxane
Me	Methyl, CH_3
mes	Mesityl, 2,4,6-$Me_3C_6H_2$
NHC	*N*-heterocyclic carbene
NMR	Nuclear Magnetic Resonance
o	Ortho
p	Para
Ph	Phenyl, C_6H_5
p-tolyl	4-MeC_6H_4
q	Quartet
s	Singlet
sept	Septet
t	Triplet
^{t}Bu	Tertiarybutyl, $C(CH_3)_3$
thf	Tetrahydrofuran
tmeda	Tetramethylethylenediamine
tz	3,5-$^{i}Pr_2$-1,2,4-triazolato

Chapter 1: Introduction

This introductory chapter is divided into three parts relating to the research presented in this thesis. These two sections describe the main classes of ligand employed, outlining the basic physical and chemical properties of each type, illustrated by representative examples:

1) Monoanionic amidinates, guanidinates and phosphaguanidinates

2) Dianionic bis(amido)silanes

1.1 – Amidinates, Guanidinates and Phosphaguanidinates

1.1.1 General Definitions

The study of metal complexes that incorporate amidinate, guanidinate and phosphaguanidinate ligands has been a major focus in the Coles research group for a number of years. These monoanionic ligands all share the common feature of a heteroallylic, delocalised N-C-N core, and differ only in the substituent on the central carbon atom. Amidinates have either alkyl, aryl, or in the case of formamidinates, a proton in this position whereas guanidinates and phosphaguanidinates have amido ($-NR_2$) or phosphido ($-PR_2$) groups, respectively (Figure 1.1).

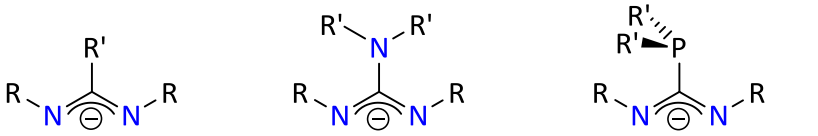

Figure 1.1 – General structure of amidinates, guanidinates and phosphaguanidinates (R′ = H, alkyl, aryl)

Metal-amidinate, -guanidinate and -phosphaguanidinate complexes are generally synthesised *via* one of three methods (Scheme 1.1):

1) Insertion of a carbodiimide into a metal-carbon, -amide or -phosphide bond
2) Deprotonation of the neutral pro-ligand by a metal-alkyl or -amide reagent
3) Salt metathesis between a metal-halide and the lithiated ligand (usually generated by method 1 or 2)

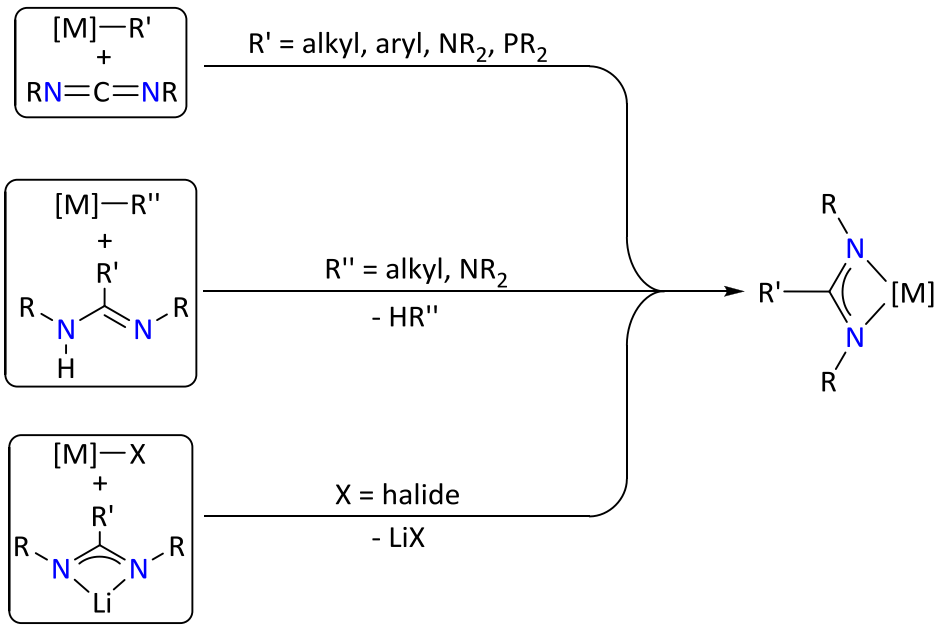

Scheme 1.1 – General routes to metal-amidinate, -guanidinate and -phosphaguanidinate complexes

1.1.2 Electronic Structures and Geometric Considerations

Guanidinate ligands possess three possible resonance structures (Scheme 1.2); the first two (**A**/**A'**) are also observed for amidinate and phosphaguanidinate ligands. The third (**B**) is unique to guanidinates and invokes contribution from the lone pair of the tertiary amido group into the Y-shaped CN_3 π-system, forming an imidinium/diamide zwitterionic structure. Evidence for this Y-shaped delocalisation should become apparent when looking at the C-N bond lengths of the CN_3 core, where an equal contribution from **B** would result in all three distances being approximately equal. An illustrative example in which this is observed in the titanium guanidinate complex $Ti(Et_2NC\{NPh\}_2)_2Cl_2$, where the C-N bond lengths are found to be 1.341(6) Å for the uncoordinated nitrogen atom and 1.343(6) and 1.341(6) Å for the coordinated nitrogen atoms.[1] However, analysis of the bond lengths of structurally characterised acyclic guanidinate complexes show that this additional delocalisation is not always present.

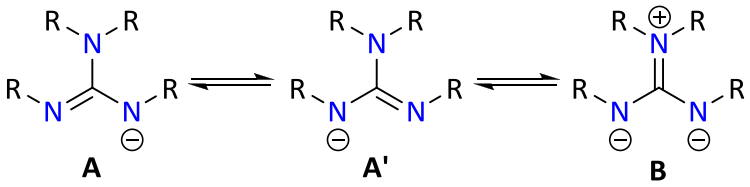

Scheme 1.2 – Resonance structures of guanidinate ligands

The contribution of resonance structure **B** means that guanidinate ligands are more basic and hence stronger donors than their amidinate counterparts. This is illustrated by the comparison of the redox potentials of the dinuclear molybdenum amidinate and guanidinate 'paddle wheel' complexes $Mo_2(\{N(p\text{-tolyl})\}_2CH)_4$ and $Mo_2(\{NPh\}_2CNHPh)_4$.[2,3] Cyclovoltametric studies of the amidinate complex shows a redox potential at +0.21 V and an irreversible oxidation at +1.3 V (*vs.* Ag/AgCl). The guanidinate complex shows two redox potentials at -0.05 V and

+0.85 V (*vs.* Ag/AgCl), providing evidence of the increased donor capabilities of the guanidinate ligand and therefore its superior ability to stabilise high oxidation state metals.

For delocalisation to occur the p-orbitals of the central carbon atom and amido nitrogen must align to some degree. However, due to steric interactions between the nitrogen substituents, the NR_2 moiety tends to twist so that it does not lie in the same plane as the heteroallylic N-C-N core. This twisting, defined as torsion angle θ (Figure 1.2), is less pronounced with smaller nitrogen substituents.

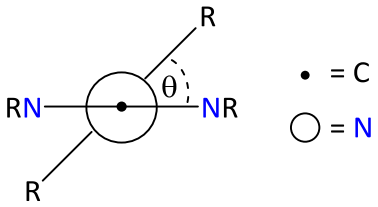

Figure 1.2 – Definition of torsion angle θ

A particularly interesting class of guanidinate ligands are the {n:m}-bicyclic derivatives (Figure 1.3). These ligands have the nitrogen atoms of the heteroallylic core tethered to the amido substituent on the central carbon atom, with the two most commonly used being the anions of the {6:6} and {5:5} bicyclic guanidines 1,3,4,6,7,8-hexahydro-2*H*-pyrimido[1,2-a]pyrimidine (hpp-H) and 1,4,6-triaza-bicyclo-[3.3.0]oct-4-ene (tbo-H). The tethering of the nitrogen substituents fixes the orientation of the amido groups such that they tend toward co-planarity with the heteroallylic core, resulting in more favourable conditions for π-orbital overlap.

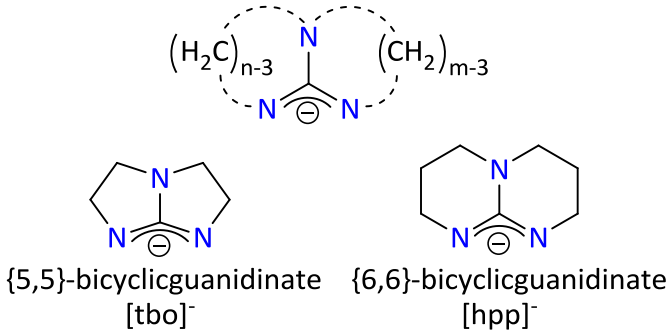

Figure 1.3 – General structure of {n:m}-bicyclic guanidinates

1.1.3 Structural Trends in Metal-Guanidinate Compounds

Analysis of structural data from acyclic and bicyclic guanidinate complexes, obtained from the Cambridge Structural Database, shows a positive correlation between torsion angle θ and the R_2N-CN_2 bond length.* These data are represented graphically in Figure 1.4, which displays a plot of the R_2N-CN_2 distance against θ. The general trend is for a greater torsion angle to coincide with a longer R_2N-CN_2 bond length, expected if one considers larger θ angles decreasing the effective overlap between the nitrogen lone-pair and the empty p-orbital on the central sp^2 carbon of the heteroallylic fragment.

* No differentiation between the different bonding modes observed for guanidinate ligands have been made in Figure 1.4 as it has been assumed that the bonding mode of the ligand has little effect on the R_2N-CN_2.

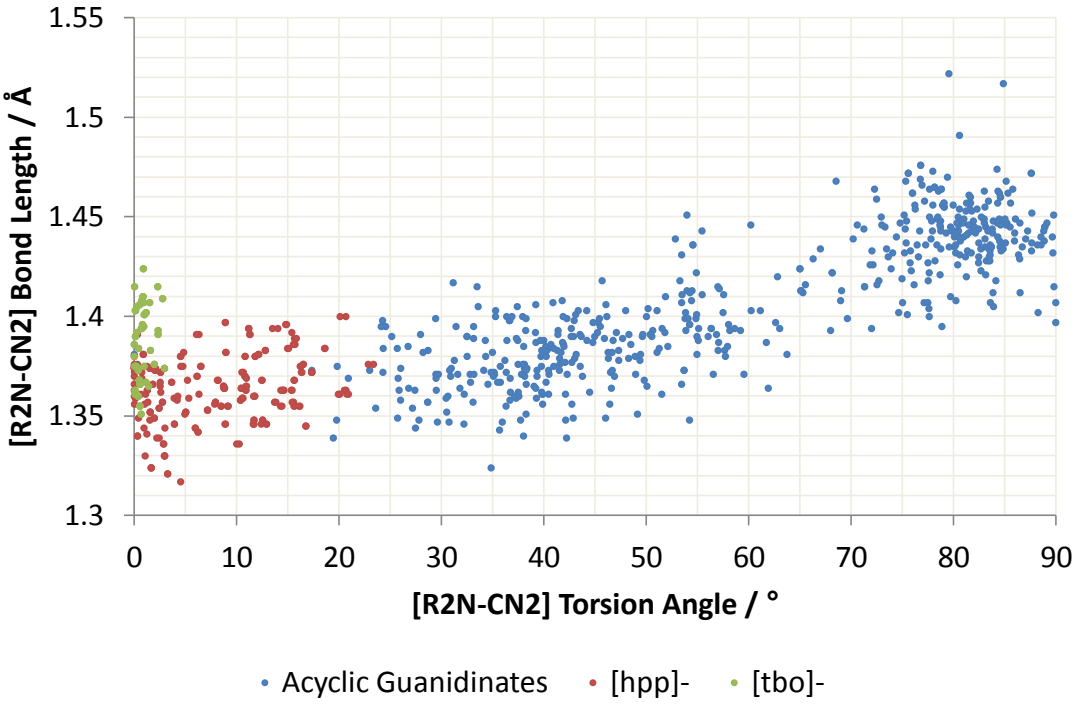

Figure 1.4 – Plot of R_2N-CN_2 Torsion angle of guanidinate ligands *vs* R_2N-CN_2 bond length

It is also observed in Figure 1.4 that the R_2N-CN_2 bond lengths for the complexes containing the $[tbo]^-$ ligand do not fit the trend observed for the acyclic guanidinates and $[hpp]^-$ data. That is to say that bond lengths greater than 1.4 Å are observed despite the measured torsion angles all being less than 5°. This suggests that another factor is affecting the degree of orbital overlap. The amido nitrogen of the $[hpp]^-$ ligand is usually planar, whereas the {5:5} bicyclic system of $[tbo]^-$ inflicts strain on the rings of the ligand resulting in the amido nitrogen having a more pyramidal geometry. It is thought that this non-planar geometry is much less favourable for the orbital overlap necessary for delocalisation of the lone pair of electrons of the amido nitrogen into the R_2N-CN_2 bond. In an attempt to probe whether this pyrimalisation contributes to a lengthening of the R_2N-CN_2 bond, a plot of the degree of pyramidalisation (DP %; Figure 1.5) of the tertiary nitrogen vs the R_2N-CN_2 bond length of $[tbo]^-$ ligands is shown in Figure 1.6. The plot tentatively shows a slight positive correlation however it is not significant

enough to make any definitive conclusions meaning more data (i.e. more $[tbo]^-$ complexes) are needed.

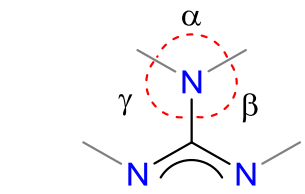

$$DP\ \% = \frac{360 - (\alpha + \beta + \gamma)}{0.9}$$

Figure 1.5 – Defininition of degree of pyramidalisation (DP %)

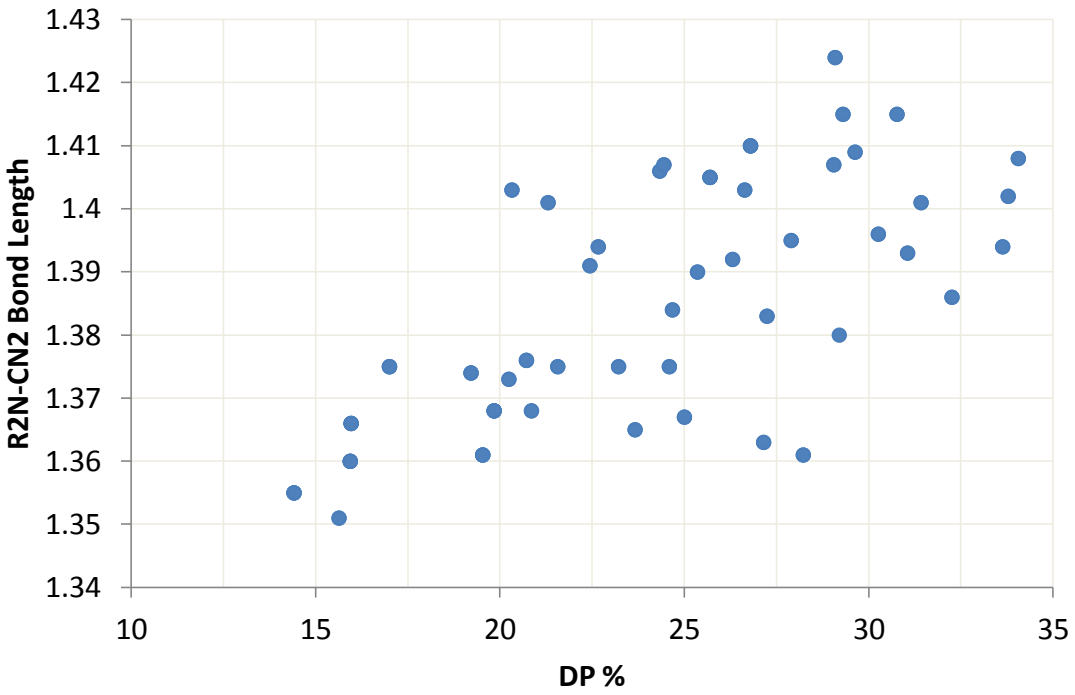

Figure 1.6 – Plot of DP % of $[tbo]^-$ ligands *vs* $R_2N\text{-}CN_2$ bond length

1.1.4 Coordination Modes at Metal Centres

Amidinate, guanidinate and phosphaguanidinate ligands have been shown to adopt a number of different coordination modes (Figure 1.7). The most commonly observed are chelating mode **B** and bridging mode **C**.

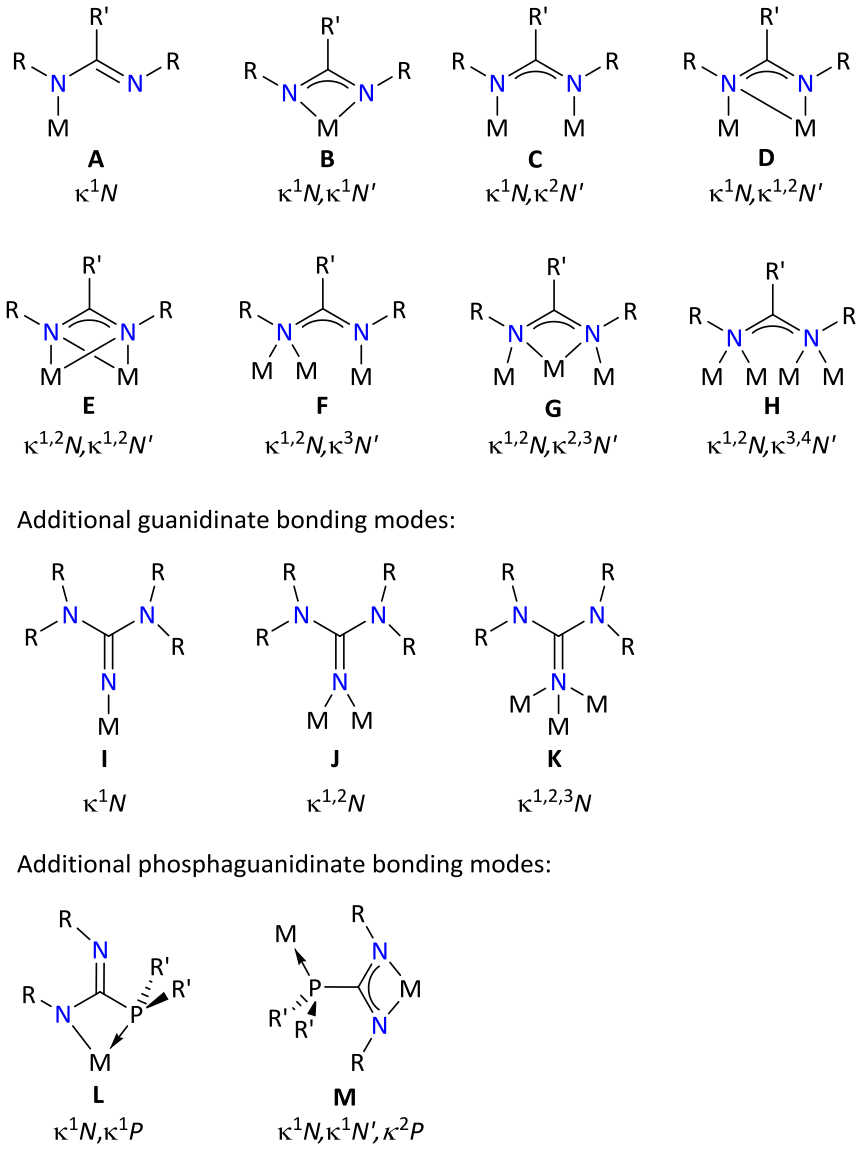

Figure 1.7 – Amidinate, guanidinate and phosphaguanidinate bonding modes with nomenclature (R = alkyl, aryl or $SiMe_3$, R′ = alkyl, aryl, H or NR_2)

1.1.5 Metal-Amidinate, -Guanidinate and -Phosphaguanidinate Complexes

The first metal amidinate complex, Li(PhC{NSiMe$_3$}$_2$), was reported by Sanger in 1973.[4] However, it was not until after the work of Boeré *et al.* in 1987, demonstrating that a range of different *N*,*N*,*N*'-tris(trimethylsilyl)amidines could be synthesised using a refined version of Sanger's method (Scheme 1.3), that amidinates started increasing in popularity as a class of ligand.[5]

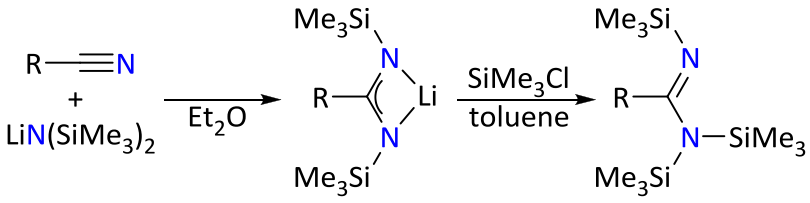

Scheme 1.3 – Synthesis of *N*,*N*,*N*'-tris(trimethylsilyl)amidines (R = Ph, *p*-tolyl, *p*-ClC$_6$H$_4$, *p*-MeOC$_6$H$_4$, *p*-Me$_2$NC$_6$H$_4$, *p*-CF$_3$C$_6$H$_4$, *p*-C$_6$H$_5$C$_6$H$_4$ and CF$_3$)

Within a couple of years, amidinate complexes of metals from across the periodic table had been reported; the first comprehensive review of metal amidinate complexes was published in 1990.[6]

The first guanidinate complex was reported in 1968 by Wade *et al*., who found that the lithium guanidinate LiN=C(NMe$_2$)$_2$ (**I**) was formed on treatment of *N*,*N*,*N*',*N*'-tetramethylguanidine with LiMe in Et$_2$O.[7] Cryoscopic measurements indicated that the complex was dimeric in a benzene solution and NMR spectroscopy showed that the guanidinate ligand was bound to lithium by the imine nitrogen. Wade *et al.* published the solid state structure of LiN=C(NMe$_2$)$_2$ fifteen years later, showing it to exist as the hexamer [**I**]$_6$ in the solid-state, with each guanidinate ligand adopting bonding mode **K**, bridging between three Li atoms *via* the imine nitrogen (Figure 1.8).

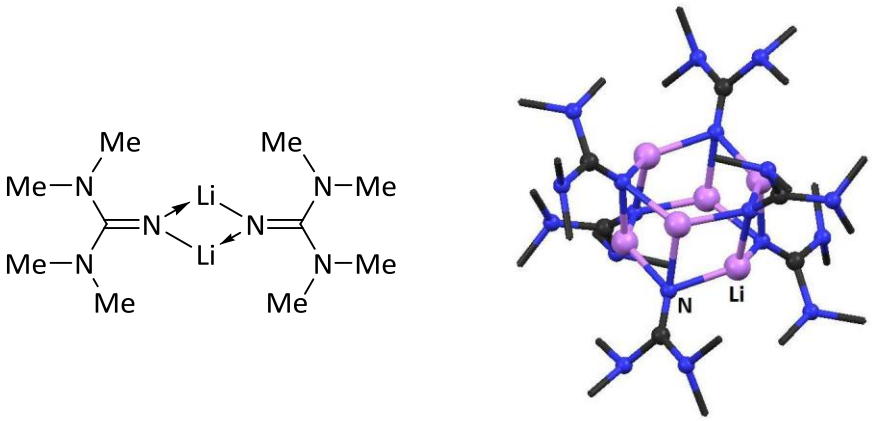

Figure 1.8 – Solution and solid state structures of $LiN=C(NMe_2)_2$ (**I**)

It is somewhat surprising that bridging bonding mode **C** was not observed for guanidinate ligands until 1990 when Kostic *et al*. reported a number of bimetallic terpyridineplatinum complexes.[8] Even more surprising is that chelating bonding mode **B** was not observed until 1996 when Bailey *et al*. reported the synthesis of the rhodium cyclopentadienyl complex RhCp*({NPh}$_2$CNHPh)Cl and the ruthenium arene complex Ru(1-Me-4-^{i}PrC$_6$H$_4$)({NPh}$_2$CNHPh)Cl.[9]

It was realised early in the development of amidinate ligands that, being isoelectronic with carboxylate anions, they could be useful in stabilising bimetallic, 'paddlewheel' complexes when they adopt bonding mode **C**. Since the first reports of such amidinate complexes by Cotton *et al.* in 1975,[10,11] over 100 other examples have been reported. The use of amidinate ligands in this field has seen a number of advances including the first example of a V≡V triple bond (V_2(HC{N-*p*-tolyl}$_2$)$_4$; **II**),[12] the first tribridged dinuclear complexes (e.g. Fe_2(HC{NPh}$_2$)$_3$; **III**)[13,14] and the first quadrupley bonded Ir complex (Ir_2(HC{N-*p*-tolyl}$_2$)$_4$; **IV**)[15] (Figure 1.9).

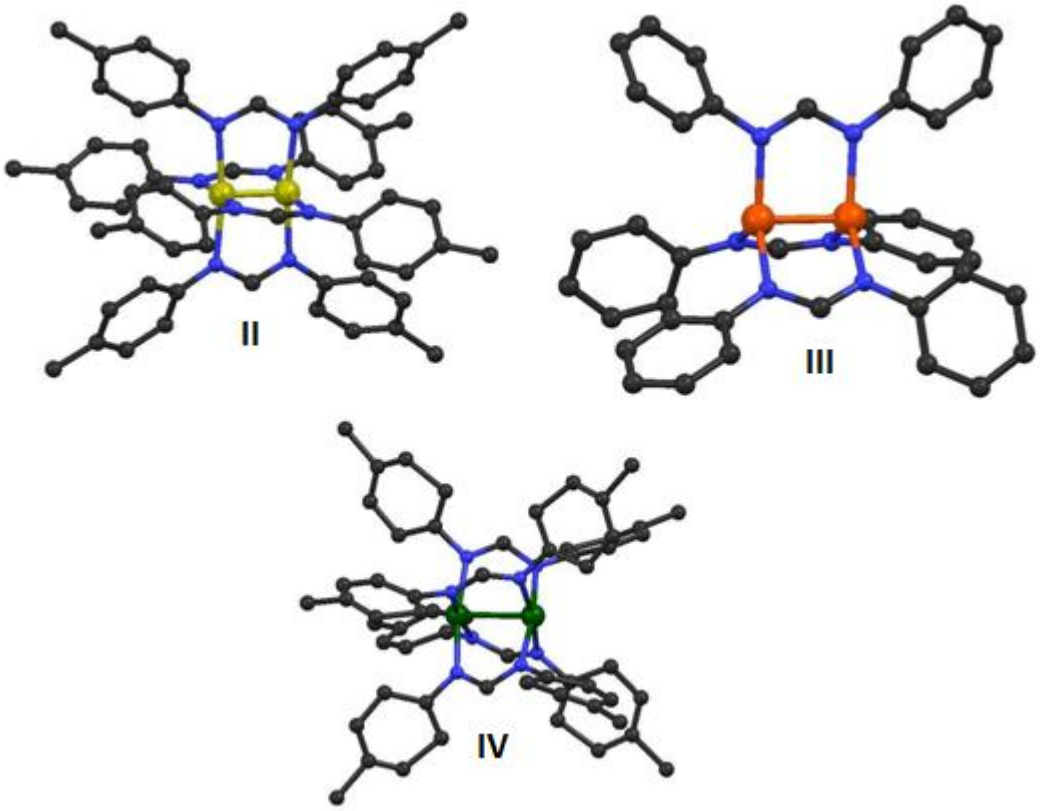

Figure 1.9 – Notable examples of amidinate bridged metal-metal multiply bonded complexes; $V_2(HC\{N\text{-}p\text{-tolyl}\}_2)_4$ (**II**),[12] $Fe_2(HC\{NPh\}_2)_3$ (**III**),[13,14] $Ir_2(HC\{N\text{-}p\text{-tolyl}\}_2)_4$ (**IV**)[15]

While the use of formamidinates allowed a significant advance in the synthesis of paddlewheel complexes, the discovery that these ligands were cleaved by low valent metals, such as Nb^{II} and Ta^{II},[16,17] prompted the search for more robust ligand systems. Attention turned to the $[hpp]^-$ anion following its use in the synthesis of the first guanidinate stabilised paddlewheel complex $Ru_2(hpp)_4Cl_2$ by Bear *et al*. in 1996.[18] The following year Cotton *et al.* succeeded in the synthesis of the first triply bonded dinuclear Nb^{II} complex $Nb_2(hpp)_4$ (**V**) from the reaction of $NbCl_3(dme)$ with a mixture of Lihpp and KC_8 (Figure 1.10).[19]

Another notable guanidinate stabilised paddlewheel complex is the dichromium complex $Cr_2(\{NPh\}_2CN(CH_2)_4)_4$ (**VI**; Figure 1.9), which was the first dichromium compound to be oxidised without decomposition.[20] This compound displayed a redox potential at +0.02 V (*vs.* Ag/AgCl)

and the cationic complex was isolated following oxidation of $Cr_2(\{NPh\}_2CN(CH_2)_4)_4$ by $AgPF_6$, forming $[Cr_2(\{NPh\}_2CN(CH_2)_4)_4][PF_6]$.

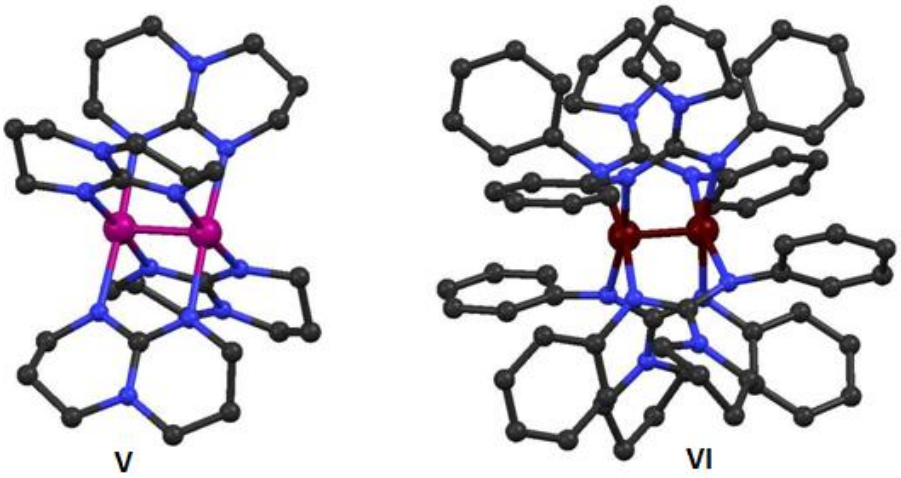

Figure 1.10 – Solid state structures of notable guanidinate paddle wheel complexes; $Nb_2(hpp)_4$ (**V**),[19] $Cr_2(\{NPh\}_2CN(CH_2)_4)_4$ (**VI**)[20]

The first reported synthesis of a neutral phosphaguanidine was published in 1980 by Issleib *et al.* who isolated the silylated phosphaguanidines, $\{Me_3Si\}RPC(NR)(NR\{SiMe_3\})$ (R = Cy or Ph) from the insertion of a carbodiimide into the P-Si bond of a bis(silyl)phosphine.[21] In the same year it was also reported that the reaction of diphenylphosphine with di-*p*-tolylcarbodiimide results in the formation of the protonated derivative $Ph_2PC(NR)(NHR)$ (R = *p*-tolyl).[22]

The first example of a metal complex bearing an anionic phosphaguanidinate ligand was the Rh^I compound $Rh(PPh_3)_2(Ph_2PC\{NR\}_2)$ (R = *p*-tolyl), synthesised *via* the addition of Li^nBu to a 1:1 mixture of $Rh(PPh_3)_3Cl$ and $Ph_2PC(NR)(NHR)$.[23] An alternative route to synthesise a metal phosphaguanidinate complex was reported by Hey-Hawkins and Lindenberg who found that a carbodiimide can be inserted in the M-P bond of a metal phosphide.[24,25]

The chemistry of phosphaguanidinate complexes is still in its infancy and it has only really started to be investigated over the last decade. Interest in phosphaguanidinate complexes in the Coles group began in 2002 with the synthesis of Li($Ph_2PC\{N^iPr\}_2$)(thf) (**VII**) from the reaction of *N,N'*-di-*iso*-propylcarbodiimide with an *in situ* generated lithium phosphide, $LiPPh_2$.[26] The solid-state structure shows **VII** to be dimeric with the phosphaguanidinate ligand adopting a bridging bonding mode **D** (Figure 1.11). Addition of tmeda to a toluene solution of **VII** results in displacement of the coordinated thf to form the monomeric complex Li($Ph_2PC\{N^iPr\}_2$)(tmeda) (**VIII**) where the phosphaguanidinate ligand adopts bonding mode **L** (Figure 1.11). Both lithium complexes were shown to act as ligand transfer reagents when reacted with $AlMe_2Cl$, generating the κ^1N,κ^1N' bonded phosphaguanidinate complex $AlMe_2(Ph_2PC\{N^iPr\}_2)$ (**IX**; Figure 1.11). Compound **IX** can act as a metal-functionalised phosphine as demonstrated by the by its reaction with $PtMe_2(COD)$, resulting in the formation of $PtMe_2(Ph_2PC\{N^iPr\}_2AlMe_2)_2$. Spectroscopic data showed that the phosphaguanidinate ligand adopts bonding mode **M**.[26]

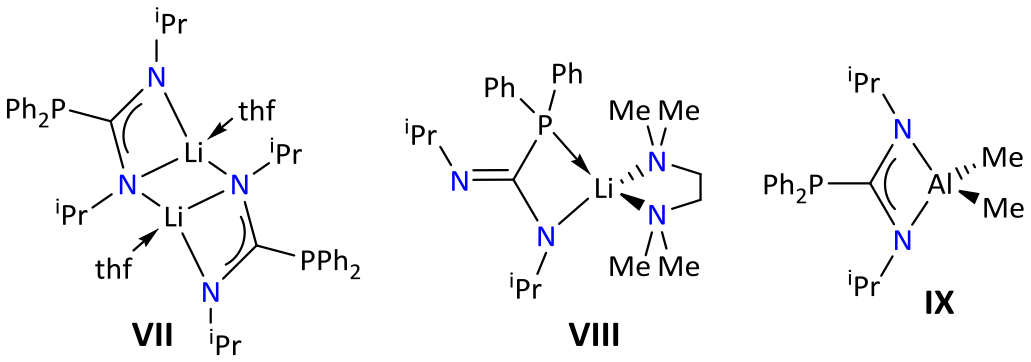

Figure 1.11 – Metal complexes of the phosphaguanidinate ligand $[Ph_2PC\{N^iPr\}_2]^-$

The first crystallographically characterised example of **IX** as a metal-functionalised phosphine was the copper complex $CuBr(Ph_2PC\{N^iPr\}_2AlMe_2)_2$ (**X**),[27] synthesised *via* reaction of the P-bound *bis*-phosphaguanidine complex $CuBr(Ph_2PC\{N^iPr\}\{NH^iPr\})_2$ with $AlMe_3$ (Scheme 1.4).

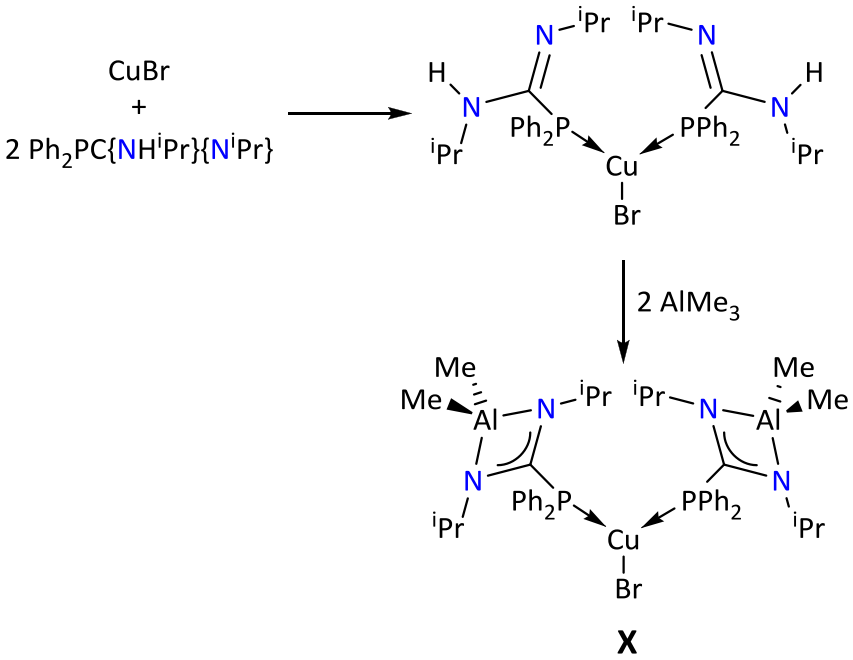

Scheme 1.4 – Synthesis of $CuBr(Ph_2PC\{N^iPr\}_2AlMe_2)_2$ (**X**)

The family of lithium phosphaguanidinate complexes was extended in 2006 by the synthesis of the *P*-dicylcohexyl derivative "$Li(Cy_2PC\{N^iPr\}_2)$".[28] Unlike $Li(Ph_2PC\{N^iPr\}_2)(thf)$, which is dimeric in the solid-state, $Li(Cy_2PC\{N^iPr\}_2)$ crystallises as a cyclic hexamer. Each phosphaguanidinate ligand exhibits a $\kappa^1N,\kappa^1P,\kappa^2N'$ bonding mode, being *P,N*-bound to a lithium centre with the imine nitrogen coordinating to an adjacent lithium atom.

1.1.6 Magnesium Amidinates, Guanidinates and Phosphaguanidinates

The first examples of magnesium amidinate compounds, reported in 1992 by Westerhausen and Hausen, were thf and benzonitrile adducts of the bis(amidinate), $Mg(PhC\{NSiMe_3\}_2)_2$.[29] These compounds were synthesised from the reaction of benzonitrile with $Mg(N\{SiMe_3\}_2)_2$ in toluene to yield the benzonitrile adduct $Mg(PhC\{NSiMe_3\}_2)_2(NCPh)$, which was converted to the bis(thf) adduct $Mg(PhC\{NSiMe_3\}_2)_2(thf)_2$ (**XI**) following the addition of thf. The solid-state

structure of **XI** was reported by Walther *et al*. a few years later showing a monomeric structure with the amidinate ligands chelating to a distorted octahedral magnesium centre.[30]

Since then, only a small number of magnesium amidinate complexes have been described in the literature, somewhat surprising given the attention that amidinate ligands have attracted over the last 30 years. The reaction chemistry of magnesium amidinate complexes is also relatively unexplored and, until now, has been limited to their use as ligand transfer reagents[30] and investigations into their use as chemical vapour deposition precursors for Mg doped semi-conductors.[31]

Most structurally characterised examples are magnesium bis(amidinate) complexes and are generally synthesized from the reaction of the neutral amidine pro-ligand with a dialkyl magnesium reagent (*e.g*. $MgBu_2$) or from salt metathesis reactions between a lithiated amidinate with MgX_2 (X = Cl or Br).[30–33]

In the presence of thf, magnesium bis(amidinate) complexes tend to be monomeric with 6-coordinate, distorted octahedral magnesium centres in the solid-state. This is illustrated by the crystal structures of compound **XI**[30] and $Mg(PhC\{N^iPr\}_2)_2(thf)_2$ (**XII**)[33] in which the amidinate ligands lie in the same plane with *trans*-coordinated thf (Figure 1.12). The use of bidentate donor solvents results in a more distorted pseudo-octahedral geometry of the magnesium centre in which the amidinate ligands no longer lie in the same plane, shown by the crystal structures of $Mg(HC\{N\text{-}p\text{-}tolyl\}_2)(dme)$ (**XIII**) and $Mg(HC\{N\text{-}p\text{-}tolyl\}_2)(tmeda)$ (**XIV**) (Figure 1.12).[34]

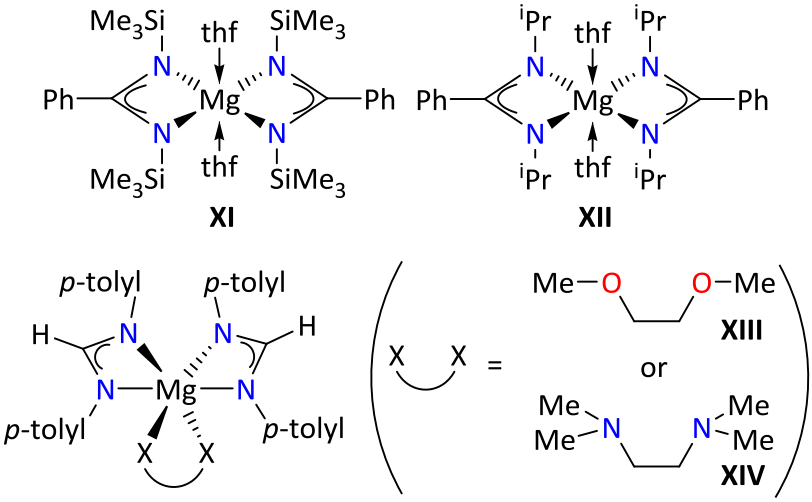

Figure 1.12 – Examples of magnesium bis(amidinate) complexes

In the absence of a sufficiently strong donor molecule, magnesium complexes with different amidinate bonding modes are formed in the solid-state, depending on the size of nitrogen substituents. When ^{t}Bu groups are used, monomeric structures in which the amidinate ligands adopting chelating bonding mode **B** results, *e.g.* Mg(MeC{N^{t}Bu}$_2$)$_2$ (**XV**) and Mg(PhC{N^{t}Bu}$_2$)$_2$ (**XVI**), while with less bulky ^{i}Pr groups a dimeric structure is adopted with the amidinate ligands present in both chelating and bridging modes (**B** and **C**), *e.g.* [Mg(MeC{N^{i}Pr}$_2$)$_2$]$_2$ (**XVII**).[31] A dimeric structure is also observed for the asymmetric amidinate complex [Mg(MeC{NEt}{N^{t}Bu})$_2$]$_2$ (**XVIII**); however the bridging amidinate ligands are present in bonding mode **D** with the ethyl substituted nitrogen bridging both magnesium centres (Figure 1.13).[31]

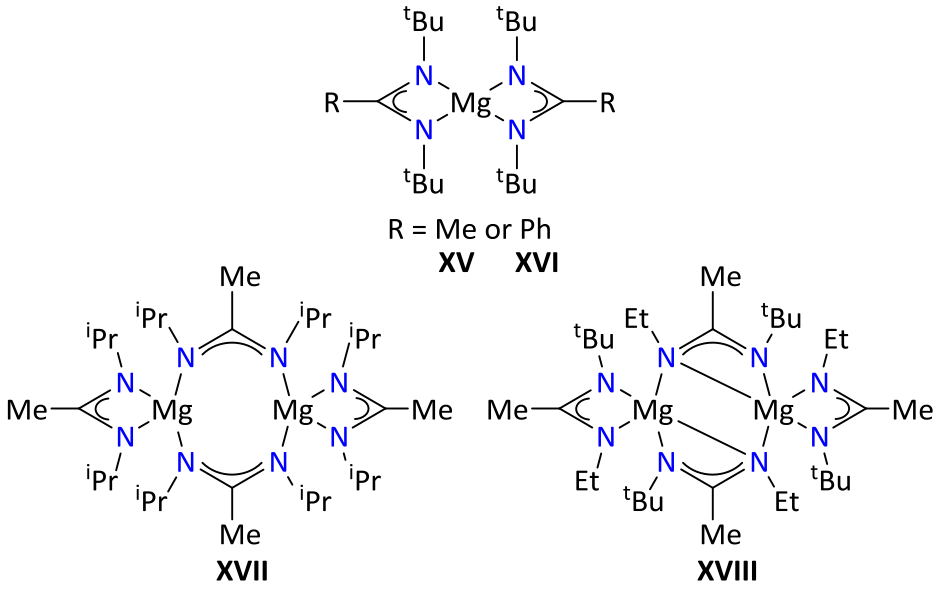

Figure 1.13 – Non-solvated magnesium bis(amidinate) complexes[31]

In earlier studies on the synthesis of magnesium amidinate compounds, conducted during the final year project of my MChem degree, it was found that the equimolar reaction of *N*,*N*′-dicyclohexylcarbodiimide (DCC) with Mg(*p*-tolyl)Br formed the bis(amidinate), Mg(*p*-tolylC{NCy}$_2$)$_2$(thf)$_2$ (**XIX**) rather than the expected mono(amidinate) halide complex. The formation of the bis(amidinate) is rationalized in Scheme 1.5. The different postulated routes are:

1) The carbodiimide reacts preferentially with the MgR_2 component of the Schlenk equilibrium of the *p*-tolyl Grignard starting material

Or

2) Once formed, the mono(amidinate) also exists in a Schlenk-like equilibrium and the bis(amidinate) component crystallises preferentially.

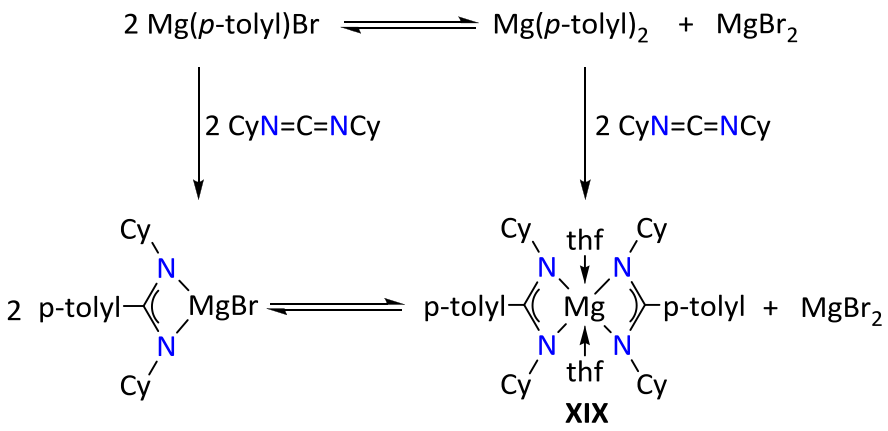

Scheme 1.5 – Postulated routes resulting in the formation of Mg(*p*-tolylC{NCy}$_2$)$_2$(thf)$_2$ (**XIX**)

In contrast to the reaction with Mg(*p*-tolyl)Br, the reaction of Mg(mes)Br with one equivalent of DCC yields the dimeric mono(amidinate) halide complex [Mg(mesC{NCy}$_2$)Br(Et$_2$O)]$_2$ (**XX**; Scheme 1.6).[35] These results show that when synthesising magnesium amidinates *via* the insertion of a carbodiimide into the Mg-C bond of a Grignard, the choice of alkyl/aryl group may determine whether a mono- or bis(amidinate) is formed.

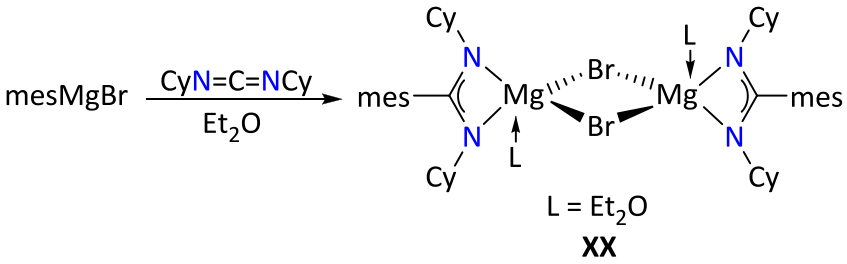

Scheme 1.6 – Synthesis of [Mg(mesC{NCy}$_2$)Br(Et$_2$O)]$_2$ (**XX**)

Examples of magnesium guanidinate complexes are even scarcer in the literature than amidinate complexes. Prior to 2011, only four structurally characterised examples had been reported, the first being the bis(guanidinate) Mg(^{i}Pr$_2$NC{N^{i}Pr$_2$}$_2$)$_2$(thf), synthesised from the reaction of *N*,*N*'-diisopropylcarbodiimide with Mg(N^{i}Pr$_2$)$_2$.[33] Despite the paucity of such compounds, one of the most significant discoveries in magnesium chemistry, the isolation of

the first stable Mg^{I} complexes, was made using a magnesium guanidinate. In 2007 Green *et al*. showed that the dimeric magnesium guanidinate $[LMg(\mu\text{-}I)_2Mg(OEt_2)L]$ (L = $[^{i}Pr_2NC\{NAr^{iPr}\}_2]^-$) (**XXIb**), and the related β-diketiminate complex $Mg(HC\{C(Me)NAr^{iPr}\}_2)I(Et_2O)$ (**XXIIa**), is reduced by potassium resulting in the formation of $(L)Mg\text{-}Mg(L)(OEt_2)$ (L = $[^{i}Pr_2NC\{NAr^{iPr}\}_2]^-$; **XXIb**, Scheme 1.7) and (L)Mg-Mg(L) (L = $[HC(C(Me)NAr^{iPr})_2]^-$; **XXIIb**, Scheme 1.7).[36]

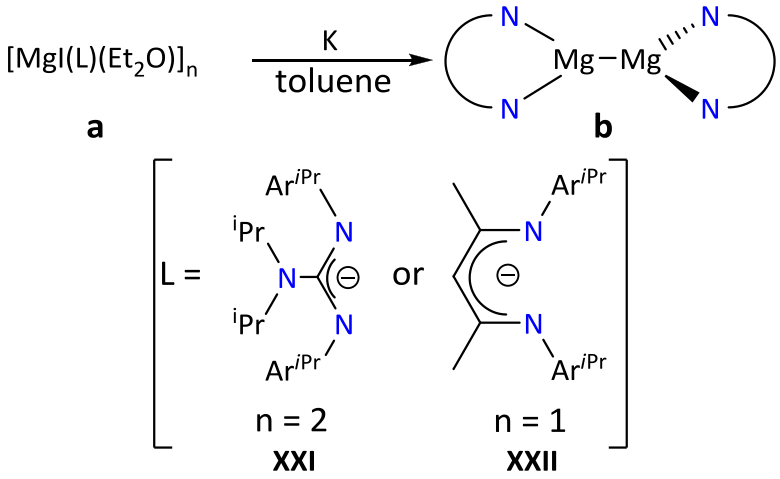

Scheme 1.7 – Synthesis of the first Mg(I) complexes[36]

During the course of our studies in this area, a report on bicyclic guanidinate magnesium complexes utilising the $[hpp]^-$ ligand was published.[37] Ciobanu *et al.* isolated a small number of colourless crystals from the reaction of hpp-H with MgMeBr in Et_2O. Single crystal X-ray crystallography showed the structure to be tetrameric $[MgBr(hpp)]_4$ (**XXIII**) with the $[hpp]^-$ ligands adopting bonding mode **G** (Figure 1.14).[37] Interestingly, previous work in our research group had found that the analogous reaction with MgMeCl in thf yielded $Mg(thf)_2(hpp)_2MgCl_2$ (**XXIV**) with the $[hpp]^-$ ligands adopting bonding mode **D**.[38]

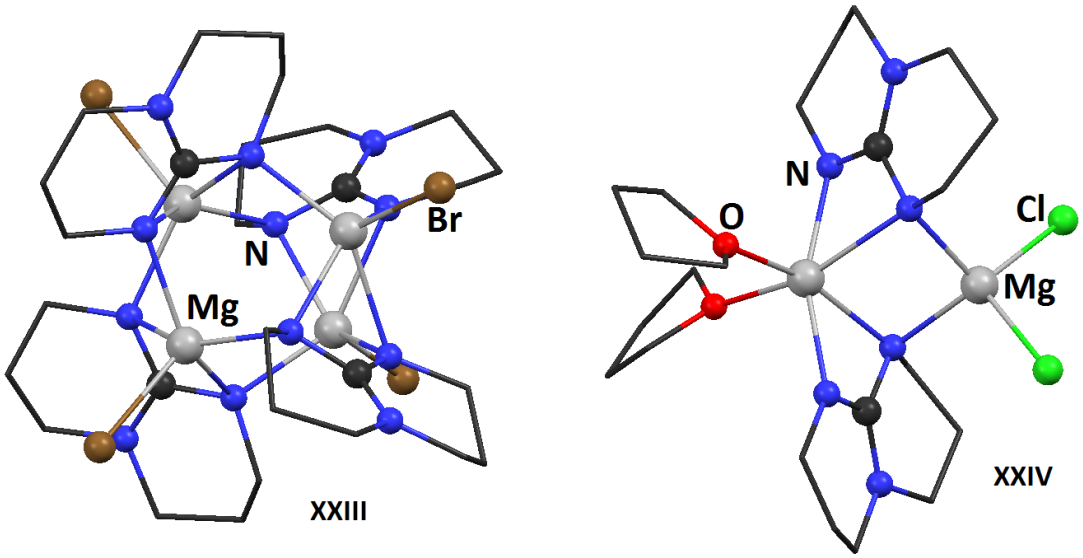

Figure 1.14 – Solid state structures of $[MgBr(hpp)]_4$ (**XXIII**) and $Mg(thf)_2(hpp)_2MgCl_2$ (**XXIV**)

There are no published reports of magnesium phosphaguanidinate complexes, although a few examples have been made previously within the Coles group (Figure 1.15). These complexes were synthesised *via* the reaction of the neutral phosphaguanidine pro-ligands with MgMeCl to give $[Mg(R_2PC\{NR'\}_2)Cl(thf)]_2$ (R = Ph, R' = Cy (**XXV**) or R = Cy R' = ^{i}Pr (**XXVI**)). Selected complexes were reacted with lithium salts Li(O-2,6-^{t}Bu-4-Me-C_6H_2) and $Li(N\{SiMe_3\}_2)$ to afford $Mg(Ph_2PC\{NCy\}_2)$(O-2,6-^{t}Bu-4-MeC_6H_2)(thf) (**XXVII**) and $Mg(Ph_2PC\{NCy\}_2)(N\{SiMe_3\}_2)$(thf) (**XXVIII**). [39]

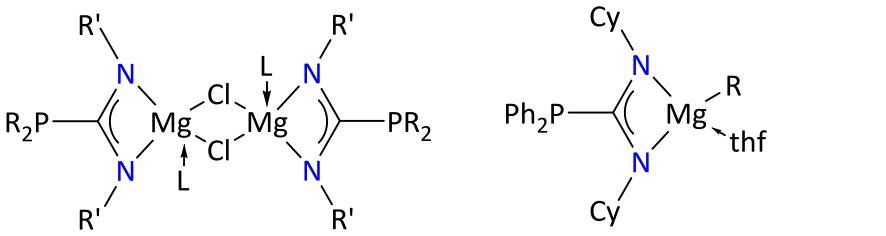

XXV R = Ph, R' = Cy, L = thf
XXVI R = Cy, R' = ^{i}Pr, L = thf

XXVII R = O-2,6-^{t}Bu-4-MeC_6H_2
XXVIII R = $N\{SiMe_3\}_2$

Figure 1.15 – Magnesium phosphaguanidinate complexes previously synthesised in the Coles group

1.1.7 – Amidinate and Guanidinate complexes in Catalysis

The use of group 4 metallocene complexes as olefin polymerisation catalysts has been studied in great depth since the Nobel prize winning research by Ziegler and Natta in the 1950s.[40–42]

Over the last 20 years a great deal of research has focused on the development of olefin polymerisation catalysts with alternative, non-cyclopentadienyl, ligand systems, in part to avoid issues with the increasingly restrictive patent literature. It was pointed out by Edelmann *et al.* that amidinates can be considered as 'steric cyclopentadienyl equivalents',[43] a concept first discussed by Wolczanski *et al.* with respect to a series of complexes using the tri-tertiarybutylmethoxide ligand.[44] This steric similarity to cyclopentadienyl ligands makes complexes of amidinates, and by association guanidinates, attractive alternatives in the development of olefin polymerisation catalysts.

The first use of a transition metal amidinate as an olefin polymerisation catalyst was reported by Green *et al.* in 1993. It was found that the half sandwich zirconium complex $ZrCp(PhC\{NSiMe_3\}_2)Cl_2$ (**XXIX**; Figure 1.16) acts as a precatalyst for the polymerisation of ethylene and propylene upon activation with a large excess of MAO.[45] Numerous other examples of mono- bi- and tris- amidinate or guanidinate complexes of titanium, zirconium and hafnium have been reported for the polymerisation of ethylene with varying degrees of activity.[46]

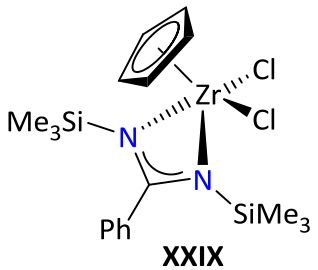

XXIX

Figure 1.16 – The first transition metal amidinate olefin polymerisation catalyst; $ZrCp(PhC\{NSiMe_3\}_2)Cl_2$ (**XXIX**)

Organolanthanide complexes represent another class of particularly interesting catalysts for various transformations. The vast majority of organolanthanide complexes contain cyclopentadienyl derivatives as supporting ligands. Amidinates and guanidinates represent two of the most successfully implemented alternative ligand systems, being bulky enough for steric saturation of the coordination sphere of lanthanide ions. In addition to this, the ease at which the steric and, to a lesser extent, electronic properties of amidinate ligands can be altered make them as versatile as cyclopentadienyl ligands.

Interest in lanthanide amidinate complexes as catalysts was stimulated by the discovery that lanthanide tris(amidinates) and -(guanidinates), $Ln(RC\{NCy\}_2)_3(thf)_n$ (R = Me, Ln = Nd, Gd, Yb, n = 0; R = NMe_2, Ln = Nd, Y, Yb, n = 2; Figure 1.17), were highly active catalysts for the ring opening polymerisation of ε-caprolactone.[47] Although promising results have been observed for the polymerisation of olefins by lanthanide amidinates, the majority of work has focused on the polymerisation of polar substrates such as ε-caprolactone and methylmethacrylate.[48]

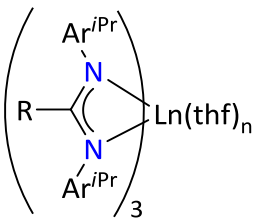

R = Me, Ln = Nd, Gd, Yb, n = 0
R = NMe_2, Ln = Nd, Y, Yb, n = 2

Figure 1.17 – Lanthanide tris(amidinate) and -(guanidinate) ε-caprolactone polymerisation catalysts; $Ln(RC\{NCy\}_2)_3(thf)_n$

The use of metal amidinates in catalysis is not restricted to polymerisation reactions. Ru^{II} and Ru^{III} amidinates have been shown to be effective catalysts for the intramolecular Kharasch

reaction (the addition of polyhaloalkanes to olefins)[49] while a number of examples have been reported for their activity in the heterofunctionalisation of olefins, e.g. $Y(RC\{NAr^{iPr}\}_2)(CH_2SiMe_3)_2$ (R = NMe_2 or Ph) for hydrosilation[50] and $Lu(PhC\{NCH(CH_3)Ph\}_2)_2(N\{SiMe_3\}_2)$ for hydroamination.[51]

1.2 – Bis(amido)silane Ligands

Dianionic, bidentate bis(amido)silane ligands, $[R_2Si\{NR'\}_2]^{2-}$, have been utilised in coordination chemistry since the 1970s. They are sterically similar to amidinates, guanidinates and phosphaguanidinates (*vide supra*) in that a single atom bridges two nitrogen atoms that have the potential to interact with a metal centre. However, electronically they are fundamentally different as in their fully deprotonated state they are dianionic. Metallic complexes using these ligands are generally synthesised from the metathesis reaction of a dilithiated bis(amido)silane, $R_2Si\{NR'Li\}_2$, with a metal halide. Although many examples of transition metal complexes incorporating bis(amido)silane ligands are known, they do not fall within the remit of this introduction and will not be discussed.

1.2.1 Synthesis of Bis(amino)silanes, $R_2Si\{N(H)R'\}_2$, and Corresponding Lithium Salts, $[R_2Si\{NR'Li\}_2]$

The synthesis of the lithium complexes is achieved by the reaction of a neutral bis(amino)silane, $R_2Si\{N(H)R'\}_2$, with an lithium alkyl, e.g. Li^nBu, LiMe. The bis(amino) precursors are usually synthesised from either (a) the reaction of two equivalents of an *in situ* lithiated primary amine with a dichlorosilane or (b) directly from the reaction of four equivalents of the amine with the silane, where 2 equivalents of the amine act as a base removing HCl to form an ammonium salt (Scheme 1.8).

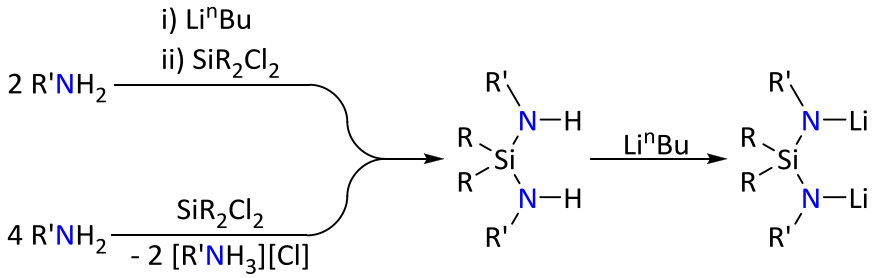

Scheme 1.8 – General synthesis of bi(amino)- and dilithiated bis(amido)silanes

X-ray diffraction studies of the dilithium salts have shown a range of interesting structural conformations (Figure 1.18).

The first example to be studied, $Me_2Si\{N^tBuLi\}_2$ (**XXX**), was found to be dimeric in the solid-state with each nitrogen bonding to three lithium atoms to form a $(N_2Li_2)_2$ tetragonal core.[52] When synthesised in the presence of thf, $Me_2Si\{N^tBuLi\}_2$ was crystallised as the solvated monomer, $Me_2Si\{N^tBu\}_2Li_2(thf)_3$ (**XXXI**). In this structure each lithium atoms is coordinated by a terminal thf, with a bridging thf molecule between them; the nitrogen atoms both coordinate to each of the lithium atoms.[53]

Replacing the ^{t}Bu groups with aryl or benzyl-derived groups results in structures in which weak π-interactions between Li and the aromatic rings are observed. Power *et al.* synthesised the mesityl derivative $Me_2Si\{NmesLi\}_2$ (**XXXII**) which crystallised as a dimer with a ladder-type core formed from joining two LiN_2Si rings (Figure 1.18).[54] The two lithium atoms in this core are each coordinated by three nitrogen atoms while the remaining two lithium atoms are bound by one nitrogen atom and have close interactions with two nearby mesityl rings; one in an η^6 fashion and one in an η^2 fashion to the carbons in the *ipso* and *ortho* positions. Hill and Hitchcock reported $Me_2Si\{NAr^{iPr}Li\}_2$ (**XXXIII**), which also crystallised as a dimer but does not form the ladder-core seen for **XXXII**.[55] In this case two of the lithium atoms are coordinated by three nitrogen atoms, as observed for $[Me_2Si\{NmesLi\}_2]_2$, with the other two bound to two

nitrogen atoms with two close contacts to the *ipso* carbons of the diisopropylphenyl rings (Figure 1.18).

The substituted-benzyl derivative $Me_2Si\{N(CH(Me)Ph)Li\}_2$ (**XXXIV**), reported by Liu *et al.*, is also dimeric in the solid state with a similar tetragonal structure to that of $[Me_2Si\{N^tBuLi\}_2]_2$, with each nitrogen atom coordinating to three lithium atoms, but with the two N_2Li_2 rings in a more eclipsed orientations forming an cubane-like $(N_2Li_2)_2$ core (Figure 1.18). Each of the lithium atoms also forms η^2 contacts with the *ipso* and *ortho* phenyl carbon atoms

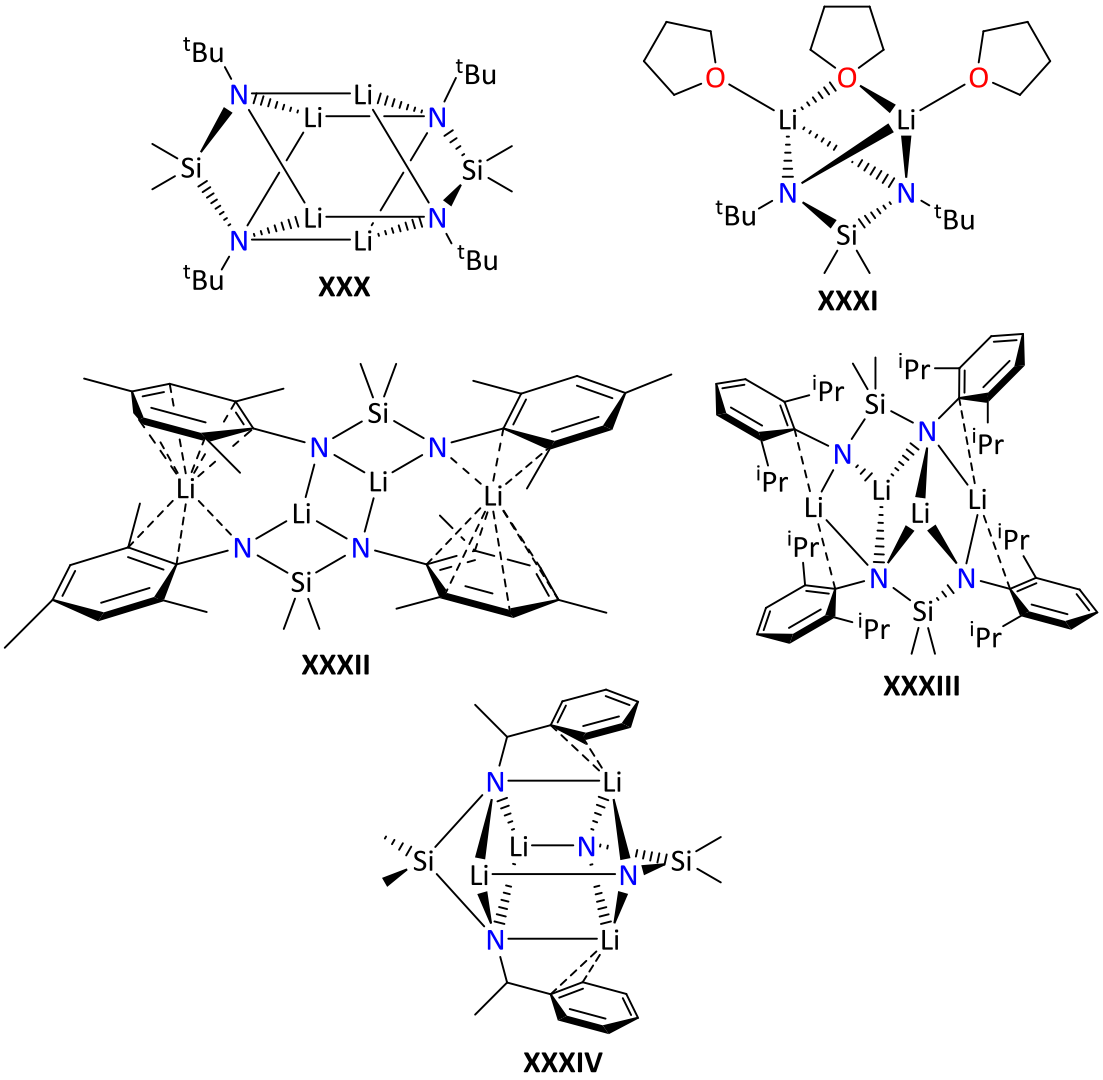

.

Figure 1.18 – Examples of dilithiated bis(amido)silanes (Note: two of the CH(Me)Ph groups of **XXXIV** have been removed for clarity)

1.2.3 Group 14 Derivatives of bis(amido)silanes

Research into main group complexes of bis(amido)silanes has largely focused on divalent tin and germanium complexes, commonly referred to as *N*-heterocyclic-stannylenes and -germylenes. The first example was $Sn\{N^tBu\}_2SiMe_2$ (**XXXV**), reported by Veith in 1975.[56] In the solid state, **XXXV** was found to exist as both monomeric and dimeric molecules arranged in a chain with short contacts (3.675 Å; considerably less than sum of the van Der Waals radii = 4.34 Å)[57] between the tin atoms of the monomeric and dimeric units (Figure 1.19).

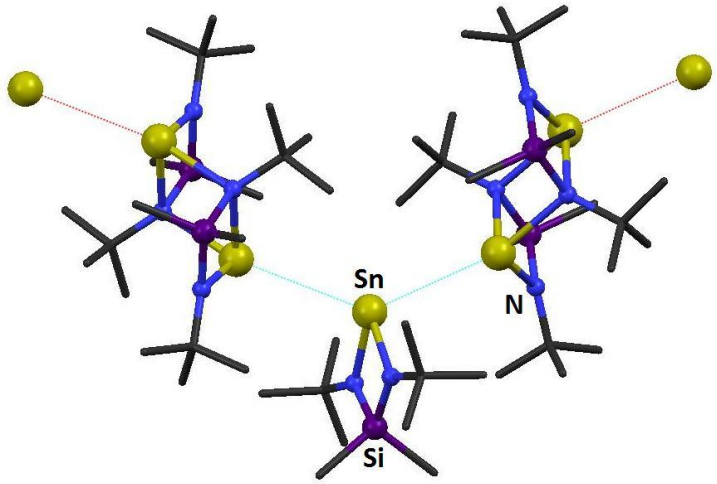

Figure 1.19 – Solid-state structure of $Sn\{N^tBu\}_2SiMe_2$ (**XXXV**) showing short contacts between the dimeric and monomeric molecules

A number of derivatives have since been reported (Figure 1.20)[34,58] but the majority of the reactivity studies of bis(amino)stannylenes has been performed by Veith and co-workers using **XXXV**.

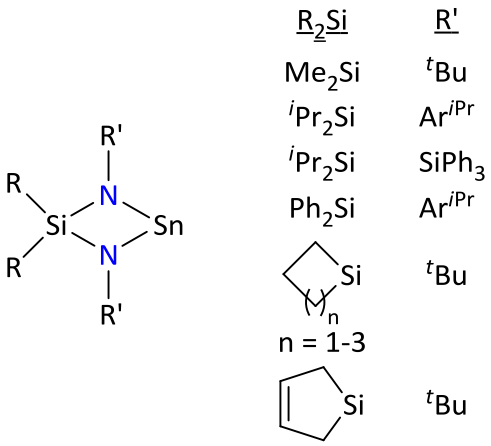

Figure 1.20 – Examples of bis(amino)stannylenes

1.2.4 Sn({N^{t}Bu}$_2$SiMe$_2$ as a ligand

Stannylenes can be described as being Lewis-amphoteric due to the filled 5*s* and empty 5*p* orbitals of the Sn(II) centre, enabling them to both accept and donate an electron pair. This property was exploited by Veith *et al.* during the investigation of **XXXV** as a coordinating ligand. In 1981, Veith *et al*. showed that **XXXV** reacted with $M(CO)_6$ (M = Cr or Mo) under UV-irradiation, displacing a carbonyl ligand, to form the pentacarbonyl stannylene complex $M(CO)_5(Sn\{N^tBu\}_2SiMe_2)$. In the case of the molybdenum example, a second carbonyl ligand can be eliminated to form the bis-stannylene complex $Mo(CO)_4(Sn\{N^tBu\}_2SiMe_2)_2$.[59] Veith *et al.* then studied the reactivity of **XXXV** with transition metal halide complexes, beginning with Wilkinson's catalyst in 1989.[60] The reaction of two equivalents of $Sn\{N^tBu\}_2SiMe_2$ with $RhCl(PPh_3)_3$ at -20 °C resulted in the displacement of one of the phosphine ligands and the insertion of two stannylene molecules into the Rh-Cl bond, forming *cis*-$Rh(PPh_3)_2((\mu\text{-}Sn\{N^tBu\}_2SiMe_2)_2Cl)$ (**XXXVI**; Scheme 1.9). When allowed to warm to room temperature a second product is observed in which the remaining two phosphine ligands are replaced by an additional three stannylene molecules, to give $Rh(Sn\{N^tBu\}_2SiMe_2)_3((\mu\text{-}Sn\{N^tBu\}_2SiMe_2)_2Cl)$ (**XXXVII**); this compound can also be made in near quantitative yield from the reaction of five equivalents of **XXXV** with $RhCl(PPh_3)_3$ at 60 °C (Scheme 1.9).

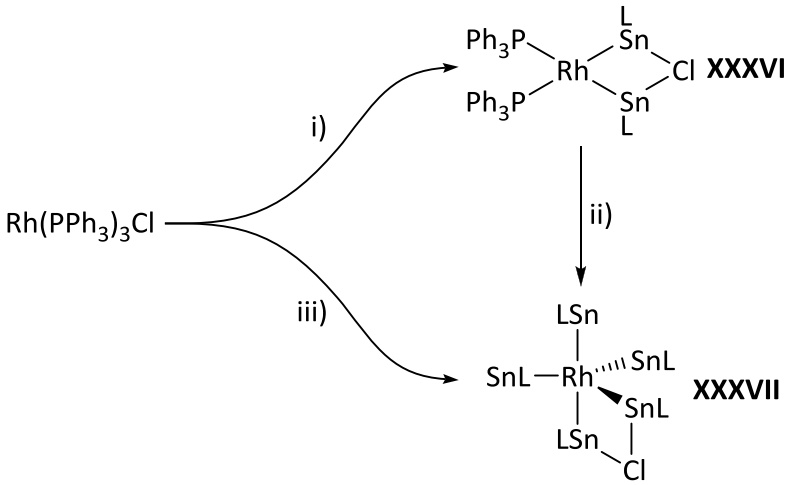

Scheme 1.9 – Reactions of Sn{N^{t}Bu}$_2$SiMe$_2$ (**XXXV**) with Wilkinson's catalyst (L = [{N^{t}Bu}$_2$SiMe$_2$]$^{2-}$). i) 2 **XXXV**, toluene, -20 °C ii) warm to room temperature iii) 5 **XXXV**, toluene, 60 °C

The ligating properties of **XXXV** was further demonstrated by the synthesis of Ni(Sn{N^{t}Bu}$_2$SiMe$_2$)$_4$ (**XXXVIII**), the first example of a homoleptic, zero valent first row transition metal stannylene complex.[61]

The Lewis-amphoteric nature of **XXXV** was further probed by its reaction with nickelocene,[62] a compound that usually reacts with nucleophiles (electron donors) at the Ni centre and at the cyclopentadienyl ring with electrophiles (electron acceptors).[63] The product from this reaction was NiCp({Sn{N^{t}Bu}$_2$SiMe$_2$}$_2$Cp) (**XXXIX**), in which two stannylene molecules have inserted between one of the Cp rings and Ni (i.e. reacting as both an electrophile and a nucleophile, Figure 1.21). In contrast, the germanium analogue of **XXXV**, Ge{N^{t}Bu}$_2$SiMe$_2$, reacts with NiCp$_2$ *via* one molecule inserting between Ni and one of the Cp rings and another molecule coordinating to Ni forming NiCp(Ge{N^{t}Bu}$_2$SiMe$_2$)(Ge({N^{t}Bu}$_2$SiMe$_2$)Cp) (**XL**; Figure 1.21).

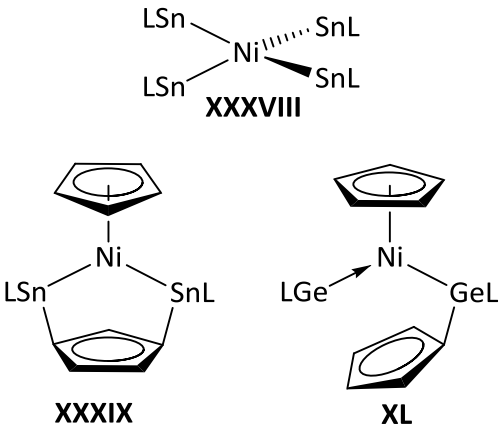

Figure 1.21 – Products of the reactions of $E\{N^tBu\}_2SiMe_2$ (E = Sn or Ge) with $Ni(COD)_2$ and $NiCp_2$ ($L = [\{N^tBu\}_2SiMe_2]^{2-}$)

In addition to behaving as a two electron donor ligand *via* the lone pair of tin, it was also shown that ligation through the nitrogen lone pairs is also possible. Veith *et al*. investigated this by reacting **XXXV** with a range of divalent transition metal halides, MCl_2 (M = Cr, Fe, Co, Ni, Zn, Pt, Pd) and MBr_2 (M = Ni, Zn).[64] It was found that while the group 10 halide salts reacted with four equivalents of **XXXV** to form $M(Sn\{N^tBu\}_2SiMe_2)_4X_2$,[†] the other salts only reacted with two equivalents to form $M((Sn\{N^tBu\}_2SiMe_2)_2Cl)_2$. Solid-state structures were obtained of the products from the reactions of **XXXV** with $CoCl_2$, $ZnCl_2$, $NiBr_2$ and $PdCl_2$, showing three different coordination modes of **XXXV**. $Co(Sn\{N^tBu\}_2SiMe_2)Cl_2$ (**XLI**) and $Zn(Sn\{N^tBu\}_2SiMe_2)Cl_2$ (**XLII**) both crystallised as chloride bridged dimers but while the stannylene ligand of the Co complex chelated to the cobalt *via* both nitrogen atoms, only one of the nitrogen atoms coordinated in the Zn complex (Figure 1.22). The tin centre in both complexes form Lewis acid-base adducts with one chloride. The Ni and Pd complexes, $M(Sn\{N^tBu\}_2SiMe_2)_4X_2$ (**XLIII**; M = Ni, X= Br; M= Pd, X = Cl), are described as being isostructural with two stannylene molecules inserting into each of the M-X bonds, forming two XSn_2M metallacycles (Figure 1.22).

[†] NOTE: $NiCl_2$ did not react with $Sn\{N^tBu\}_2SiMe_2$

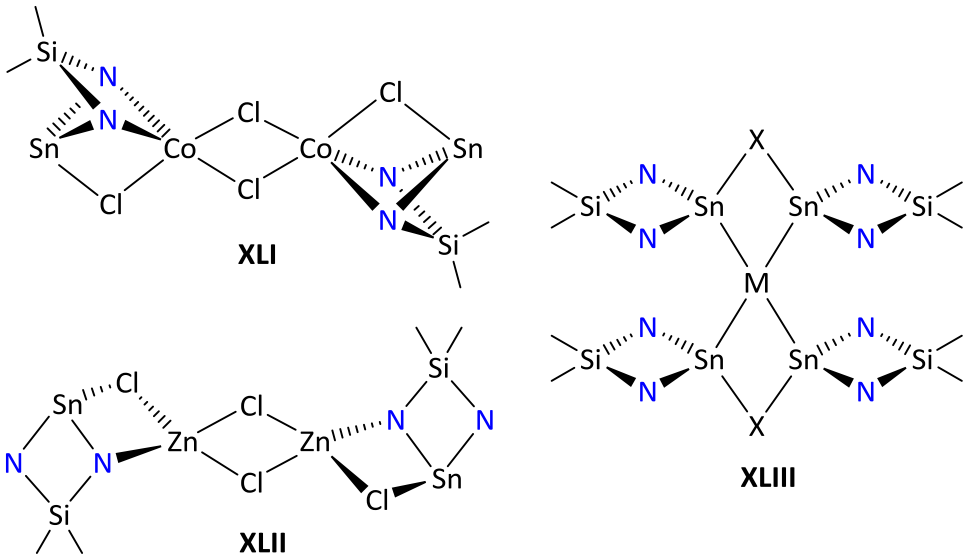

Figure 1.22 – Products from the reactions of **XXXV** with divalent transition metal halides

Recently we synthesised the bis(amido) stannylene Sn{NAr^{iPr}}$_2$SiMe$_2$ (**XLIV**), a bulkier derivative of Veith's stannylene, **XXXV**. The increased size of the nitrogen substituents of **XLIII** is sufficient to prevent aggregation in the solid-state (Figure 1.23) unlike **XXXV** which is found to exist as a mixture monomers and dimers (Figure 1.19). The synthesis and structure of stannylene **XLIV** was recently reported by Zheng *et al*..[65,66]

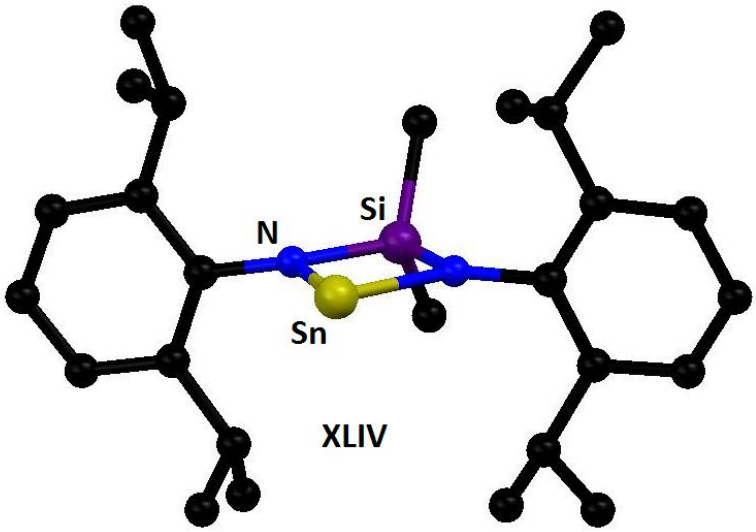

Figure 1.23 – Solid state structure of Sn({NAr^{iPr}}$_2$SiMe$_2$) (**XLIV**)

Initial studies of the reactivity of **XLIV** focussed on the oxidative addition of various iodide substrates (Scheme 1.10).[‡] **XLIV** was found to react with iodine and iodomethane to form the Sn^{IV} complexes $Sn(\{NAr^{iPr}\}_2SiMe_2)I_2$ (**XLV**) and $Sn(\{NAr^{iPr}\}_2SiMe_2)(Me)(I)$ (**XLVI**). Compound **XLV** was also synthesised from the reaction of $Me_2Si(NAr^{iPr}Li)_2$ with SnI_4. The reaction of **XLIV** with diphenylchlorophosphine resulted in the formation of tetraphenyldiphosphine (identified by ^{31}P NMR spectroscopy). The Sn containing product was thought to be either $Sn(\{NAr^{iPr}\}_2SiMe_2)Cl_2$ or the distannane $(Me_2Si\{NAr^{iPr}\}_2(Cl)SnSn(Cl)(\{NAr^{iPr}\}_2SiMe_2)$ based upon the reported reactivity of $Sn\{N^tBu\}_2SiMe_2$ with chlorinated phosphines by Veith *et al*.[67,68] and West and Stahl.[69] However, sufficient analytical data was not collected to definitively prove this hypothesis.

We were also interested in the formation of metal-tin bonds using **XLIV** as a substrate. This was initially investigated by reacting **XLIV** with $FeCp(I)(CO)_2$ (Scheme 1.10), resulting in the insertion of **XLIV** into the Fe-I bond to generate $FeCp(SnI(\{NAr^{iPr}\}_2SiMe_2))(CO)_2$ (**XLVII**).

[‡] This work was performed by Becky M. Donovan for her MChem research project under my supervision, see reference 135

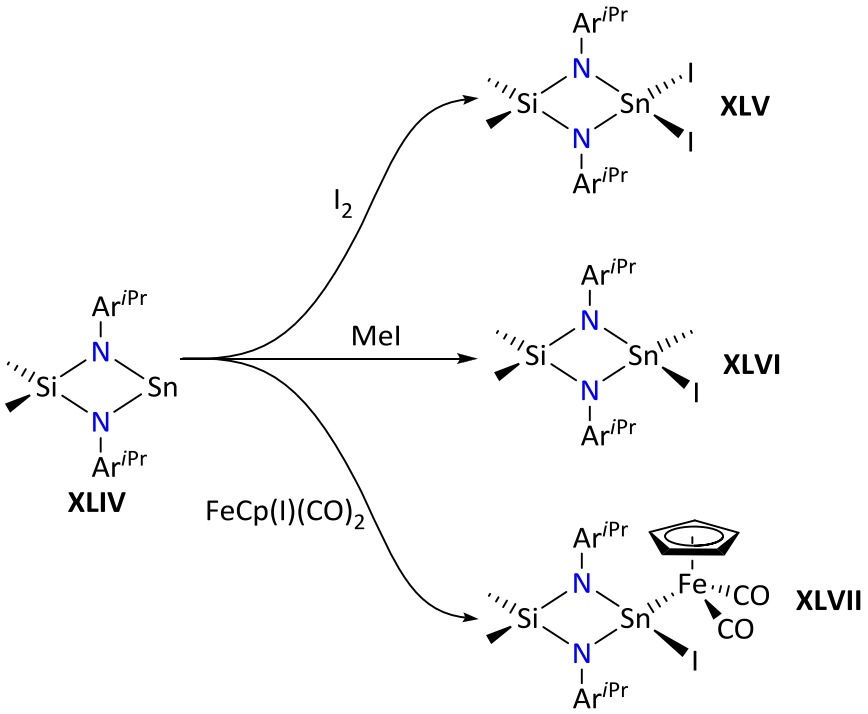

Scheme 1.10 – Reactions of $Sn\{NAr^{iPr}\}_2SiMe_2$ (**XLIV**) with MeI, I_2 and $FeCp(I)(CO)_2$

Chapter 2: Synthesis of Amidinate, Guanidinate and Phosphaguanidinate Complexes of Magnesium

The application of magnesium compounds as (pre)catalysts in organic transformations requires the development of a suitable ancillary ligand set to support the metal during the catalytic cycle. The target ligands had a number of key features which was felt would maximize their potential in this role:

a) monoanionic – to allow a second Mg-X functionality to be present in the molecule, to serve as the site of reactivity

b) chelating – to occupy more than one coordination site on the metal and infer stability to the complex

c) facile access to a range of derivatives – to allow steric and electronic tuning to take place during refinement of catalytic activity

The amidinate, guanidinate and phosphaguanidinate ligands were deemed to be suitable candidates and the synthesis of a range of compounds was therefore attempted, building on previous work conducted in the group.[35,39]

2.1 – Synthesis of Mg(mesC{NCy}$_2$)(N{SiMe$_3$}$_2$)(thf) (1) and Structure of Mg(mesC{NCy}$_2$)(O-2,6-^{t}Bu$_2$C$_6$H$_3$)(thf) (2)

The reaction of Li(N{SiMe$_3$}$_2$) with [Mg(mesC{NCy}$_2$)Br(Et$_2$O)]$_2$ (**XX**, Chapter 1) in thf results in the formation of the magnesium amide complex Mg(mesC{NCy}$_2$)(N{SiMe$_3$}$_2$)(thf) (**1**). Compound **1** was also synthesised in a one-pot procedure without the isolation of **XX**, with an increase in overall yield[§] of **1** obtained (82.2 % vs 71.5 %; Scheme 2.1). The product was crystallised by slow cooling of a hot (60 °C) hexane solution ambient temperature and the purity confirmed by elemental analysis.

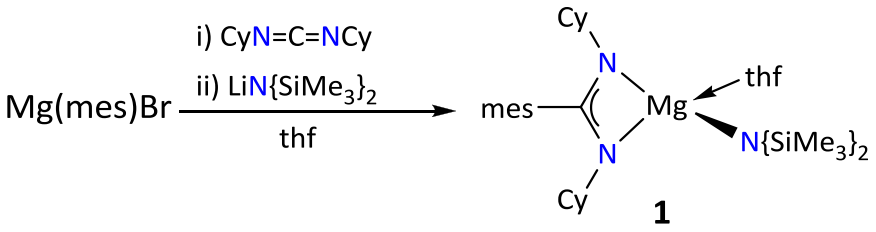

Scheme 2.1 – Synthesis of Mg(mesC{NCy}$_2$)(N{SiMe$_3$}$_2$)(thf) (**1**)

The ^{1}H NMR spectrum of **1** in D$_6$-benzene shows that the amidinate ligand is bound to magnesium in a symmetrical fashion, as evident from the single resonance for the cyclohexyl α-CH protons at δ_H 2.68 ppm. Only one resonance is observed at δ_H 2.34 ppm for the methyl groups in the *ortho* positions of the mesityl ring implying free rotation of mesityl group in solution. The thf resonances at δ_H 3.83 and 1.33 ppm are shifted from the chemical shifts of the non-complexed molecule in D$_6$-benzene (δ_H 3.57 and 1.40 ppm) indicating the thf is bound to magnesium in solution. The methyl protons of the trimethylsilyl groups are equivalent and have a chemical shift of δ_H 0.51 ppm.

[§] Calculated from quantity of Mg(mes)Br used

The solid-state structure of **1** was determined by single crystal X-ray diffraction. Compound **1** crystallises in the monoclinic $P2_1/c$ space group and was shown to be monomeric in the solid-state (Figure 2.1). The geometry of the four coordinate magnesium centre is distorted tetrahedral [range of angles = 65.54(7) - 134.26(8)°] with the smallest angle defined by the N1-Mg-N2 bite angle of the chelating amidinate ligand. The bond lengths and angles of the amidinate-Mg moiety do not differ dramatically from those found for **XX**,[35] despite a change in the coordination number from five to four, implying that the ligand is relatively insensitive to the metal environment.

The Mg-N1 and Mg-N2 bond lengths of 2.077(2) and 2.081(2) Å are identical (within 3σ) and are only slightly longer than the Mg-N3 bond length of 1.997(2) Å. The C1-N1 and C1-N2 bond lengths of 1.336(3) and 1.333(3) Å are also identical (within 3σ) indicating that the negative charge is fully delocalised across the hetero-allylic N-C-N core. The internal angles of the planar CN_2Mg metallacycle [sum of angles = 359.9°] are as expected for a chelating magnesium amidinate complex, all being with the standard deviations of the mean values obtained from the 19 other structurally characterised magnesium amidinates reported by the Cambridge Crystallographic Data Centre (CCDC).[70,71]

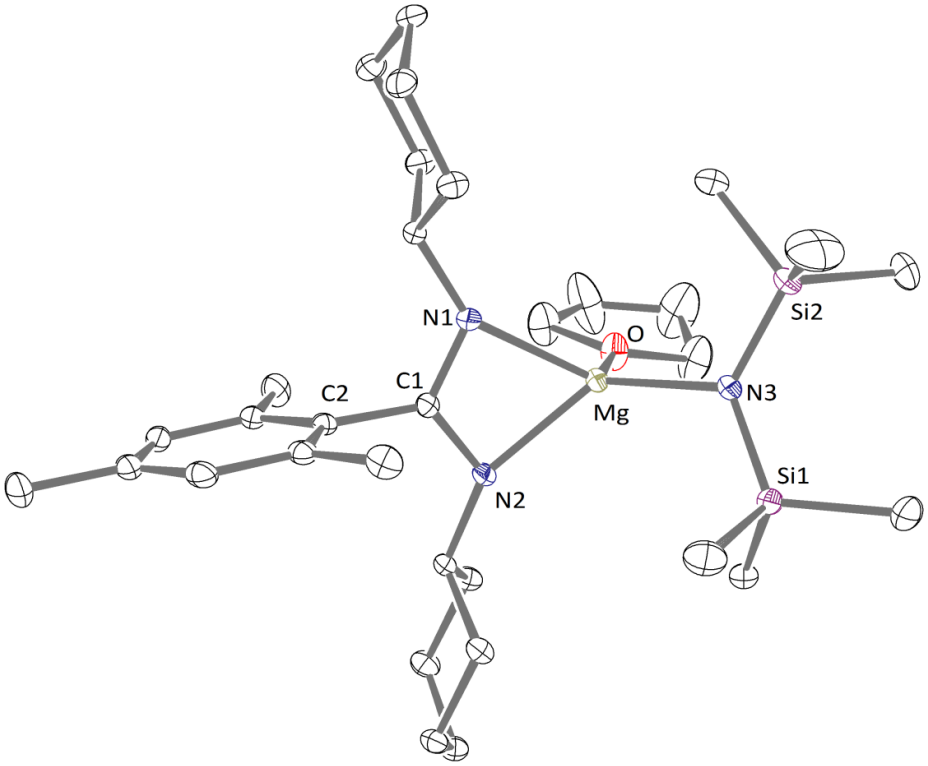

Figure 2.1 – ORTEP representation of Mg(mesC{NCy}$_2$)(N{SiMe$_3$}$_2$)(thf) (**1**) (with thermal ellipsoids at 30% level), hydrogen atoms omitted for clarity. Selected bond lengths and angles are listed in Table 2.1

Table 2.1 – Selected Bond Lengths (Å) and Angles (°) for 1			
Mg-N1	2.077(2)	**C1-N2**	1.333(3)
Mg-N2	2.081(2)	**C1-C2**	1.508(3)
Mg-N3	1.997(2)	**N3-Si2**	1.6937(19)
Mg-O	2.0205(18)	**N3-Si1**	1.697(2)
C1-N1	1.336(3)		
N1-Mg-N2	65.54(7)	**Mg-N2-C1**	89.62(13)
N1-Mg-N3	134.26(8)	**Mg-N3-Si1**	115.41(10)
N1-Mg-O	108.30(8)	**Mg-N3-Si2**	117.05(10)
N2-Mg-N3	130.83(8)	**Si1-N3-Si2**	127.24(12)
N2-Mg-O	106.34(8)	**N1-C1-N2**	115.0(2)
N3-Mg-O	105.60(8)	**N1-C1-C2**	122.90(19)
Mg-N1-C1	89.71(13)	**N2-C1-C2**	122.04(19)

Previous work within group showed that **XX** reacts with Li(O-2,6-^{t}Bu$_2$C$_6$H$_3$) to give the magnesium aryloxide, Mg(mesC{NCy}$_2$)(O-2,6-^{t}Bu$_2$C$_6$H$_3$)(thf) (**2**; Scheme 2.2).[35] Although this compound was characterised spectroscopically, a solid-state structure had not been obtained. Slow cooling of a hot (see above) hexane solution of **2** yielded crystals of sufficient quality for

analysis by single crystal X-ray diffraction. Satisfactory elemental analysis was not obtained despite multiple attempts. This is believed to be due to difficulties in separation from the LiBr side product.

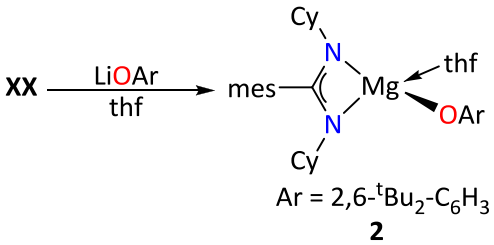

2

Scheme 2.2 – Synthesis of Mg(mesC{NCy}$_2$)(O-2,6-^{t}Bu$_2$C$_6$H$_3$)(thf) (**2**)

Like compound **1**, aryloxide **2** crystallises in the monoclinic $P2_1/c$ space group and is monomeric in the solid state (Figure 2.2). The amidinate ligand chelates to a distorted tetrahedral magnesium centre with no significant differences in the amidinate bond lengths and angles compared with **1**. The Mg-O1-C23 angle (163.38(18)°) is large and there is a relatively short Mg-O1 bond length (1.8431(19) Å), as observed in related magnesium complexes containing a terminal [O-2,6-^{t}BuC$_6$H$_3$]$^-$ ligand.[72,73]

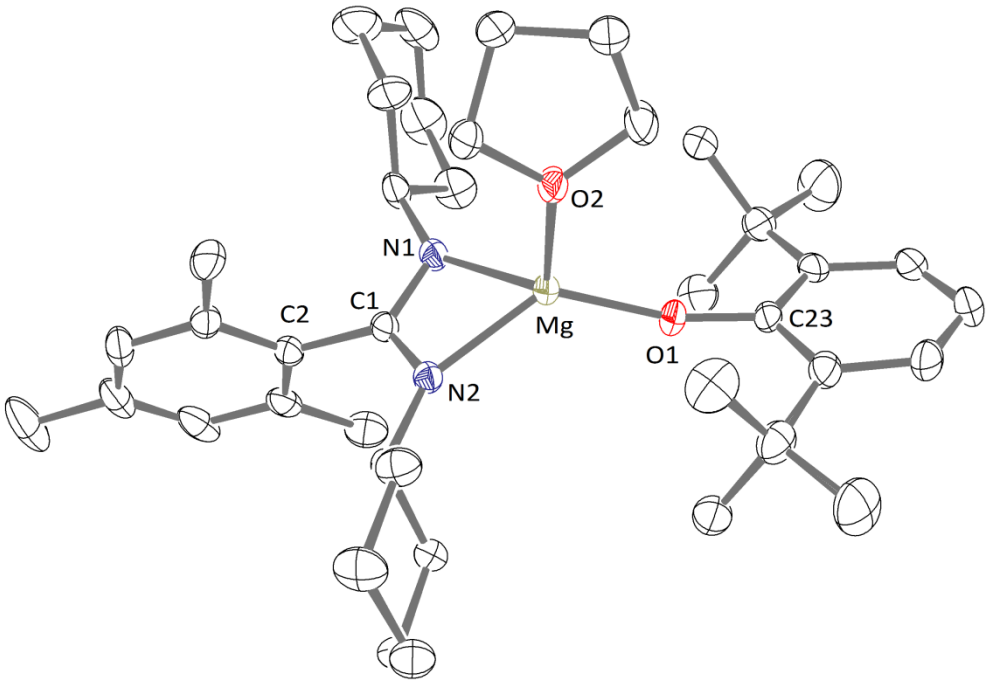

Figure 2.2 – ORTEP representation of Mg(mesC{NCy}$_2$)(O-2,6-^{t}BuC$_6$H$_3$)(thf) (**2**) (with thermal ellipsoids at 30% level), hydrogen atoms omitted for clarity. Selected bond lengths and angles are listed in Table 2.2

Table 2.2 – Selected Bond Lengths (Å) and Angles (°) of 2			
Mg-N1	2.067(2)	**C1-N1**	1.328(3)
Mg-N2	2.054(2)	**C1-N2**	1.329(3)
Mg-O1	1.8431(19)	**C1-C2**	1.509(4)
Mg-O2	2.005(2)	**O1-C23**	1.333(3)
N1-Mg-N2	65.89(9)	**Mg-N1-C1**	89.31(16)
N1-Mg-O1	134.82(10)	**Mg-N2-C1**	89.84(15)
N1-Mg-O2	106.29(9)	**Mg-O1-C23**	163.38(18)
N2-Mg-O1	131.25(9)	**N1-C1-N2**	114.9(2)
N2-Mg-O2	111.31(9)	**N1-C1-C2**	122.3(2)
O1-Mg-O2	103.07(9)	**N2-C1-C2**	122.8(2)

2.2 – Synthesis of $Mg(tbo)Br(thf)_n$ (3) and $Mg(tbo)\{N(SiMe_3)_2\}(thf)$ (4)

The reaction of the bicyclic guanidine 1,4,6-triazabicyclo[3.3.0]oct-4-ene (H-tbo) with MgMeBr in thf resulted in the formation of a compound of general formula $Mg(tbo)Br(thf)_n$ (**3**, n = 1 or 1.5; Scheme 2.3). The ^{1}H NMR spectrum of **3** showed two resonances for the $[tbo]^-$ methylene protons at δ_H 3.70 (overlapping with a thf resonance) and 2.70 ppm, indicating a symmetrical ligand environment, and two thf resonances at δ_H 3.70 (overlapping with a $[tbo]^-$ methylene resonance) and 1.40 ppm. The ratio of the integrals of these signals was consistent with 1.5 molecules of thf for each $[tbo]^-$ ligand, which implied that the product had the formula $Mg(tbo)Br(thf)_{1.5}$. These crystals rapidly became opaque when placed under vacuum suggesting desolvation under these conditions. Elemental analysis results of a sample of **3** that had been exposed to vacuum were correct for an empirical formula of **3** where n = 1.

The reaction of **3** with $Li(N\{SiMe_3\}_2)$ gave a crystalline product following work up and recrystallisation from hexane. The elemental analysis results of this product were consistent with the formula $Mg(tbo)(N\{SiMe_3\}_2)(thf)$ (**4**; Scheme 2.3). The ^{1}H NMR spectrum shows two $[tbo]^-$ methylene resonances at δ_H 3.93 and 2.63 indicating that the ligand has remained in a symmetrical environment. The $SiMe_3$ groups of the amide ligand give rise to a single resonance at δ_H 0.37 ppm and the presence of coordinated thf is evident from the resonances at δ_H 2.75 and 1.45 ppm.

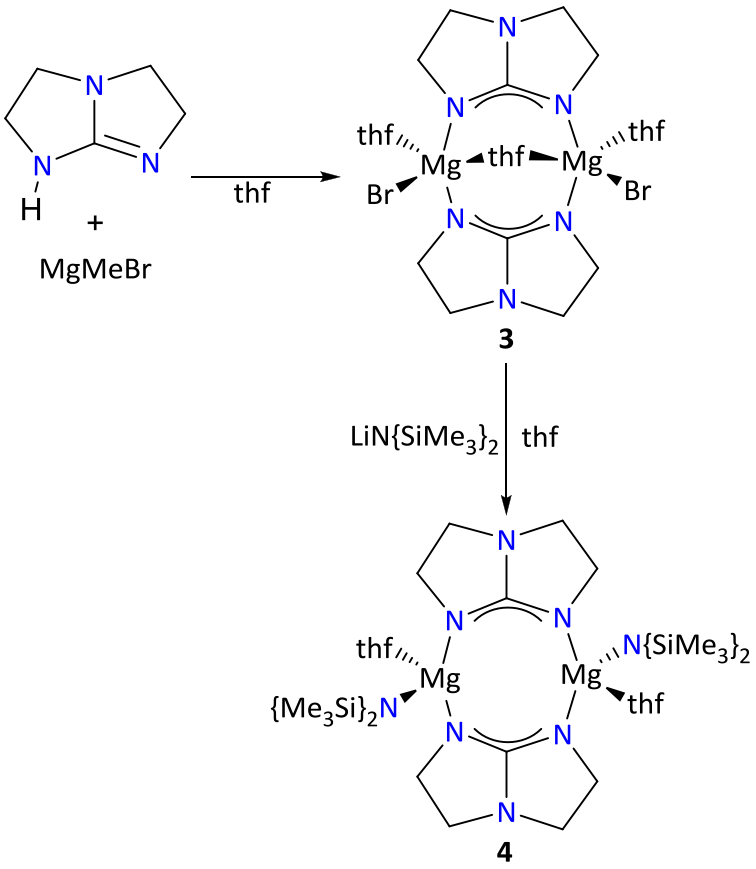

Scheme 2.3 – Synthesis of $[Mg(tbo)Br(thf)_n]_2$ (**3;** n = 1.5) and $[Mg(tbo)(N\{SiMe_3\}_2)(thf)]_2$ (**4**)

The solid-state structures of **3** and **4** were determined by single crystal X-ray diffraction (Figures 2.3 and 2.4). **3** and **4** crystallise in the orthorhombic *Pnan* space group and the monoclinic $P2_1/c$ space group respectively. Both compounds are bimetallic with two magnesium centres bridged by two $[tbo]^-$ ligands, each adopting the κ^1N,κ^2N'-bonding mode, and a terminal coordinated thf molecule; **3** also has a μ-thf molecule between the magnesium atoms bridging *via* the oxygen atom. The structure of **4** is very different from the analogous $[hpp]^-$ complex, $[Mg(hpp)(N\{SiMe_3\}_2)]_2$ (**XLVIII**), in which the guanidinate ligands adopt a $\kappa^1N,\kappa^{1,2}N'$-bonding mode and there is no coordinated thf (Figure 2.5).[38]

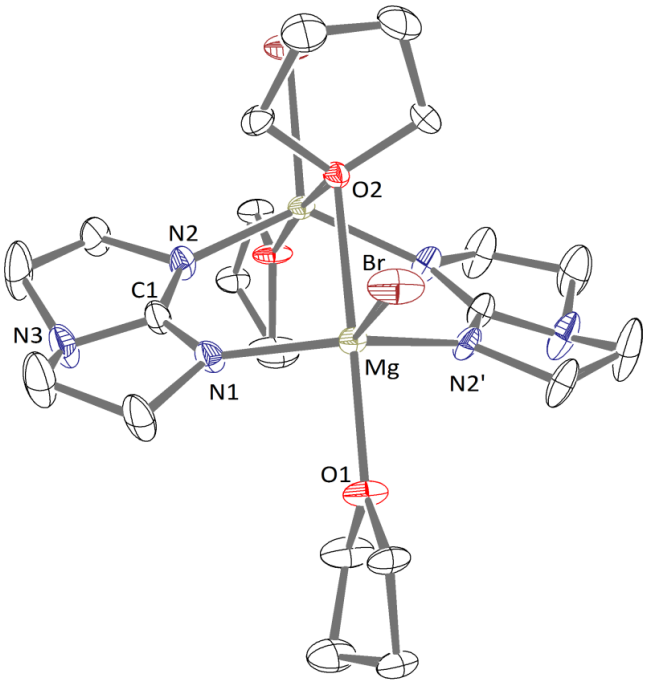

Figure 2.3 – ORTEP representation of $[Mg(tbo)Br(thf)_{1.5}]_2$ (**3**) (with thermal ellipsoids at 30% level), hydrogen atoms omitted for clarity. Selected bond lengths and angles are listed in Table 2.3

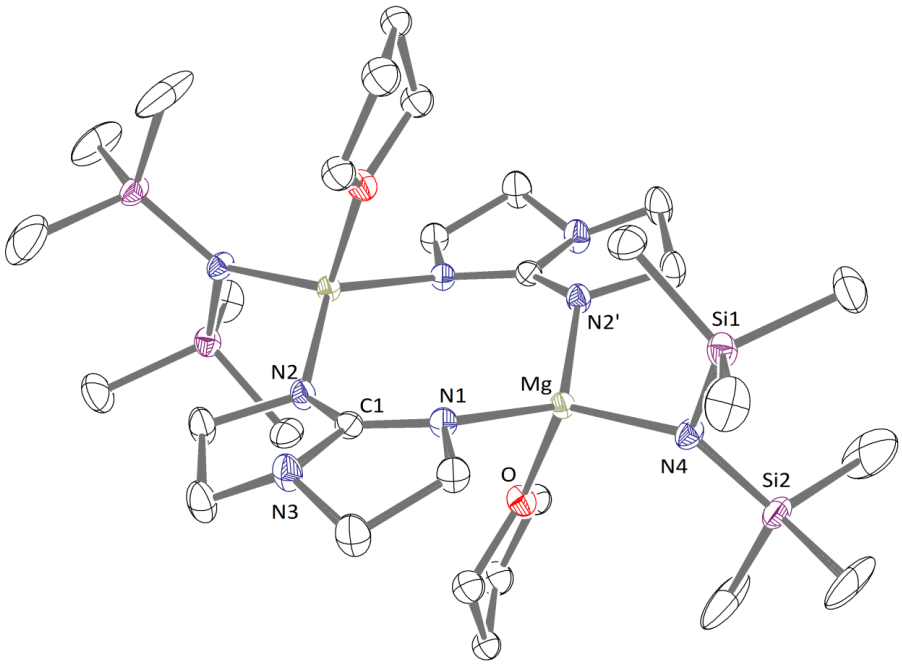

Figure 2.4 – ORTEP representation of $[Mg(tbo)(N\{SiMe_3\}_2)(thf)]_2$ (**4**) (with thermal ellipsoids at 30% level), hydrogen atoms omitted for clarity. Selected bond lengths and angles are listed in Table 2.3

Table 2.3 – Selected Bond Lengths (Å) and Angles (°) of 3 and 4					
Bond Lengths (Å)	**3**	**4**	**Angles (°)**	**3**	**4**
Mg-N1	2.039(4)	2.0468(15)	**N1-Mg-N2′**	128.66(15)	124.50(6)
Mg-N2′	2.033(4)	2.0507(15)	**N1-Mg-N4**	-	111.32(6)
Mg-N4	-	2.0205(15)	**N1-Mg-O1**	90.25(14)	95.94(6)
Mg-O1	2.094(3)	2.0578(14)	**N1-Mg-O2**	84.41(11)	-
Mg-O2	2.426(3)	-	**N1-Mg-Br**	117.38(12)	-
Mg-Br	2.4512(13)	-	**N2′-Mg-N4**	-	110.73(6)
C1-N1	1.335(5)	1.323(2)	**N2′-Mg-O1**	90.45(14)	96.28(6)
C1-N2	1.304(5)	1.325(2)	**N2′-Mg-O2**	84.41(11)	-
C1-N3	1.385(9)	1.401(2)	**N2′-Mg-Br**	113.50(11)	-
			O1-Mg-O2	170.46(11)	-
			N1-C1-N2	131.1(4)	132.07(15)
			N1-C1-N3	114.3(4)	113.93(15)
			N2-C1-N3	114.5(4)	113.99(15)

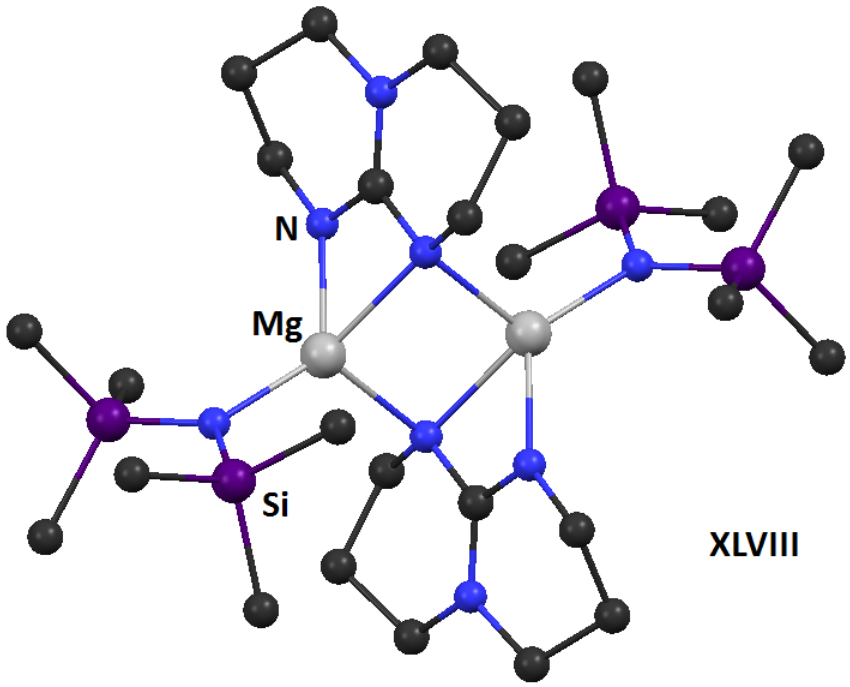

Figure 2.5 – Molecular structure of $[Mg(hpp)(N\{SiMe_3\}_2)]_2$ (**XLVIII**)

The observation that the $[tbo]^-$ ligand preferentially adopts a bridging bonding mode rather than chelating to a metal is not surprising when the {5:5} bicyclic structure of the ligand is considered. This constrained geometry has a marked effect on the direction of the donor orbitals of the bonding nitrogen atoms, forcing them to point away from the 'mouth' of the

ligand (Figure 2.6). Indeed the other eleven structurally characterised examples of metal-[tbo] complexes (found *via* the CCDC)[70,71] all have the $[tbo]^-$ ligand bridging between two or more metal centres. This is in contrast to acyclic guanidinates whose donor orbitals point towards the mouth of the ligand due to the steric interactions between the nitrogen substituents, resulting in a tendency to adopt a chelating bonding mode (although not exclusively). The {6:6} bicyclic structure of $[hpp]^-$ has the effect of the donor orbitals adopting a parallel projection. This can be thought of as an intermediate projection between the donor orbitals of $[tbo]^-$ and acyclic guanidinates and this idea fits with the solid-state structure of **XLVIII** where the $[hpp]^-$ ligands both chelate to and bridge between the magnesium centres.

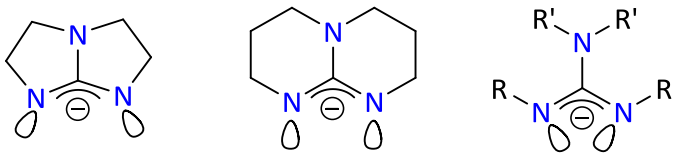

Figure 2.6 – Projections of the N-donor orbitals of $[tbo]^-$, $[hpp]^-$ and acyclic guanidinates

There are two main ideal geometries adopted by 5-coordinate complexes, trigonal bipyramidal and square pyramidal. The geometric parameter τ was defined by Addison *et al.* to describe the 'degree of trigonality' of a 5 coordinate complex using the formula $\tau = (\beta - \alpha) / 60$.[74] For a truly square pyramidal complex $\tau = 0$ whereas for a perfectly trigonal bipyramidal complex $\tau = 1$ (Figure 2.7).

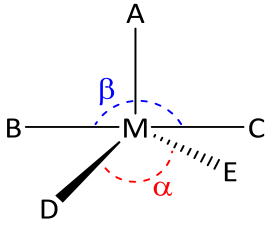

Figure 2.7 – Definition of α and β used for calculating degree of trigonality

The geometry around the five-coordinate magnesium atom in **3** approaches trigonal bipyramidal (τ = 0.70)[74] with the bridging and terminal thf molecules occupying the axial positions [O1-Mg-O2 angle = 170.46(11)°] and the $[tbo]^-$ and bromide ligands in the equatorial positions. The four coordinate magnesium atoms in **4** have distorted tetrahedral geometries [range of angles = 95.94(6) - 124.50(6) **°**] with the largest angle between the coordinated nitrogen atoms of the two $[tbo]^-$ ligands.

Within each structure, the Mg-N1 and Mg-N2′ bond lengths are identical (within 3σ), with those in **3** (2.039(4) and 2.033(4) Å) being shorter than those in **4** (2.0468(15) and 2.0507(15) Å). From a steric argument it may expected that longer bonds would be observed around the more crowded, five coordinate Mg centres in **3**. The fact that this is not the case suggests that this parameter is also influenced by the presence of the electronegative bromide ligand in **3**, relative to the amide ligand in **4**, generating a more electropositive Mg atom and therefore shorter Mg-N bonds.

The C1-N1 and C1-N2 bond lengths are identical (within 3σ) in **4** (1.323(2) and 1.325(2) Å), indicating delocalisation of the negative charge across the hetero-allylic N-C-N core. In **3**, however, they are significantly different (1.335(5) and 1.304(5) Å), consistent with a larger contribution from the localised π-bond resonance structure depicted in Scheme 1.2.

2.3 – Crystal Structure of a Tetrametallic Product from the Hydrolysis of 4

Storage of a toluene solution of **4** at -50 °C for 10 weeks in an attempt to obtain a second crop of the amide afforded a small number of colourless crystals. Analysis of these crystals by X-ray crystallography showed them to be the μ_4-oxo tetra-metallic complex $Mg_4(\mu_4\text{-}O)(tbo)_4(N\{SiMe_3\}_2)_2$ (**5**; Figure 2.8). Although no other data was collected on this complex, the structure is of interest for a number of reasons described below.

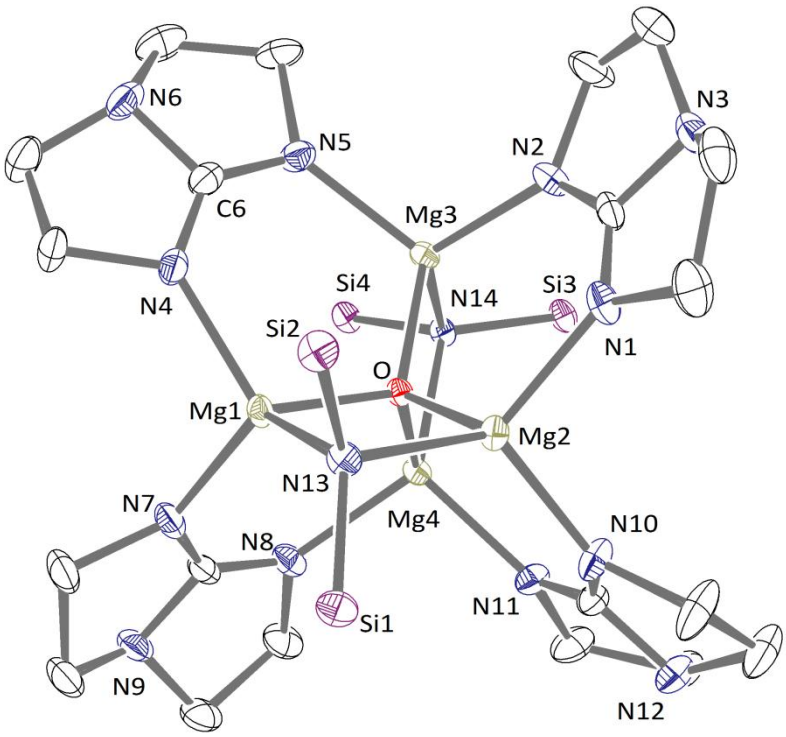

Figure 2.8 – ORTEP representation of $Mg_4(\mu_4\text{-}O)(tbo)_4(N\{SiMe_3\}_2)_2$ (**5**) (with thermal ellipsoids at 30% level), hydrogen atoms and Me groups omitted for clarity. Selected bond lengths and angles are listed in Table 2.4

Table 2.4 – Selected Bond Lengths (Å) and Angles (°) of 5					
Mg1-O	1.939(4)	**Mg4-N8**	2.050(5)	**C6-N4**	1.321(8)
Mg2-O	1.937(4)	**Mg4-N11**	2.035(5)	**C6-N5**	1.325(8)
Mg3-O	1.932(4)	**Mg1-N13**	2.174(5)	**C6-N6**	1.403(7)
Mg4-O	1.932(4)	**Mg2-N13**	2.185(5)	**C11-N7**	1.323(8)
Mg1-N4	2.052(5)	**Mg3-N14**	2.179(5)	**C11-N8**	1.317(8)
Mg1-N7	2.041(5)	**Mg4-N14**	2.181(4)	**C11-N9**	1.406(7)
Mg2-N1	2.039(5)	**C1-N1**	1.316(8)	**C16-N10**	1.322(8)
Mg2-N10	2.057(5)	**C1-N2**	1.323(8)	**C16-N11**	1.316(8)
Mg3-N2	2.056(5)	**C1-N3**	1.399(7)	**C16-N12**	1.406(7)
Mg3-N5	2.039(5)				
Mg1-O-Mg2	96.14(16)	**Mg2-O-Mg4**	116.64(18)	**N1-C1-N2**	131.4(5)
Mg1-O-Mg3	116.54(18)	**Mg3-O-Mg4**	96.07(16)	**N4-C6-N5**	131.9(5)
Mg1-O-Mg4	116.26(18)	**Mg1-N13-Mg2**	82.84(16)	**N7-C11-N8**	132.2(5)
Mg2-O-Mg3	116.72(18)	**Mg3-N14-Mg4**	82.43(15)	**N10-C16-N11**	132.1(5)

Compound **5** consists of four 6-membered CN_2Mg_2O metallacycles and two 4-membered NMg_2O metallacycles, formed by a bridging $[tbo]^-$ or $[N\{SiMe_3\}_2]^-$ ligands between two Mg atoms of an oxygen centred $[Mg_4O]^{6+}$ tetrahedron. The structure of compound **5** is reminiscent of a number of magnesium and zinc μ_4-oxo complexes (for examples see Figure 2.9).

The Mg1-O-Mg2 and Mg3-O-Mg4 angles, 96.14(16)° and 96.07(16)°, respectively, are more acute than the ideal tetrahedral angle, with the remaining Mg-O-Mg angles in the range 116.26(18) – 116.72(18)°. The Mg-O bond lengths are identical (within 3σ) with a range of 1.932(4) – 1.939(4) Å.

The Mg-N(tbo) bond lengths are in the range 2.035(5) – 2.057(5) Å and are comparable with those in **3** and **4**. The C-N bond lengths of the CN_3 core of each $[tbo]^-$ ligand indicate delocalisation of the negative charge across the hetero-allylic moiety (C-N bond length range 1.316(8) – 1.325(8) Å) but not the rear tertiary amido nitrogen (C-N bond length range: 1.399(7) – 1.406(7) Å).

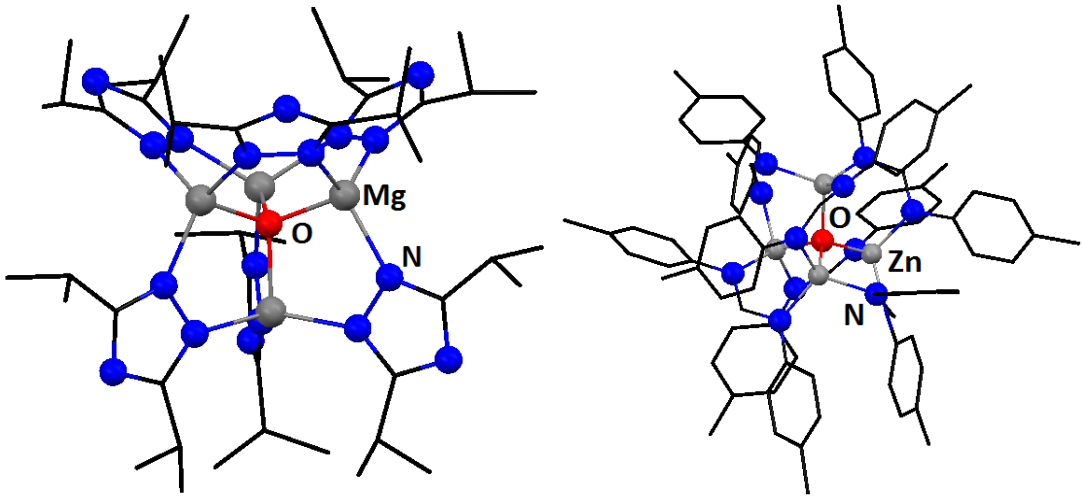

Figure 2.9 – Examples of magnesium and zinc μ_4-oxo complexes: $Mg_4(\mu_4\text{-}O)(tz)_6$[75] and $Zn_4(\mu_4\text{-}O)(HC\{N\text{-}p\text{-}tolyl\}_2)_6$[34]

A likely explanation for the formation of **5** is the accidental contamination of the sample with H_2O, which is doubly deprotonation by two equivalents of the amide ligand, $[N\{SiMe_3\}_2]^-$, to form **5**. However, attempts to deliberately synthesis **5** *via* the stoichiometric addition of H_2O (in a thf solution) to **4** were unsuccessful, with the only identifiable substance being unreacted **4**. It should be noted that oxide species like compound **5** have also been observed following exposure of organomagnesium compounds to O_2; an illustrative example is the formation of $Mg_4(\mu_4\text{-}O)Br_6(Et_2O)_4$ from MgPhBr (Figure 2.10).[76,77]

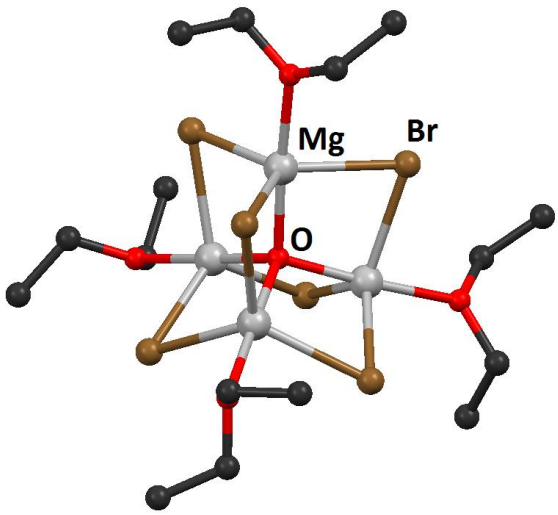

Figure 2.10 – Solid state structure of $Mg_4(\mu_4\text{-}O)Br_6(Et_2O)_4$

2.4 – Synthesis of $Mg(Cy_2PC\{NCy\}_2)Br(Et_2O)$ (6) and $Mg(Cy_2PC\{NCy\}_2)(N\{SiMe_3\}_2)(thf)$ (7)

The phosphaguanidine, $Cy_2PC(NCy)(NHCy)$, is synthesised from the insertion of DCC into the Li-P bond of the *in situ* generated lithium phosphide $LiPCy_2$, followed by quenching with $[HNEt_3][Cl]$.[78] The reaction of the phosphaguanidine with MgMeBr afforded $Mg(Cy_2PC\{NCy\}_2)Br(Et_2O)$ (**6**) with elimination of methane (Scheme 2.6). The reaction of **6** with $Li(N\{SiMe_3\}_2)$ gave the amide $Mg(Cy_2PC\{NCy\}_2)(N\{SiMe_3\}_2)(thf)$ (**7**; Scheme 2.6).

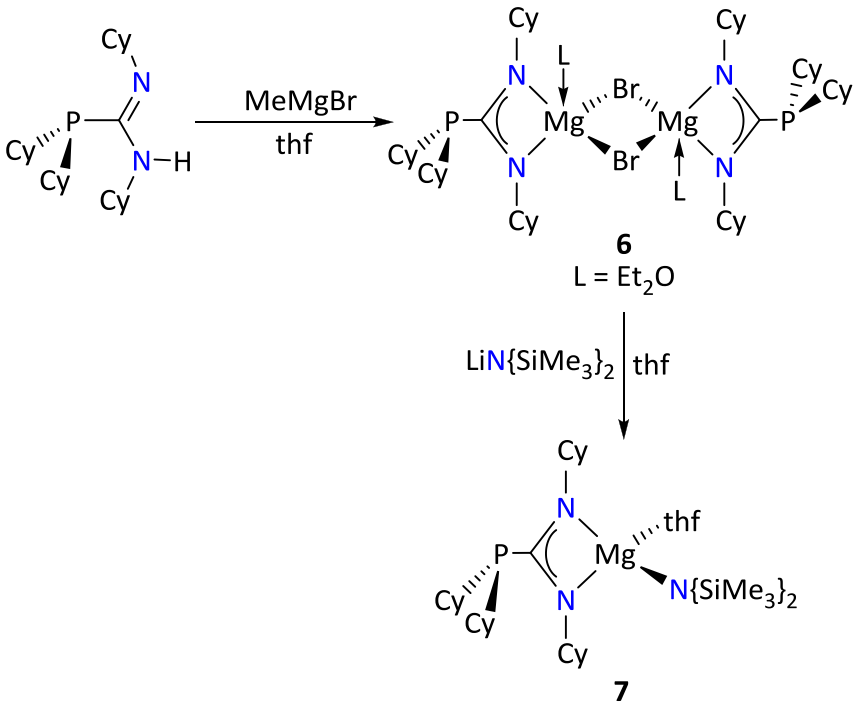

Scheme 2.6 – Synthesis of $Mg(Cy_2PC\{NCy\}_2)Br(Et_2O)$ (**6**) and $Mg(Cy_2PC\{NCy\}_2)(N\{SiMe_3\}_2)(thf)$ (**7**)

Satisfactory NMR data were not obtained for **6** owing to the low yield of the reaction (9.7 %); however the elemental analysis results and an X-ray diffraction study (*vide infra*) confirmed the proposed molecular formula.

The ^{1}H NMR spectrum of **7** shows a complex region of overlapping multiplets between δ_H 2.11 – 1.11 ppm for the *P*- and *N*-cyclohexyl protons with the exception of the *α*-CH of *P*-cyclohexyl groups which are observed as a multiplet at δ_H 2.30 ppm (confirmed by ^{1}H/^{31}P HMBC NMR experiment). The Si*Me*$_3$ resonances are observed as a singlet at 0.46 ppm.

The solid-state structures for **6** and **7** were determined by single crystal X-ray diffraction (Figures 2.10 and 2.11). Compound **6** crystallizes in the triclinic $P\bar{1}$ space group and lies on an inversion centre (symmetry transformations used to generate equivalent atoms: -x+1, -y+2, -z+2). It is therefore dimeric in the solid-state, with bromides bridging between two magnesium centres. The geometry around the magnesium centres is best described as distorted square pyramidal (τ = 0.40)[74] with the coordinated Et_2O molecule in the apical site and the two bromides and chelating amidinate ligand in the axial positions. This molecular structure is similar to that observed for amidinate complex **XX**[35] (Scheme 1.6) and two previously described phosphaguanidinate complexes **XXV** and **XXVI** (Figure 1.15).[39] The C1-N1 (1.341(3) Å) and C1-N2 (1.330(3) Å) bond lengths of the phosphaguanidinate ligand are identical (within 3σ) implying that the negative charge is delocalised across the heteroallylic core. The C1-P bond length (1.898(3) Å) is comparable to the analogous bonds in **XXV** (1.8905(17) Å) and **XXVI** (1.889(4) Å).

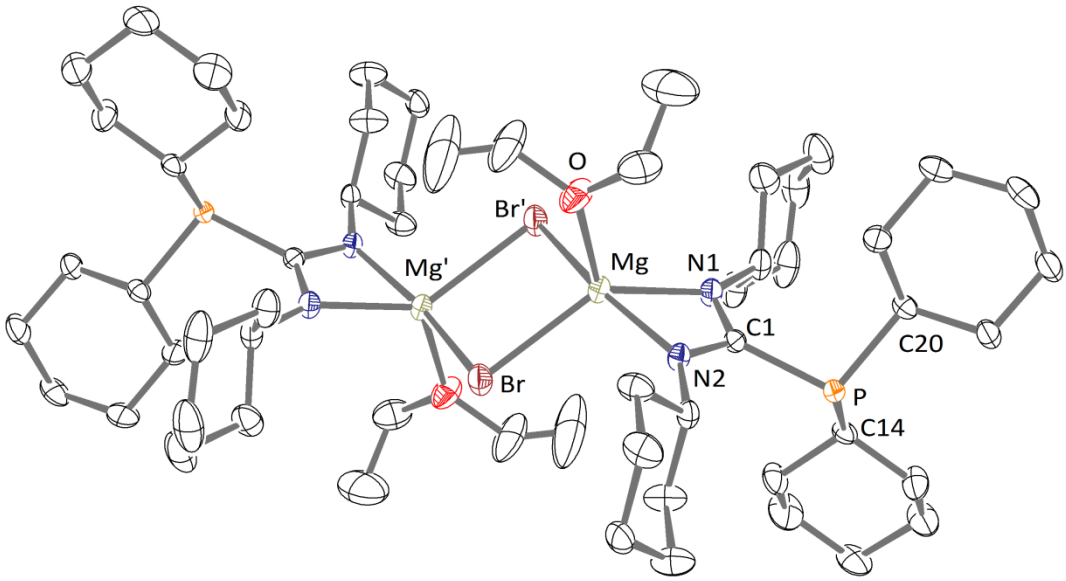

Figure 2.10 – ORTEP representation of $[Mg(Cy_2PC\{NCy\}_2)Br(Et_2O)]_2$ (**6**) (with thermal ellipsoids at 30% level), hydrogen atoms omitted for clarity. Selected bond lengths and angles are listed in Table 2.5

Table 2.5 – Selected Bond Lengths (Å) and Angles (°) of 6			
Mg-N1	2.071(2)	**N1-Mg-Br'**	99.03(7)
Mg-N2	2.108(2)	**N1-Mg-O**	113.43(10)
Mg-Br	2.5818(10)	**N2-Mg-Br**	100.53(7)
Mg-Br'	2.6882(10)	**N2-Mg-Br'**	161.48(7)
Mg-O	2.062(2)	**N2-Mg-O**	101.19(11)
C1-N1	1.341(3)	**Br-Mg-Br'**	86.46(3)
C1-N2	1.330(3)	**Br-Mg-O**	108.25(8)
C1-P	1.898(3)	**Br'-Mg-O**	92.71(7)
		N1-C1-N2	112.7(2)
N1-Mg-N2	64.27(9)	**N1-C1-P**	128.7(2)
N1-Mg-Br	137.56(8)	**N2-C1-P**	118.63(18)

Compound **7** is monomeric in the solid state and also crystallises in the triclinic $P\bar{1}$ space (Figure 2.11). The four-coordinate magnesium centre has a distorted tetrahedral geometry and the overall structure is comparable with that of the phosphaguanidinate complex **XXVIII** (Figure 1.15)[39] and amidinate complex **1**. There are no notable differences in the bond lengths and angles around magnesium or the N-C-N hetro-allylic core of the ligand. There is also no significant change in the C1-P bond length compared to **6** indicating that the change in the magnesium coordination sphere does not strongly influence the phosphaguanidinate ligand.

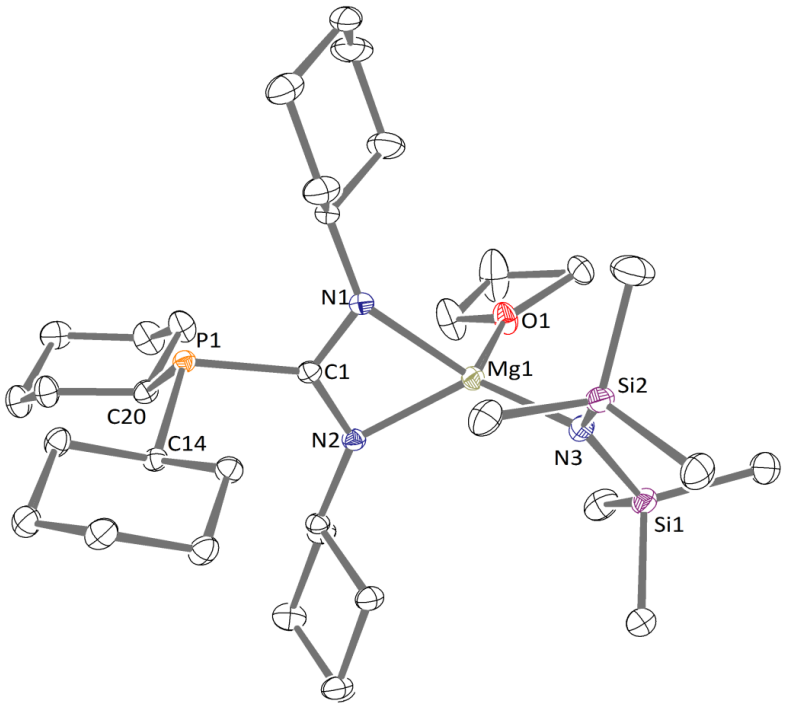

Figure 2.11 – ORTEP representation of $Mg(Cy_2PC\{NCy\}_2)(N\{SiMe_3\}_2)(thf)$ (**7**) (with thermal ellipsoids at 30% level), hydrogen atoms omitted for clarity. Selected bond lengths and angles are listed in Table 2.6

Table 2.6 – Selected Bond Lengths (Å) and Angles (°) of 7			
Mg-N1	2.084(2)	**N1-Mg-N3**	134.88(8)
Mg-N2	2.0611(19)	**N1-Mg-O**	101.08(8)
Mg-N3	1.992(2)	**N2-Mg-N3**	127.07(8)
Mg-O	2.0611(19)	**N2-Mg-O**	108.61(8)
C1-N1	1.337(3)	**N3-Mg-O**	111.38(8)
C1-N2	1.335(3)	**N1-C1-N2**	113.45(19)
C1-P	1.895(2)	**N1-C1-P**	118.11(16)
		N2-C1-P	128.43(16)
N1-Mg-N2	65.20(7)		

2.5 – Summary

The synthesis of several new amidinate, guanidinate and phosphaguanidinate complexes of magnesium have been described, including the first examples of magnesium complexes utilising the bicylic guanidinate $[tbo]^-$. The syntheses of the complexes follow straight-forward procedures and, with the exception of **6**, they are all obtained in good yields (60.0 – 84.1 %). The bidentate amidinate and phosphaguanidinate ligands are found to chelate to magnesium while the $[tbo]^-$ ligand is found to bridge between two metal centres in both **3** and **4**. The bromide complex **6** is dimeric in the solid-state resembling the previously known amidinate, guanidinate and phosphaguanidinate compounds **1**, **XXIa**, **XXV** and **XXVI**. In contrast to these halide bridged precursors, the amide and aryloxide complexes **1**, **2** and **7**, generated from the metathesis reactions of **1** and **6** with the appropriate lithium salt, are monomeric in the solid-state, analogous to the magnesium phosphaguanidinates **XXVII** and **XXVIII**.

2.6 – Experimental Procedures for Chapter 2

General Information

MgMeBr solution was purchased from Sigma Aldrich and transferred in to ampoules under N_2 before use. $LiN\{SiMe_3\}_2$ and *N,N*-dicyclohexylcarbodiimide were also purchased from Sigma Aldrich and were used without any further purification following being transferred into the glovebox.

Mg(mes)Br solution was made from the reaction of 2-bromomesitylene with magnesium turnings in ether. $Cy_2PC\{NCyH\}\{NCy\}$[78] and tbo-H[79] were synthesised following literature procedures while LiO-2,6-$^tBu_2C_6H_3$ was isolated following the addition of 1 equivalent of Li^{n}Bu to 2,6-di-*tert*-butylphenol in hexane.

For all other general experimental procedure see Appendix A.

Synthesis of Mg(mesC{NCy}$_2$)(N{SiMe$_3$}$_2$)(thf) (1)

A 0.6 M solution of Mg(mes)Br (6.1 mL, 3.7 mmol, 1 equiv.) in thf was added to a stirring solution of *N,N*-dicyclohexylcarbodiimide (0.760 g, 3.7 mmol, 1 equiv.) in thf at ambient temperature. The resultant solution was left to stir for 18 h before the addition of a thf solution of $LiN(SiMe_3)_2$ (0.619 g, 3.7 mmol, 1 equiv.). Stirring for a further 16 h at ambient temperature followed by removal of volatiles *in vacuo* afforded a white solid. Extraction of the product in hot hexane with slow cooling to ambient temperature yielded colourless crystals of **1**. Further crops of crystal of **1** were obtained after concentration of the mother liquor and storage at -20 °C. Yield = 2.0 g, 82.2 %

Anal. Calcd. for $C_{32}H_{59}N_3OSi_2Mg$ (582.31): C, 66.00%; H, 10.21%; N, 7.22%. **Found:** C, 65.89%; H, 10.16%; N, 7.11%

^{1}H NMR (500 MHz, D_6-benzene)**:** δ 6.79 (s, 2H, m-H, mesityl C*H*), 3.83 (m, 4H, THF), 2.68 (m, 2H, Cy *α-H*), 2.34 (s, 6H, mesityl *o*-CH_3), 2.10 (s, 3H, mesityl *p*-CH_3), 1.33 (m, 4H, THF), 0.51 (s, 18H, Si(CH_3)$_3$)

^{13}C {^{1}H} NMR (125 MHz, D_6-benzene): δ 175.4 (*C*N_2), 137.3 (*C*), 134.5 (*C*), 133.9 (*C*), 128.8 (*C*H), 69.3 (thf *C*H_2), 56.1 (Cy *α*-*C*H), 38.2 (Cy *C*H_2), 26.6 (2 × overlapping Cy *C*H_2), 25.5 (thf *C*H_2), 21.5 (mesityl *p*-*C*H_3), 21.0 (mesityl *o*-*C*H_3), 6.97 (Si(*C*H_3)$_3$)

Synthesis of Mg(mesC{NCy}$_2$)(O-2,6-^{t}Bu$_2$C$_6$H$_3$)(thf) (2)

Compound **2** was synthesised using the same procedure used to make **1** using Mg(mes)Br (11.0 ml, 6.6 mmol, 1 equiv.), *N,N*-dicyclohexylcarbodiimide (1.36 g, 6.6 mmol, 1 equiv.) and LiO-2,6-^{t}Bu$_2$C$_6$H$_3$ (1.40 g, 6.6 mmol, 1 equiv.). Yield: 2.91 g, 70.3 %.

NMR spectra was in full agreement with the previously recorded data.[35]

^{1}H NMR (400 MHz, D_6-benzene): δ 7.51 (d, $^3J_{HH}$ = 7.6, 2H, Ar *m*-C*H*), 6.90 (t, $^3J_{HH}$ = 7.6, 1H, Ar *p*-C*H*), 6.80 (s, 2H, C$_6$*H$_2$*), 3.71 (br m, 4H, thf C*H$_2$*), 2.71 (m, 2H, Cy *α*-C*H*), 2.31 (s, 6H, *o*-C*H$_3$*), 2.10 (s, 3H, *p*-C*H$_3$*), 1.79 (s, 18H, C(C*H$_3$*)$_3$), 1.74-1.41 (m, 20H, Cy-C*H$_2$*), 1.23 (m, thf C*H$_2$*).

^{13}C {^{1}H} NMR (100 MHz, D_6-benzene): δ 175.8 (*C*N_2), 163.8 (Ar *i*-*C*), 138.1 (*C$_6$*H$_2$), 137.5 (Ar *o*-*C*), 134.5, 133.6, 128.9 (*C$_6$*H$_2$), 125.5, 114.41 (C$_6$*H$_3$*), 69.9 (thf *C*H_2), 55.9 (Cy *α*-*C*H), 38.2 (Cy-*C*H_2), 36.0 (*C*(CH_3)$_3$), 32.1 (C(*C*H_3)$_3$), 26.6, 26.5 (Cy-*C*H_2), 25.4 (thf *C*H_2), 21.5 (*p*-*C*H_3), 21.0 (*o*-*C*H_3)

Synthesis of Mg(tbo)Br(thf)$_n$ (3)

A 3 M solution of MgMeBr (1.6 ml, 4.8 mmol, 1.04 equiv.) was added to a stirring solution of 1,4,6-triazabicyclo[3.3.0]oct-4-ene (Htbo) (0.511 g, 4.6 mmol, 1 equiv.) at ambient temperature. Gas evolved on addition and a small amount of a white precipitate formed within 15 min. After stirring for 4 h the solution was concentrated, gently heated to ~65 °C and filtered. Slow cooling to ambient temperature yielded colourless crystals of **3**. Yield = 0.93 g, 60.0 %.

Anal. Calcd. for $C_9H_{16}N_3OMgBr$ (n = 1; 286.45): C, 37.61%; H, 5.61%; N, 14.62%. **Found:** C, 37.65%; H, 5.56%; N, 14.42%.

^{1}H NMR (500MHz, D_6-benzene)**:** δ 3.80-3.65 (m, 10H, tbo-CH_2 + thf), 2.70 (m, 8H, tbo-CH_2), 1.40 (m, 6H, thf)

^{13}C {^{1}H} NMR (125MHz, D_6-benzene)**:** δ *, 68.7 (thf), 54.5 (br, tbo-CH$_2$), 50.5 (br, tbo-CH$_2$), 26.0 (thf)

*resonance for CN$_3$ not observed

Synthesis of Mg(tbo){N(SiMe$_3$)$_2$}(thf) (4)

A 3 M solution of MgMeBr (1.3 ml, 3.9 mmol, 1.03 equiv.) was added to a stirring solution of 1,4,6-triazabicyclo[3.3.0]oct-4-ene (Htbo) (0.420 g, 3.8 mmol, 1 equiv.) at ambient temperature. Gas evolved on addition and a small amount of a white precipitate formed within 15 min. The resultant solution was left to stir for 4 h before the addition of a thf solution of LiN(SiMe$_3$)$_2$ (0.632 g, 3.8 mmol, 1 equiv.). The resultant solution was left to stir at ambient temperature for 20 h followed by the removal of volitiles *in vacuo* leaving a white solid. Extraction of the product in hot hexane with slow cooling to ambient temperature yielded colourless crystals of **4**. Yield 1.00 g, 72.0 %.

Anal. Calcd. for $C_{15}H_{34}N_4OSi_2Mg$ (366.93): C, 49.10%; H, 9.34%; N, 15.27%. **Found:** C, 49.05%; H, 9.35 %; N, 15.26%.

^{1}H NMR (500 MHz, D_6-benzene): δ 3.93 (t, $^{3}J_{HH}$ = 7.7Hz, 4H, tbo-CH_2), 3.75 (m, 4H, thf), 2.63 (t, $^{3}J_{HH}$ = 7.7Hz, 4H, tbo-CH_2), 1.45 (m, 4H, thf), 0.37 (s, 18H, Si(CH_3)$_3$)

^{13}C {^{1}H} NMR (125 MHz, D_6-benzene): δ 180.6 (CN$_3$), 69.6 (thf), 56.1 and 50.7 (tbo-CH$_2$), 25.6 (thf), 6.5 (Si(CH$_3$)$_3$)

Synthesis of MgBr{Cy$_2$PC(NCy)$_2$}(Et$_2$O) (6)

A 3 M solution of MgMeBr in Et_2O (0.25 ml, 0.75 mmol, 1.2 equiv.) was added to a stirring Et_2O solution of *P,P,N,N'*-tetrakis(cyclohexyl)phosphaguanidine (250 mg, 0.62 mmol, 1 equiv.) at ambient temperature and the resultant solution left to stir for 3 h, by which time a white precipitate had formed. The solution was warmed gently to dissolve the precipitate and a

small number of colourless crystals of **6** were obtained after storage at 5 °C for 3 days. Yield = 35 mg, 9.7 %.

Anal. Calcd. for $C_{29}H_{54}N_2OPBrMg$ (581.9): C, 59.85 %; H, 9.35 %; N, 4.81 %. **Found:** C, 59.71 %; H, 9.57 %; N,42.72 %.

Synthesis of Mg(Cy$_2$PC{NCy}$_2$)(N{SiMe$_3$}$_2$)(thf) (7)

A 3 M solution of MgMeBr in Et_2O (0.6 ml, 1.8 mmol, 1 equiv.) was added to a stirring thf solution of *P,P,N,N'*-tetra(cyclohexyl)phosphaguanidine (730 mg, 1.8 mmol, 1 equiv.) at ambient temperature. The resultant solution was left to stir for 5 h before the addition of a thf solution of $LiN(SiMe_3)_2$ (300 mg, 1.8 mmol, 1 equiv.) and was then left to stir for an additional 18 h.

The removal of volatiles *in vacuo* gave a white solid from which the product was extracted in hot hexane. Slow cooling of the hot hexane solution yielded colourless crystals of **7**. Yield = 1.0 g, 84.1 %.

Anal. Calcd. for $C_{35}H_{70}N_3OSi_2PMg$ (660.4): C, 63.65 %; H, 10.68 %; N, 6.36 %. **Found:** C, 63.51 %; H, 10.53 %; N, 6.26 %.

^{1}H NMR (400 MHz, D_6-benzene): δ 3.71 (m, 4H, thf CH_2), 2.30 (m, 2H, *P*-Cy *α*-C*H*), 2.11-1.11 (m, 42H, *P*- and *N*-Cy), 1.27 (m, 4H, thf C*H*$_2$), 0.46 (s, 18H, Si*Me*$_3$)

^{13}C {^{1}H} NMR (100 MHz, D_6-benzene): δ 174.8 (d, $^1J_{CP}$ = 49.7 Hz, *C*PN_2), 68.7 (s, thf *C*H_2), 38.0 (br), 36.0 (d, $^2J_{CP}$ = 17.8 Hz, *P*-Cy *α*-*C*H), 33.5 (d, J_{CP} = 22.7 Hz, *P*-Cy *C*H_2), 32.0 (d, J_{CP} = 12.4 Hz, *P*-Cy *C*H_2), 27.4 (d, J_{CP} = 20.7 Hz, *P*-Cy *C*H_2), 27.4 (s, *N*-Cy *C*H_2), 26.6 (s, *N*-Cy *C*H_2), 26.5 (s, *N*-Cy *C*H_2), 25.2 (s, thf *C*H_2), 6.6 (s, Si*Me*$_3$)

^{31}P {^{1}H} NMR (161 MHz, D_6-benzene): δ -8.3

Chapter 3: Magnesium Amidinates, Guanidinates and Phosphguanidinates as Pre-catalysts for the Tischenko Reaction

It has been known for over a century that aldehydes can be converted to esters in the presence of a suitable catalyst (Scheme 3.1). This transformation was first reported by Claisen who, while investigating the related Cannizzaro reaction, discovered that benzaldehyde would dimerise in the presence of sodium alkoxides to give benzyl benzoate.[80] Nearly two decades later Tischenko, after whom the reaction has been named, found that aluminium alkoxides were superior catalysts converting enolisable and aliphatic aldehydes into their corresponding esters in addition to non-enolisable, aromatic aldehydes such as benzaldehyde.

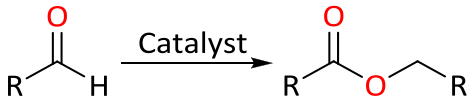

Scheme 3.1 – The Tischenko reaction

Since Tischenko's discovery, aluminium alkoxides have remained the most widely used catalysts for the Tischenko reaction. In the early to mid 20th century, a considerable body of work was performed investigating both the scope and mechanistic details of the reaction. For example, in the 1920s Child and Adkins examined the effects of solvent, different alkoxides catalysts and the addition of transition metal halide salts as co-catalysts.[81,82] The $Al(OEt)_3$ catalysed Tischenko esterification of acetaldehdye was studied in chlorinated, aromatic and alkyl solvents. It was noted that, while the reaction would almost reach completion (yield = 98

%) in 8 h when performed in tetrachloromethane, the same reaction in chloroform reached only 48 % yield in this time. Reactions performed in benzene or xylenes reached a similar yield of 49 % in 8 h while a 71 % yield was obtained after 8 h in heptanes. $Al(O^iPr)_3$ and $Al(OBu)_3$ were both found to be more active catalysts than $Al(OEt)_3$ for the esterification of acetaldehyde in xylenes, reaching yields of 97 % and 95 % in 24 h respectively compared to the 65 % obtained using $Al(OEt)_3$. Perhaps the most important result in terms of future industrial applications was the discovery that the rate of reaction could be increased by using various transition metal chloride salts as promoters. It was found that $ZnCl_2$ gave the most rapid promotion and later this salt would be utilised in the industrial scale production of ethyl acetate (*vide infra*).

It was hypothesised by Lin and Day that the reaction proceeded *via* a mechanism in which the aluminium alkoxide acted as a Lewis acid catalyst, with the carbonyl group of an aldehyde molecule attacking the activated carbonyl carbon of a coordinated aldehyde with the ester generated *via* an intermolecular hydride shift (Scheme 3.2).[83]

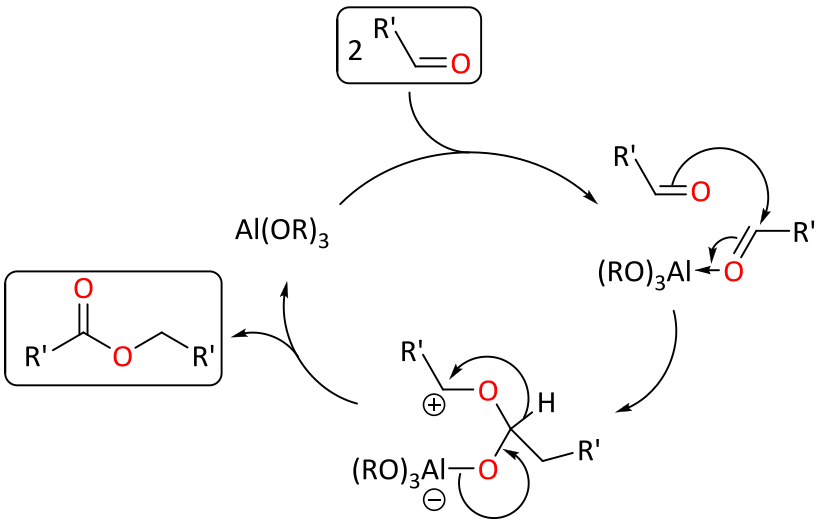

Scheme 3.2 – Lin and Day's proposed mechanism

Ogata *et al*. found that the mixed ester, isopropylacetate (**A**), was formed as well as the expected ester, ethyl acetate (**B**), when using aluminium triisopropoxide to catalyse the esterification of acetaldehyde (Scheme 3.3) After performing a number of experiments to rule out transesterification, they suggested a new mechanism involving transfer of an alkoxide ligand to the aldehyde, forming a new alkoxide (**C**), in their case an ethoxide, following a hydride shift to a second molecule of aldehdye. It is this new alkoxide which reacts to generate homoester **B**. This proposed mechanism became the generally accepted mechanism for the aluminium alkoxide catalysed Tischenko reaction.[84]

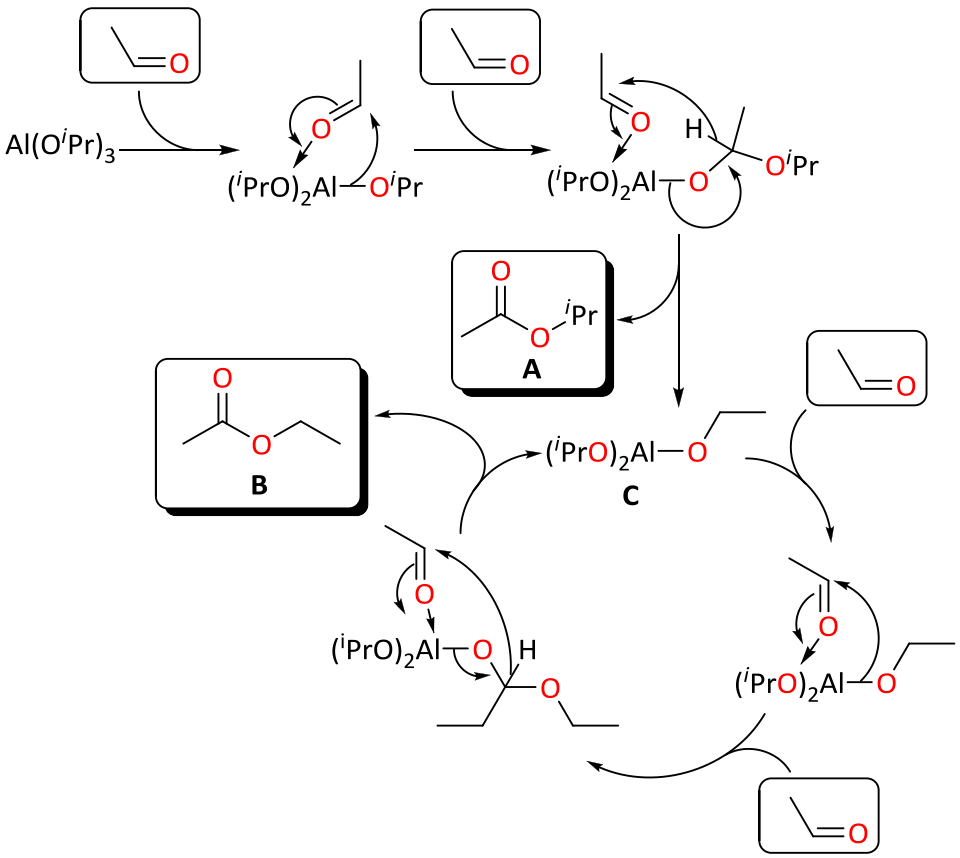

Scheme 3.3 – Ogata *et al.*'s proposed mechanism

The Tischenko reaction has become an industrially important reaction for the production of ethyl acetate, especially in countries where acetaldehyde is available in sufficient quantities or

ethanol supplies are scarce or expensive making the esterification of ethanol with ethanoic acid a less commercially viable process.[85] The catalyst system used is a solution of aluminium ethoxide in ethanol/ethyl acetate with a $ZnCl_2$ co-catalyst. The exothermic reaction is maintained at a temperature between 0-5 °C to inhibit side reactions such as aldol condensations.[86] An industrial process was first developed and put into operation at the Hoechst plant near Frankfurt under licence from the Consortium für Elektrochemie and Wacker-Chemie in 1931.[87]

Since the 1970s, many other compounds have been found to be catalytically active for the Tischenko reaction with examples of main group, transition metal, lanthanide and actinide complexes being reported. With a few notable exceptions, transition metal catalysts have generally performed poorly. Recently a rhodium (III) hydride complex bearing a tripodal phosphinoborate ligand, $Rh(PhB\{CH_2CH_2PPh_2\}_3)(H)_2(NCMe)$, was reported to have exceptional activities for the esterification of a number of aromatic and aliphatic aldehydes.[88] Although highly active, the esterification of aromatic aldehydes using this rhodium catalyst was required to be performed under an atmosphere of H_2.

Ogoshi *et al*. have recently shown that $Ni(COD)_2$/*N*-heterocyclic carbene (NHC) systems can also be used for the symmetric esterification of aldehdyes.[89] In comparison to other catalysts, the $Ni(COD)_2$/NHC systems perform poorly due to the elevated temperature (60 °C) required for efficient conversion. They do however excel in the mixed Tischenko reaction generating cross-coupled esters,[90] an area that remains relatively unexplored.

Lanthanide complexes have received a lot of attention as catalysts for the Tischenko reaction over the last 10-15 years, in part due to their inherent Lewis acidity and their successful application to numerous other catalytic processes. Most notable of these are the homoleptic lanthanide amides, $Ln(N\{SiMe_3\}_2)_3$ (Ln = La or Sm),[91,92] and lanthanum formamidinates, $La\{HC(NR)_2\}_3(thf)_x$ (R = *o*-tolyl, 2,6-dimethylphenyl or 2,6-diethylphenyl.[93] Both classes of

catalysts were shown to convert a number of different aromatic and aliphatic aldehydes to their corresponding esters, with the formamidinate complex La{HC(N-*o*-tolyl)$_2$}$_3$(thf)$_2$ showing particularly impressive activities with a number of substrates.

Recent work by Eisen *et al.* has demonstrated the catalytic activity of some thorium complexes; ThCp$^*_2$Me$_2$, Th(NEtMe)$_4$ and Th(Me$_2$SiCp″$_2$)(C$_4$H$_9$)$_2$.[94,95] The activities of these complexes are varied, with ThCp$^*_2$Me$_2$ and Th(NEtMe)$_4$ giving only 65 % and 85 % conversions of benzaldehyde to benzylbenzoate in 48 h and Th(Me$_2$SiCp″$_2$)(C$_4$H$_9$)$_2$ giving a 96 % yield in 24 h. The studies by Eisen *et al.* also include a detailed kinetic study showing the reaction to be first order with respect to both catalyst and substrate and that the reaction procedes by a mechanism resembling that proposed by Ogata et al (*vide supra*).

Apart from aluminium alkoxides, catalysts based around main group elements are scarce. The only other group 13 catalyst reported is boric acid. However, practical utility is unlikely as harsh reaction conditions are required (temperatures above 200 °C) and the yields of ester are low (34 % conversion of benzaldehyde to benzyl benzoate).[34] The heavy alkaline earth metal amides M(N{SiMe$_3$}$_2$)$_2$(thf)$_n$ (M = Ca, Sr, Ba) were all found to be effective catalysts for the esterification of aromatic, heteroaromatic, and aliphatic aldehydes.[96]

The only examples of homogeneous magnesium based catalytic systems are *in situ* generated bromomagnesium thiolates, formed from the reaction of MgPhBr with thiols.[97] Although these systems catalyse the Tischenko reaction, elevated temperatures and long reaction times are required for high yields to be obtained. These systems were also investigated as catalyst for generating cross-coupled, mixed esters from the reaction of aldehydes with trifluoromethyl ketones with promising results despite slow reaction times (24-67 h). MgO was shown to be an active heterogeneous catalyst for the Tischenko reaction and has been demonstrated to be able to generate both homo- and mixed-esters.[98,99]

Previous work within the Coles group has shown that monomeric phosphaguanidinate complexes Mg($Ph_2PC\{NCy\}_2$)(O-2,6-$^tBu_2$-4-MeC_6H_2)(thf), Mg($Ph_2PC\{NCy\}_2$)($N\{SiMe_3\}_2$)(thf) (Figure 1.15; **XXVII** and **XXVIII**) and the dimeric guanidinate [Mg(hpp)($N\{SiMe_3\}_2$)]$_2$ (Figure 2.5; **XLVIII**) catalyse the ring opening polymerisation of *rac*-lactide, with the $[hpp]^-$ complex showing impressive reactivity (100 % conversion of 500 equivalents of *rac*-lactide to polylactide within 30 minutes).[39] It was therefore of interest to investigate the potential catalytic activity of amidinate, guanidinate and phosphaguanidinate supported magnesium aryloxides and amides with respect to other transformations involving organic, carbonyl containing substrates.

This chapter investigates the activity of the amide complexes reported in Chapter 2, in addition to the previously reported complexes Mg($mesC\{NCy\}_2$)(O-2,6-$^tBu_2C_6H_3$)(thf) (Figure 2.2; **2**), **XXVIII** and **XLVIII** as pre-catalysts for the Tischenko reaction.

3.1 – Magnesium Bicyclic Guanidinate Compounds as Pre-Catalysts

Compound **4** and the related $[hpp]^-$ complex **XLVIII** (Figure 3.1) were selected for preliminary investigations into the potential of magnesium complexes as catalysts for the Tischenko reaction.

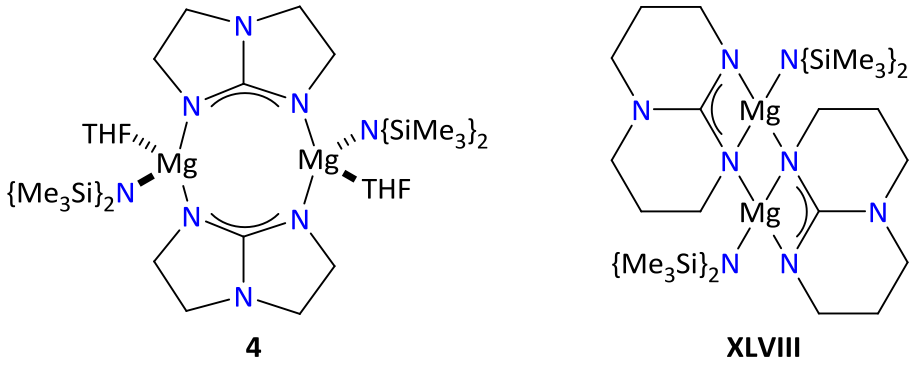

Figure 3.1 – $[Mg(tbo)(N\{SiMe_3\}_2)(thf)]_2$ (**4**) and $[Mg(hpp)(N\{SiMe_3\}_2)]_2$ (**XLVIII**)

Initial catalytic testing was performed on an NMR scale in D_6-benzene using 1,4-dimethoxybenzene as the internal standard and benzaldehyde as the substrate (Scheme 3.4). The progress of the reaction was monitored by ^1H NMR spectroscopy, with spectra typically taken at 20 s intervals for the first hour, and then at 60 s intervals until completion of the experiment. The temperature of reaction was maintained at 30 °C in the NMR probe. The yield of benzyl benzoate was calculated from the values of the integrals of the methylene protons of the ester relative to the 1,4-dimethoxybenzene resonances. Full experimental details are given in Section 3.6.

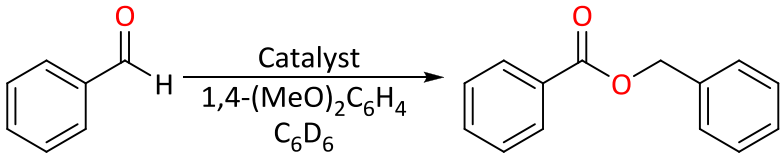

Scheme 3.4 – Catalytic testing of the conversion of benzaldehyde to benzyl benzoate

The results of the reactions using 10 mol % of **4** and **XLVIII** are represented graphically in Figure 3.2. In both cases, benzylbenzoate is generated immediately, with **4** and **XLVIII** producing yields of 38 % and 33 %, respectively, after 5 min. The production of benzylbenzoate by **XLVIII** is likely to be hindered by its poor solubility in benzene, meaning that there will be a small induction time during which the catalyst is activated (*vide infra*). After 5 min, the rates of ester production begin to decrease with 50 % yields achieved by both catalysts after approximately 15 min. After 60 min both rates have decreased significantly with yields of 58 % and 64 % produced by **4** and **XLVIII**, respectively. This reduction in the rate of product formation is attributed to mass transport effects as the substrate is consumed within the sample tube and competitive binding with thf at high conversions/low concentrations of aldehyde for **4**.

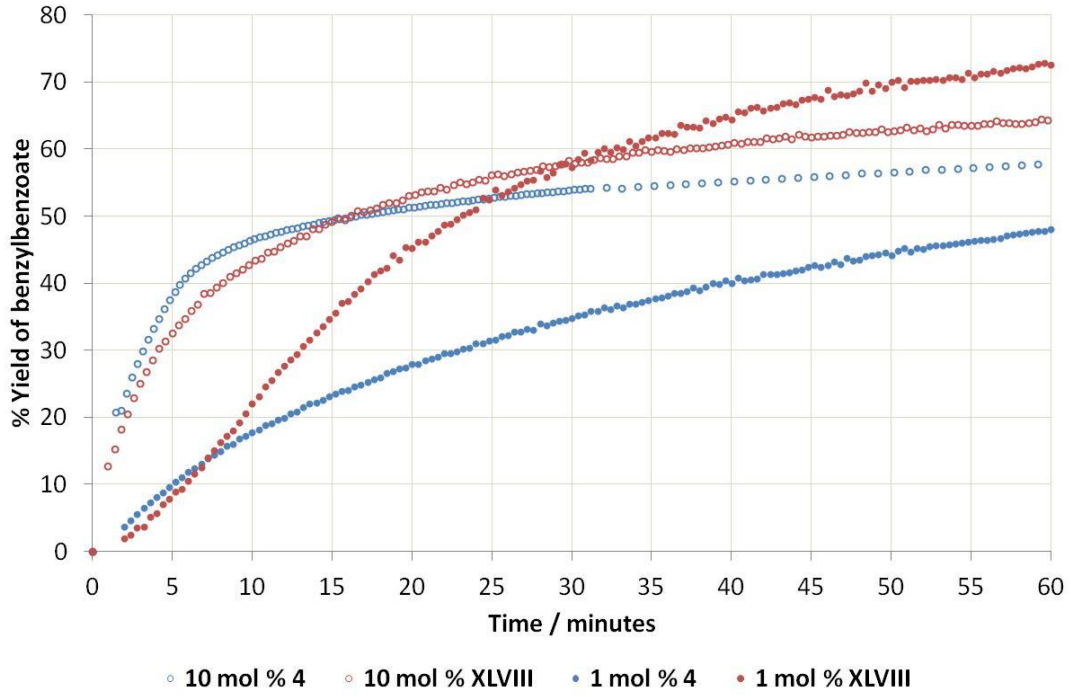

Figure 3.2 – Plot of % yields of benzylbenzoate vs. time for experiments using 10 mol % **4**, 1 mol % **4**, 10 mol % **XLVIII** and 1 mol % **XLVIII**. Values calculated from NMR integrals relative to 1,4-dimethoxybenzene internal standard, monitored for 60 min

The reactions were repeated using a catalyst loading of 1 mol %; the results are also shown in Figure 3.2. The lower catalyst concentration resulted in less than 10 % yield after 5 min. At this point in the experiment, the rate of ester formation with **4** slowly begins to decrease, until after 60 min the yield of benzylbenzoate is 48 %. NMR analysis of the reaction after 24 h showed approximately 90 % yield of benzylbenzoate, indicating that slow conversion continues beyond the initial 60 min.

During the first 5 min the rate of production of benzylbenzoate using 1 mol % of **XLVIII** increases, which is likely due to the conversion of **XLVIII** to soluble, active compounds as the reaction proceeds. A steady rate of ester formation is then reached which is maintained for the next 15 min before beginning to slow, producing an overall yield of 45 % after 20 min. After 60 min a yield of 73 % has been reached and > 90 % conversion is reached after 4 h.

After the reactions with 1 mol% catalyst loading had reached completion (*i.e.* no further production of ester detected by NMR integration and minimal concentrations of benzaldehyde were detected by NMR) an additional 100 equivalents of benzaldehyde were added. The consumption of aldehyde and production of ester immediately re-commenced. The results of this experiment using compound **XLVIII** are displayed in Figure 3.3. A similar rate of conversion for the first 10 min after addition of the second portion of benzaldehyde compared to the rate of the first 100 equivalents is noted. This suggesting the presence of the ester product does not hinder the catalysis and that the observed decrease in the rate of production over time in these experiments is due to the reduction in the relative concentration of benzaldehyde. After 10 min the rate of ester formation begins to slow and after 60 min the yield of benzyl benzoate is 60 %, 13 % less than the yield obtained from the first 100 equivalents after 60 min (Figure 3.3). These data suggest that the catalytic species does not decompose in solution upon consumption of all of the substrate and may be adopting a resting-state.

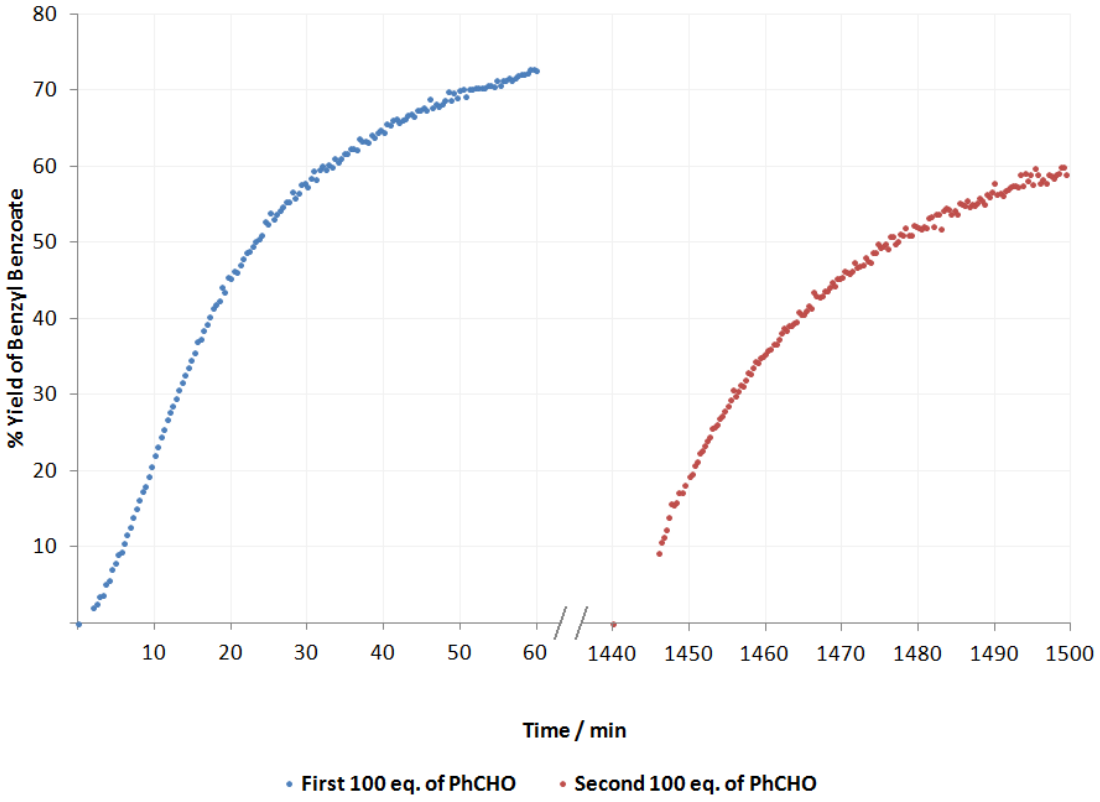

Figure 3.3 – Plot showing the % yield of benzyl benzoate *vs* time from the consecutive addition of 2 x 100 equivalents of benzaldehyde

3.2 – Magnesium Amidinates and Phosphaguanidinates as Pre-Catalysts

The effect of altering the ancillary ligand-set and the Mg-heteroatom bond on the conversion of benzaldehyde to benzyl benzoate was investigated using the amidinate complexes **1** and **2** and the phosphaguanindinate complexes **7** and **XXVIII** (Figure 3.4).

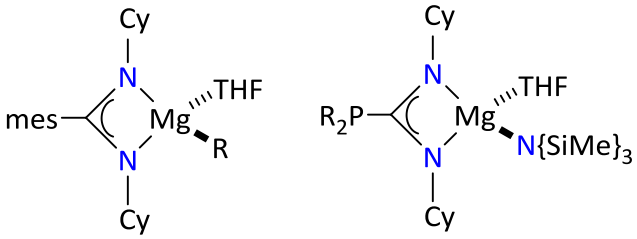

R = $N\{SiMe_3\}_2$ **1**
R = O-2,6-$^tBu_2C_6H_3$ **2**

R = Cy **7**
R = Ph **XXVIII**

Figure 3.4 – $Mg(mesC\{NCy\}_2)(N\{SiMe_3\}_2)(thf)$ (**1**), $Mg(mesC\{NCy\}_2)(O\text{-}2,6\text{-}^tBu_2C_6H_3)(thf)$ (**2**), $Mg(Cy_2PC\{NCy\}_2)(N\{SiMe_3\}_2)(thf)$ (**7**) and $Mg(Ph_2PC\{NCy\}_2)(N\{SiMe_3\}_2)(thf)$ (**XXVIII**)

These experiments were performed using the same conditions as those described in Section 3.2.1 for **4** and **XLVIII**, using a catalyst loading of 1 mol %; the results are displayed in Figure 3.5. Comparing the results of amides **1**, **7** and **XXVIII** with those of **4** and **XLVIII** above, it is apparent that the initial rates of conversion are strongly affected by changing the chelating ligand, with all rates of ester formation increasing. The phosphaguanidinate complex **XXVIII** has the highest rate of conversion followed by **7** then **1**. In the first 10 min **1**, **7**, and **XXVIII** produce 37 %, 46 % and 60 % yields of benzyl benzoate respectively.

After 10 min, the rates of ester production by the phosphaguanidinate catalysts **7** and **XXVIII** have started to decrease and after 30 min yields of 60 % and 70 % are obtained, respectively. Amidinate compound **1** has produced a yield of 65 % of benzyl benzoate after this time, although it is noted that the rate of production has also begun to decrease.

Over the next 30 min the reactions using **7** and **XXVIII** only produce minor amounts of product (4-5 %), giving overall yields of 65 % and 74 %, respectively. The reaction using **1** continues at a steady rate over this time period to produce a final yield of 74 % after 60 min.

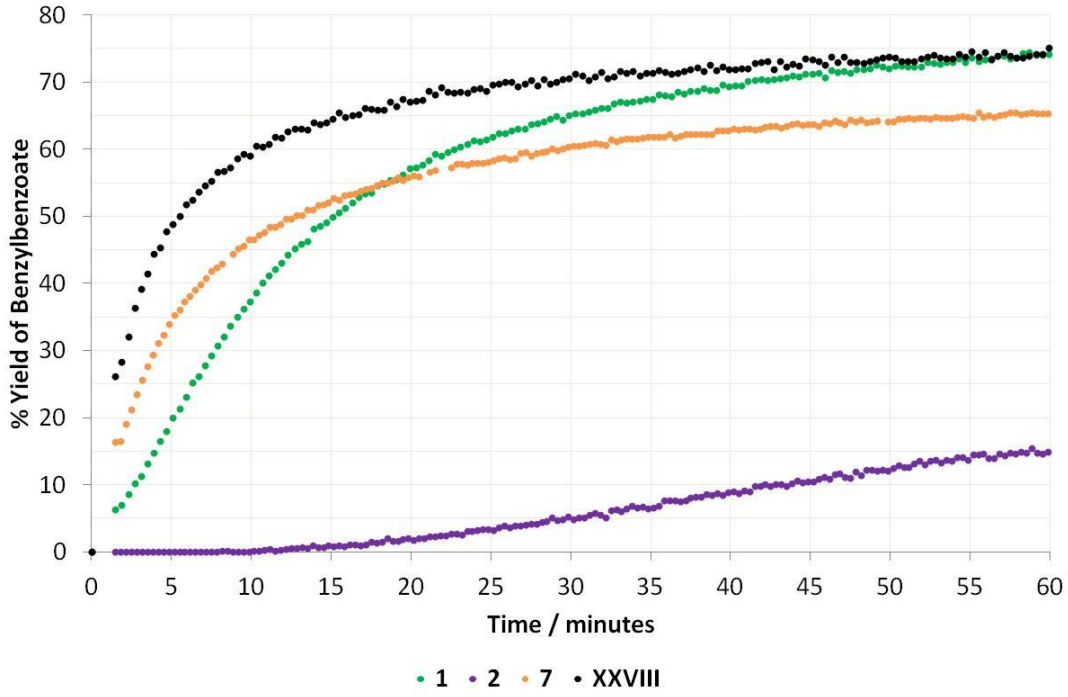

Figure 3.5 – Plot of % yields of benzylbenzoate vs. time for experiments using 1 mol % of **1**, **2**, **7** and **XXVIII**. Values calculated from NMR integrals relative to 1,4-dimethoxybenzene internal standard, monitored for 60 min

Compound **1** was also shown to convert benzaldehyde to benzyl benzoate under solvent free conditions. This reaction was performed by adding 0.1 mol % of **1** to a stirring sample of benzaldehyde (9.1 mmol), resulting in an exothermic reaction. A 24 mg sample of the reaction mixture was taken after 24 h and added to 0.5 mL of a 0.11 M solution of 1,4-dimethoxybenzene in D_6-benzene. Immediate analysis by ^{1}H NMR spectroscopy showed that a 98 % yield of benzyl benzoate had been reached.

The catalytic profile of the aryloxide **2** is markedly different to that of the amides examined. Detectable amounts of ester are only observed after 10 min (Figure 3.5), representing a very low rate of product formation. Once initiated, the production of benzyl benzoate by **2** continues slowly, with a 5 % yield of ester after 30 min and only 15 % after 60 min. Figure 3.6 shows the progress of the reaction of **2** over 18 hrs. After the first 60 min the rate begins to slow, producing only a further 10 % yield of ester in the next 60 min and another 5 % in the subsequent 60 min. The rate continues to slowly decrease and a yield of just over 50 % is reached after 18 h (Figure 3.6). The poor rate of reaction of **2** is thought to be due to the activation of the catalyst being slowed by the bulky aryloxide hindering association of the aldehyde substrate to the magnesium centre.

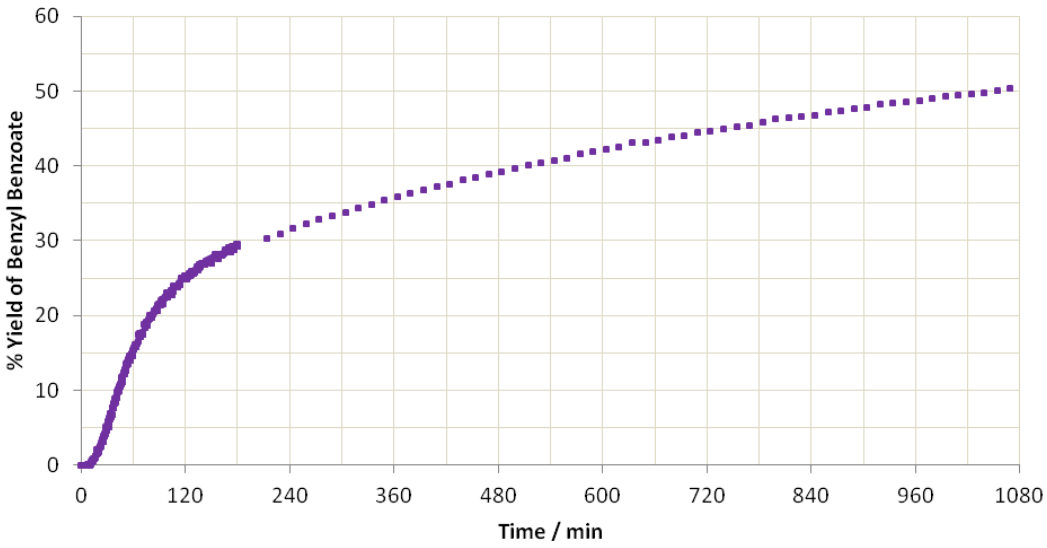

Figure 3.6 – Plot of % yields of benzylbenzoate vs. Time using 1 mol % of **2**. Values calculated from NMR integrals relative to 1,4-dimethoxybenzene internal standard, monitored for 18 h

3.3 – Preliminary Mechanistic Studies

The rate of consumption of benzaldehdye was examined in an attempt to gain some preliminary kinetic insights that may shed light on the mechanism by which the pre-catalysts react. This examination proved inconclusive (see Appendix B).

It was hypothesised that the magnesium catalysed Tischenko reaction would proceed *via* a similar mechanism to that described by Ogata *et al*. for aluminium alkoxide catalysts and Eisen *et al.* for their thorium systems, illustrated in Scheme 3.5 for the magnesium-amide catalysed process. If this pathway was operating, *N*,*N*-bis(trimethylsilyl)benzamide would be formed as a by-product upon activation of the pre-catalyst. To probe this, 2 equivalents of benzaldehyde were added to NMR samples of **1** and **7** in C_6D_6 and the resultant solutions were analysed by GC-MS.

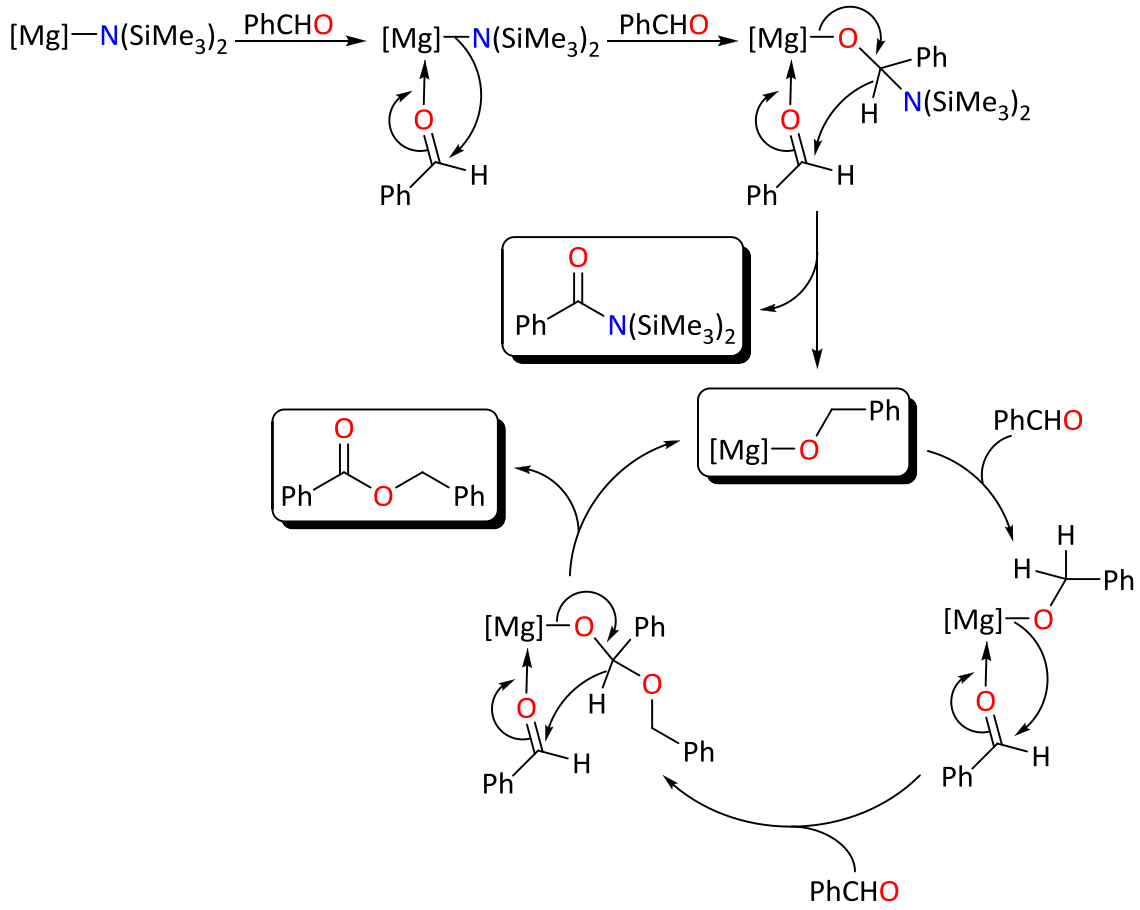

Scheme 3.5 – Proposed mechanism for the magnesium-amide catalysed Tischenko reaction

The gas chromatograph from the reaction with **1** shows six organic species, identified by comparison of known mass spectra (using the NIST Mass Spectral Search Program) as benzaldehyde, benzylalcohol, benzyl trimethylsilylether, *N,N*-bis(trimethylsilyl)benzamide, *N*-(trimethylsilyl)benzamide and benzyl benzoate (Figure 3.6a). The same products were observed in the chromatograph from the reaction with **7**; in addition the presence of dicyclohexylphosphine and DCC is noted (Figure 3.6b). As no dicyclohexylphosphine is observed in the ^{31}P NMR spectrum prior to the preparation of the GC-MS sample (δ_P of $PHCy_2$ in D_6-benzene = -27.4 ppm)[100] we conclude that its presence, along with that of DCC, are due to hydrolysis of the phosphaguanidinate ligand after exposure to air during the preparation of

the GCMS sample. Facile cleavage of the P-C bond of the *P*-diphenyl phosphaguanidine $Ph_2PC(NCy)(NHCy)$ has recently been shown to occur in the presence of water and oxygen.[101]

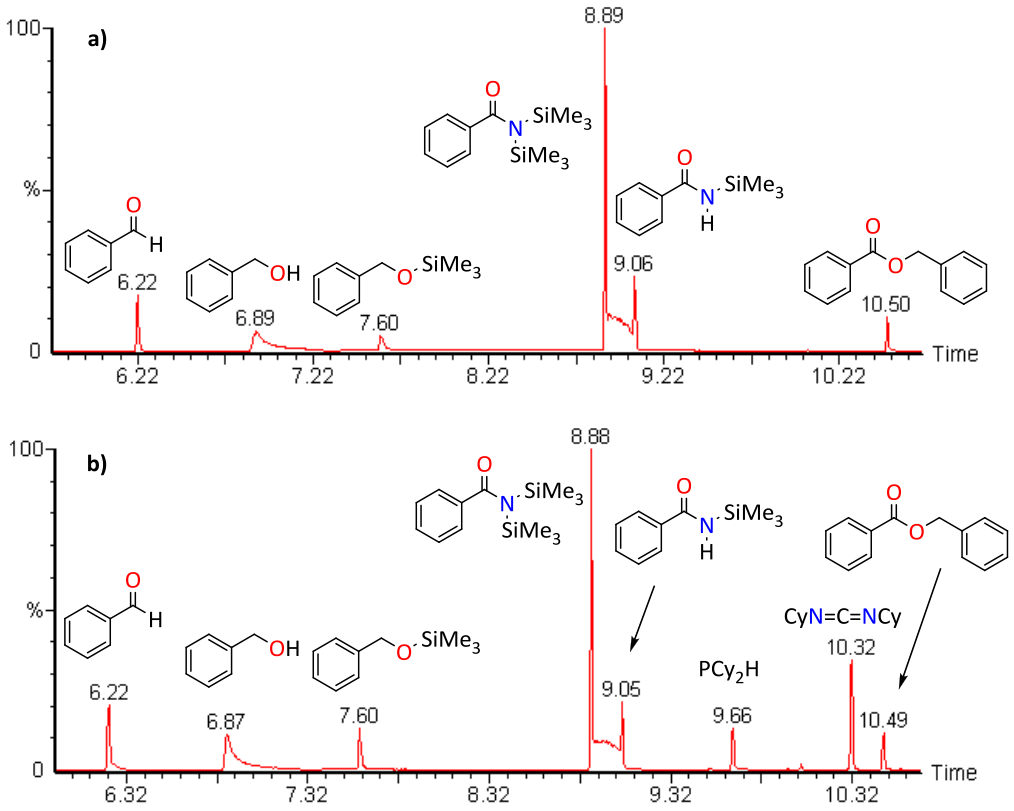

Figure 3.6 – Gas chromatographs from the reactions of 2 equivalents benzaldehdye with a) **1** and b) **7**

The observation of *N,N*-bis(trimethylsilyl)benzamide by GC-MS supports the proposed mechanism outlined in Scheme 3.5. The presence of benzyl trimethylsilyl ether and *N*-(trimethylsilyl)benzamide are likely due to benzyl alcohol reacting with *N,N*-bis(trimethylsilyl)benzamide resulting in the exchange of a silyl group with the alcoholic proton.

Both chromatographs also show the presence of the neutral amidine and phosphaguanidine (regions not shown in Figure 3.6). In a previously reported investigation, the presence of the

neutral pro-ligand, BDI-H, was observed by ^{1}H NMR spectroscopy during the Tischenko reaction catalysed by the β-diketiminate calcium amide [Ca(BDI)(N{SiMe$_3$}$_2$)(thf)] (BDI = [HC{C(Me)NAr^{iPr}}$_2$]$^-$).[96] One of the advantages of the phosphaguanidinate ligands in **7** and **XXVIII** is the presence of a single characteristic peak in the ^{31}P NMR spectrum at δ_P = -28.1 ppm and δ_P = -16.9 ppm,[39] respectively, that provides a method to determine whether a similar loss of ligand occurs with the magnesium catalyst. The ^{31}P NMR spectra of the catalytic reaction mixtures of **7** and **XXVIII** after 24 h show no evidence of the presence of the neutral phosphaguanidines (Ph$_2$PC(NCy)(NHCy) δ_P = -16.9 ppm; Cy$_2$PC(NCy)(NHCy) δ_P = -21.1 and -4.1 ppm for E$_{syn}$ and Z$_{anti}$ isomers resectively)[78,102] implying their presence in the chromatographs is likely due to hydrolysis of magnesium species during GCMS sample preparation. To rule out the possibility of the ligand being lost in the early stages of the reaction and reacting further, 2 equivalents of benzaldehyde were added to NMR samples of **7** and **XXVIII**. Again, the ^{31}P NMR spectra shows no evidence of the presence of the neutral phosphaguanidines.

If the proposed mechanism in Scheme 3.5 is correct, the catalytic species generated upon activation is a benzoxide-containing species. This species would be identical for the reactions of compounds **1** and **2** and should result in both of these reactions displaying similar rates of conversion. However, such a direct comparison cannot be made due to the slow activation of **2.**

3.4 – Scope of Reaction

To probe the scope of reaction, compounds **1** and **XLVIII** were reacted with trimethylacetaldehyde (**A**), cyclohexanecarboxaldehyde (**B**), isobutyraldehyde (**C**) and acetaldehdye (**D**) (Figure 3.6). The experiments were performed under the same conditions used for the catalytic experiments previously described (Section 3.3.1), using 1 mol % of catalyst.[**]

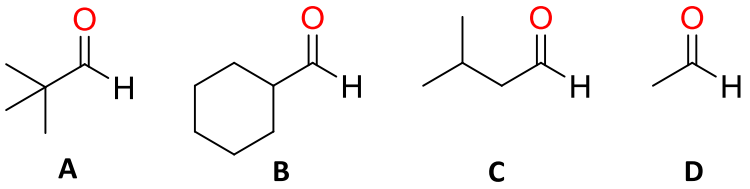

Figure 3.6 – Trimethylacetaldehyde (**A**), cyclohexanecarboxaldehyde (**B**), isobutyraldehyde (**C**) and acetaldehdye (**D**)

Compounds **1** and **XLVIII** both catalyse the production of 2,2-dimethylpropyl 2,2-dimethylpropionate from the dimerisation of trimethylacetaldehyde **A** (Figure 3.7). The reaction with **1** proceeds at a much higher rate than with **XLVIII**, producing an 84 % yield of ester after 60 min compared to the ~55 % yield produced by **XLVIII**. After 180 min, **1** converts nearly all of **A** (<5 % remaining) to the corresponding ester, with a yield of 96 %. During the same time, **XLVIII** only produced a 62 % yield of ester.

[**] Note: due to demand on the NMR instrument by other users, the progress of the reaction was monitored less frequently.

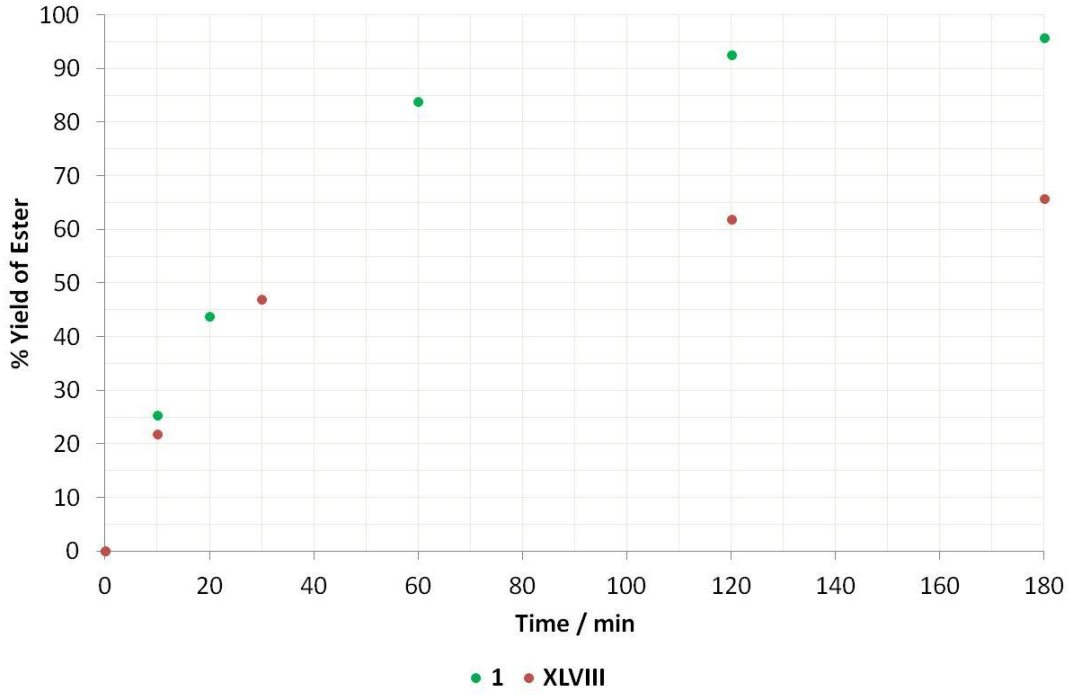

Figure 3.7 – Plot of % yields of 2,2-dimethylpropyl 2,2-dimethylpropionate vs. time for experiments using 1 mol % of **1** and **XLVIII**. Values calculated from NMR integrals relative to 1,4-dimethoxybenzene internal standard, monitored for 3 h

The formation of cyclohexylcyclohexanoate, $CyC(O)OCH_2Cy$, from cyclohexanecarboxaldehyde (**B**) with compound **XLVIII** occurs slightly faster than the reaction with **1** (Figure 3.8). Yields of 52 % and 61 % are obtained after 60 min with **1** and **XLVIII**, respectively; over the next 2 h the yields only increase slightly to 59 % and 64 %. After reacting for 4 h, approximately 18 % of the original quantity of **B** remains for the reaction with compound **1** while <3 % of **B** remains for the reaction with **XLVIII**. These data suggest that **B** is also being consumed in competing reactions, forming as yet unidentified side products.

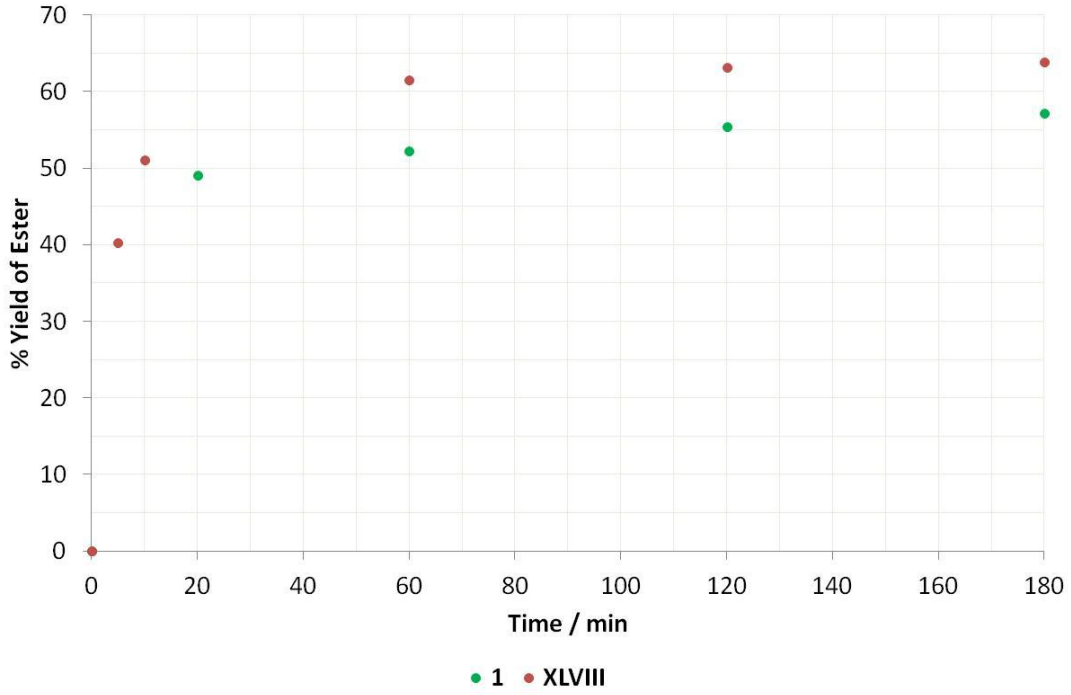

Figure 3.8 – Plot of % yields of cyclohexyl cyclohexanoate vs. time for experiments using 1 mol % of **1** and **XLVIII**. Values calculated from NMR integrals relative to 1,4-dimethoxybenzene internal standard, monitored for 3 h

The reactions of **1** and **XLVIII** with isobutyraldehyde and acetaldehdye produced a complex mixture of products with no evidence of ethyl acetate or isobutyl isobutyrate observed by GC-MS or NMR spectroscopy (no observable peaks in the ^{1}H NMR spectra at δ_H 3.89 ppm[103] and δ_H 3.75 ppm[88] corresponding to the methylene signals of ethyl acetate and isobutyl isobutyrate, respectively). This complex mixture is thought to be due to the basic nature of magnesium amides and the fact that both acetaldehdye and isobutyraldehyde are easily enolisable aldehydes. It is likely therefore that competing aldol reactions, similar to those observed by Henderson *et al.* using $Mg(N\{SiMe_3\}_2)_2$ (Scheme 3.7),[104] are occurring in preference to the desired coupling. It is likely that competing aldol reactions are also responsible for lower than expected yields obtained in the reactions of **1** and **XLVIII** with aldehdye **B**.[††]

[††] Cyclohexanecarboxaldehyde is enolisable due to the presence of a proton on the α-carbon, however this enolisation is slow therefore allowing the Tischenko reaction to take place

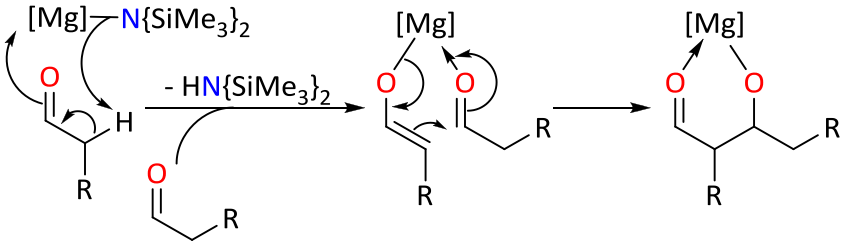

Scheme 3.7 – Aldol reaction promoted by a $Mg(N\{SiMe_3\}_2)_2$

3.5 – Summary and Comparison with Other Recent Catalysts

Magnesium amidinate, guanidinate and phosphaguanidinate complexes represent a new class of catalysts for the Tischenko reaction. Varying degrees of activity are observed using complexes **1**, **2**, **4**, **7**, **XLVIII** and **XXVIII** as pre-catalysts for the esterification of benzaldehyde. Aryl oxide **2** is the least active while the phosphaguanidinate complexes **7** and **5** show rapid formation of the ester under the conditions investigated. Amidinate complex **1** and guanidinate complex **4** may be considered the most impressive pre-catalysts based on rapid initial formation of ester and having the highest conversion after 60 min. Results from GC-MS and NMR spectroscopy suggest the mechanism of the reaction involves the generation of a benzyloxide intermediate, which may be considered the catalytically active species. Unfortunately, attempts to synthesise an analogue of this benzyloxide complex were unsuccessful.

Compounds **1** and **XLVIII** were selected to examine the potential scope of the reaction, demonstrating that these pre-catalysts will catalyse the esterification of aliphatic aldehydes in addition to aromatic aldehydes, but do not promote esterification of easily enolisable aldehydes.

Turn over frequencies (TOFs) can be used to compare the activities of the magnesium complexes with other reported catalysts (Table 3.1). TOFs are a measure of the number of moles of product produced per mole of catalyst per unit of time (usually per hour, h^{-1}). The TOFs for the magnesium compounds tested in this work were calculated at the time taken for 50 % conversion, and after 60 min.

Table 3.1 Comparison of TOFs				
Catalyst	**mol %**	**TOF / h^{-1}**		**Reference**
1	1	199[a]	74[b]	This work
2	1	3[a]	15[b]	This work
4	1	44[a]	35[b]	This work
7	1	234[a]	65[b]	This work
XLVIII	1	129[a]	72[b]	This work
XXVIII	1	545[a]	75[b]	This work
$Rh(PhBP_3)(H)_2(NCMe)$[c]	1	2830		75
$Ni(COD)_2$/IPrCl[d]	2	33[e]		76
$La(N\{SiMe_3\}_2)_3$	1	87		78, 79
$La\{HC(N\text{-}o\text{-}tolyl)_2\}_3(thf)_2$	1	200		80
$Ca(N\{SiMe_3\}_2)(thf)_2$	1	52		81
MgPhBr/$PhCH_2SH$	10	1.4[f]		82
MgPhBr/$PhCH_2SH$	20	4.1[f]		82

[a] TOF at 50 % conversion; [b] TOF after 60 min; [c] $PhBP_3$ = $PhB(CH_2CH_2PPh_2)_3$; [d] IPrCl = 1,3-bis-(2,6-diisopropylphenyl)-4,5-dichloroimidazol-2-ylidene; [e] reaction performed at 60 °C; [f] reaction performed at 65 °C

The TOF values calculated at 50 % conversion and after 60 min differ greatly. For example, at 50 % conversion phosphaguanidinate **XXVIII** has a TOF of 545 h^{-1}, surpassing all reported catalysts for the Tischenko reaction of benzaldehdye, with the exception of the previously mentioned rhodium phosphinoborate complex (TOF 2830 h^{-1}).[88] However, the value calculated for **XXVIII** after 60 min (75 h^{-1}) is much more modest, illustrating that TOFs alone can not be used to grade catalyst and that the reaction profile as a whole should be taken into account. Due to having the fastest rates of ester production after 1 h, we believe that, of the pre-catalysts described here, compounds **1** and **XLVIII** are the most promising.

With the exception of **2**, the trend of a higher TOF after 50 % conversion than after 60 min is observed for all magnesium complexes tested during this study. Although tempting to use the 50 % conversion values for comparative purposes, thereby presenting the magnesium complexes as extemely active catalysts, the values after 60 min give a more realistic representation.

The first direct comparison to make is against Conner *et al.*'s magnesium thiolate systems.[97] The most promising system reported in this study is the 1:1 mixture of MgPhBr and

benzylmercaptan, which has TOFs for the esterification of benzaldehdye of 1.4 h^{-1} and 4.1 h^{-1} with 10 mol % and 20 mol % catalyst loading respectively. Clearly, the amide complexes reported here all have greater activities and have the added advantage that they do not require elevated temperatures (65 °C) for high conversions. The same can be said when comparing the Ni^0/NHC systems reported by Ogoshi *et al.*, where the most active system, $Ni(COD)_2$/IPrCl, has a TOF of 33 h^{-1} using 2 mol % of catalysts at 60 °C.[89]

The TOFs of the magneisum amide complexes compare favourably with the calcium amide catalyst reported by Hill *et al.*, which has a TOF of 52 h^{-1} for the esterification of benzaldehyde.[96] In contrast, $Ca(N\{SiMe_3\}_2)_2(thf)$ is a more active catalyst for the esterification of the aliphatic aldehydes trimethylacetaldehyde and cyclohexanecarboxaldehyde, having TOFs >100 h^{-1} compared to 84 h^{-1} and 52 h^{-1} respectively for **1** and 47 h^{-1} and 61 h^{-1} respectively for **XLVIII**. Under solvent free conditions, 0.1 mol % of compound **1** converted benzaldehyde to benzyl benzoate near quantitatively within 24 h. In comparison 0.1 mol % of $Ca(N\{SiMe_3\}_2)_2(thf)$ was shown to produce only a 63 % yield in 88 h, however it was noted that this may have been due to the catalyst being destroyed by the presence of trace amounts of impurities or water in the benzaldehyde.

While the lanthanum amide complex $La(N\{SiMe_3\}_2)_3$ is only slightly more active (TOF = 87 h^{-1}) for the esterification of benzaldehdye than the most active of the compounds tested in this chapter, the formamidinate $La\{HC(N\text{-}o\text{-}tolyl)_2\}_3(THF)_2$ has a higher TOF of 200 h^{-1}.[91–93] Both these lanthanum catalysts also have extremely impressive TOFs for the esterification of cyclohexanecarboxaldehyde (>1500 h^{-1}). Interestingly, while $La(N\{SiMe_3\}_2)_3$ maintains this high TOF when utilised for the esterification of trimethylacetaldehyde, the TOF observed using $La\{HC(N\text{-}o\text{-}tolyl)_2\}_3(THF)_2$ for this transformation is found to be greatly reduced at a value of 45 h^{-1}, lower than that observed for both **1** and **XLVIII**.

Despite being much less active than the rhodium catalyst of Tejel *et al.*,[88] the magnesium complexes described here have the advantage of being simple to make and the readily availably starting materials are considerably cheaper.

The inability of the magnesium complexes investigated here to convert easily enolisable aldehydes to their corresponding esters is clearly a major drawback; however this investigation highlights the potential usefulness of magnesium complexes in catalysis.

3.6 – Experimental Procedures for Chapter 3

General Information

Benzaldehyde, trimethylacetaldehyde, cyclohexanecarboxaldehyde, isobutyraldehyde and acetaldehyde were purchased from Sigma Aldrich and were distilled and stored in ampoules over molecular sieves in the glovebox before use.

$[Mg(hpp)(N\{SiMe_3\}_2)]_2$ and $Mg(Ph_2PC\{NCy\}_2)(N\{SiMe_3\}_2)(thf)$ were synthesised following literature procedures.[39,38]

For all other general experimental procedure see Appendix A.

General Procedure for the Dimerisation of Benzaldehyde

In an inert atmosphere glovebox, an NMR tube fitted with a J. Young's tap were charged with 1 or 10 mol % of pre-catalyst followed by the addition of 0.5 ml of a D_6-benzene solution of 1,4-dimethoxybenzene (0.11 M). The NMR instrument was locked and shimmed to this sample and an experiment set up to record ^{1}H NMR spectra (1 scan every 30 s) for the duration of the experiment. 0.1 ml of a D_6-benzene solution of benzaldehyde (4.77 M) was then added to the sample, again in the glovebox, and was immediately taken and inserted into the NMR instrument. The experiment was started as soon as the sample was in the probe (maximum time elapsed after mixing = 2 min).

General Procedure for the Dimerisation of Trimethylacetaldehyde, Cyclohexanecarboxaldehyde, Isobutyraldehyde and Acetaldehdye

Similar method to the dimerisation of benzaldehyde using 1 mol % of pre-catalyst and 100 µL of aldehyde.

Solvent Free Dimerisation of benzaldehyde by Compound 1

In an inert atmosphere glovebox, a vial was charged with finely ground **1** (5.3 mg, 0.009 mmol, 1 equiv.) and a magnetic stirrer bar. Benzaldehyde (0.966 g, 9.1 mmol, 1000 equiv.) was added with heat given off immediately. The resultant sample stirred for 24 h before analysis of a 24 mg sample by ^{1}H NMR.

Workup of Raw Data From NMR Experiments

The data was worked up by comparison of integrals of the methylene protons, RC(O)OC$\underline{H_2}$R, of the ester against the aryl or methyl protons of the 1,4-dimethoxybenzene standard. The concentrations of ester in solution were calculated using the following equation:

$$[\text{ester}] = ([\text{standard}] \times I_{\text{ester}} \times n) / I_{\text{standard}}$$

n = 2 if using integrals of the aryl protons of the standard

n = 3 if using integrals of the methyl protons of the standard

Chapter 4: Synthesis and Reactivity of the Phospha-Grignard Reagent Mg(P{SiMe$_3$}$_2$)Br(thf)

4.1 – Introduction

One of the most common synthetic techniques used to introduce a ligand to a metal centre is salt metathesis between the lithium salt of the ligand and a metal halide. This method has generally served organometallic chemists well due to the relative ease of converting many neutral pre-ligands to lithium salts using readily available organolithium reagents such as Li^{n}Bu. There are occasions, however, when lithium salts reduce the metal substrate rather than (or in addition to) serving as a ligand transfer reagent.

Lithium phosphides, LiPR$_2$ (R = H, alkyl, aryl or silyl), can be generated from the reaction of an alkyl lithium reagent with a primary, PRH$_2$, or secondary phosphine, PR$_2$H. In some cases, a tertiary phosphine can be converted to the secondary phosphide anion by reacting with lithium metal, e.g. PPh$_3$. These compounds are useful phosphide transfer agents and are usually generated *in situ*.[105]

An illustrative example of a lithium phosphide reacting as a reducing agent was reported by Lappert *et al*. in 1988.[106] It was noted that 1 or 2 equivalents of the lithium phosphide LiP{SiMe$_3$}$_2$(thf)$_2$ (**XLIX**) react with ZrCp$_2$Cl$_2$ to give the corresponding mono- and bis-phosphides, ZrCp$_2$(P{SiMe$_3$}$_2$)Cl (**L**) and ZrCp$_2$(P{SiMe$_3$}$_2$)$_2$ (**LI**), respectively. However, the same reaction with TiCp$_2$Cl$_2$ gave the reduced Ti^{III} complex TiCp$_2$Cl(thf) (**LII**) (Scheme 4.1). It was also found that phosphide **XLIX** reduced TiCpCl$_3$(thf) and UCp″$_2$Cl$_2$ (Cp″ = 1,3-{SiMe$_3$}$_2$C$_5$H$_3$) to TiCpCl$_2$(thf) (**LIII**) and UCp″$_2$(μ-Cl$_2$)Li(thf)$_2$ (**LIV**), respectively (Scheme 4.1). In such cases where

reduction by the lithium salt presents a problem, Grignard reagents, RMgX (R = ligand and X = halide), may be investigated as an alternatives reagent.

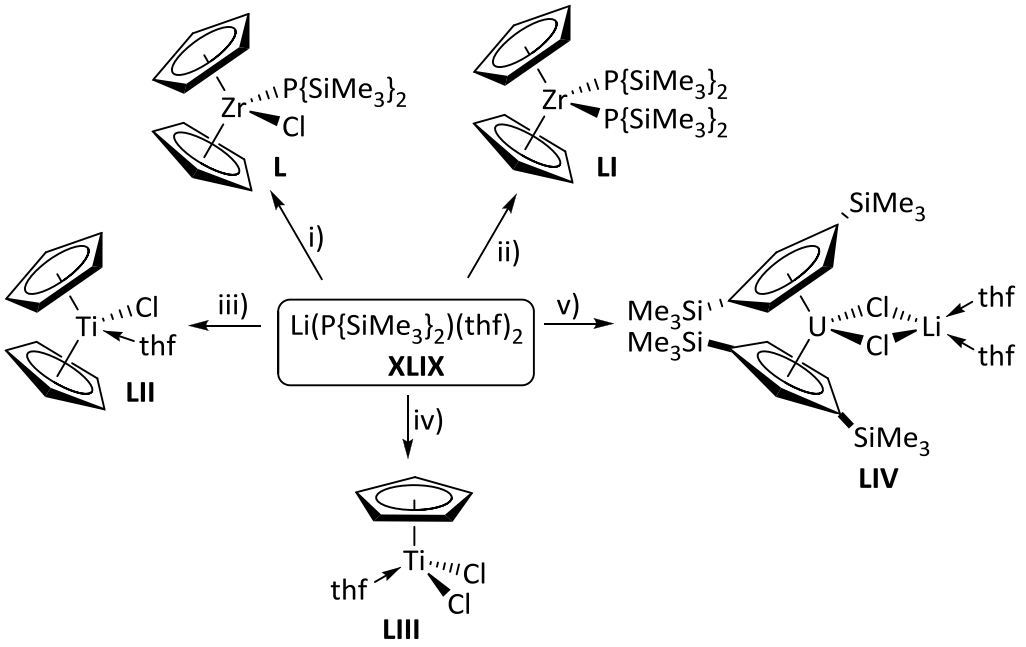

Scheme 4.1 – Reactivity of $Li(P\{SiMe_3\}_2)(thf)_2$ (**XLIX**) with (i) $ZrCp_2Cl_2$, (ii) 0.5 $ZrCp_2Cl_2$, (iii) $TiCp_2Cl_2$, (iv) $TiCpCl_3$ and (v) UCp''_2Cl_2

The first molecular magnesium phosphides were synthesized over 40 years ago and consisted of $Mg(PPh_2)_2$, $MgEt(PPh_2)$, $Mg(PHPh)_2$ and MgEt(PHPh).[107] These compounds were characterised spectroscopically and since then only a few other examples have been reported, the majority of which are homoleptic *bis*-phosphides, $Mg(PR_2)_2$. The first structurally characterised magnesium phosphide was $Mg(PHPh)_2(tmeda)$ (**LV**), published in 1987 by Hey *et al*. (Figure 4.1).[108]

A number of structural permutations of the *bis*-(trimethylsilyl)phosphide $Mg(P\{SiMe_3\}_2)_2$ have been reported; the thf and dme adducts (**LVI** and **LVII**) are monomeric in the solid-state whereas the base-free compound crystallises as a trimetallic oligomer (**LVIII**) (Figure 4.1).[34,109] Compound **LVIII** was shown to exist in a dimer-trimer equilibrium in solution.

There are very few *mono*-phosphide magnesium complexes with the only structurally characterised examples being $[MgEt(PPh_2)(L)]_\infty$ (**LIX**; L = Et_2O[107] or thf[110]), $[(PhC(P\{SiMe_3\}_2)(CR''))Mg(\mu\text{-}P\{SiMe_3\}_2)]_2$ (**LX**; R″ = C≡CPh)[111] and $[MgBu\{P(CH\{SiMe_3\}_2)Ar\}]_2$ (Ar = C_6H_4-2-OMe, C_6H_3-2-OMe-3-Me) (**LXI**)[112] (Figure 4.1).

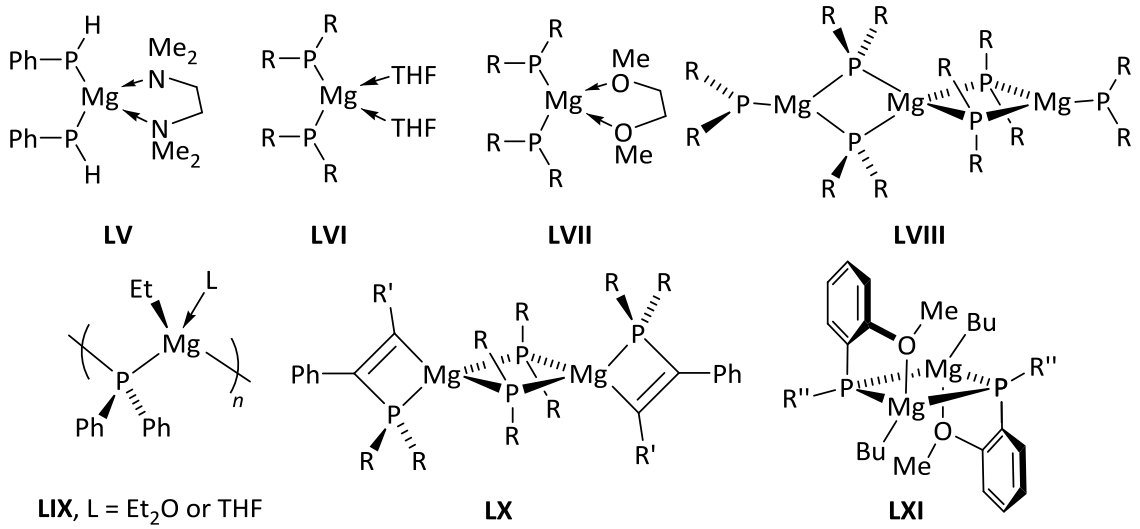

Figure 4.1 – Structurally characterised examples of magnesium phosphides (R = $SiMe_3$, R′ = C≡CPh, R″ = $C(H)(SiMe_3)_2$

This chapter describes the synthesis and characterisation of the first true 'phospha-Grignard' complex with the general formula $Mg(PR_2)X$ (X = halide). Preliminary reactivity studies with group 4 metallocenes MCp_2Cl_2 (M = Ti, Zr) are also described.

4.2 – Synthesis of MgX(P{SiMe$_3$}$_2$)(thf) (X = Br or Me) (8/8′)

The equimolar reaction of MgMeBr and PH(SiMe$_3$)$_2$ in Et$_2$O resulted in the precipitation of a white solid, which was crystallised from a toluene/thf mixture (approximate ratio of 10:1) as colourless crystals. Elemental analysis of these crystals gave results that were consistent with the formula Mg(P{SiMe$_3$}$_2$)Br(thf) (**8**).

The ^{1}H NMR spectrum of **8** in D$_8$-thf showed a broad resonance for the trimethylsilyl groups at δ_H 0.15 ppm and a signal at δ_H -1.62 ppm (relative ratio 20:1). The low frequency signal is in the region of the NMR spectrum associated with Mg-Me groups[113] and was shown to be spatially related to SiMe$_3$ using Nuclear Overhauser Effect Spectroscopy (Figure 4.2). This suggested contamination of the bromide **8** with Mg(P{SiMe$_3$}$_2$)Me(thf)$_n$ (**8'**). An explanation for the presence of **8'** is the reaction of PH(SiMe$_3$)$_2$ with MgMe$_2$, a component of the MgMeBr solution due to the Schlenk equilibrium (Scheme 4.2).[114, ‡‡] Initial batches of crystals were consistent with a sample high in bromide **8**, whilst subsequent batches showed a higher proportion of methyl compound **8′**.

‡‡ It should be noted that any solution or sample of **8** mentioned from this point on contains a minor component of **8′**, however given the relatively small amount of **8′** (<10 %) and the presumed similarity in chemical behaviour the remainder of the chapter will refer to the major component only.

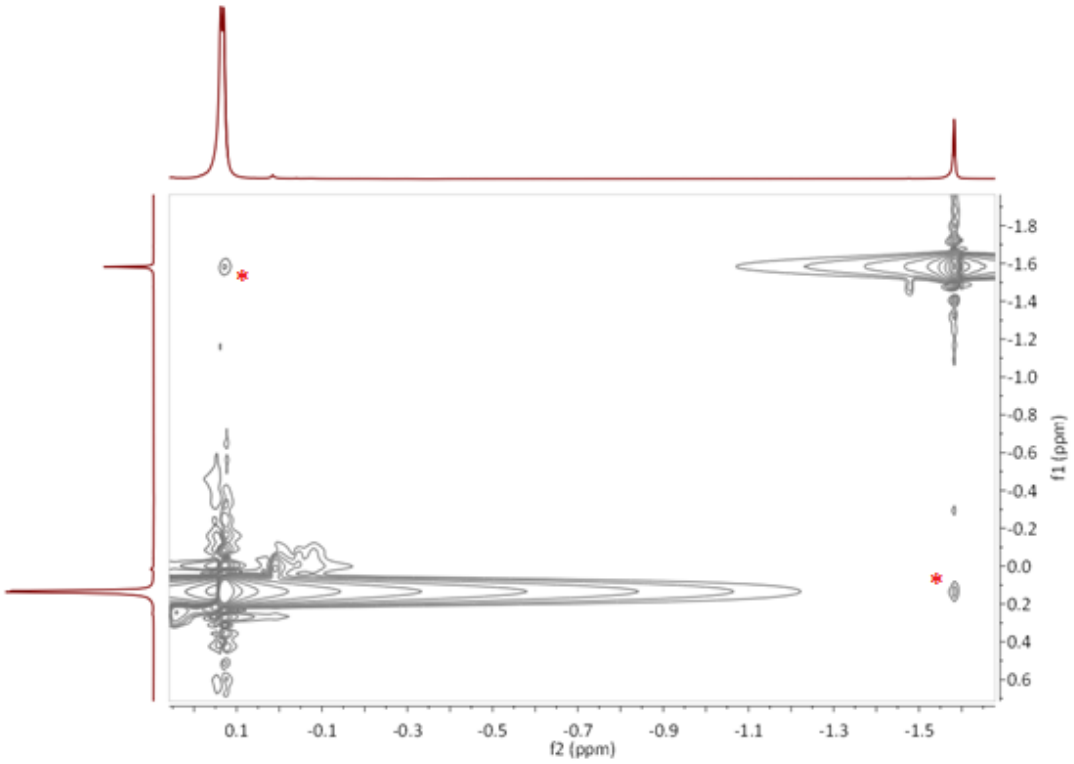

Figure 4.2 – NOESY NMR spectrum of **8/8'**; * = $SiMe_3$/Mg-Me cross peaks

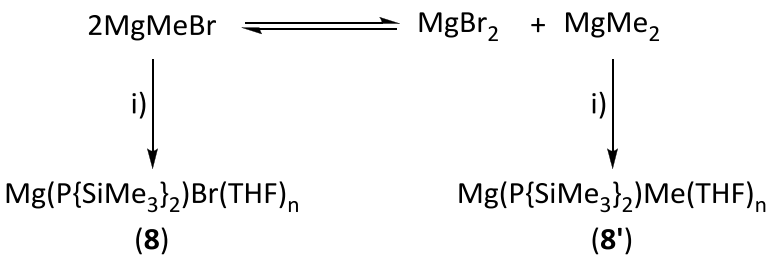

Scheme 4.2 – Postulated pathways for the generation of **8** and **8'**, i) $PH\{SiMe_3\}_2$

The $^{31}P\{^1H\}$ NMR spectrum of **8/8'** in D_8-thf shows two broad resonances at δ_P -296.9 and -305.1 ppm in an approximate 2:3 ratio. The broad nature of the signals suggests a fluxional system in solution, which is a reasonable assumption given the tendency for compounds of this nature to form equilibrium mixtures in coordinating solvents. The higher frequency signal is close to the reported chemical shift of the *bis*-phosphide complex $Mg(P\{SiMe_3\}_2)_2(thf)_n$ (δ_P -

294.7 ppm[34]) which would be an expected component of the Schlenk equilibrium of **8**. The lower frequency signal is assigned to coincident signals of **8** and **8'**.

To investigate whether **8/8'** exists as a Schlenk equilibrium in solution, a slight excess of 1,4-dioxane was added to an NMR sample in a mixture of D_6-benzene and thf, with the expectation that it would react with $MgBr_2$ forming insoluble $[MgBr_2(\mu\text{-1,4-dioxane})]_\infty$ polymer (Scheme 4.3). Precipitation of this solid from solution would enrich the sample with the *bis*(phosphide) component, $Mg(P\{SiMe_3\}_2)_2(thf)_n$. This procedure is used during the preparation of dialkylmagnesium compounds from Grignard reagents.[115]

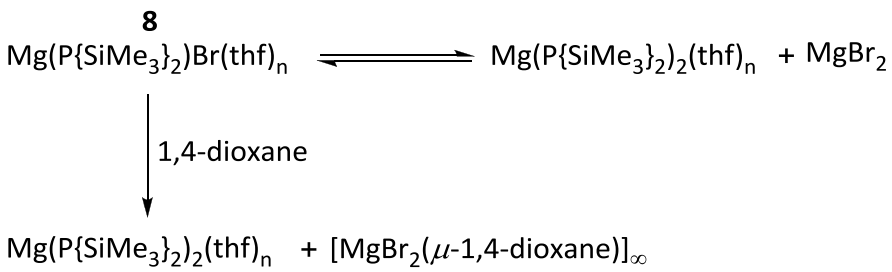

Scheme 4.3 – Schlenk equilibrium of **8** and reaction with 1,4-dioxane

Addition of an excess of 1,4-dioxane to a sample of **8/8'** resulted in the instant formation of a white precipitate, suggesting the formation of $[MgBr_2(\mu\text{-1,4-dioxane})]_\infty$. This was accompanied by a change in the $^{31}P\{^1H\}$ NMR spectrum. The broad signals sharpened and the relative integrals of the resonance assigned to $Mg(P\{SiMe_3\}_2)_2(thf)_n$ increased in intensity with a concomitant decrease of the integral for the resonance assigned to **8/8'** (Figure 4.3). The residual signal at 304.5 ppm is assigned to **8'** as the excess of dioxane should have shifted the equilibrium involving **8** such that only the *bis*-phosphide is left. The addition of 1,4-dioxane to a sample enriched in **8'** resulted in very little change to the ^{31}P signals, with no precipitate

observed. The change in chemical shift is due to the new solvent system as a result of the addition of 1,4-dioxane.

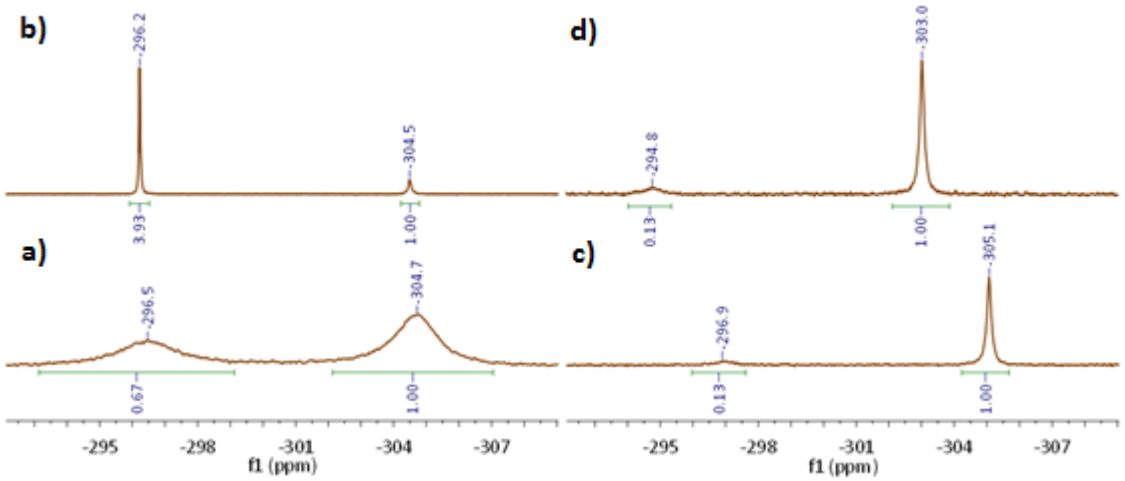

Figure 4.3 - (a) ^{31}P NMR spectrum of **8**/**8'** (161 MHz, thf/D_6-benzene); (b) ^{31}P NMR spectrum of of the same sample after addition of excess 1,4-dioxane; (c) ^{31}P NMR spectrum of a methyl-enriched sample (**8'**; 161 MHz, D_8-thf); (d) ^{31}P NMR spectrum of methyl-enriched sample after addition of excess 1,4-dioxane.

It is possible that additional equilibria involvoing oligomers of **8**, e.g. monomer-dimer equilibrium, may also contribute to the broad ^{31}P signals observed. Although the data presented here can not discount this possibility, it is not thought that such equilibria are likely due to the presence of the strong donor solvent thf, which is commonly found to break up aggregated complexes. This belief is supported by observation that although the solvent free complex **LVIII** is isolated as a trimer in the solid state and exists in a dimer-trimer equilibrium, the thf solvated complex **LVI** is monomeric in the solid state and shows no sign of any oligomeric equilibria in a thf solution.

Such equilibria for **8'** are also not thought to be likely due to the sharp resonance observed in the **8'** enriched NMR spectra (Figure 4.3 (c)) which remains unchanged following the addition of 1,4-dioxane in addition to the arguments above.

Single crystal X-ray crystallography showed **8** crystallises in the triclinic $P\bar{1}$ space group and is dimeric in the solid state (Figure 4.4). The molecule lies on an inversion centre with two phosphides bridging the magnesium atoms, forming a planar Mg_2P_2 metallacycle with internal angles of 94.27(5)° and 85.73(5)° at magnesium and phosphorus, respectively. The magnesium and phosphorus atoms have distorted tetrahedral geometries with identical (within 3σ) Mg-P bond lengths (2.5624(16) Å and 2.5621(16) Å). These bond lengths are comparable with other bridging magnesium bis(trimethylsilyl)phosphide complexes (**LVIII** = range: 2.536(3)–2.678(2) Å,[109] **LX** = 2.559(2) Å and 2.569(2) Å[111]).

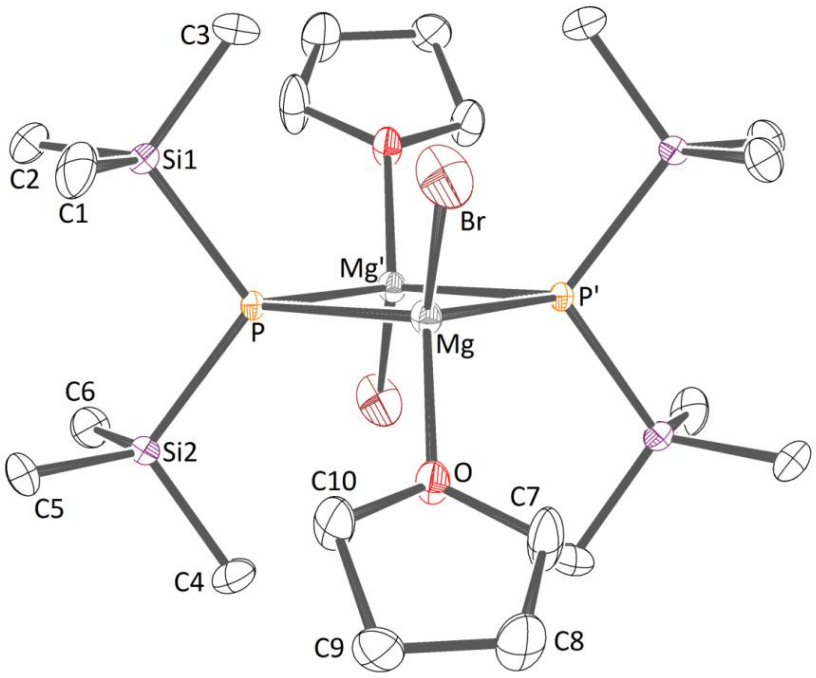

Figure 4.4 – ORTEP representation of $[Mg(P\{SiMe_3\}_2)Br(thf)]_2$ ($[\mathbf{8}]_2$) with thermal ellipsoid probability at 30 % (H atoms omitted for clarity, symmetry operation: ' = –x, –y + 1, –z). Selected bond lengths and angles in Table 4.1

Table 4.1 - Selected bond lengths [Å] and angles [°] for $[8]_2$			
Mg-P	2.5624(16)	**Mg-P′**	2.5631(16)
Mg-O	2.026(3)	**Mg-Br**	2.4235(15)
P-Si1	2.2245(14)	**P-Si2**	2.2362(14)
P-Mg-P′	94.27(5)	**Mg-P-Mg′**	85.73(5)
Si1-P-Si2	108.94(5)	**Si1-P-Mg**	108.69(6)
Si1-P-Mg′	120.78(6)	**Si2-P-Mg**	122.39(5)
Si2-P-Mg′	109.60(6)	**O-Mg-Br**	103.31(12)
O-Mg-P	108.84(11)	**O-Mg-P′**	112.73(11)
Br-Mg-P	118.95(6)	**Br-Mg-P′**	118.81(6)

The reactions of MgMeBr with $PHCy_2$ and $PHPh_2$ in Et_2O were also investigated. With $PHCy_2$, no reaction was observed at ambient temperature (analysis by ^{31}P NMR showed only $HPCy_2$) and upon heating to 70 °C in toluene, an insoluble white solid was precipitated that could not be identified. The reaction of $PHPh_2$ and MgMeBr in Et_2O yielded a white powder which dissolved in thf to give a yellow solution. The ^{31}P NMR spectrum (thf + D_6-benzene as a lock solvent) of this crude solid showed several phosphorus resonances, including one major signal at -47.3 ppm. This signal is in a region consistent with other Mg-PPh_2 complexes (*e.g.* $[MgEt(PPh_2)(thf)]_\infty$ = δ_P -45.2 ppm, $Mg(PPh_2)_2(thf)_4$ = δ_P -39.7 ppm).[110] Unfortunately attempts to isolate a clean sample of the product proved unsuccessful and definitive assignment of this resonance as corresponding to a Mg-PPh_2 unit cannot be made.

4.3 – Reactivity with Group 4 Metallocenes

Despite alkyl and aryl Grignard reagents being common alternatives to organolithium reagents, the lack of phospha-Grignards in the literature means that no studies of the corresponding reactivity have been reported. The only attempt to use a magnesium phosphido species as a phosphide transfer reagent was by Hey *et al*., reacting **LV** with $NiCl_2$(dcpe).[108] The result was the formation of the diphosphene complex Ni(dcpe)(η^2-PhP=PPh) (**LXII**) rather than the expected nickel phosphide (Scheme 4.4). This product had previously been synthesised by Schäfer *et al*. from the reaction of $NiCl_2$(dcpe) with $PPh(SiMe_3)_2$.[116]

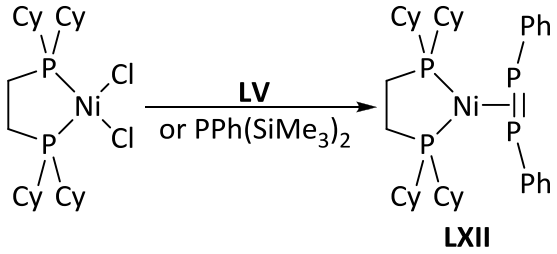

Scheme 4.4 – Synthesis of Ni(dcpe)(η^2-PhP=PPh) (**LXII**)

Compound **8** was tested as an alternative to lithium reagent **XLIX** in the reaction with $ZrCp_2Cl_2$ and $TiCp_2Cl_2$, with particular interest in whether it would act as a phosphide transfer reagent in the titanium system without reducing the metal centre.

The NMR scale reaction of $ZrCp_2Cl_2$ with 1 equivalent of **8** resulted in the appearance of three resonances in the $^{31}P\{^1H\}$ NMR at δ_P 109.8 (**i**), -78.4 (**ii**) and -72.4 (**iii**) ppm (Figure 4.5). Resonances (**i**) and (**iii**) are consistent with the previously report chemical shifts for zirconium phosphido complexes $ZrCp_2(P\{SiMe_3\}_2)Cl$[117] and $ZrCp_2(P\{SiMe_3\}_2)_2$[118] respectively, demonstrating that **8** is an effective phosphide transfer reagent.

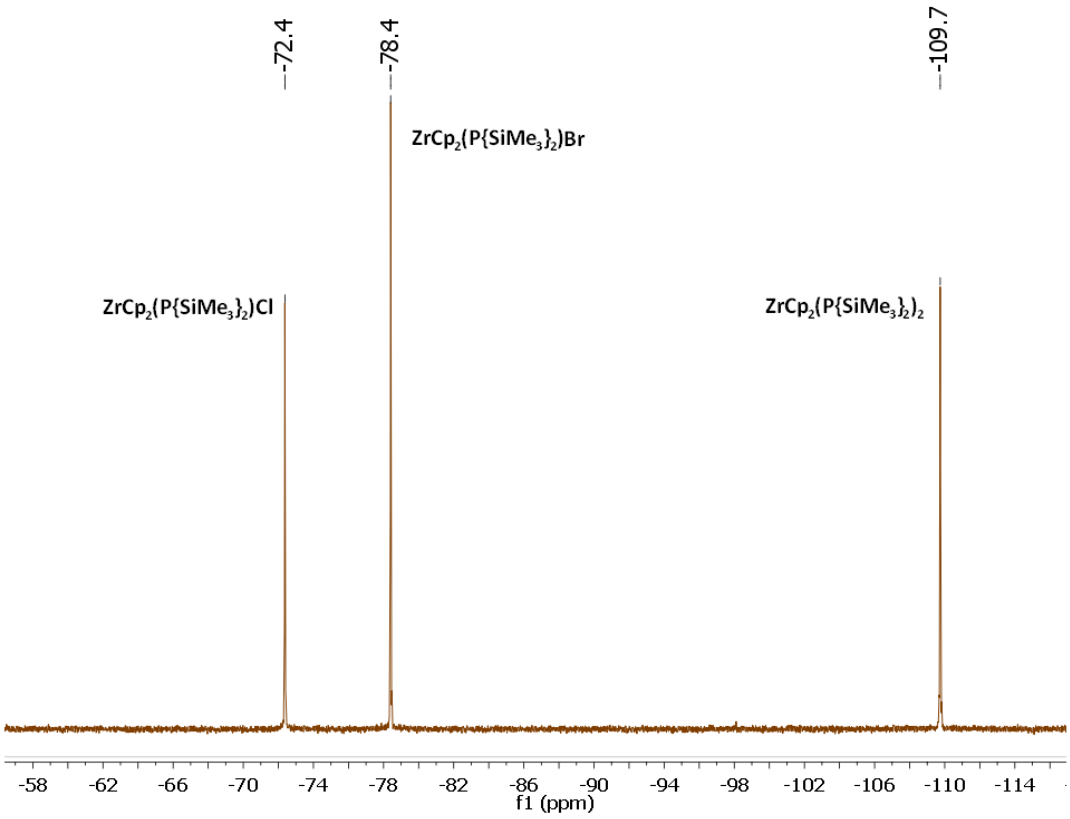

Figure 4.5 – $^{31}P\{^{1}H\}$ NMR spectrum of the reaction mixture following the addition of **8** to $ZrCp_2Cl_2$

Analysis by electron impact (EI) mass spectrometry of the residue left after removing the solvent from the reaction mixture showed molecular ion peaks at *m/z* = 432 ($ZrCp_2(P\{SiMe_3\}_2)Cl$) and 575 ($ZrCp_2(P\{SiMe_3\}_2)_2$). Also observed was a peak at *m/z* = 478 corresponding to the bromide species $ZrCp_2(P\{SiMe_3\}_2)Br$, formed *via* halide exchange during the course of the reaction. We assign resonance (**ii**) from the $^{31}P\{^{1}H\}$ NMR spectrum to this species.

The reaction of $TiCp_2Cl_2$ with 1 equivalent of **8**, initially performed on a NMR scale, resulted in an immediate colour change from red to orange/brown. The $^{31}P\{^{1}H\}$ NMR spectrum displayed only one resonance at δ_P -217.0 ppm which is consistent with the diphosphine, $\{Me_3Si\}_2P\text{-}P\{SiMe_3\}_2$.[119] The reaction was then repeated on a preparative scale in thf. A dark green

pentane solution was obtained after work up from which a no clean product could be isolated. However, on standing a small number of pale blue crystals formed from a D_6-benzene NMR sample of the crude residue. These crystals were shown to be the hexametallic dimer $[TiCp_2(\mu\text{-}X)_2Mg(thf)(\mu\text{-}X)_2Mg(thf)_2(\mu\text{-}X)]_2$ (X = Br or Cl) (**9**) by single crystal X-ray diffraction (Figure 4.5).

The halide bridged hexametallic structure consists of a *tetra*magnesium $[MgX_2]_4$ core capped at either end by $TiCp_2X$. The Ti^{III} centres have distorted tetrahedral centres while the geometry about Mg is distorted octahedral. Atomic displacement parameters were found to be too small when the initial refinement assigned all the halides as chloride. Given that the production of $ZrCp_2(P\{SiMe_3\}_2)Br$ from the reaction of **8** with $ZrCp_2Cl_2$ demonstrates halide exchange processes can occur, the structure was re-examined, allowing the halide positions to freely refine as a mixture of chloride and bromide atoms. The result suggested that the bromide atoms are predominantly located in the Ti(μ-X)Mg positions (average 27% Br) and the remaining positions being only marginally contaminated by Br (average 4.9% Br). The contamination of halide positions by bromide means that meaningful discussion of bond lengths and angles cannot be made.

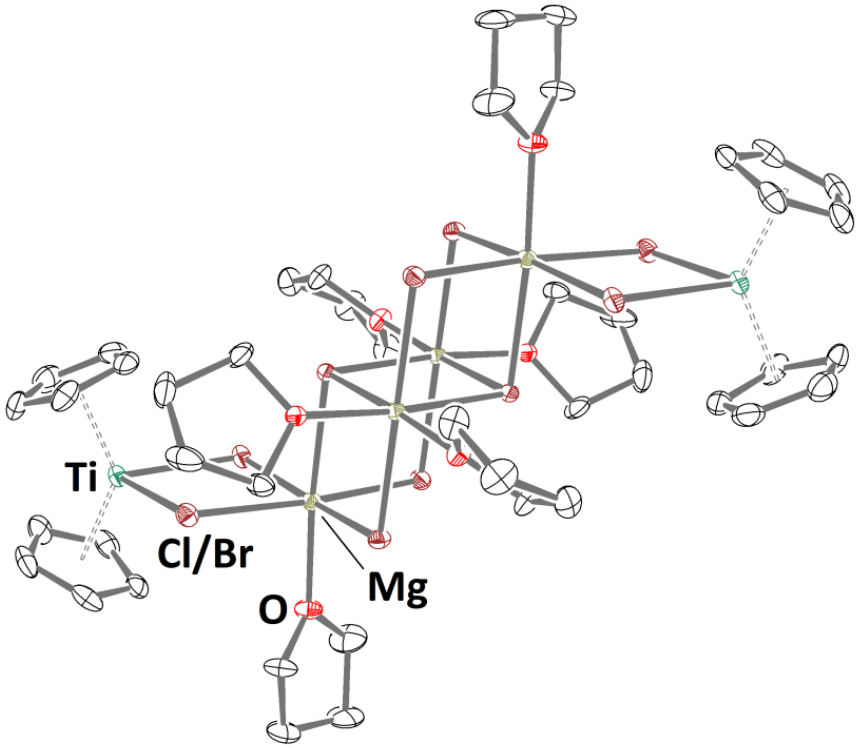

Figure 4.5 – ORTEP representation of **9** with thermal ellipsoid probability at 30 % (H atoms omitted for clarity)

The structure of **9** is reminiscent of the MgX_2 bridged Ti^{III} complexes $(Cp_2Ti\{\mu\text{-}Cl\}_2)_2Mg(thf)_2$ (**LXIII**) and $[TiCp_2(\mu\text{-}Cl)_2Mg(thf)_2(\mu\text{-}Cl)]_2$ (**LXIV**), isolated in low yields from the reduction of $TiCp_2Cl_2$ by Mg in the presence of phosphorus donors (Scheme 4.5).[120] **LXIII** was also synthesised by the stoichiometric reaction of $[TiCp_2(\mu\text{-}Cl)]_2$ and $MgCl_2$, although it is noted that **LXIV** could not be made by reaction $[TiCp_2(\mu\text{-}Cl)]_2$ with two equivalents of $MgCl_2$.

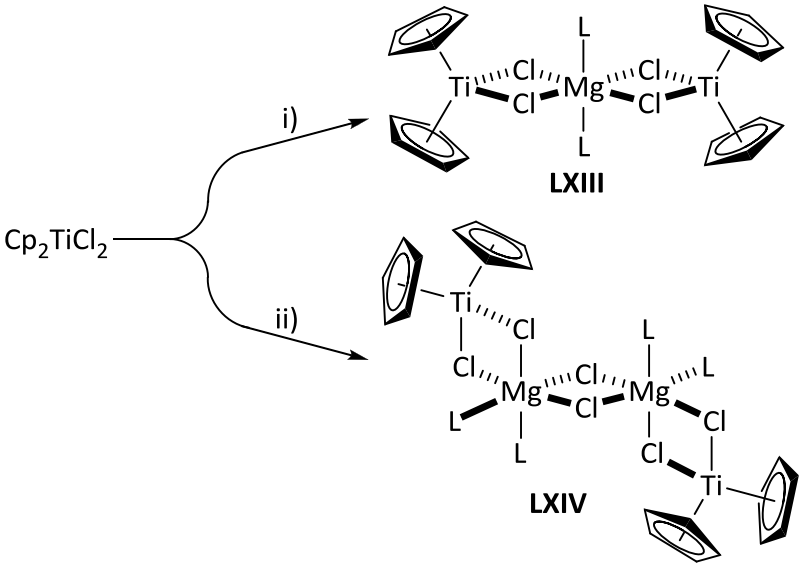

Scheme 4.5 – Reaction of $TiCp_2Cl_2$ with i) excess Mg, P_4 and ii) excess Mg, PH_2R (R = Cy or Ph)[120]; L = thf

The formation of **LXIII** and **LXIV** contrasts with the reduction of $TiCp_2Cl_2$ by Mg in the presence of the strong σ-donor PMe_3, which affords the Ti^{II} complex $TiCp_2(PMe_3)_2$.[121] The addition of PMe_3 to **LXIII** and **LXIV** resulted in the formation of the previously reported Ti^{III} complex $TiCp_2Cl(PMe_3)$[122], which can be further reduced by Mg in the presence of more PMe_3 to $TiCp_2(PMe_3)_2$. Following this work it was postulated that Ti/Mg aggregates such as **LXIII** and **LXIV** are formed during the initial reduction of Ti^{IV} to Ti^{III}, and that these react rapidly with PMe_3 to give $TiCp_2Cl(PMe_3)$. Compound **9** represents an example of another intermediate that may be formed during such reactions.

The observation that **LXIV** was formed from the reduction of $TiCp_2Cl_2$ in the presence of PH_2R (R = Cy or Ph) but was not successfully synthesised from the correct stoichiometric mixture of $[TiCp_2(\mu\text{-}Cl)]_2$ and $MgCl_2$ (unlike **LXIII**) suggests that the phosphorus donors play an important role in the generation of these Ti/Mg aggregates. The exact nature of this role, however, remains unclear.

4.4 – Summary

The reaction of MgMeBr with the secondary phosphine $PH\{SiMe_3\}_2$ resulted the formation of $MgBr(P\{SiMe_3\}_2)(thf)$ (**8**) and $MgMe(P\{SiMe_3\}_2)(thf)_n$ (**8'**). The formation of this mixture is likely due to the Schlenk equilibrium of the Grignard starting material. Compound **8** has been shown to act as phosphide transfer reagent when reacted with $ZrCp_2Cl_2$, but was noted to reduce titanium in $TiCp_2Cl_2$ to Ti^{III}.

The similar reactivity of **8** compared to the lithium phosphide **XLIX**, and the detection of $\{Me_3Si\}_2P\text{-}P\{SiMe_3\}_2$ as the only phosphorus containing product from this reaction suggests that the magnesium component of **8** may not be responsible for the reduction of titanium. Rather one can postulate it is the conversion of the phosphide anion to the diphosphine that is the driving force.

The Ti^{III} complex $[Cp_2Ti(\mu\text{-}X)_2Mg(thf)(\mu\text{-}X)_2Mg(thf)_2(\mu\text{-}X)]_2$ (X = Br or Cl) (**9**) was isolated from the reaction of **8** with $TiCp_2Cl_2$ and may represent an intermediate in the reduction of $TiCp_2Cl_2$ to Ti^{II} by Mg.[120] Interest in species of this type arise from the fact that highly active, industrial heterogeneous catalysts for the polymerization of α-olefins have been generated from mixed Ti/Mg systems.[123] For example, $[Mg_2(\mu\text{-}Cl)_3(thf)_6][TiCl_5(thf)]$,[124] supported on SiO_2, is used commercially with an organometallic co-catalyst for the polymerization of ethylene.[125] Compound **9**, along with the related complexes **LXIII** and **LXIV**, may represent useful model systems for studying $MgCl_2$ supported titanium based olefin polymerisation catalysts.

4.5 – Experimental Procedures for Chapter 4

General Information

MgMeBr was purchased from Sigma Aldrich and was transferred to an ampoule before use. $ZrCp_2Cl_2$ and $TiCp_2Cl_2$ were also purchased from Sigma Aldrich and were used without any further purification following being transferred in to the glovebox. $PH\{SiMe_3\}_2$ was donated by Dr. Ian Crossely.

For all other general experimental procedure see Appendix A.

Synthesis of [Mg(P{SiMe$_3$}$_2$)X(thf)] [X = Br/Me (8/8')]

A solution of MgMeBr (3.1 mL of a 3.0 M solution, 9.3 mmol) in Et_2O was added dropwise through a syringe to a solution of $PH\{SiMe_3\}_2$ (2.0 mL, 9.2 mmol) in Et_2O (ca. 10 mL) at –78 °C. The solution was stirred and warmed to ambient temperature. After stirring for 3 h, a white precipitate formed that was isolated by filtration and washed with a small amount of cold Et_2O (ca. 10 mL). Slow cooling of a warm (60 °C) toluene/thf solution to ambient temperature yielded colourless crystals, which proved to be a mixture of $Mg(P\{SiMe_3\}_2)Br(thf)$ (**8**) and $Mg(P\{SiMe_3\}_2)Me(thf)$ (**8'**). Overall yield = 2.14 g. Initial batches of crystals were consistent with a sample high in bromide **8**, whilst subsequent batches showed a higher proportion of methyl compound **8'**.

Analysis of **8**: $C_{10}H_{26}BrMgOPSi_2$ (353.67): calcd. C 33.96, H 7.41; found C 33.82, H 7.50

NMR of **8**:

^{1}H NMR (400 MHz, D_8-thf): δ = 0.15 (br, Si*Me*$_3$)

^{13}C {^{1}H} NMR (100 MHz, D_8-thf): δ = 7.2 (br, Si*Me*$_3$)

^{31}P {^{1}H} NMR (161 MHz, D_8-thf): δ = -296.9 (br), -305.1 (br.)

^{29}Si {^{1}H} NMR (79 MHz, D_8-thf): δ = 2.9 (br, *Si*Me$_3$)

NMR of **8'**:

^{1}H NMR (400 MHz, D_8-thf) δ = 0.14 (br, Si*Me*$_3$), –1.62 (s, Mg*Me*)

^{13}C {^{1}H} NMR (100 MHz, D_8-thf): δ = 7.2 ($^{2}J_{CP}$ = 9 Hz, Si*Me*$_3$), -14.6 (Mg*Me*)

^{31}P {^{1}H} NMR (161 MHz, D_8-thf): δ = -305.1 (br.)

^{29}Si {^{1}H} NMR (79 MHz, D_8-thf): δ = 1.4 (d, $^{1}J_{SiP}$ = 39 Hz, *Si*Me$_3$)

NMR reaction of 8 with $ZrCp_2Cl_2$

8 (20.8 mg, 0.059 mmol) was dissolved in thf (0.3 mL) and added to a solution of $ZrCp_2Cl_2$ (17.2 mg, 0.059 mmol) in D_6-benzene (ca. 0.3 mL) in a vial in an inert atmosphere glovebox. An instant colour change from colourless to red/purple was observed. An NMR tube was charged with the solution, and NMR spectra were recorded. After 24 h, the solvent was removed and the residue dissolved in pure D_6-benzene, and the final products were analysed by NMR spectroscopy.

^{31}P {^{1}H} NMR (161 MHz, D_6-benzene): δ = -72.4 ($ZrCp_2(P\{SiMe_3\}_2)Cl$), -78.4 ($ZrCp_2(P\{SiMe_3\}_2)Br$), -109.7 ($ZrCp_2(P\{SiMe_3\}_2)_2$)

NMR reaction of 8 with $TiCp_2Cl_2$

$TiCp_2Cl_2$ (12.3 mg, 0.049 mmol) was dissolved in D_6-benzene (0.3 mL) and added to **8** (17.5 mg, 0.049 mmol) in a vial in an inert atmosphere glovebox. The reaction mixture was swirled until **8** had completely dissolved. A colour change from red to orange/brown was observed. An NMR tube was charged with the solution and was analysed by ^{31}P NMR spectroscopy.

^{31}P {^{1}H} NMR (161 MHz, D_6-benzene): δ = -217.0 ($\{Me_3Si\}_2P$-$P\{SiMe_3\}_2$)

Preparative scale reaction of 8 with $TiCp_2Cl_2$

Compound **8** (100.9 mg, 0.285 mmol) was dissolved in thf (10 mL) and added dropwise to a stirred solution of $TiCp_2Cl_2$ (71 mg, 0.285 mmol) in thf (10 mL). The solution gradually turned dark green over a period of 2 h. The solvent was removed in vacuo and the residue washed with pentane to afford a green solution. Despite trying numerous conditions, no clean product could be obtained from this mixture. A sample of the residue was dissolved in D_6-benzene,

from which turquoise crystals of **9** were deposited over a period of 2 d. As both the composition of reagent **8** (mixed Br/Me) and the product **9** (mixed Br/Cl) are variable, and the reaction between **8** and $TiCp_2Cl_2$ leading to **9** is non-stoichiometric, we are unable to report a reliable synthesis of **9** in this work. In addition further characterization of **9** by elemental analysis is not viable (due to the variable Br/Cl composition of the crystals), and NMR analysis is hampered by the paramagnetic nature of the Ti^{III} centres.

Chapter 5: Reactions of a Cyclic Bis(amino)stannylene With Platinum(II) Chlorido Complexes

5.1 – Introduction

Divalent tin species are known to readily insert into Pt-Cl bonds. The most commonly studied systems involve the reaction of $SnCl_2$ with dichloroplatinum diphosphine complexes, e.g. *cis*- or *trans*-$PtCl_2(PPh_3)_2$, to form trichlorostannyl platinum complexes, $Pt(SnCl_3)_{2-n}(Cl)_n(PR_3)_2$ (n = 0 or 1). Complexes of this type, where n = 1, have attracted a lot of interest due to their activity as hydroformylation catalysts.[126–133]

In contrast to $SnCl_2$, very little work involving the reactivity of other Sn^{II} compounds with platinum complexes has been conducted. Two examples that have been studied are the bis(alkyl) and bis(amido) stannylenes $Sn(CH\{SiMe_3\}_2)_2$ (**LXV**) and $Sn(N\{SiMe_3\}_2)_2$ (**LXVI**). The chemistry of these stannylenes was investigated in depth by Lappert and co-workers during the 1970s and 1980s.[134–138] In 1976 it was shown that an excess of stannylene **LXV** reacts with the chloride bridged platinum complex $[PtCl(\mu\text{-}Cl)(PEt_3)]_2$ to form the monometallic compound $PtCl(SnCl(CH\{SiMe_3\}_2)_2)(Sn(CH\{SiMe_3\}_2)_2)(PEt_3)$ (**LXVII**), in which **LXV** has inserted into the terminal Pt-Cl bond of each platinum, and an additional equivalent acts as a neutral σ-donor (Figure 5.1).[135] In a stoichiometric ratio, this reaction was shown to yield bimetallic $[Pt(\mu\text{-}Cl)(SnCl\{CH\{SiMe_3\}_2\}_2)(PEt_3)]_2$ (**LXVIII**), in which **LXV** has inserted into the terminal Pt-Cl with retention of the bridging chlorides (Figure 5.1). The reaction of the amido-stannylene **LXVI** with $[PtCl(\mu\text{-}Cl)(PEt_3)]_2$ resulted in formation of a mixture of *cis*- and *trans*-$[Pt(\mu\text{-}Cl)(SnCl(N\{SiMe_3\}_2)_2)(PEt_3)]_2$ (**LXIX**) and not the analogue of **LXVII** (Figure 5.1).[138] It was shown that heating a solution of **LXIX** resulted in the isomerisation of the *cis*-isomer to the *trans*-

isomer. **LXVI** was also shown to insert into both Pt-Cl bonds of $Pt(COD)Cl_2$ to form $Pt(COD)(SnCl(N\{SiMe_3\}_2)_2)_2$ (**LXX**).[138]

The reactivity of **LXVI** towards Pt^0 complexes was also examined. It was shown that three equivalents of **LXVI** will displace the cyclooctadiene ligands of $Pt(COD)_2$ to form $Pt(Sn(N\{SiMe_3\}_2)_2)_3$ (**LXXI**),[34] in which each stannylene is acting as a *σ*-donor ligand to the Pt centre (Figure 5.1). Compound **LXXI** was the first example of a Pt^0 stannylene complex and to date the only other examples were reported by Hahn *et al*. in 2008, utilising benzannulated bis(stannylene) ligands (**LXXII** and **LXXIII**; Figure 5.1).[139]

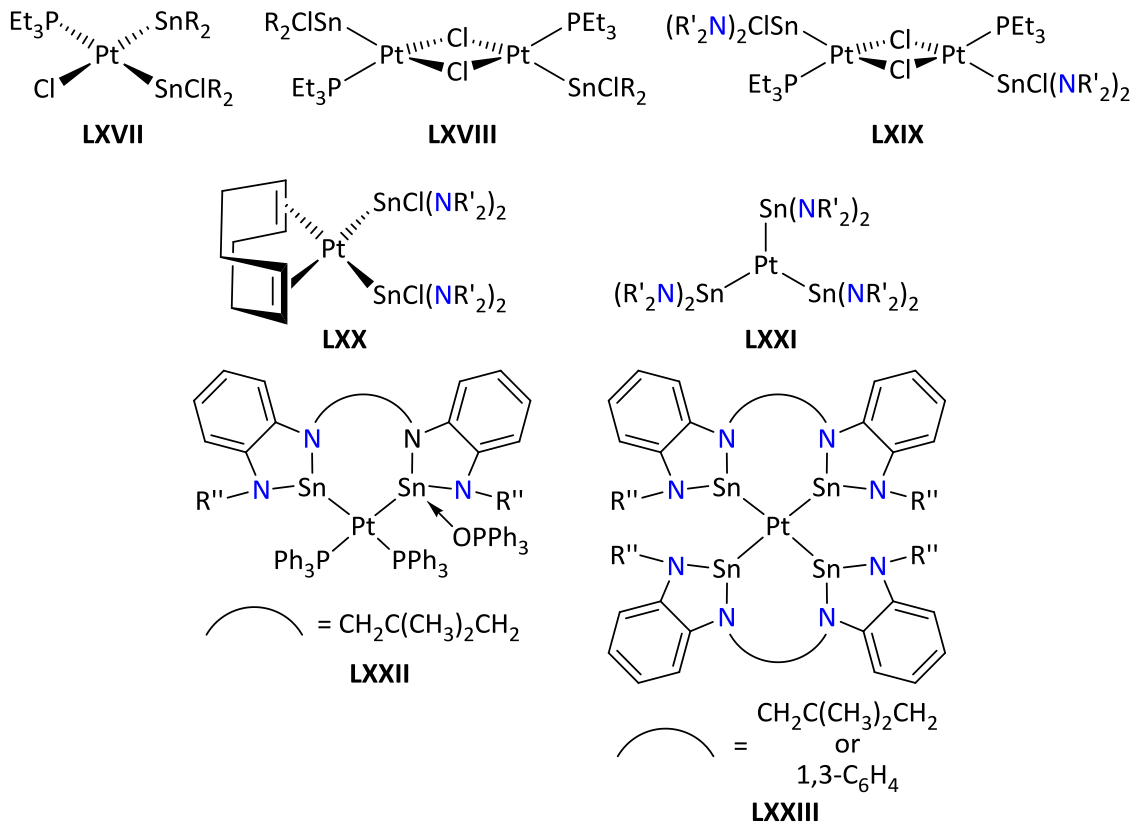

Figure 5.1 – Examples of complexes formed from the reaction of stannylenes with various platinum compounds; R = $CH\{SiMe_3\}_2$, R′ = $SiMe_3$, R″ = neopentyl

Section 1.2.4 described some of the work of Veith *et al.* investigating the reactivity of the cyclic bis(amino)stannylene Sn{N^{t}Bu}$_2$SiMe$_2$ (**XXXV**; Figure 1.19) with a number of different transition metal halides. It also introduced our preliminary reactivity studies of the related stannylene Sn{NAr^{iPr}}$_2$SiMe$_2$ (**XLIII**; Figure 1.23). This chapter describes work performed on the reactivity of **XLIII** with the platinum-chloride species $PtCl_2(PPh_3)_2$, $PtCl_2$(COD), $[PtCl(\mu\text{-}Cl)(PEt_3)]_2$ and $PtCl_2$, showing a number of different modes of reactivity for the stannylene. In addition, the activity one of the resultant compounds as a hydroformylation catalyst is examined.

5.2 – Reaction of $Sn\{NAr^{iPr}\}_2SiMe_2$ (XLIII) with *cis*-$PtCl_2(PPh_3)_2$, $PtCl_2(COD)$ and $[PtCl(\mu\text{-}Cl)(PEt_3)]_2$

The reaction of **XLIII** with *cis*-$PtCl_2(PPh_3)_2$ was initially performed on an NMR scale in D_6-benzene. Analysis of the solution by NMR spectroscopy identified the product as *cis*-$PtCl(SnCl(\{NAr^{iPr}\}_2SiMe_2))(PPh_3)_2$ (**10**) (*vide infra*). Elemental analysis results of a yellow-orange powder obtained from a preparative scale reaction in toluene were consistent with this formula.

The ^1H NMR spectrum of **10** showed two singlets of equal intensity for the Si*Me*$_2$ methyl groups. This contrasts with the single resonance observed for **XLIII**, indicating a reduction in the symmetry of the stannylene component from C_{2v} to C_s. This is interpreted as being caused by addition of non-equivalent groups to the tin centre in a pseudo-tetrahedral geometry, as noted for $Sn(\{NAr^{iPr}\}_2SiMe_2)(Me)(I)$ and $FeCp(SnI(\{NAr^{iPr}\}_2SiMe_2))(CO)_2$ (**XLIV** and **XLVI** in Scheme 1.10).

The ^{31}P NMR of **10** showed two sets of mutually coupled doublets at δ_P 19.9 (**A**) and 31.7 (**B**) ppm ($^2J_{PP}$ = 15 Hz), each with Sn and Pt satellites (Figure 5.2). Both ^{117}Sn and ^{119}Sn satellites are resolved for phosphorus resonance **B**, with $^2J_{SnP}$ coupling constants of 3367 and 3522 Hz respectively; these data are consistent with a *trans* coupling to tin. The only tin coupling observed for phosphorus resonance **A** is 136 Hz, consistent with a *cis* coupling to Sn. The $^1J_{PtP}$ coupling constants of **A** and **B** are 3886 and 2597 Hz respectively.

The ^{119}Sn and ^{195}Pt NMR spectra both display doublet of doublets (δ_{Sn} -167 ppm and δ_{Pt} -4695 ppm) with $^2J_{SnP}$ and $^1J_{PtP}$ coupling constants consistent with those observed in the ^{31}P NMR spectrum. ^{195}Pt satellites are observed in the ^{119}Sn NMR spectrum with a $^1J_{SnPt}$ coupling constant of 15436 Hz.

The addition of two equivalents of **XLIII** to $PtCl_2(PPh_3)_2$ also yields **10**, with one equivalent of **XLIII** unreacted (by ^{119}Sn and ^{31}P NMR). Insertion into both Pt-Cl bonds is therefore not observed and is most likely due to the large steric profile of **XLIII**.

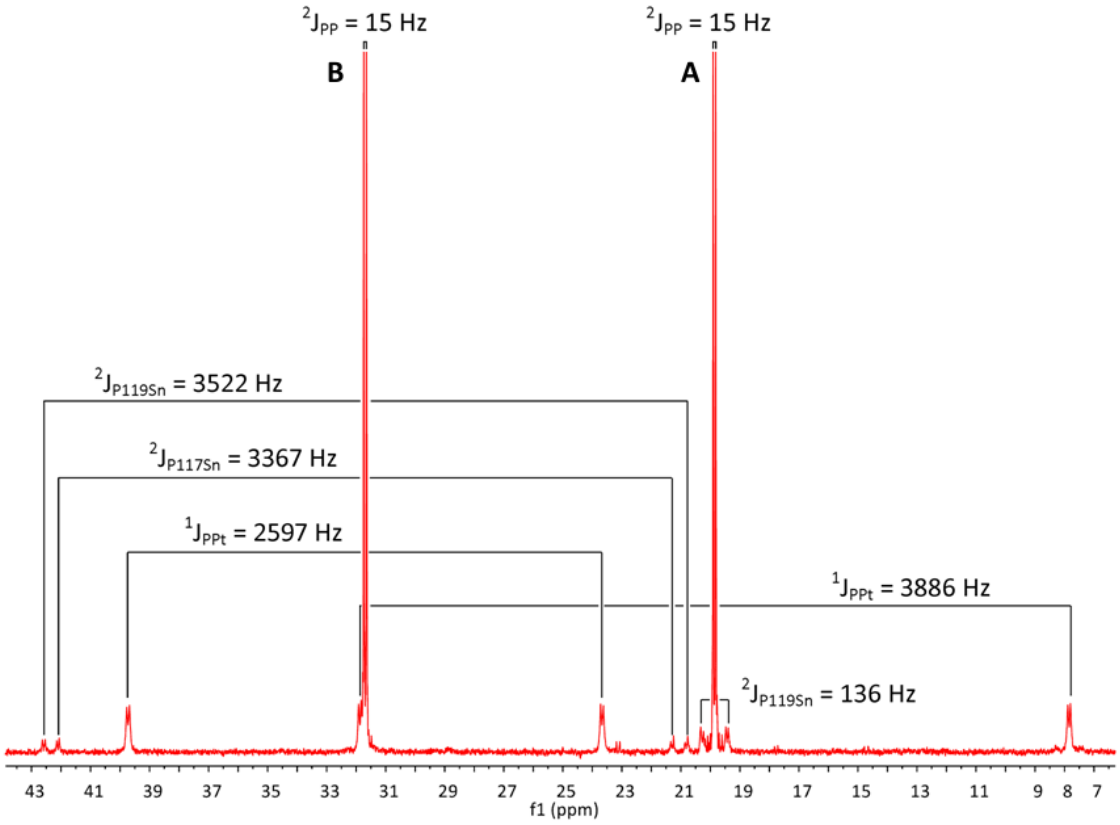

Figure 5.2 – ^{31}P NMR spectrum of *cis*-PtCl(SnCl({NAr^{iPr}}$_2SiMe_2$))$(PPh_3)_2$ (**10**)

Single crystal X-ray diffraction studies of crystals deposited from a D_6-benzene NMR sample showed that **10** crystallises in the triclinic $P\bar{1}$ space group and confirms that stannylene **XLIII** has inserted into one of the Pt-Cl bonds (Figure 5.3). The geometry about the four-coordinate tin centre is distorted tetrahedral [range of angles = 74.84(8)-128.05(6)°] with the N1-Sn-N2 bite angle of the bis(amido) ligand defining the smallest angle. The Sn-N bond lengths (2.078(2) and 2.068(2) Å) are almost identical to the analogous bond lengths of the free stannylene **XLIII** (2.090(4) and 2.080(4) Å).[140,66] This is slightly surprising as it was predicted that the coordination of two additional groups at tin would result in a rehybridisation from sp^2

(with an empty *p*-orbital to accept electron density from the amido nitrogen) to sp^3 with no empty orbitals as well as a change from a two coordinate, sterically unsaturated Sn(II) centre to a smaller four coordinate, 'crowded' Sn(IV) centre. The other geometric parameters of the SnN_2Si metallacycle are also comparable with those found for **XLIII**, suggesting that any differences due to changes in the electronic configuration at tin are minimal. The Sn-Cl1 bond length of 2.4061(7) Å is similar to the Sn-Cl bond lengths observed in other complexes synthesised from the insertion of a divalent tin amide in to a metal-Cl bond, e.g. Rh(η^6-C_6H_5Me)(η^2-C_8H_{15})(SnCl(N{$SiMe_3$}$_2$)) (2.437 Å) and *trans*-[Pt(μ-Cl)(SnCl(N{$SiMe_3$}$_2$))(PEt_3)]$_2$ (2.401 Å).[137,34]

The platinum centre has a distorted square planar geometry [sum of angles = 359.86°]. The P1-Pt-P2 angle of 97.59(2)° is the largest and is comparable to the analogous angle reported for various structures reported for *cis*-$PtCl_2(PPh_3)_2$ [range = 97.265-99.121°].[141–143] The most acute angle is the Sn-Pt-Cl2 angle which is 78.757(17)°. The Pt-P1 (phosphine *trans* to Cl) bond length of 2.2576(6) Å is comparable than the Pt-P bond lengths reported for *cis*-$PtCl_2(PPh_3)_2$ [range = 2.248-2.271 Å] while the Pt-P2 (phosphine *trans* to Sn) bond length of 2.3346(6) Å is significantly longer. This is likely due to the [SnCl({NAr^{iPr}}$_2$$SiMe_2$)]$^-$ ligand imparting a stronger *trans* influence than the chloride ligand.

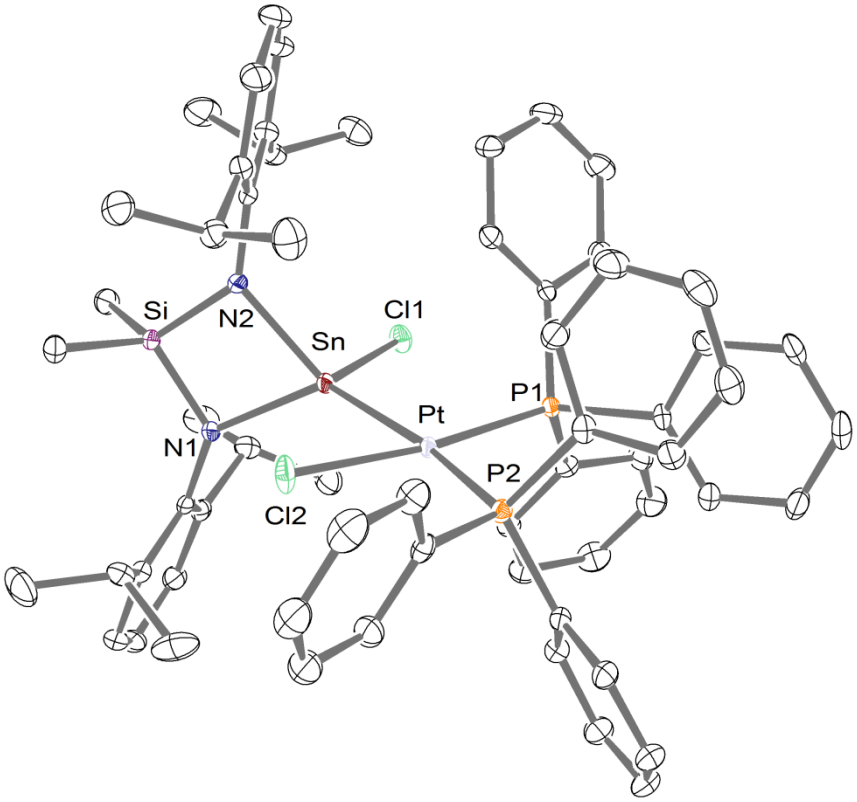

Figure 5.3 – ORTEP representation of *cis*-PtCl(SnCl({NAr^{iPr}}$_2$SiMe$_2$))(PPh$_3$)$_2$ (**10**) (with thermal ellipsoids at 30% level), hydrogen atoms and 3 benzene solvate molecules omitted for clarity. Selected bond lengths and angles are listed in Table 5.1

Table 5.1 – Selected bond lengths (Å) and angles (°) of 10			
Pt-Sn	2.61549(18)	**Sn-N2**	2.068(2)
Pt-P1	2.2576(6)	**Sn-Cl1**	2.4061(7)
Pt-P2	2.3346(6)	**Si-N1**	1.736(2)
Pt-Cl2	2.3346(6)	**Si-N2**	1.729(2)
Sn-N1	2.078(2)		
P1-Pt-P2	97.59(2)	**Pt-Sn-Cl1**	113.554(16)
P1-Pt-Sn	93.546(17)	**N1-Sn-N2**	74.84(8)
P1-Pt-Cl2	171.67(2)	**N1-Sn-Cl1**	105.95(6)
P2-Pt-Cl2	89.97(2)	**N2-Sn-Cl1**	100.40(6)
P2-Pt-Sn	168.535(17)	**Sn-N1-Si**	95.64(9)
Sn-Pt-Cl2	78.757(17)	**Sn-N2-Si**	96.22(9)
Pt-Sn-N1	128.05(6)	**N1-Si-N2**	93.29(10)
Pt-Sn-N2	126.33(6)		

The reaction of **XLIII** with PtCl$_2$(COD) and [PtCl(μ-Cl)(PEt$_3$)]$_2$ also resulted in the insertion of the stannylene into one of the Pt-Cl bonds, to form PtCl(SnCl({NAr^{iPr}}$_2$SiMe$_2$))(COD) (**11**; Scheme

5.1) and [Pt(μ-Cl)(SnCl({NAr^{iPr}}$_2$SiMe$_2$))(PEt$_3$)]$_2$ (**12**; Scheme 5.1). Compounds **11** and **12** were identified by ^{1}H, ^{119}Sn and ^{195}Pt NMR spectroscopy.

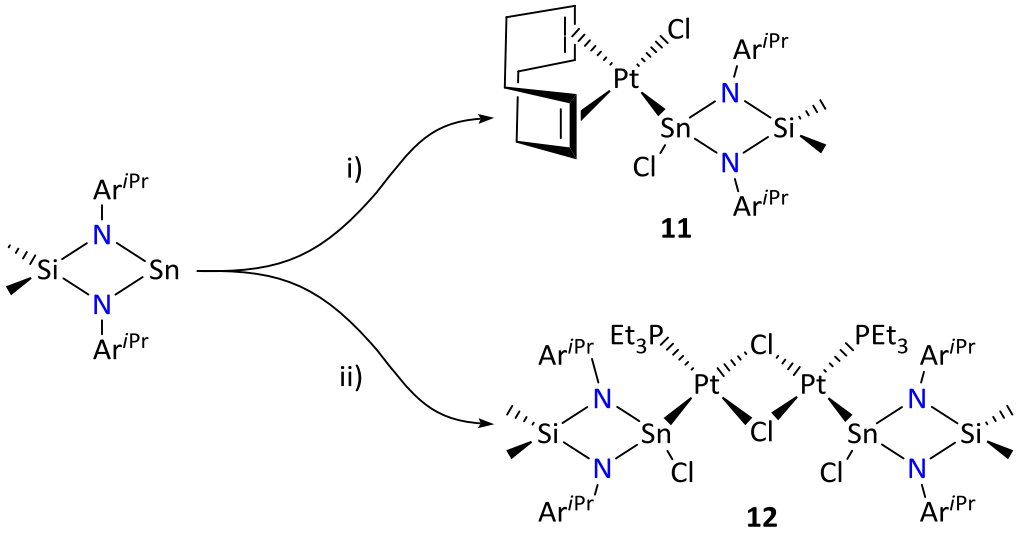

Scheme 5.1 – Synthesis of PtCl(SnCl({NAr^{iPr}}$_2$SiMe$_2$))(COD) (**11**) and [Pt(μ-Cl)(SnCl({NAr^{iPr}}$_2$SiMe$_2$))(PEt$_3$)]$_2$ (**12**); i) Pt(COD)Cl$_2$, C$_6$D$_6$; ii) ½ [PtCl(μ-Cl)(PEt)]$_2$, C$_6$D$_6$

The ^{1}H NMR spectrum of **11** shows two multiplets at δ_H 4.85 and 5.28 ppm assigned to inequivalent alkenyl protons of the cyclooctadiene ligand. This is attributed to the insertion of **XLIII** into one of the Pt-Cl bonds. Each of these signals has platinum satellites corresponding to $^2J_{PtH}$ coupling constants of 67 Hz (*trans* to Cl) and 37 Hz (*trans* to Sn), respectively. The methylene protons of the cyclooctadiene ligand are also inequivalent, giving rise to two broad signals at 4.85 and 5.28 ppm. As for **10**, the Si*Me$_2$* methyl groups are observed as two equal intensity singlets at δ_H 0.47 and 0.55 ppm, reflecting the expected loss of symmetry. The ^{119}Sn NMR spectrum of **11** shows a significant shift of the tin resonance (δ_{Sn} -222 ppm) compared to **XLIII** (δ_{Sn} -522 ppm); platinum satellites corresponding to a coupling constant of 21576 Hz are observed. The magnitude of this coupling is consistent with the formation of a Sn-Pt bond.

The ^{195}Pt NMR spectrum shows a single resonance at δ_{Pt} -3669 ppm with resolved ^{117}Sn and ^{119}Sn couplings ($^{1}J_{PtSn}$ = 20618 Hz and 21576 Hz respectively).

We note that the addition of two equivalents of **XLIII** to $PtCl_2$(COD) does not result in the insertion of **XLIII** into both Pt-Cl bonds. ^{1}H NMR spectra clearly show that only the monoinsertion product **11** is formed. This is in contrast to the analogous reaction reported by Lappert *et al.* using two equivalents of **LXVI**, in which the double insertion product **LXX** is formed.[138]

The ^{1}H NMR spectrum of **12** shows the ethyl groups of the phosphine ligands as two multiplets at δ_H 0.65 and 1.11 ppm for the methyl and methylene protons respectively. The Si*Me*$_2$ groups are again observed as two singlets, at δ_H 0.23 and 0.73 ppm. The ^{31}P NMR spectrum shows a single environment for the phosphine ligands (δ_P 17.5 ppm) with coupling to tin and platinum ($^{2}J_{PSn}$ = 178 Hz, $^{1}J_{PPt}$ = 3761 Hz). The ^{119}Sn NMR spectrum is a doublet at δ_{Sn} -402 ppm ($^{2}J_{SnP}$ = 178 Hz) with platinum satellites ($^{1}J_{SnPt}$ = 27026 Hz). A doublet is also observed in the ^{195}Pt NMR spectrum at δ_{Pt} -4058 Hz ($^{1}J_{PtP}$ = 3761 Hz); no tin satellites were resolved in this experiment.

It is likely that a *trans*- geometry is adopted for **12** given the bulk of the N-heterocyclic stannylene and the relatively small $^{1}J_{PPt}$ coupling compared to *cis*- and *trans*-[Pt(μ-Cl){Sn(N{SiMe$_3$}$_2$Cl}(PEt$_3$)]$_2$ (4109 Hz and 3960 Hz respectively).

5.3 – Reaction of $Sn\{NAr^{iPr}\}_2SiMe_2$ (XLIII) with $PtCl_2$

Veith *et al.* previously reported the reaction of four equivalents of $Sn\{N^tBu\}_2SiMe_2$ with $PtCl_2$ resulted in the insertion of two stannylene molecules into each Pt-Cl bonds to form $Pt((Sn\{N^tBu\}_2SiMe_2)_2Cl)_2$ (see Section 1.2.4). As previously demonstrated, multiple insertions of **XLIII** into the Pt-Cl bonds of 4-coordinate platinum complexes do not occur, presumably due to the steric profile **XLIII**. We were curious as to whether this trend in reactivity extended to the reaction of **XLIII** with coordinatively unsaturated platinum compounds. To investigate this, a fourfold excess of **XLIII** was added to a suspension of $PtCl_2$ in D_6-benzene. An immediate reaction was evident from the formation of a red solution upon mixing; however, not all of the $PtCl_2$ was consumed and solid $PtCl_2$ remained unreacted, settling to the bottom of the NMR tube. The reaction was therefore heated at 60 °C for 3 days. During this time a number of red crystals were deposited in the NMR tube.

Analysis of the crystals by single crystal X-ray diffraction showed that the molecular structure of the platinum complex was $Pt((SnCl_2\{NAr^{iPr}\})_2SiMe_2)(Sn\{NAr^{iPr}\}_2SiMe_2)_2$ (**13**; Figure 5.4). Compound **13** crystallises in the triclinic $P\bar{1}$ space group and consists of a platinum centre coordinated by two molecules of stannylene **XLIII** in a *cis*-arrangement and a novel chelating bis(dichloroaminostannate) ligand $[Me_2Si\{N(Ar^{iPr})SnCl_2\}_2]^{2-}$. The geometry around the platinum centre is best described as highly distorted square planar [sum of angles = 366.5°]. The distortion is most likely due to the steric interactions of the bulky ligands around Pt. The Sn-Pt-Sn angles are in the range 81.447(14)° – 105.320(15)° with a 27.05(2)° twist between the Sn1-Pt-Sn2 and Sn3-Pt-Sn4 planes.

The four Pt-Sn bond lengths are all similar [range = 2.5392(5)-2.5606(4) Å], despite there being two very different tin environments. The Sn centres of the coordinated stannylene ligands are almost planar [sum of angles = 358.1° and 357.5°]. The N-Sn-N bite angles of 75.91(18)° and

76.2(2)° are identical (within 3σ) and are comparable with the analogous bite angle of **10** and **XLIII**; the remaining geometric parameters of the SnN_2Si metallacycle also show very little difference between these compounds, suggesting this is a robust unit.

The main feature of interest in compound **13** is the newly formed bis(stannate) ligand, which chelates to platinum *via* Sn1 and Sn2 (Sn1-Pt-Sn2 bite angle = 81.477(14)°) forming a unique 6-membered SiN_2Sn_2Pt metallacycle in a twisted boat conformation. The Sn atoms are distorted tetrahedral [range of angles = 100.73(5)-123.61(14)° and 100.87(7)-124.30(13)°] with the smallest angles described by the two terminal chloride atoms. The two Sn-N bond lengths (2.037(4) Å and 2.040(5) Å) are comparable to the Sn-N bond lengths of the neutral stannylene ligands.

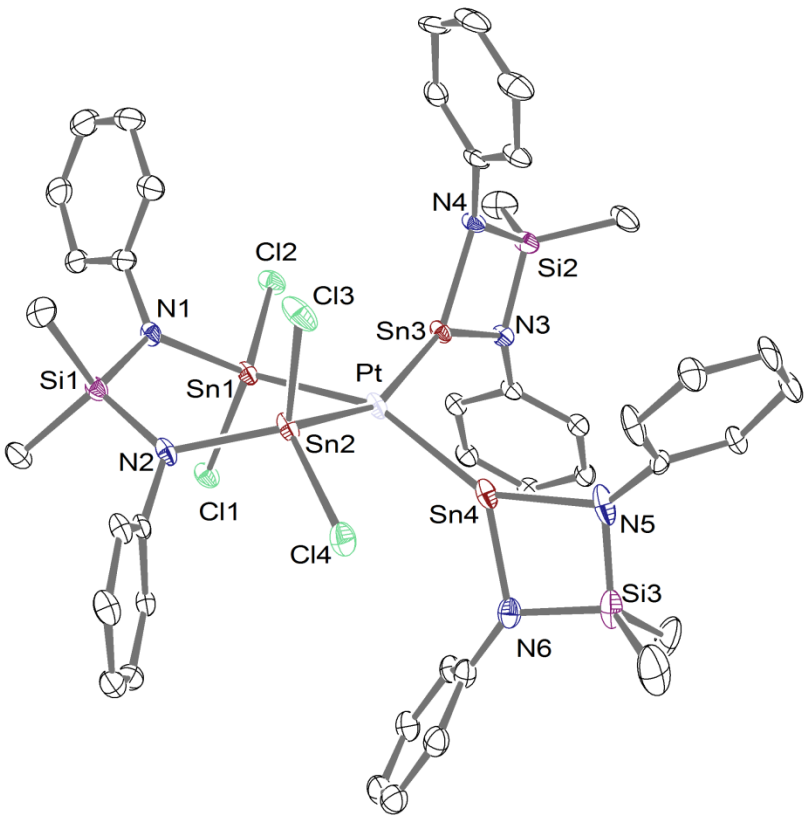

Figure 5.4 – ORTEP representation of $Pt(\{SnCl_2NAr\}_2SiMe_2)(Sn\{NAr\}_2SiMe_2)_2$ (**13**) (with thermal ellipsoids at 30% level), hydrogen atoms and ^{i}Pr groups omitted for clarity. Selected bond lengths and angles are listed in Table 5.2

Table 5.2 – Selected bond lengths (Å) and angles (°) of 13					
Pt-Sn1	2.5392(5)	**Sn2-N2**	2.040(5)	**Si1-N1**	1.748(5)
Pt-Sn2	2.5524(4)	**Sn2-Cl3**	2.3460(16)	**Si1-N2**	1.747(5)
Pt-Sn3	2.5606(4)	**Sn2-Cl4**	2.3766(18)	**Si2-N3**	1.748(5)
Pt-Sn4	2.5532(5)	**Sn3-N3**	2.034(4)	**Si2-N4**	1.741(5)
Sn1-N1	2.037(4)	**Sn3-N4**	2.042(5)	**Si3-N5**	1.758(7)
Sn1-Cl1	2.3537(14)	**Sn4-N5**	2.046(5)	**Si3-N6**	1.750(5)
Sn1-Cl2	2.3793(15)	**Sn4-N6**	2.028(6)		
Sn1-Pt-Sn2	81.477(14)	**N1-Sn1-Cl2**	105.82(15)	**N3-Sn3-N4**	75.91(18)
Sn1-Pt-Sn3	88.857(15)	**Cl1-Sn1-Cl2**	100.73(5)	**Pt-Sn4-N5**	148.34(19)
Sn1-Pt-Sn4	157.386(16)	**N2-Sn2-Pt**	124.30(13)	**Pt-Sn4-N6**	133.00(15)
Sn2-Pt-Sn3	156.915(17)	**N2-Sn2-Cl3**	105.24(14)	**N5-Sn4-N6**	76.2(2)
Sn2-Pt-Sn4	90.850(15)	**N2-Sn2-Cl4**	104.27(15)	**N1-Si1-N2**	106.7(2)
Sn3-Pt-Sn4	105.320(15)	**Cl3-Sn2-Cl4**	100.87(7)	**N3-Si2-N4**	91.9(2)
N1-Sn1-Pt	123.61(14)	**Pt-Sn3-N3**	148.22(14)	**N5-Si3-N6**	91.6(3)
N1-Sn1-Cl1	106.20(14)	**Pt-Sn3-N4**	133.97(13)		

The mechanism by which the bis(stannate)ligand is formed is not known. A possible mechanism involves the stannylene initially acting as a ligand transfer reagent, reacting with $PtCl_2$ to form a cyclic bis(amido)platinum complex and $SnCl_2$. Insertion of $SnCl_2$ into each of the Pt-N bonds would then result in the formation of the bis(stannate) ligand observed in the structure of **13** (Scheme 5.2).

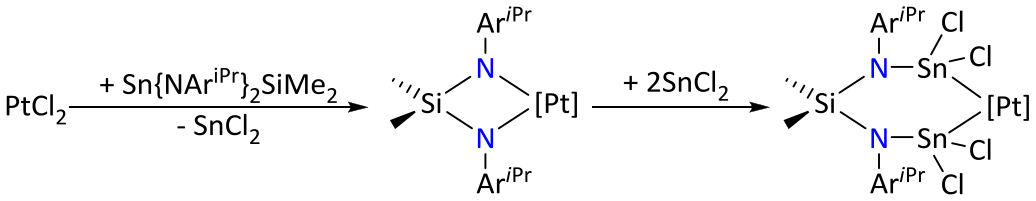

Scheme 5.2 – Postulated reaction to form bis(stannate) ligand $[Me_2Si\{N(Ar^{iPr})SnCl_2\}_2]^{2-}$

The transfer of the bis(amido)silane ligand from tin to another metal has previously been observed in the reaction of $Sn\{N^tBu\}_2SiMe_2$ with $AlH_2(OR)$ (R = ^{t}Bu, $SiMe_3$, Si^tBuMe_2), which

resulted in formation of Al({N^{t}Bu}$_2$SiMe$_2$)(OR).[144,145] Although there is not any precedent in the literature for the insertion of tin into a Pt-N bond, it has been shown that CO, which is isoelectronic to divalent tin species, will insert into the Pt-N bond of PtMe(N(H)CH$_2$Ph)(dppe) to form PtMe(C(O)N(H)CH$_2$Ph)(dppe) (Scheme 5.3).[146]

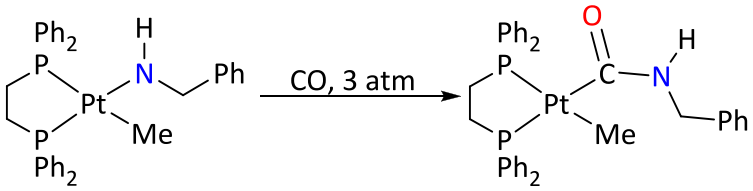

Scheme 5.3 – Insertion of CO into a Pt-N bond

5.4 – Investigation of *cis*-PtCl(SnCl({NAr^{iPr}}$_2$SiMe$_2$))(PPh$_3$)$_2$ as a Hydroformylation Catalyst

As discussed in Section 5.1, complexes of the type Pt($SnCl_3$)(Cl)(PR_3)$_2$, usually generated *in situ* from the reaction of $PtCl_2(PR_3)_2$ with $SnCl_2$, are active catalysts for hydroformylation. However, it is not been definitively shown whether the $[SnCl_3]^-$ remains bound to platinum or dissociates, forming a stable anion, in the initial activation step (Figure 5.4). While investigation of this initial step by high pressure NMR have showed that substitution of $[SnCl_3]^-$ by CO provides an ionic pathway for hydroformylation,[147] recent computational studies favour retention of the Pt-Sn bond.[148–150]

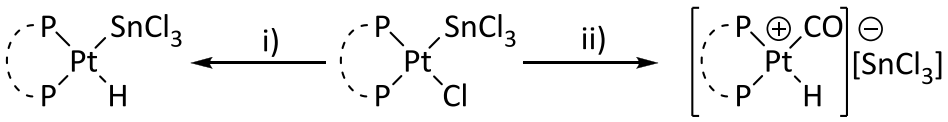

Scheme 5.4 – Possible active species in the catalytic hydroformylation of olefins by Pt($SnCl_3$)(Cl)(PR_3)$_2$; i) H_2, ii) CO/H_2

While a considerable amount of research has focused on the development of alternative supporting phosphine ligands, the effect using an alternative Sn^{II} cocatalyst has not been investigated.

A typical hydroformylation reaction using 1-hexene as a substrate was used to examine the catalytic activity of compound **10**. The results were compared to those obtained using Pt($SnCl_3$)(PPh_3)$_2$ (mixture of *cis*- and *trans*- isomers, ratio = 2:1) under the same conditions,[§§] and are shown in Table 5.3.

The activity of Pt($SnCl_3$)(PPh_3)$_2$ was comparable to that reported for an *in situ* generated catalyst from $PtCl_2(PPh_3)_2$ and $SnCl_2$.[151] Low hydroformylation activity was observed for

[§§] Experiments performed by Dr. Phil Dyer at the University of Durham

compound **10** with only very small quantities of heptanal detected although the *l*:*b* ratio was superior to that observed for $PtCl(SnCl_3)(PPh_3)_2$. Moderate activity was observed for the hydrogenation of 1-hexene by **10**. The use proton sponge (1,8-bis(dimethylamino)naphthalene) to remove any potential problems in catalytic performance (that commonly arise from advantageous hydrolysis of the $[SnCl_3]^-$ moiety, generating HCl)[151,152] resulted in the inhibition of the hydroformylation reaction. In all runs, significant levels of isomerism of 1-hexene were observed.

Table 5.3 – Catalytic testing results for the hydroformyation of 1-hexene (toluene, 90 °C, 40 bar pressure of 1:1 syngas feed, 3 h)

Catalyst	C_7 aldehdyes (%)	*l*:*b*[d,g]	n-Hexane (%)[g]	Hexenes (%)[e,g]	1-C_6 (%)[f]
10[a]	3	2.5	17	80	3
10[b]	4	1.3	13	83	2
10[a,c]	<1	n/a	~2	~98	3
$PtCl(SnCl_3)(PPh_3)_2$[a]	50	6.1	8	42	13
$PtCl(SnCl_3)(PPh_3)_2$[b]	51	6.2	9	40	19

[a] [Pt] = 0.5 mmol, [b] [Pt] = 1.0 mmol, [c] with 0.005 mmol proton sponge, [d] linear to branched product distribution, [e] total amount of hexenes, [f] percentage of 1-hexenes, [g] data are an average of two identical runs

5.3 – Summary

Stannylene **XLIII** has been shown to readily insert into a Pt-Cl bond of 4 coordinate Pt^{II} dichloride complexes, reacting with $PtCl_2(PPh_3)_2$, $PtCl_2(COD)$ and $[PtCl(\mu\text{-}Cl)(PEt_3)]_2$ to form $PtCl(SnCl(\{NAr^{iPr}\}_2SiMe_2))(PPh_3)_2$ (**10**), $PtCl(SnCl(\{NAr^{iPr}\}_2SiMe_2))(COD)$ (**11**) and $[Pt(\mu\text{-}Cl)(SnCl(\{NAr^{iPr}\}_2SiMe_2))(PEt_3)]_2$ (**12**) respectively.

The reaction of **XLIII** with $PtCl_2$ afforded the pentametallic complex $Pt((SnCl_2\{NAr^{iPr}\})_2SiMe_2)(Sn\{NAr^{iPr}\}_2SiMe_2)_2$ (**13**). This complex contains a novel chelating bis(dichloroaminostannate), $[Me_2Si\{N(Ar^{iPr})SnCl_2\}_2]^{2-}$, and is the first example of a Pt^{II} complex containing neutral coordinating stannylene.

The activity of compound **10** as a hydroformylation catalyst was examined however only low activity is observed. If the mechanism involves the retention of the Pt-Sn bond, the bulk of the "$SnCl(\{NAr^{iPr}\}_2SiMe_2$" moiety will disfavour olefin coordination and hence the formation of a 5-coordinate platinum intermediate. If a mechanism involving an ionic pathway is in operation, it may be that $[SnCl(\{NAr^{iPr}\}_2SiMe_2]^-$ is an unstable ionic intermediate, therefore limiting reactivity. The data presented here demonstrates the importance of the role of the tin co-catalysts in the hydroformylation of olefins by Pt/Sn systems.

5.4 – Experimental Procedures for Chapter 5

General Information

$PtCl_2(PPh_3)_2$,[153] $PtCl_2(COD)$,[154] $[PtCl(\mu\text{-}Cl)(PEt_3)]_2$[155] and $Sn\{NAr^{iPr}\}_2SiMe_2$[66,140] were prepared following literature procedures. $PtCl_2$ was purchased from Johnson Matthey and used as received.

For all other general experimental procedure see Appendix A.

Synthesis of cis-PtCl(SnCl{(NAr^{iPr})$_2$SiMe$_2$})(PPh$_3$)$_2$ (10)

NMR Scale:

A yellow solution of $Sn\{NAr^{iPr}\}_2SiMe_2$ (**XLIII**) (30.4 mg, 0.06 mmol, 2 equiv.) in C_6D_6 was added to a NMR tube fitted with a J. Youngs tap that had previously been charged with $PtCl_2(PPh_3)_2$ (22.8 mg, 0.03 mmol, 1 equiv.). The $PtCl_2(PPh_3)_2$ quickly dissolved and the solution turned orange immediately. NMR Spectra were consistent with *cis*-$PtCl(SnCl(\{NAr^{iPr}\}_2SiMe_2))(PPh_3)_2$

Preparative Scale:

A solution of $Sn\{NAr^{iPr}\}_2SiMe_2$ (**XLIII**) (158 mg, 0.30 mmol, 1 equiv.) in toluene was added drop wise to a suspension of $PtCl_2(PPh_3)_2$ (240 mg, 0.30 mmol, 1 equiv.) in toluene. The solution went clear and orange after complete addition and stirring for 10 min. The reaction mixture was stirred for a further 18 h. The solution was concentrated, filtered and stored at –20 °C, affording orange crystals of **10**. Note: these crystals readily desolvate under vacuum to give a yellow powder. Yield = 256 mg, 67 %.

Anal. Calcd. For $C_{62}H_{70}Cl_2N_2P_2PtSiSn$ (1317.96): C 56.50, H 5.35, N 2.13 %. Found: C 56.62, H 5.26, N 2.05 %.

^{1}H NMR (C_6D_6, 400 MHz): δ 7.42 (m, 6H, *o*-CH of PPh_3), 7.36 (d, 4H, *m*-CH of Ar), 7.28 (m, 6H, *o*-CH of PPh_3), 7.21 (t, 2H, *p*-CH of Ar), 6.93-6.74 (m, 12H, *m*-CH of PPh_3), 6.51 (m, 6H, *p*-CH of

PPh_3), 5.05 (br, 2H, CH of ^{i}Pr), 4.64 (br, 2H, CH of ^{i}Pr), 1.81-1.21 (br, 24H, CH_3 of ^{i}Pr), 0.66 (s, 3H, CH_3 of $SiMe_2$), 0.43 (s, 3H, CH_3 of $SiMe_2$)

^{13}C {^{1}H} NMR (C_6D_6, 100 MHz): δ 149.0 (br, *o*-C of Ar), 143.7 (s, *i*-C of Ar), 135.0 (2 x d overlapping, *o*-CH of PPh_3), 133.0 (d, *i*-C of PPh_3), 131.1 (s, *m*-CH of PPh_3), 130.9 (s, *m*-CH of PPh_3), 129.5 (d, *i*-C of PPh_3), 128.1 (s, *m*-CH of PPh_3), 123.9 (s, *m*-CH of Ar), 123.3 (s, *p*-CH of Ar), 27.4 (s, CH of ^{i}Pr), 26.6 (br, CH_3 of ^{i}Pr), 5.0 (s, CH_3 of $SiMe_2$), 4.2 (CH_3 of $SiMe_2$)

^{31}P {^{1}H} NMR (D_6-benzene, 162 MHz): δ 31.7 (d, $^{2}J_{PP}$ = 15 Hz, $^{2}J_{P119Sn}$ = 3522 Hz, $^{2}J_{P117Sn}$ = 3367 Hz, $^{1}J_{PPt}$ = 2597 Hz), 19.9 (d, $^{2}J_{PP}$ = 15 Hz, $^{2}J_{P119Sn}$ = 136 Hz, $^{1}J_{PPt}$ = 3886 Hz

^{119}Sn {^{1}H} NMR (D_6-benzene, 149 MHz): δ -167 (dd, $^{2}J_{SnP}$ = 136 Hz, $^{2}J_{SnP}$ = 3522 Hz, $^{1}J_{SnPt}$ = 15436 Hz)

^{195}Pt {^{1}H} NMR (D_6-benzene, 85 MHz): δ -4695 (dd, $^{1}J_{PtP}$ = 2597 Hz, $^{1}J_{PtP}$ = 3886 Hz)

Synthesis of PtCl(SnCl{(NAr)$_2$SiMe$_2$})(COD) (11)

NMR Scale:

Compound **11** was prepared as for **10**, using $Sn\{NAr^{iPr}\}_2SiMe_2$ (**XLIII**) (19.3 mg, 0.037 mmol) and $PtCl_2$(COD) (13.7 mg, 0.037 mmol). NMR spectra were consistent with PtCl(SnCl{$Me_2Si(NAr)_2$})(COD) (**11**).

^{1}H NMR (D_6-benzene, 400 MHz): δ 7.25 (d, $^{3}J_{HH}$ = 7.1 Hz, 4H, *m*-CH of Ar), 7.12 (t, $^{3}J_{HH}$ = 7.1 Hz, 2H, *p*-CH of Ar), 5.28 (br, $^{2}J_{HPt}$ = 37.0 Hz,2H, CH of COD), 4.85 (br, $^{2}J_{HPt}$ = 67.0 Hz, 2H, CH of COD), 4.65 (sept, 4H, $^{3}J_{HH}$ = 6.8 Hz CH of ^{i}Pr), 1.56 (d, $^{3}J_{HH}$ = 6.7 Hz 12H, CH_3 of ^{i}Pr), 1.49 (d, $^{3}J_{HH}$ = 6.7 Hz, 12H, CH_3 of ^{i}Pr), 1.19 (m, 4H, CH_2 of COD), 0.99 (m, 4H, CH_2 of COD), 0.55 (s, 3H, CH_3 of $SiMe_2$), 0.47 (s, 3H, CH_3 of $SiMe_2$)

^{13}C {^{1}H} NMR (D_6-benzene, 100 MHz): δ 148.1 (s, *o*-C of Ar), 141.7 (s, *i*-C of Ar), 124.4 (s, *m*-CH of Ar), 124.1 (s, *p*-CH of Ar), 121.9 (s, CH of COD), 87.7 (s, CH of COD), 32.0 (s, CH_2 of COD), 27.6

(s, CH_2 of COD), 27.2 (s, CH of ^{i}Pr), 26.6 (br, CH_3 of ^{i}Pr), 4.4 (s, CH_3 of $SiMe_2$), 4.0 (s, CH_3 of $SiMe_2$)

^{119}Sn {^{1}H} NMR (D_6-benzene, 149 MHz): δ -221.7 (s, $^{1}J_{SnPt}$ = 21576 Hz)

^{195}Pt {^{1}H} NMR (D_6-benzene, 85 MHz): δ -3669.3 (s, $^{1}J_{Pt117Sn}$ = 20618 Hz, $^{1}J_{Pt119Sn}$ = 21569 Hz)

Synthesis of [Pt(μ-Cl)(SnCl({NAr^{iPr}}$_2$SiMe$_2$))(PEt$_3$)]$_2$ (12)

NMR Scale:

Compound **12** was prepared as for **10**, using Sn{NAr^{iPr}}$_2$SiMe$_2$ (**XLIII**) (15.4 mg, 0.029 mmol, 2 equiv.) and [PtCl(μ-Cl)(PEt$_3$)]$_2$ (11.5 mg, 0.015 mmol, 1 equiv.). NMR spectra were consistent with [Pt(μ-Cl){(Me$_2$Si{NAr}$_2$)SnCl}(PEt$_3$)]$_2$ (**12**).

^{1}H NMR (D_6-benzene, 400 MHz): δ 7.06 (d, $^{3}J_{HH}$ = 7.5 Hz, 4H, *m*-C_6H_3), 6.97 (t, $^{3}J_{HH}$ = 7.5 Hz, 2H, *p*-C_6H_3), 4.37 (br, 4H, C*H*Me_2), 1.45 (br, 12H, CH*Me*$_2$), 1.37 (d, $^{3}J_{HH}$ = 6.2 Hz 12H, CH*Me*$_2$), 1.11 (m, 6H, PCH_2CH$_3$), 0.73 (s, 3H, Si*Me*$_2$), 0.65 (dt, 9H, $^{3}J_{HH}$ = 7.5 Hz, $^{3}J_{HP}$ = 18.0 Hz, PCH$_2$CH_3), 0.23 (s, 3H, Si*Me*$_2$).

^{31}P{^{1}H} NMR (D_6-benzene, 162 MHz): δ 17.5 (s, $^{2}J_{PSn}$ = 178 Hz, $^{1}J_{PPt}$ = 3761 Hz).

^{119}Sn{^{1}H} NMR (D_6-benzene, 149 MHz): δ -402 (d, $^{2}J_{PSn}$ = 180 Hz, $^{1}J_{SnPt}$ = 26999 Hz).

^{195}Pt{^{1}H} NMR (D_6-benzene, 85 MHz): δ -4058 (d, $^{1}J_{PtP}$ = 3742 Hz).

Synthesis of Pt((SnCl$_2${NAr^{iPr}})$_2$SiMe$_2$)(Sn{NAr^{iPr}}$_2$SiMe$_2$)$_2$ (13)

NMR Scale:

Compound **13** was prepared as for **10**, using Sn{NAr^{iPr}}$_2$SiMe$_2$ (**XLIII**) (81.0 mg, 0.15 mmol, 4 equiv.) and $PtCl_2$ (10.0 mg, 0.038 mmol, 1 equiv.). The sample was heated at 60 °C for 3 days, during which time the product crystallised as red crystals.

Chapter 6: Bis(amido) Complexes of Antimony and Bismuth

6.1 – Introduction

Bismuth stands apart from its neighbouring heavy main group elements in the periodic table, namely Sn, Pb, Sb, Te and Po, in being relatively non-toxic.[156] Indeed, a number of bismuth compounds are used medicinally to treat a range of conditions, key examples being bismuth subsalicylate for the treatment stomach and gasterointestinal complaints, bismuth subgallate as an internal deodorant and bibrocathol for the treatment of eye infections (Figure 6.1).

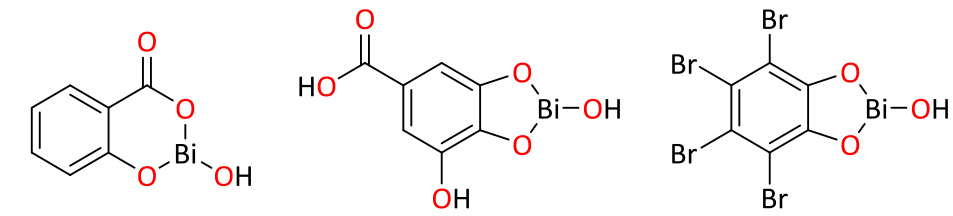

Bismuth Subsalicylate Bismuth Subgallate Bibrocathol

Figure 6.1 – Medicinally important bismuth complexes

The chemistry of bismuth remains relatively neglected in comparison to its lighter group 15 congeners. Despite this, bismuth compounds have been utilised for a number of different chemical processes, in addition to the previously mentioned medicinal applications. In organic synthesis, simple bismuth(III) compounds such as $BiCl_3$, $Bi(NO_3)_3$, $Bi(OTf)_3$ and $Bi(OAc)_3$ have been shown to act as useful catalysts and reagents for a number of transformations, including oxidation and reduction reactions, the removal of protecting groups and C-E bond formation (E = C, N, O).[157] Bismuth has long played an important role in material science, for example in the

development of high temperature superconductors.[158] One of the most well known bismuth compounds is bismuth molybdate, $Bi_2O_3.MoO_3$, used in the SOHIO (Standard Oil of Ohio) process for the oxidation/ammoxidation of propene to make acrolein and acrylonitrile. Bismuth is known to play an integral part in the rate determining and latter steps of this reaction.[159,160] Investigation of this catalytic process prompted the development of molecular organometallic model systems. Hanna *et al*. recently reported the first molecular bismuth system with reactivity similar to that observed in the SOHIO process.[161] They demonstrated that the reaction of $BiCl_3$ with 3 equivalents of $LiOAr^{tBu}$ resulted in the formation of a mixture of organic products (**LXXIV**, **LXXV**, **LXXVI**; Scheme 6.1), bismuth metal and possibly other unidentifiable Bi^{III} products rather than the homoleptic bismuth aryloxide complex, $Bi(OAr^{tBu})_3$. It was concluded that this reactivity showed that bismuth aryloxides can act as one electron oxidising agents, generating Bi^{II} radicals in a similar manner to $Bi_2O_3.MoO_3$ during the oxidation of propene (Scheme 6.1).[159]

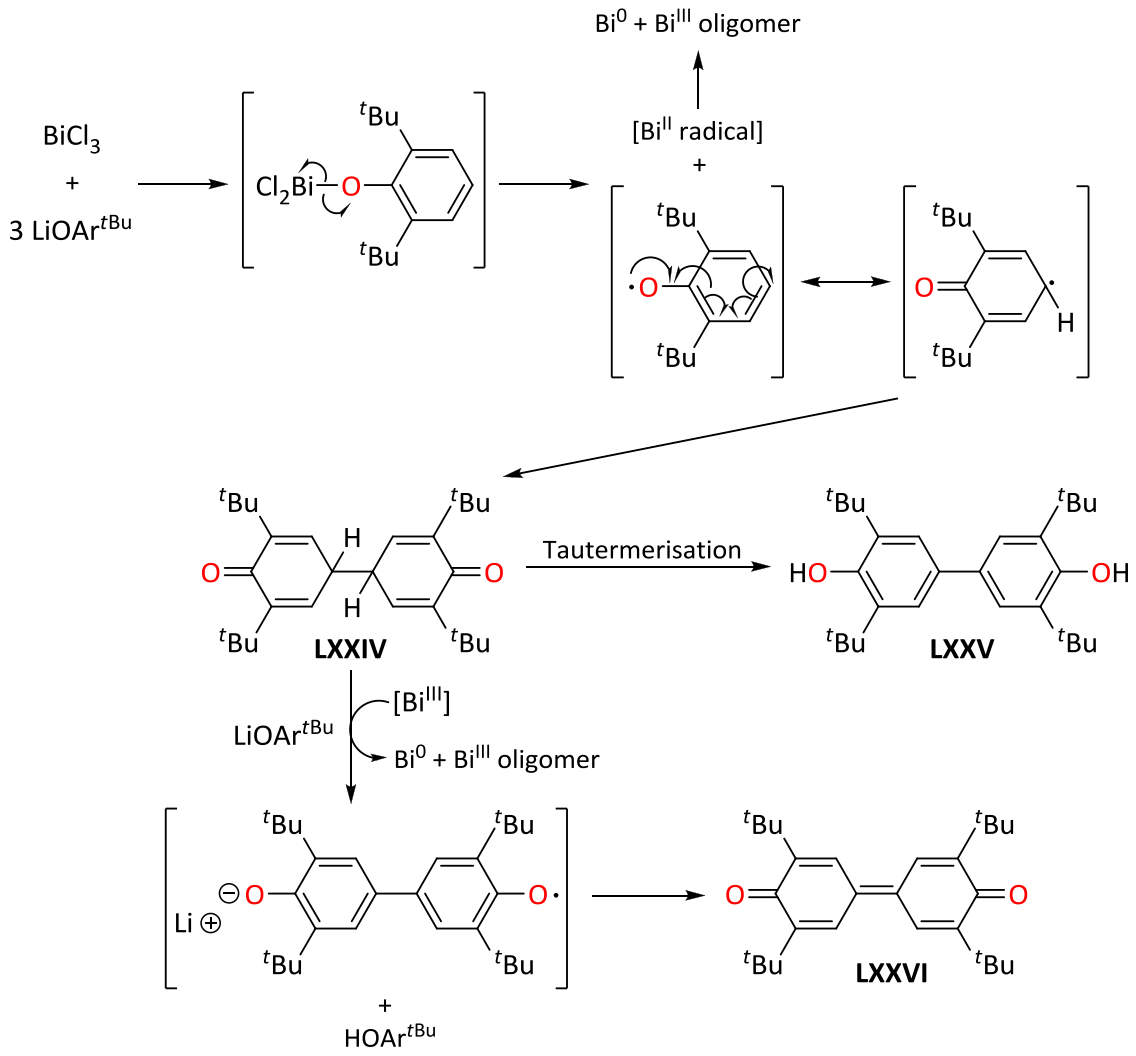

Scheme 6.1 – Hanna *et al.*'s proposed mechanism for the reaction of $BiCl_3$ with $LiOAr^{tBu}$

A recent publication by Evans *et al.* showed that the reaction of $BiCl_2Ar^{NCN}$ (**LXXVII**; Ar^{NCN} is the NCN-pincer ligand [2,6-$(Me_2NCH_2)_2C_6H_3]^-$) with 2 equivalents of $KOAr^{tBu}$ resulted in the formation of the oxyaryl dianion containing $BiAr^{NCN}(C_6H_2$-3,5-^{t}Bu-4-O) (**LXXVIII**), formed *via para* C-H activation of the aryl oxide ring (Scheme 6.2).[162] This is in contrast to the reactions of **LXXVII** with $KOAr^{Me}$ and $KOAr^{iPr}$, which resulted in the expected bis(aryloxide) complexes $BiAr^{NCN}(OAr^{Me})_2$ (**LXXIX**) and $BiAr^{NCN}(OAr^{iPr})_2$ (**LXXX**). It was postulated that the formation of **LXXVIII** proceeded *via* a Bi^{II} radical intermediate in a similar fashion to Hanna *et al.*'s $BiCl_3/LiOAr^{tBu}$ system.

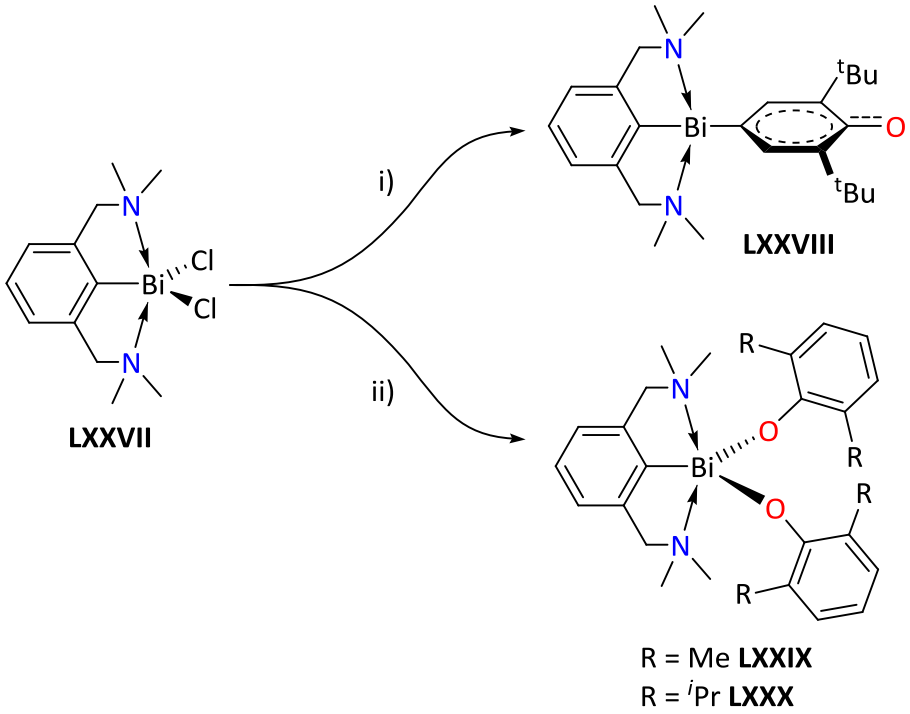

Scheme 6.2 – Reactions of $BiCl_2Ar^{NCN}$ (**LXXVII**) with Li-aryloxides; i) $LiOAr^{tBu}$, ii) $LiOAr^{Me}$ or $LiOAr^{iPr}$

Model systems containing both bismuth and molybdenum are still relatively rare however, where isolated, such systems have been shown to possess interesting C-H bond activation properties. A recent example was reported by Knispel and Limberg who found that while no reaction was observed from the mixing of the tris(amido) bismuth complex $BiL(NMe_2)$ (**LXXXI**; L = 1,8-bis[(trimethylsilyl)amino]naphthalene, $[1,8\text{-}C_{10}H_6(NSiMe_3)_2]^{2-}$), first synthesised by Roesky *et al*. (*vide infra*),[163] with $MoCp_2(O)$, the analogous reaction with $MoCp^{Me}_2(O)$ resulted in C-H activation of the cyclopentadienyl methyl substituent, forming the 'tuck over' complex $[LBi(\mu\text{-}\eta^5{:}\eta^1\text{-}(C_5H_4)CH_2)(\mu\text{-}O)MoCp^{Me}]$ (**LXXXII**; Scheme 6.3).[164]

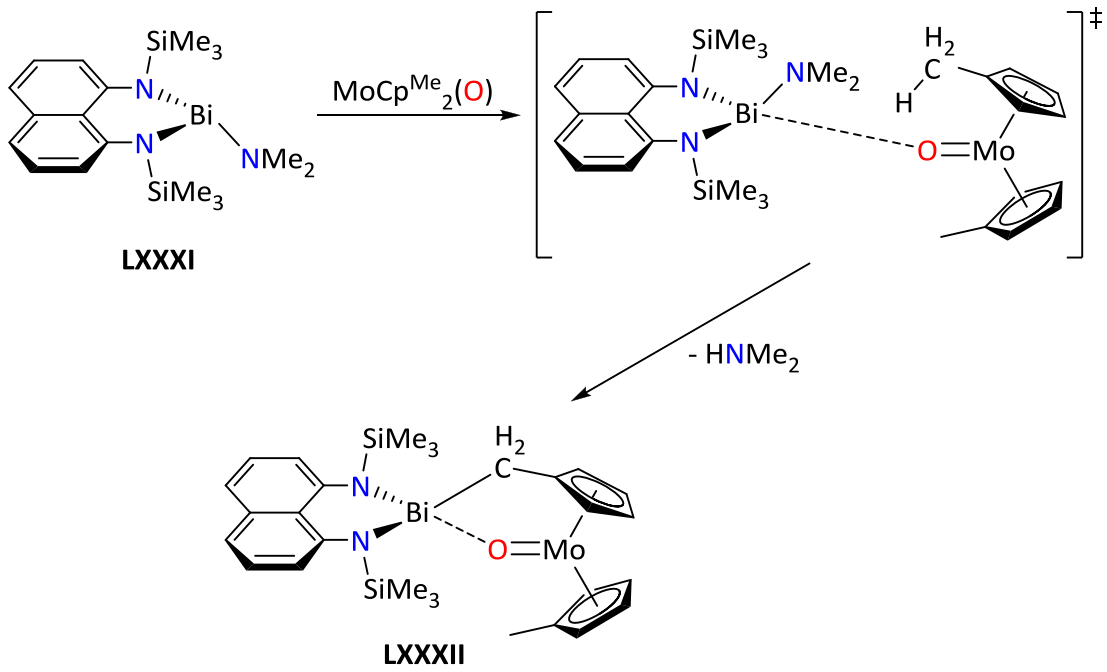

LXXXI **LXXXII**

Scheme 6.3 – Reaction of $BiL(NMe_2)$ (**LXXXI**; L = $[1,8\text{-}C_{10}H_6(NSiMe_3)_2]^{2-}$) with $MoCp_2(O)$

Bismuth (III) amides are relatively rare despite the first examples, $BiMe_n(N\{SiMe_3\}Me)_{3-n}$ (n = 1-2), being reported in 1966.[165] They are often found to be light sensitive, e.g. $Bi(NMe_2)_3$[166,167] and $Bi(N(SiMe_2CHCH_2)_2)_3$,[168] which may be a contributing factor to the lack of examples in the literature. Only a small number of homoleptic bismuth amides, $Bi(NR_2)_3$, have been structurally characterised, the first being $Bi(NPh_2)_3$;[169] other examples include $Bi(NH\{2,4,6\text{-}^tBuC_6H_2\})_3$ and $Bi(N\{SiMe_3\}_2)_3$.[167,168,170,171]

Recently Evans *et al.* found that the reaction of three equivalents of $KN\{SiMe_3\}_2$ with $BiCl_3$ resulted in the formation of the imido complex $[Bi(\mu\text{-}N\{SiMe_3\})(N\{SiMe_3\}_2)]_2$ in addition to the expected homoleptic amide, $Bi(N\{SiMe_3\}_2)_3$; the former is generated from cleavage of a N-Si bond. This kind of reactivity was not unknown for bismuth and the similar imido complexes $[Bi(\mu\text{-}NAr^{iPr})(NHAr^{iPr})]_2$ and $[Bi(\mu\text{-}N^tBu)(Ph)]_2$ have been synthesised from the reactions of $BiCl_3$ with $LiNHAr^{iPr}$ and $BiPhCl_2$ with $LiNH^tBu$ respectively.[172,173]

The aforementioned heteroleptic tris(amdio) complex **LXXXI** was generated *via* the reaction of $Bi(NMe_2)_3$ with 1,8-bis[(trimethylsilyl)amino]naphthalene and was shown by Roesky *et al*. to readily add across the unsaturated bonds of ketones, aldehydes, alkenes and alkynes.[163]

Veith and Bertsch synthesised the cyclic bis(amido)bismuth chloride complex $Bi(\{N^tBu\}_2SiMe_2)Cl$ (**LXXXIII**) in 1988.[174] However, little subsequent work was done using this compound, with the only reported studies being the generation of cationic bismuth complexes $[Bi(\{N^tBu\}_2SiMe_2)][ECl_4]$ from the reaction of **LXXXIII** with ECl_3 (E = Al, Ga or In),[175] and the synthesis of bis(amino)metallabismuthanes $M(Bi(\{N^tBu\}_2SiMe_2))Cp(CO)_n$ (M = Fe (n = 2), Mo or W (n = 3)).[176]

This chapter describes the synthesis of a new derivative of **LXXXIII** and its analogous antimony complex, incorporating bulky aryl substituents at nitrogen. The structural effect of these bulkier groups are discussed in addition to the subsequent synthesis of a heteroleptic tris(amido)bismuth compound and bismuth- and antimony-cyclopentadienyl derivatives.

6.2 – Synthesis of E({NAr^{iPr}}$_2$SiMe$_2$)Cl (E = Sb 14 or Bi 15)

The reaction of the dilithiated bis(amido)silane $Me_2Si(NAr^{iPr}Li)_2$ with one equivalent of ECl_3 (E = Sb or Bi) yields Sb({NAr^{iPr}}$_2$SiMe$_2$)Cl (**14**) and Bi({Ar^{iPr}}$_2$SiMe$_2$)Cl (**15**) as crystalline solids after work up. An insoluble black precipitate was formed during the synthesis of **15**, presumed to be elemental bismuth generated by decomposition of a light sensitive intermediate (once isolated, **15** shows no sign of light sensitivity). Evidence supporting this theory comes from the observation that when the reaction is performed in the absence of light a marked increase in yield is obtained (68 % vs. 30 % under ambient light conditions) with only a small amount of black precipitate evident.

The ^{1}H NMR spectra of **14** displays the Si*Me$_2$* groups of the bis(amide) ligand as two singlets (δ_H 0.01 and 0.63 ppm), consistent with a C_s-symmetric structure derived from a pyramidal geometry at the Sb centre. Broad resonances are observed for the *meta*-protons of the aromatic substituent (δ_H 7.12 ppm) and the isopropyl methyl (δ_H 1.16 and 1.35 ppm) and methine (δ_H 4.04 ppm) protons, implying a fluxional process involving slow rotation of the diisopropylphenyl groups. The *para*-aromatic resonance is a well resolved triplet but overlaps with the residual benzene solvent resonance.

The ^{1}H NMR spectra of **15** also displays the Si*Me$_2$* groups as two singlets (δ_H 0.07 and 0.60 ppm), again indicating a pyramidal geometry at the metal. The *para*-aromatic proton is observed as a triplet (δ_H 6.86 ppm) while the *meta*-aromatic protons (δ_H 7.23 ppm) and isopropyl methyl (δ_H 1.65 and 0.90 ppm) and methine (δ_H 4.41 ppm) protons are again observed as a broad signals.

Compound **15** was studied using variable temperature NMR (VT-NMR) spectroscopy (Figure 6.2). As a D_8-toluene sample of **15** is cooled to -80 °C, the broad isopropyl methyl and methine signals resolve into four doublets and two septets, respectively. Conversely, as the sample is

heated to 110 °C, these signals coalesce to give a single doublet and a single septet. It is also observed that as the temperature is increased, the Si*Me*$_2$ resonances coalesce, resulting in a single broad signal at δ_H 0.32 ppm.

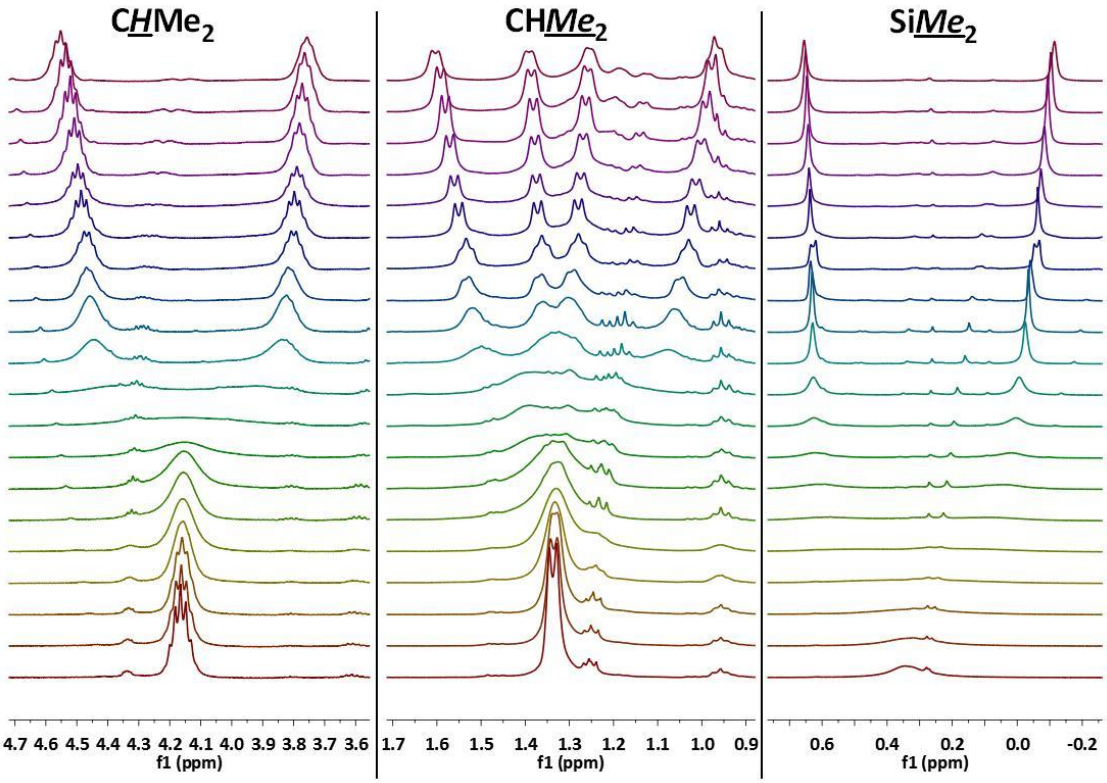

Figure 6.2 – VT NMR spectra of **15**; temperatures range = -80 – 110 °C from top to bottom at 10 °C intervals

The coalescence of the Si*Me*$_2$ resonances is consistent with one or more of the following processes occurring in solution (Scheme 6.3):

(a) Pyramidal inversion of the Bi centre through a trigonal planar transition state;

(b) Ionisation to afford the bismuth cation and re-coordination of the chloride at the opposite face of the metallacycle

(c) An intermolecular chloride transfer process

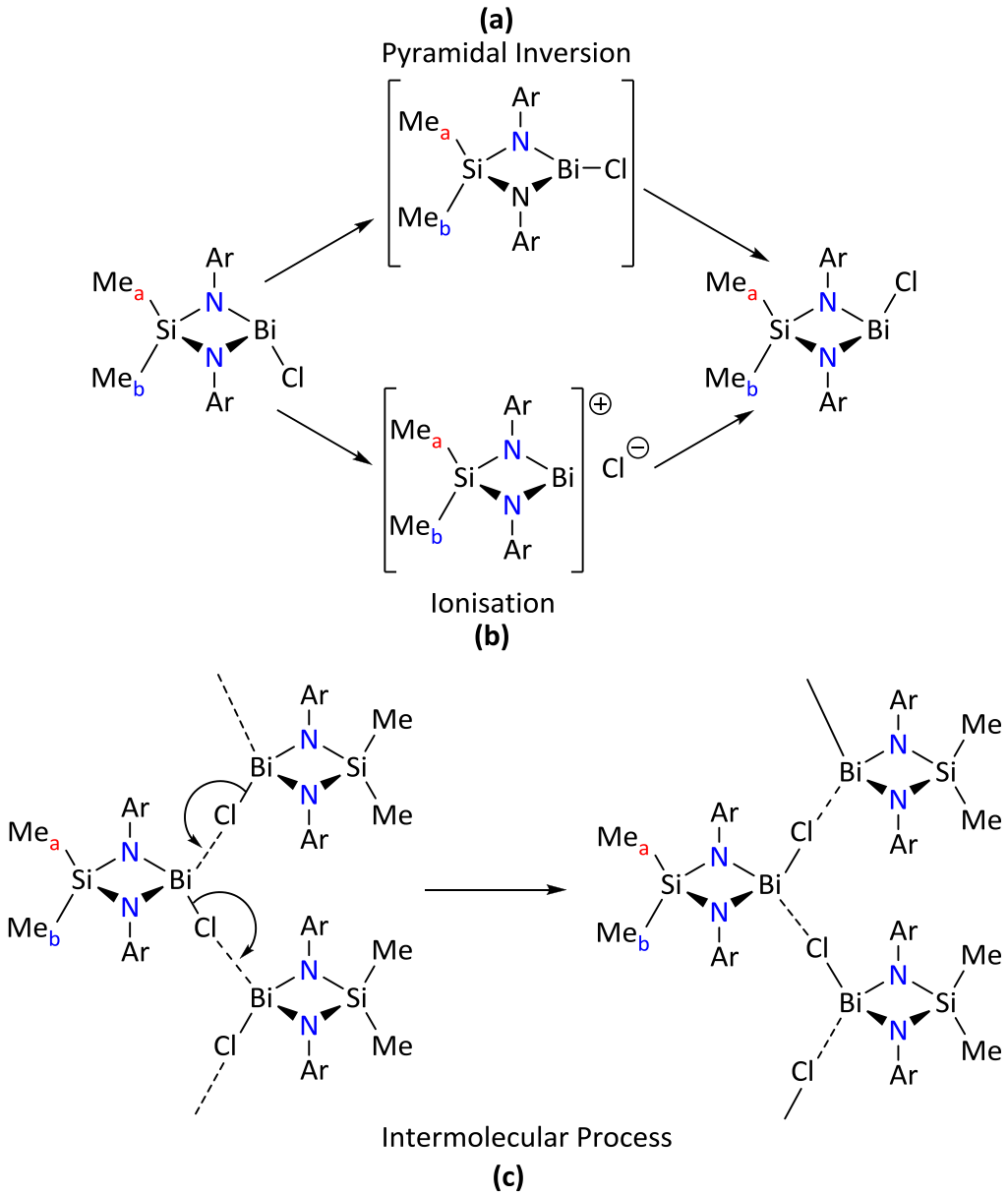

Scheme 6.3 – Possible solution state processes to explain the observation of equivalent Si*Me* protons

These processes would also account for the coalescence of the isopropyl methine signals however at least one additional process must be occur in solution in order to account for the coalescence of the isopropyl methyl signals at high temperature (Scheme 6.4):

(d) Rotation of the N–C_{ipso} bond

(e) Rotation of the C_{ipso}–C_{iPr}

No single process accounts for all the observed changes in the VT-NMR experiments therefore more than one process must be occurring.

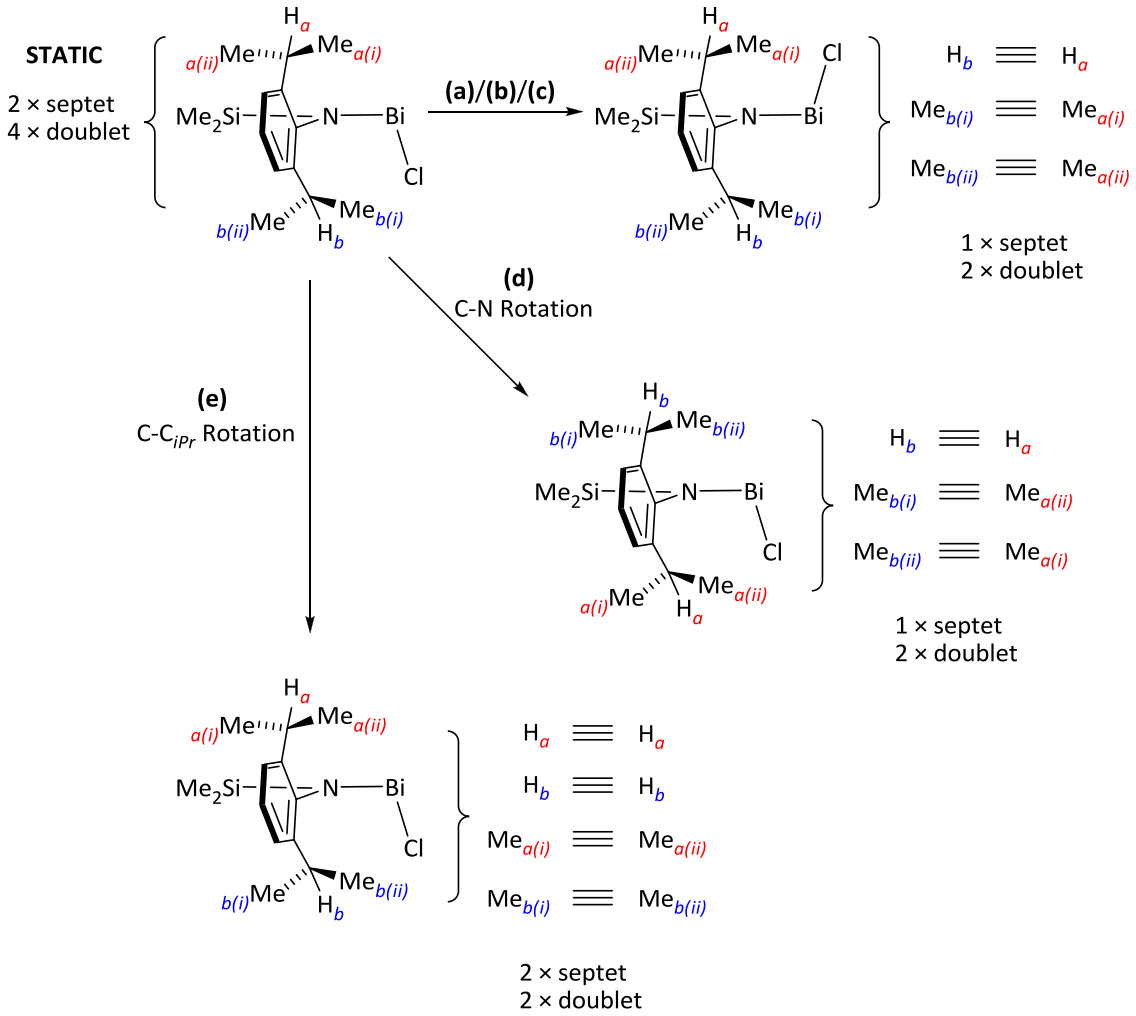

Scheme 6.4 – Hypothesised solution state processes

$$\Delta G‡ = RT_c[22.96 + \ln(T_c/\Delta\upsilon)]$$

Equation 1 – T_c = temperature (K) of coalescence , $\Delta\upsilon$ = maximum separation frequency (Hz)

Equation 1 can be used in conjunction with VT-NMR spectroscopic data to estimate the free energy of solution state fluxional processes. Using the signals for the Si*Me*$_2$, signals the energy is estimated to be, $\Delta G^{‡}$ = 69.8 kJ mol^{-1}, while using the isopropyl methine signals the estimated

energy is $\Delta G^{\ddagger}$ = 59.7 kJ mol^{-1}. However, it should be noted that as both sets of signals not fully separated at -80 °C, the values calculated are higher than the true values for any fluxional process. These data are also complicated by more than one process occurring across this temperature range.

Single crystal X-ray crystallography showed that compound **14** crystallises in the orthorhombic P*na*2_1 space group with the unit cell containing two essentially identical molecules (one of these molecules is shown in Figure 6.3). Unlike the similar compound Sb({N^{t}Bu}$_2$SiMe$_2$)Cl, which exists in the solid state as an extended chain of molecules linked by intermolecular Sb···Cl interactions,[174] compound **14** is monomeric in the solid state. This is likely due to the increase in steric bulk of the Ar^{iPr} groups compared to ^{t}Bu preventing close contacts between molecules. The geometry about the Sb centre is pyramidal [range of angles = 74.72(14)-101.66(11)°]. The bis(amido) ligand chelates to Sb forming a planar four membered SbN_2Si metallacycle [sum of internal angles = 360.0°] with the most acute angle resulting from the N1-Sb1-N2 bite angle (74.72(14)°).

The Sb1-Cl1 bond length of 2.3916(14) Å of **14** is shorter than the equivalent bond distance of Sb(Me$_2$Si{N^{t}Bu}$_2$)Cl (2.472(3) Å) due to the lack of intermolecular interactions. The two Sb1-N bond lengths (2.027(3) Å and 2.027(3) Å for Sb1-N1 and Sb1-N2 respectively) are identical (within 3σ) and are in close agreement to those in Sb(Me$_2$Si{N^{t}Bu}$_2$)Cl (1.995(6) Å). The Si1-N bond lengths only differ slightly (1.751(4) Å and 1.766(4) Å for Si1-N1 and Si1-N2 respectively) and again are close to the Si-N bond lengths of Sb(Me$_2$Si{N^{t}Bu}$_2$)Cl (1.737(6) Å).

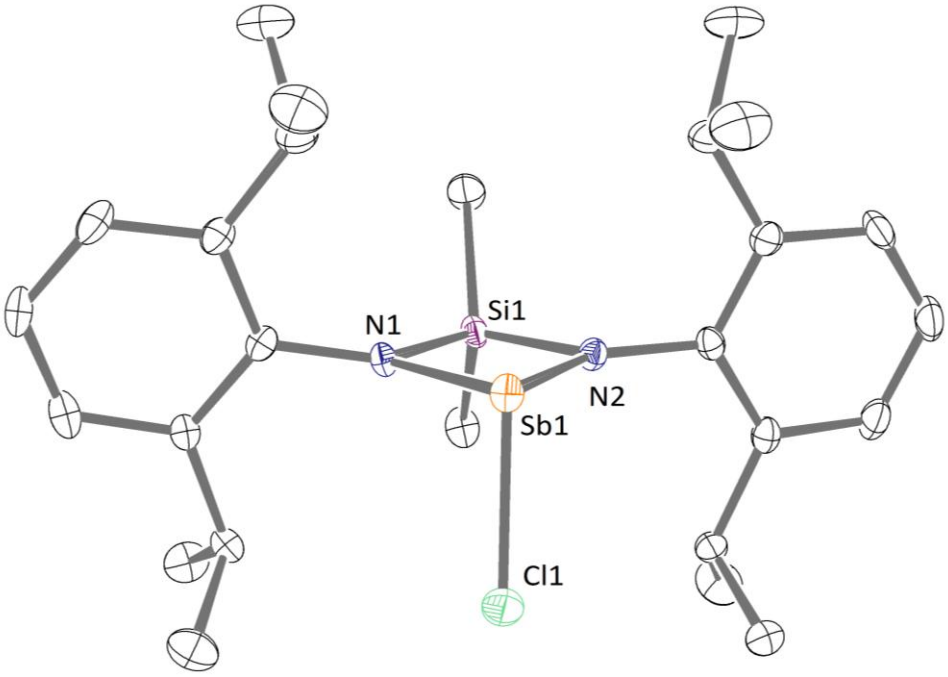

Figure 6.3 – ORTEP representation of Sb({NAr^{iPr}}$_2$SiMe$_2$)Cl (**14**) (with thermal ellipsoids at 30% level), hydrogen atoms omitted for clarity. Selected bond lengths and angles are listed in Table 6.1

Table 6.1 – Selected bond lengths (Å) and angles (°) of 14			
Sb1-Cl1	2.3916(14)	**Si1-N1**	1.751(4)
Sb1-N1	2.027(3)	**Si1-N2**	1.766(4)
Sb1-N2	2.028(3)		
Cl1-Sb1- N1	98.75(13)	**N1-Si1-N2**	88.79(16)
Cl1-Sb1- N2	101.66(11)	**Sb1-N1-Si1**	98.51(15)
N1-Sb1-N2	74.72(14)	**Sb1-N2-Si**	97.98(16)

The compound **15** was shown to crystallise in the orthorhombic *Cmc*2$_1$ space group by single crystal X-ray crystallography, with one full (molecule **A**) and one half molecule (molecule **B**) present in the unit cell. Molecule **B** lies on a mirror plane and the application of the symmetry transformation [-x+1, y, z] generates the remaining half of the molecule as well as a third molecule (**A'**) (Figure 6.4). Short contacts between molecules **A** (and **A'**) and molecule **B** are present:

(i) *via* the chloride ligands Cl1/Cl1′ and Bi2

(ii) η^6-π-aryl interactions between the bismuth atoms Bi1/Bi1′ and the aryl groups on N3/N3′.

The bond lengths and angles do not differ greatly within the different molecules, with the exception of the Bi1-Cl1 and Bi2-Cl2 bond lengths (2.5560(10) Å and 2.4857(16) Å respectively). The longer Bi1-Cl1 lengths are evidence that the perceived Bi2···Cl1 contact is a true intermolecular interaction and not just an artefact of the crystal packing. This is further supported by the Bi2···Cl1 distance of 3.199(1) Å being considerably shorter than the sum of the van der Waals radii of bismuth and chlorine (3.82 Å).[57]

The geometry of the bismuth centres is best described as pyramidal [range of angles = 71.78(11)-97.89(9)° and 70.74(16)-96.39(9)° for Bi1 and Bi2, respectively]. The lone pair on bismuth should be considered to not be stereochemically active owing to the relativistic effects experienced by the heavier main group elements (see Appendix C).

The bis(amide) ligand chelates to Bi forming a BiN_2Si planar metallacycle [sum of internal angles = 359.07° and 359.46°] with the most acute angle resulting from the N-Bi-N bite angle [71.78(11)° and 70.74(16)° for N1-Bi1-N2 and N3-Bi2-N3′ respectively]. The Bi2-N3/N3′ bond length (2.181(3) Å) is slightly longer than Bi1-N1 (2.132(3) Å) and Bi1-N2 (2.144(3) Å), possibly due to the interaction of Bi2 with Cl1/Cl1′.

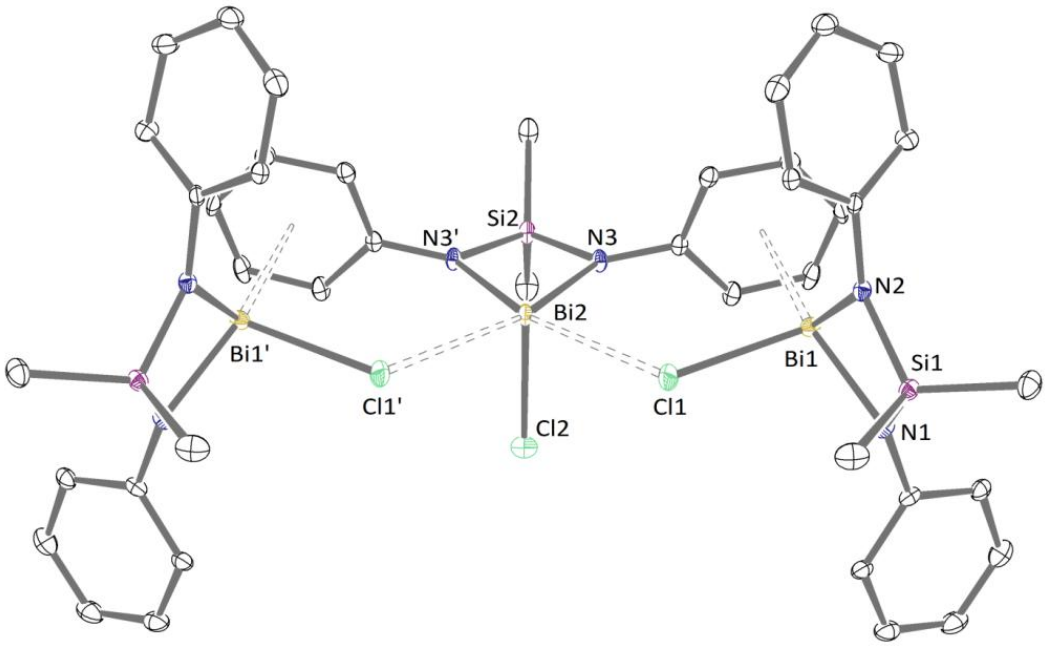

Figure 6.4 – ORTEP representation of Bi({NAr^{iPr}}$_2$SiMe$_2$)Cl (**15**) (with thermal ellipsoids at 30% level), hydrogen atoms and ^{i}Pr groups omitted for clarity. Selected bond lengths and angles are listed in Table 6.1

Table 6.2 – Selected bond lengths (Å) and angles (°) of 15			
Bi1-N1	2.132(3)	**Bi1-Ar Centroid**	3.219(6)
Bi1-N2	2.144(3)	**Bi2···Cl1**	3.199(1)
Bi1-Cl1	2.5560(10)	**Si1-N1**	1.735(3)
Bi2-N3/N3'	2.181(3)	**Si1-N2**	1.7333(3)
Bi2-Cl2	2.4857(16)	**Si2-N3/N3'**	1.736(3)
N1-Bi1-N2	71.78(11)	**Bi1-N1-Si1**	97.54(13)
N1-Bi1-Cl1	97.89(9)	**Bi1-N2-Si1**	97.17(14)
N2-Bi1-Cl1	96.34(9)	**Bi2-N3-Si2**	97.71(14)
N3-Bi2-N3'	70.74(16)	**N1-Si1-N2**	92.58(15)
N3-Bi2-Cl2	96.37(9)	**N3-Si2-N3'**	93.3(2)

The only other example of a bis(amido) bismuth complex, Bi({N^{t}Bu}$_2$SiMe$_2$)Cl (**LXXXIII**; Figure 6.5),[174] differs from **15** by having ^{t}Bu groups at nitrogen. The solid-state structure of this compound consists of an extended chain of molecules, linked by intermolecular Bi···Cl interactions. The distance of these Bi···Cl interactions is 3.047(6) Å, shorter than that observed for the Bi2···Cl1 distance in **15**. The bond lengths and angles within the metallacycle are similar

to those in **15**, with the Bi-N distances (2.124(9) Å) being identical (within 3σ) of Bi1-N1 and Bi1-N2 and slightly shorter than Bi2-N3/N3'. The Si-N bond lengths (1.728(8) Å) are also identical (within 3σ) to the angalogous bonds of **15**, as are the internal angles of the BiN_2Si metallacycle (N-Bi-N = 71.8(4)°, N-Si-N = 92.2(4)°, Si-N-Bi = 98.0(4)°). Comparing **15** and **LXXXIII** illustrates that the use of bulkier nitrogen substituents imparts little effect on the structural parameters of the metallacycle of these two examples. However, it is clear that the degree of association in the solid state is influenced, most likely due to the presence of the aryl groups enabling π-interactions with the bismuth centre.

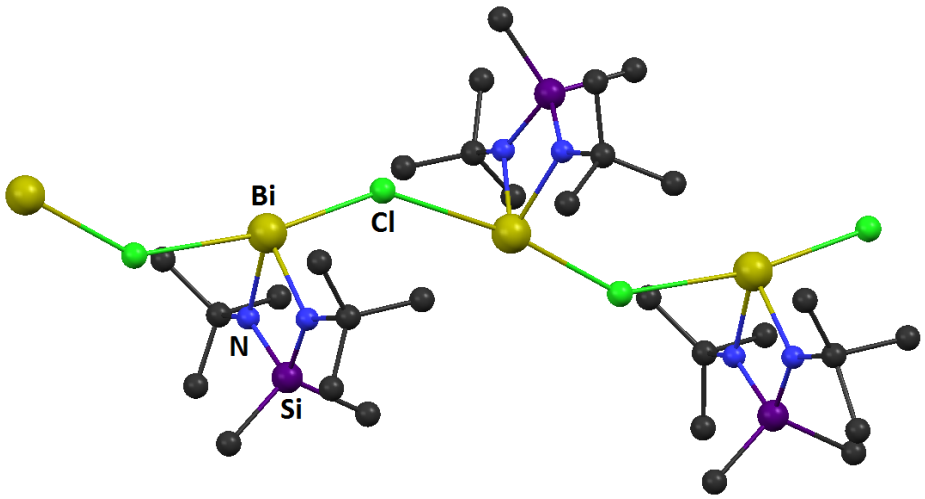

Figure 6.5 – Solid-state structure of $Bi(\{N^tBu\}_2SiMe_2)Cl$ (**LXXXIII**)

6.3 – Reaction of 15 with $AlCl_3$

It was demonstrated by Veith *et al.* that **LXXXIII** reacts with the group 13 chlorides $AlCl_3$, $GaCl_3$ and $InCl_3$ to form formally ionic complexes of the type $[Bi(Me_2Si\{N^tBu\}_2)][ECl_4]$ (E = Al, Ga or In).[175] A solid-state structure was obtained for $[Bi\{N^tBu\}_2SiMe_2][AlCl_4]$ (**LXXXIV**) and, as for **LXXXIII,** a coordination polymer was formed in the solid-state. The structure consists of alternating $[Bi\{N^tBu\}_2SiMe_2]^+$ cations and $[AlCl_4]^-$ anions linked by Bi···Cl interactions (Figure 6.6).

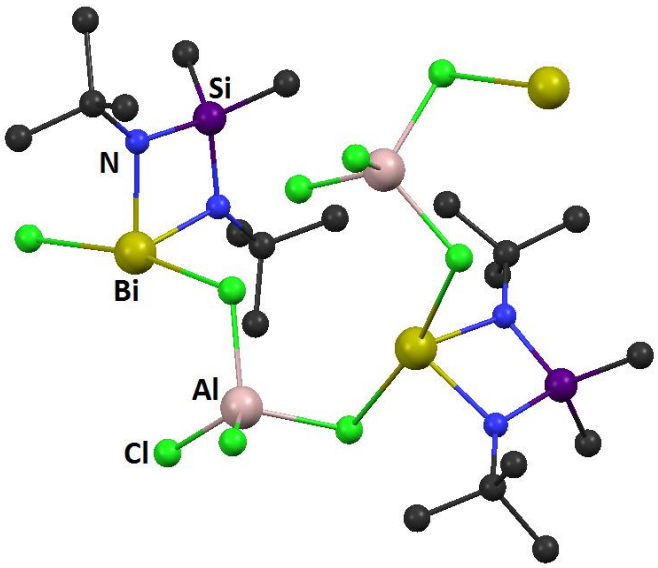

Figure 6.6 – Portion of the solid-state structure of $[Bi\{N^tBu\}_2SiMe_2][AlCl_4]$ (**LXXXIV**)

The reaction of **15** with $AlCl_3$ resulted in a dark red solution from which a small number of dark red crystals were isolated after work up and storage at -20 °C. Unfortunately a clean sample of this product was not be obtained so characterisation by NMR spectroscopy and elemental analysis was not possible; however the solid-state structure was determined by single crystal X-ray crystallography, confirming formation of the expected product, $[Bi\{NAr^{iPr}\}_2SiMe_2][AlCl_4]$ (**16**).

Compound **16** crystallises in the orthorhombic *Pbcn* space group as a dimerised contact ion pair, with two $[AlCl_4]^-$ anions each bridging *via* three of their 4 chloride ligands between two $[Bi\{NAr^{iPr}\}_2SiMe_2]^+$ cations (Figure 6.7). The bond lengths and angles of the $[Bi\{NAr^{iPr}\}_2SiMe_2]^+$ cation do not differ greatly from the corresponding bond lengths and angles of **15** (Table 6.2). The Al-Cl bond lengths of the $[AlCl_4]^-$ moiety are indicative of genuine interactions between the bismuth and chlorine atoms, where the Al-Cl2 distance (2.091(5) Å) is significantly shorter than the other Al-Cl bonds [range = 2.134(4) - 2.172(4) Å]. This is further supported by the Bi···Cl1/Cl3/Cl4 distances [range = 2.953(3) - 3.377(3) Å], which like the intermolecular Bi···Cl distances in **15**, are less than the sum of the van der Waals radii of bismuth and chlorine.[57] The shortest of these distances is the Bi···Cl1 contact and is shorter than the intermolecular Bi···Cl contacts of **15**, probably a result of the electrostatic interactions between the cation and anion.

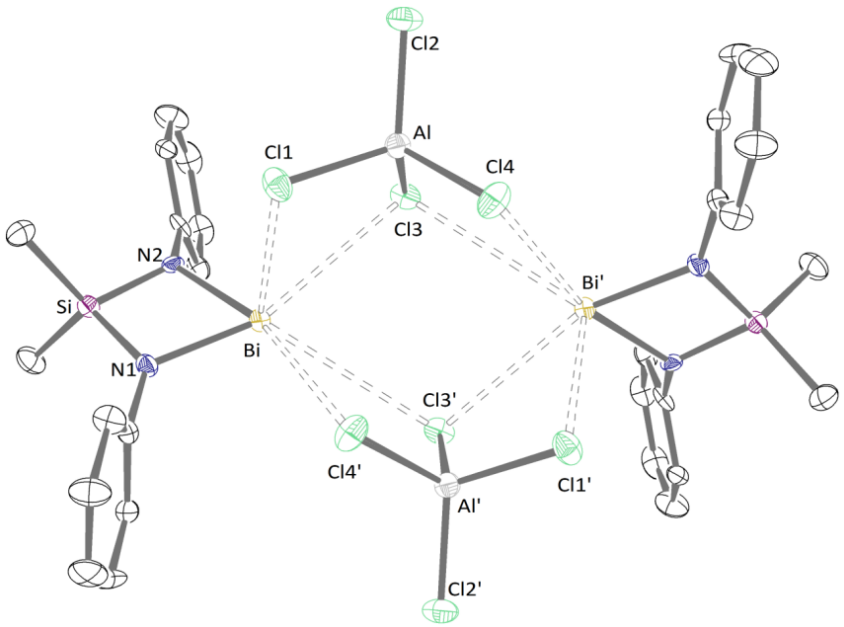

Figure 6.7 – ORTEP representation of $[Bi\{NAr^{iPr}\}_2SiMe_2][AlCl_4]$ (**16**) (with thermal ellipsoids at 30% level), hydrogen atoms and ^{i}Pr groups omitted for clarity. Selected bond lengths and angles are listed in Table 6.3

Table 6.3 – Selected bond lengths (Å) and angles (°) of 16			
Bi-N1	2.118(8)	**Bi···Cl4′**	3.296(3)
Bi-N2	2.120(8)	**Al-Cl1**	2.172(4)
Si1-N1	1.763(9)	**Al-Cl2**	2.091(5)
Si1-N2	1.765(8)	**Al-Cl3**	2.152(4)
Bi···Cl1	2.953(3)	**Al-Cl4**	1.134(4)
Bi···Cl3	3.377(3)		
N1-Bi-N2	73.7(3)	**Cl1-Al-Cl3**	105.03(17)
Bi-N1-Si	97.1(3)	**Cl1-Al-Cl4**	108.44(19)
Bi-N2-Si	97.0(3)	**Cl2-Al-Cl3**	112.91(18)
N1-Si-N2	92.1(4)	**Cl2-Al-Cl4**	107.57(18)
Cl1-Al-Cl2	110.2(2)	**Cl3-Al-Cl4**	107.57(18)

6.4 – Synthesis of Bi({NAr^{iPr}}$_2$SiMe$_2$)(N{SiMe$_3$}$_2$) (17)

The reaction of **15** with LiN{SiMe$_3$}$_2$ results in the formation of the tris(amido) complex Bi({NAr^{iPr}}$_2$SiMe$_2$)(N{SiMe$_3$}$_2$) (**17**), which is isolated as orange crystals.

In the ^{1}H NMR spectrum of **17**, the Si*Me*$_3$ groups of the hexamethyldisilazide ligand are observed as a singlet at δ_H 0.14 ppm while the Si*Me*$_2$ of the bis(amido) ligand are seen as two singlets at δ_H 0.54 and 0.10 ppm, indicating that the pyramidal geometry observed for compound **15** is maintained. Like compound **15**, the *meta* and *para* protons of the aryl groups resonate as a broad signal and a triplet at δ_H 7.19 and 6.90 ppm respectively. The isopropyl methine proton gives rise to a broad signal at δ_H 4.00 ppm while the isopropyl methyl protons are observed as two slightly broadened doublets at δ_H 1.24 and 1.36 ppm.

Complex **17** crystallises in the triclinic $P\bar{1}$ space group as determined by single crystal X-ray diffraction. There are four independent, monomeric molecules in the unit cell that differ in the orientation of the [N{SiMe$_3$}$_2$]$^-$ ligand with respect to the BiN$_2$Si metallacycle formed by the chelating bis(amide) ligand (Figure 6.8). The different orientations are defined by the [Si$_A$···Bi]-[N-Si$_B$] torsion angle θ (Figure 6.9). The values found for this angle in the four molecules are 70.03°, 70.49°, 124.59° and 137.36° for Bi1-Bi4, respectively. A full view of one of the Bi(Me$_2$Si{NAr^{iPr}}$_2$)(N{SiMe$_3$}$_2$) molecules is shown in Figure 6.10.

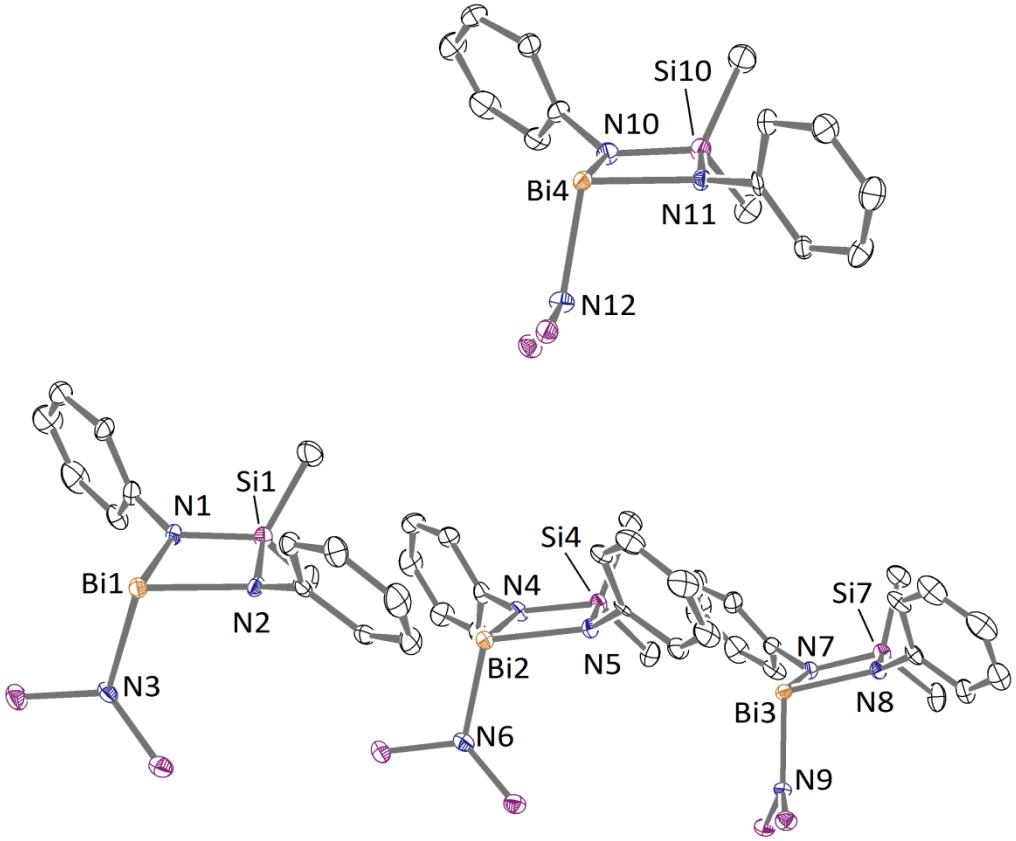

Figure 6.8 – ORTEP representation of the four molecules of Bi({NAr^{iPr}}$_2$SiMe$_2$)(N{SiMe$_3$}$_2$) (**17**) in the unit cell (with thermal ellipsoids at 30% level), hydrogen atoms, isopropyl groups and methyl groups of N{SiMe$_3$}$_2$ omitted for clarity. Selected bond lengths and angles are listed in Table 6.4

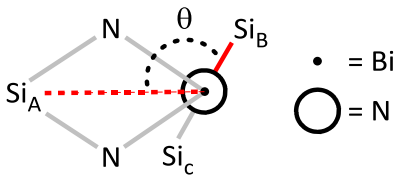

Figure 6.9 – Defining the [Si$_A$···Bi]-[N-Si$_B$] torsion angle θ, viewed looking down the Bi-N{SiMe$_3$}$_2$ bond

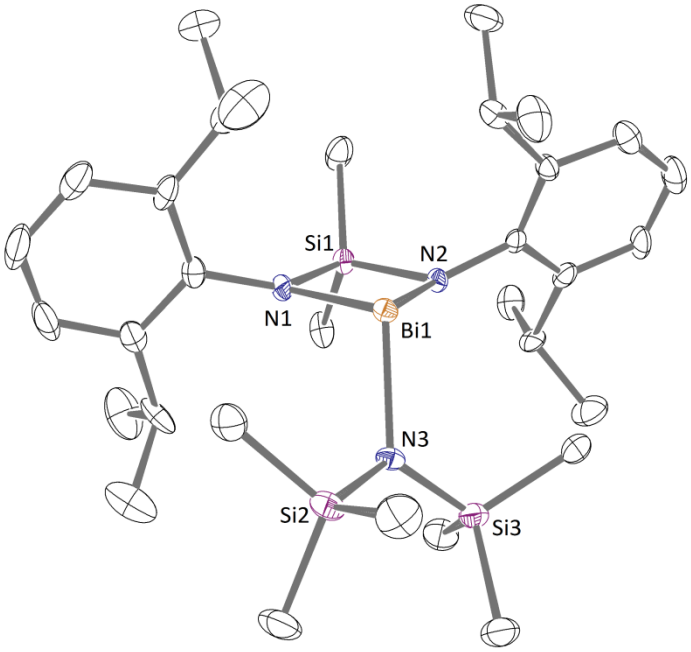

Figure 6.10 – ORTEP representation of one of the four molecules of Bi({NAr^{iPr}}$_2$SiMe$_2$)(N{SiMe$_3$)$_2$) (**17**) in the unit cell (with thermal ellipsoids at 30% level), hydrogen atoms omitted for clarity. Selected bond lengths and angles are listed in Table 6.4

The BiN$_2$Si metallacycles of each molecule have similar bond lengths and angles. The mean bite angle of the chelating bis(amide) ligand is found to be 71.19° [range = 70.90(16)-71.49(15)°] and is comparable to the analogous bite angle of **15**. In each molecule one of the Bi-N bond lengths is slightly longer than the other; the mean distance of the shorter bond is 2.166 Å [range = 2.164(4)-2.170(4) Å] while the mean value of the longer bond is 2.193 Å [range = 2.184(4)-2.201(4) Å]. The nitrogen atom of the longer bond in each molecule has a slightly more pyramidal geometry than that associated with the shorter bond and corresponds to the nitrogen atom that is spatially closest to a silyl group of the [N{SiMe$_3$}$_2$]$^-$ ligand (*i.e.* Si$_C$ in Figure 6.8). The increased pyramidal geometry is most likely caused by steric interactions between the silyl group and aryl substituent on the nitrogen atom. No statistically relevant difference is observed between the Si-N bond lengths, which are all found to be identical (within 3σ).

The Bi-N amide bond lengths are in the range 2.169(5)-2.206(5) Å, and lie at a mean angle of 109.96° from the BiN_2Si metallacycle [range = 108.61-111.61°]. The only other structurally characterised bismuth complexes with terminal Bi-N{$SiMe_3$}$_2$ bonds are Bi(N{$SiMe_3$}$_2$)$_3$, reported by Vehkamäki *et al.*, and [Bi(μ-N{$SiMe_3$})(N{$SiMe_3$}$_2$)]$_2$, reported by Evans *et al.*. The Bi-N{$SiMe_3$}$_2$ bond lengths of the former are found in the range 2.199(8)-2.272(8) Å while for the latter they are found to be 2.2040(19), in close agreement to the mean Bi-N{$SiMe_3$}$_2$ bond length of **17**.

Table 6.4 Selected bond lengths (Å) and angles (°) of 17							
Molecule 1		**Molecule 2**		**Molecule 3**		**Molecule 4**	
Metallacycle							
Bi1-N1	2.165(4)	**Bi2-N4**	2.164(4)	**Bi3-N7**	2.201(4)	**Bi4-N10**	2.196(4)
Bi1-N2	2.190(4)	**Bi2-N5**	2.184(4)	**Bi3-N8**	2.170(4)	**Bi4-N11**	2.165(4)
N1-Si1	1.731(4)	**N4-Si4**	1.737(4)	**N7-Si7**	1.740(4)	**N10-Si10**	1.740(4)
N2-Si1	1.740(4)	**N5-Si4**	1.740(4)	**N8-Si7**	1.733(4)	**N11-Si10**	1.728(4)
N1-Bi1-N2	71.17(15)	**N4-Bi2-N5**	71.49(15)	**N7-Bi3-N8**	71.20(16)	**N10-Bi4-N11**	70.90(16)
N1-Si1-N2	93.8(2)	**N4-Si4-N5**	93.8(2)	**N7-Si7-N8**	94.2(2)	**N10-Si10-N11**	93.7(2)
Bi1-N1-Si1	98.0(2)	**Bi2-N4-Si4**	97.71(19)	**Bi3-N7-Si7**	96.53(19)	**Bi4-N10-Si10**	96.72(19)
Bi1-N2-Si1	96.78(18)	**Bi2-N5-Si4**	96.88(19)	**Bi3-N8-Si7**	97.9(2)	**Bi4-N11-Si10**	98.20(19)
Bi-Amide							
Bi1-N3	2.169(5)	**Bi2-N6**	2.188(5)	**Bi3-N9**	2.185(5)	**Bi4-N12**	2.206(5)
N3-Bi1-N1	103.49(17)	**N6-Bi2-N4**	99.89(17)	**N9-Bi3-N7**	105.47(17)	**N12-Bi4-N10**	109.68(18)
N3-Bi1-N2	105.38(17)	**N6-Bi2-N5**	108.34(17)	**N9-Bi3-N8**	104.02(17)	**N12-Bi4-N11**	100.82(17)

6.5 – Synthesis of Cyclopentadienyl Derivatives of 14 and 15

Cyclopentadienyl complexes of bismuth have been known since the synthesis of $Bi(C_5H_4R)_3$ (R = H or Me) and $Bi(Cp)_2Cl$ by Fischer and Schreiner in 1960.[177] Fischer *et al.* reported that the tris(cyclopentadienyl) complex $Bi(Cp)_3$ (**LXXXV**) exists in two different, temperature dependant crystalline forms; a red form that occurs at temperatures below 15 °C that rapidly coverts to a black form above this temperature.[178] The first structurally characterised bismuth cyclopentadienyl complex was not reported until 1990 when Frank described the structure of the thermolabile and light-sensitive complex $Bi(Cp)Cl_2$ (**LXXXVI**).[179] Although shown to be monomeric in solution, in the solid-state **LXXXVI** formed polymeric $(BiCl_2)_n$ chains with Cp π-bonded to Bi in a mixture of η^2 and η^3 bonding modes (Figure 6.11). The structure of the red form of **LXXXV** was published in 1995 by Lorberth *et al.*, showing that the Cp ligands bond to Bi in an η^1 bonding mode (Figure 6.11).[180] Sitzmann and Wolmershäuser described a number of examples of bismuth halide complexes bearing the sterically crowded cyclopentadienyl derivatives $[^{i}Pr_4C_5H]^-$ and $[1,2,4\text{-}^{t}Bu_3C_5H_2]^-$.[181] The tetraisopropylcyclopentadienyl ligand adopts an η^3 bonding mode in the dimeric chloride and iodide complexes $Bi(^{i}Pr_4C_5H)X_2$ (**LXXXVII**; X = Cl or I), while in the tetra-metallic complex $[Bi_2Cl_5(^{i}Pr_4C_5H)]_2$ (**LXXXVIII**) it adopts an η^5-bonding mode (Figure 6.11). The 1,2,4-tris(tertiarybutyl)cyclopentadienyl ligand is observed to adopt both η^2- and η^3-bonding modes in the bent sandwich complex $Bi(1,2,4\text{-}^{t}Bu_3C_5H_2)_2Cl$ (**LXXXIX**; Figure 6.11). This is in contrast to the bis-Cp* bent sandwich complex $Bi(C_5Me_5)_2Cl$ (**XC**), where the cyclopentadienyl ligand adopts a η^5-bonding mode (Figure 6.11).[182]

It is clear from the examples in Figure 6.9 that Bi exhibits a range of hapticities with different Cp-derivatives. This is in contrast to antimony cyclopentadienyl complexes, for which the vast majority of cases adopt a η^1-bonding mode.

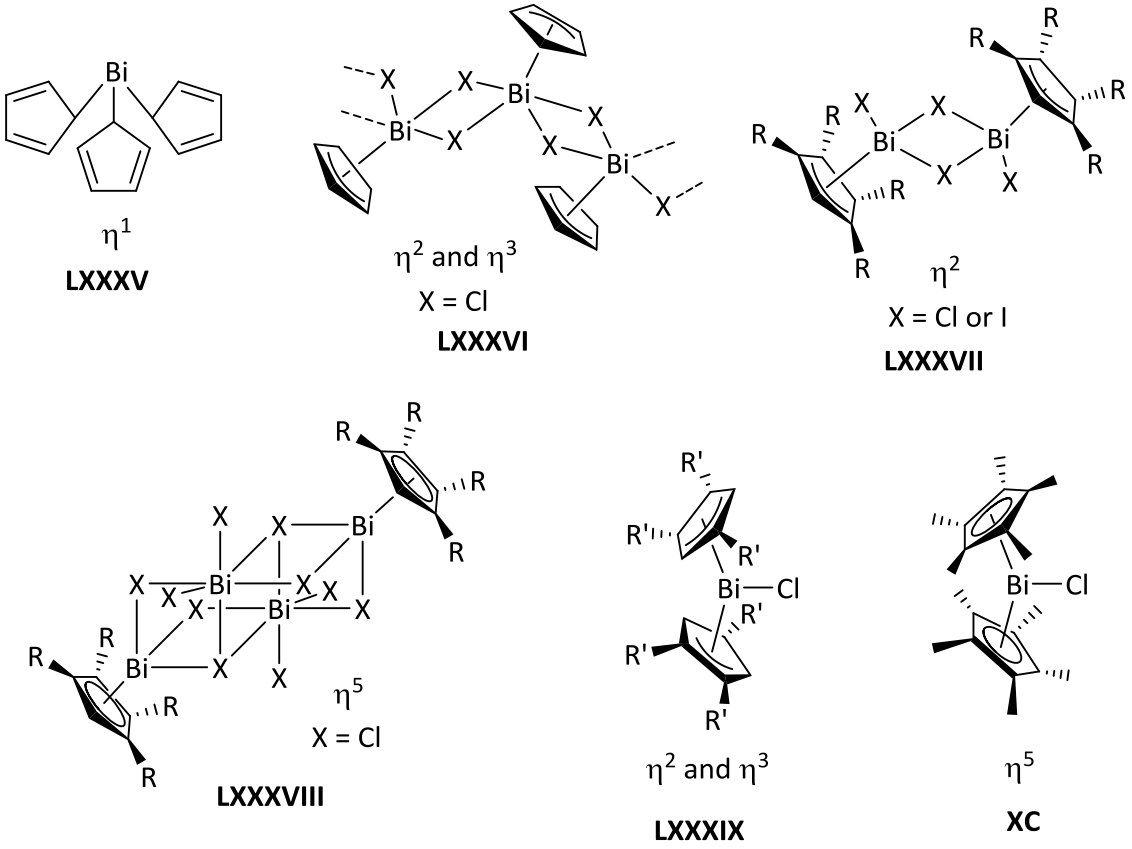

Figure 6.11 – Examples of bismuth cyclopentadienyl complexes (R = ^{i}Pr, R′ = ^{t}Bu)

The reactions of **14** and **15** with LiCp and KCp* resulted in the formation of E({NAr^{iPr}}$_2$SiMe$_2$)Cp (E = Sb, **18**; E = Bi, **19**) and E({NAr^{iPr}}$_2$SiMe$_2$)Cp* (E = Sb, **20**; E = Bi, **21**), respectively (Scheme 6.5). In all cases, the protons associated with the cyclopentadienyl ligands are observed as single resonances in the ^{1}H NMR spectra (δ_H 6.25 **18**, 6.26 **19**, 1.80 **20** and 2.08 **21**), indicating equivalent environments on the NMR timescale. Some interesting differences in the resonances of the bis(amide) ligands are, however, noted.

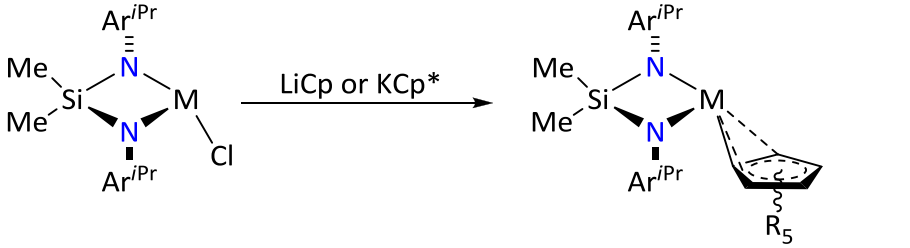

18 M = Sb R = H **20** M = Sb R = Me
19 M = Bi R = H **21** M = Bi R = Me

Scheme 6.5 – Reactions of E({NAr^{iPr}}$_2$SiMe$_2$)Cl (E = Sb **14**, Bi **15**) with LiCp and KCp*

In the ^{1}H NMR spectra of **18**, **19** and **21** at 30 °C in D$_6$-benzene the methine protons give rise to a single, well-resolved septet (δ_H 3.93 **18**, 3.94 **19** and 4.02 **21**) whereas this signal is observed as a broad resonance for **20** (δ_H 4.05 ppm). The isopropyl methyl resonances are observed as two sets of doublets for **18**, **20** and **21** (**18**: δ_H 1.32 and 1.29 ppm, **20**: δ_H 1.41 and 1.29 ppm, **21**: 1.36 and 1.30 ppm) while for compound **19** these protons resonate as one doublet (δ_H 1.29). The methyl protons of the Si*Me$_2$* group are observed as a sharp singlet for **18** (δ_H 0.30 ppm), **19** (δ_H 0.24 ppm) and **21** (δ_H 0.35 ppm) and a single broad resonance for **20** (δ_H 0.41 ppm).

One could infer that the single, sharp Si*Me$_2$* and cyclopentadienyl resonances observed for **18**, **19** and **21** are due to the metal centre adopting a trigonal-planar geometry with a η^5-bound cyclopentadienyl ring. However, this is unlikely given that the broadened SiMe$_2$ signal for **20** implies some fluxional process occurring in solution. It is also important to note that single cyclopentadienyl resonances are commonly observed for complexes that have non-η^5 hapticities in the solid-state, e.g. Bi(^{i}Pr$_4$C$_5$H)Cl$_2$, due to the low energy barrier for haptotropic shifts in solution rendering all proton environments equivalent on the NMR timescale.[183–185]

To investigate the fluxional processes taking place in solution, the Cp* complexes **20** and **21** were studied by variable temperature NMR spectroscopy in D$_8$-toluene. The key data obtained is summarised in Table 6.5.

Table 6.5 – Summary of key NMR data of compounds 18-21				
Compound	**Temp / °C**	**δ_H C*H*Me$_2$**	**δ_H CH*Me$_2$***	**δ_H Si*Me$_3$***
18	30[a]	3.93 (sept)	1.32 (d), 1.29 (d)	0.30 (s)
19	30[a]	3.94 (sept)	1.29 (d)	0.24 (s)
20	-80[b]	4.26 (sept), 3.92 (sept)	1.54 (d), 1.35 (br), 1.31 (br)	0.70 (s), 0.15 (s)
	30[a]	4.05 (br)	1.41 (d), 1.29 (d)	0.41 (br)
	50[b]	4.00 (sept)	1.37 (d), 1.25 (d)	0.39 (s)
21	-80[b]	4.07 (br)	1.39 (br), 1.32 (br)	0.38 (br)
	30[a]	4.02 (sept)	1.36 (d), 1.30 (d)	0.35 (s)

[a] solvent = D_6-benzene; [b] solvent = D_8-toluene

No change in the Cp* methyl resonance is observed when samples of **20** or **21** were cooled to -80 °C, consistent with low energy haptotropic shifts/ring whizzing of the cyclopentadienyl ligand.

As compound **20** was cooled to -80 °C, the broad signals for the $SiMe_2$ and isopropyl methine protons were observed to split into two singlets and two septets respectively (Figure 6.12). As the sample was heated to 50 °C, these signals were resolved as one singlet and one septet. Unlike **15**, the signals are observed to reach their maximum separation within the temperature limits of the NMR experiment. This enables a more accurate calculation of the free energy of the solution state fluxional processes using Equation 1. These are found to be 55.6 kJ mol^{-1} and 54.7 kJ mol^{-1} for the isopropyl methine and $SiMe_3$ resonances respectively. The isopropyl methyl signals, which are resolved as two doublets at 50 °C, broaden and begin to separate as the temperature is decreased, however they do not fully resolve at -80 °C.

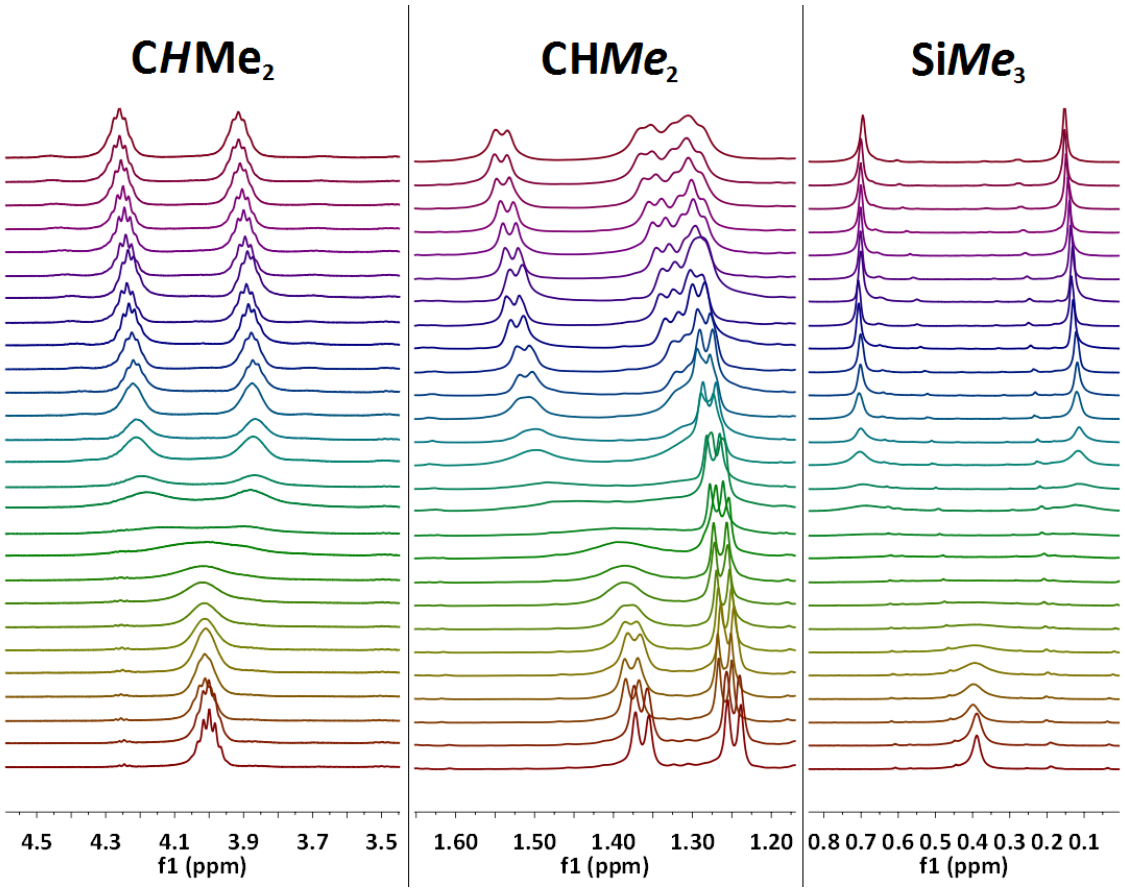

Figure 6.12 – VT NMR spectra of **20**; temperatures range = -80 – 50 °C from top to bottom at 5 °C intervals

The only notable change observed in the VT NMR spectra of **21** is that the $SiMe_2$ and isopropyl signals broaden as the temperature is decreased, with the signals still not separated at -80 °C (Figure 6.13). This implies the fluxional process for **21** are considerably lower energy processes than those of **20**, which is to be expected given that bismuth is much larger than antimony meaning that steric interaction of the ligands is reduced.

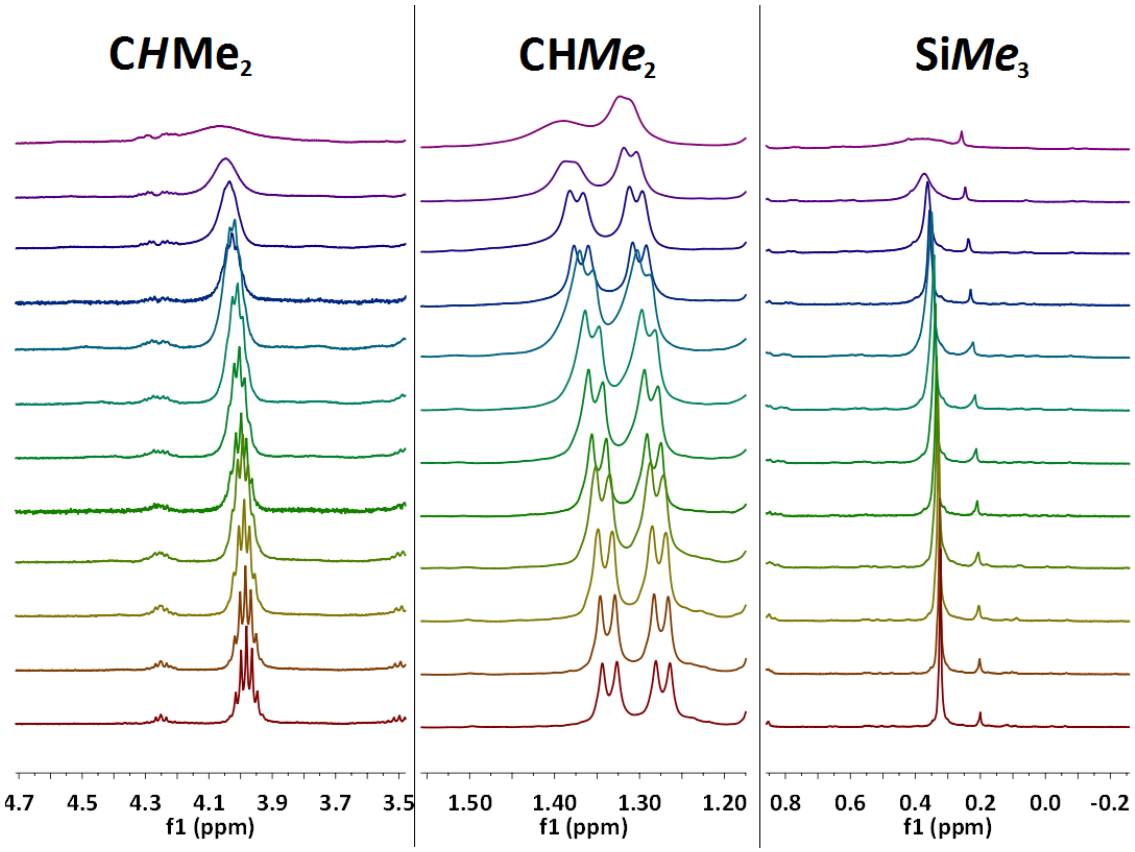

Figure 6.13 – VT NMR spectra of **21**; temperatures range = -80 – 30 °C from top to bottom at 10 °C intervals

These data are reminiscent of the VT-NMR data obtained for compound **15** (*vide supra*) so it is reasonable to believe that the same fluxional processes discussed for **15** are viable for compounds **18**-**21**.

Solid-state structures were obtained for compounds **19**, **20** and **21** from single crystal X-ray diffraction data.

Antimony complex **20** crystallises in the orthorhombic P*nma* space group and lies on a mirror plane (symmetry transformation used to generate equivalent atoms: ' = x, -y+3/2, z; Figure 6.14). The Cp* ligand bonds to antimony in an η^1 fashion (Sb-C15 bond length = 2.281(3) Å) with the C-C bond lengths are consistent with this coordination mode. The C16-C17 bond

length (1.381(3) Å) is considerably shorter than the C15-C6 (1.463(3) Å) and C17-C17′ (1.424(4) Å) bond lengths, indicating localised double bonds in the C16-C17 and C16′-C17′ positions.

The pyramidal geometry around antimony observed for **14** is retained in compound **20**. The longer Sb-N bond lengths (2.09601(16) Å) and more acute bite angle of the bis(amide) ligand (73.36(9)°) relative to compound **14** are consistent with replacing the chloride ligand of **14** with the bulkier Cp* ligand.

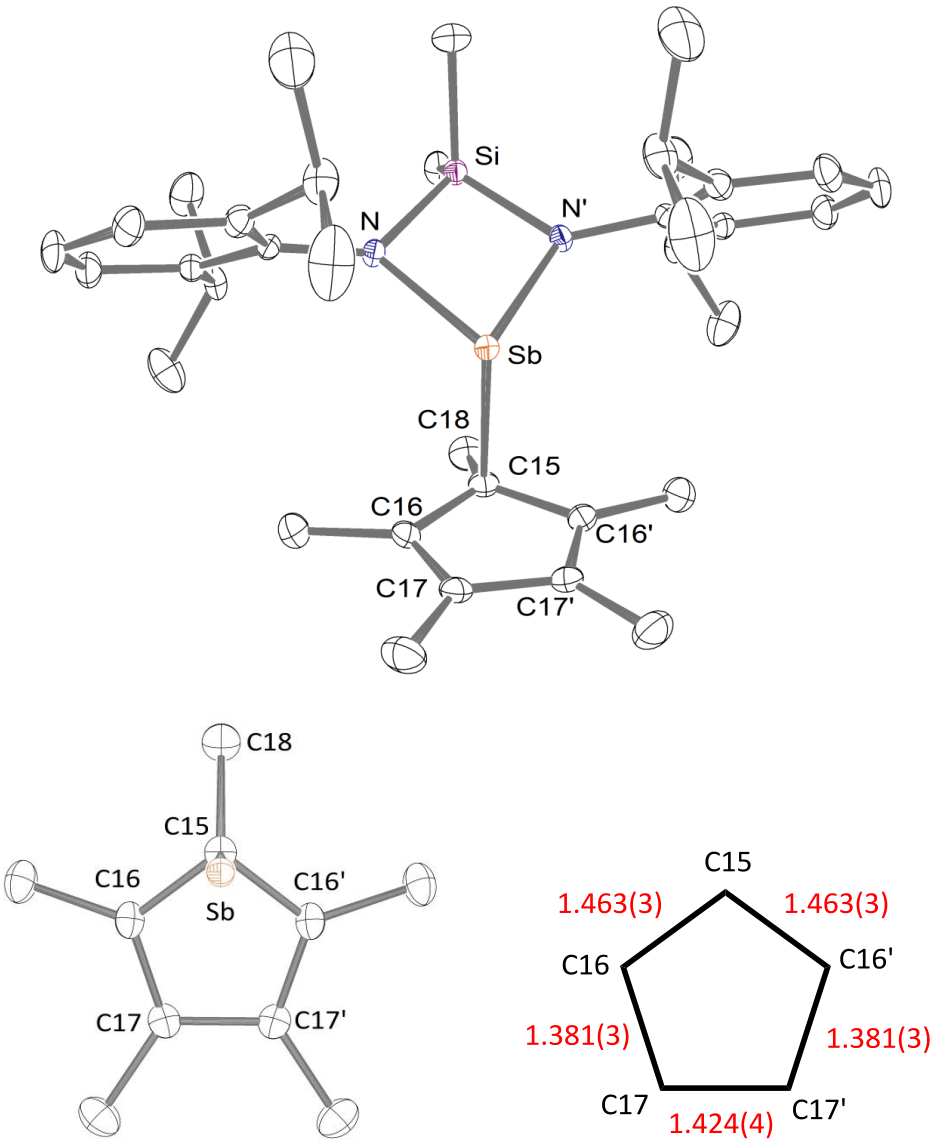

Figure 6.14 – ORTEP representation of Sb({NAr^{iPr}}$_2$SiMe$_2$)Cp* (**20**) and top down view of the Sb-Cp* moiety (with thermal ellipsoids at 30% level), hydrogen atoms omitted for clarity. Selected bond lengths and angles are listed in Table 6.6

Bismuth complexes **19** (Figure 6.16) and **21** (Figure 6.17) both crystallise in the monoclinic $P2_1/c$ space group. It is common for intermolecular Bi···Cp interactions to be observed in the solid state structures of bismuth-cyclopentadienyl complexes, e.g. $BiCp_3$,[180] however no such interactions are observed for **19** or **21**. The N1-Bi-N2 bite angles of the chelating bis(amide) ligand are 70.55(8)° and 70.11(17)° for **19** and **21** respectively. The Bi-N bond lengths of the BiN_2Si metallacycle of **21** (2.204(4) Å and 2.214(4) Å) are longer than those of **19** (2.176(2) Å and 2.180(2) Å), presumably due to the additional bulk and greater electron donating ability of the Cp* ligand.

Examination of the Bi-C bond lengths suggests that the Cp and Cp* ligands of **19** and **21** are coordinated to the bismuth centre in a η^3 bonding mode. In both compounds the Bi–C27 distance (**19** 2.468(3) Å; **21** 2.397(6) Å) is considerably shorter than the Bi–C28/C31 (**19** 2.784(3) / 2.708(3) Å; **19** 2.702(6) / 2.707(6) Å). However inspection of the C-C bond lengths of the cyclopentadienyl rings implies that the nature of this bonding may be more complex. In an ideal η^3 bonding mode, the cyclopentadienyl ring may be described as an allyl-ene (Figure 6.15). This form would have a formal double bond between C29 and C30 and coordinate to bismuth *via* C27, C28 and C31 in a π-allylic fashion. The expected effect of this coordination mode on the C-C bond lengths is that the C27-C28 and C31-C27 bonds should be identical and the C28-C29 and C30-C31 bonds should both be longer than the C27-C28, C31-C27 and C29-C30 bonds.

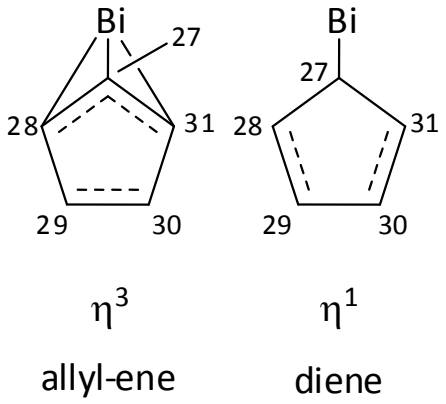

Figure 6.15 – η^3 allyl-ene and η^1 diene bonding of a cyclopentadienyl ligand

The C-C bond lengths of the Cp ligand in **19** are in the range 1.351(5)-1.428(6) Å. The shortest bond is C28-C29 while the next two shortest bonds, C29-C30 (1.385(6) Å) and C30-C31 (1.371(6) Å), are identical (within 3σ). The two longest bonds are C27-C28 (1.412(5) Å) and C31-C27 (1.428(6) Å). These bond lengths are not consistent with the expected trend of bond lengths for a η^3-coordinated Cp ligand and closer resemble the pattern of bond lengths expected for a η^1-coordination in which the Cp ligand is best described as a diene (Figure 6.13).

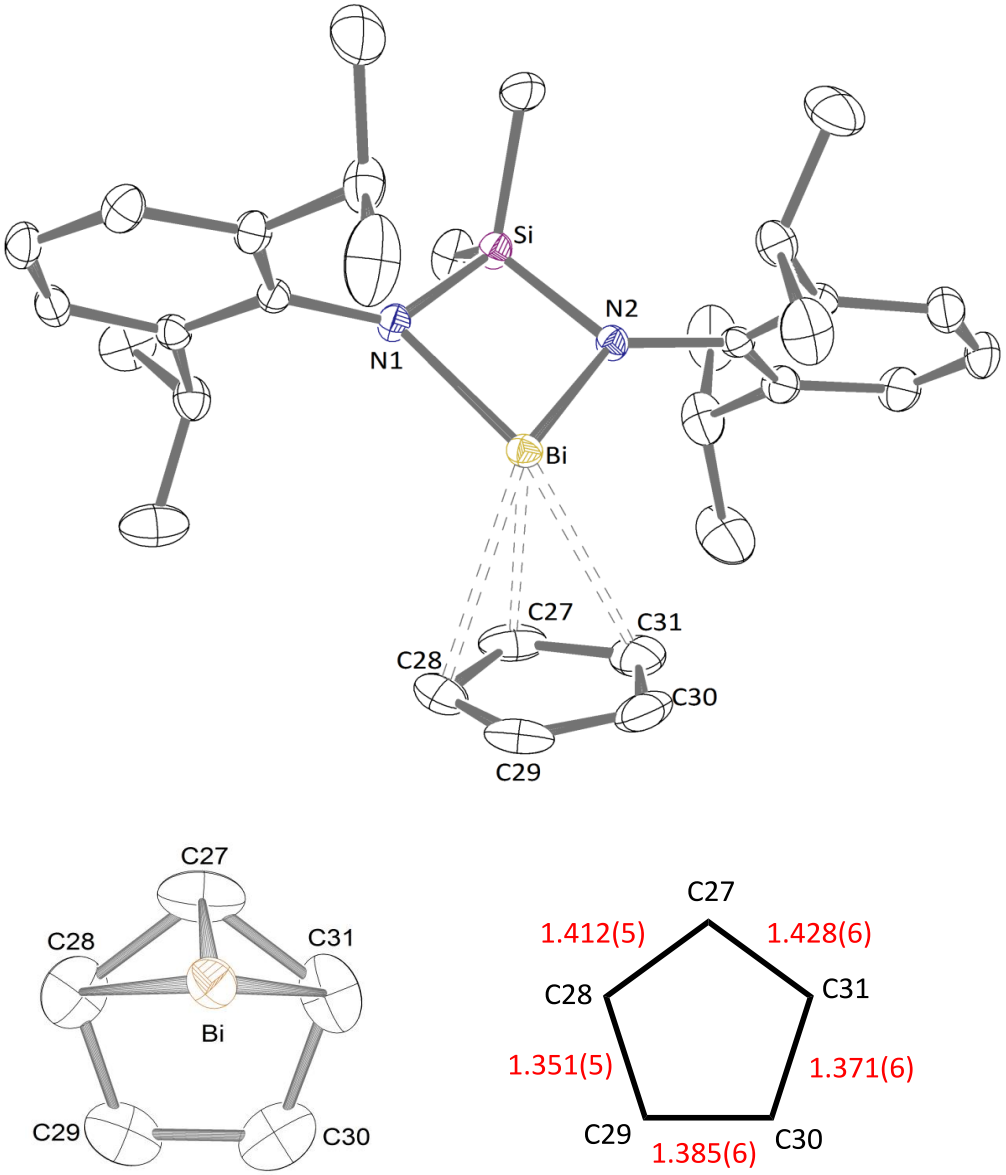

Figure 6.16 – ORTEP representation of Bi({NAr^{iPr}}$_2$SiMe$_2$)Cp (**19**) and top down view of the Bi-Cp moiety (with thermal ellipsoids at 30% level), hydrogen atoms omitted for clarity. Selected bond lengths and angles are listed in Table 6.6

The C-C bond lengths of the Cp* ligand of **21** are found in the range 1.370(9)-1.445(9) Å with each being longer than the corresponding bond of **19**. Again, the shortest bond is C28-C29, the C29-C30 and C30-C31 bonds lengths (1.395(9) Å and 1.403(11) Å, respectively) are identical (within 3σ) and the longest bonds are C27-C28 (1.445(9) Å) and C31-C27 (1.454(10) Å). These bond lengths are again is inconsistent with the expected trend of bond lengths for a η^3-coordinated Cp ligand and a closer resemble a η^1-coordination mode.

The plane of the Cp ligand in **19** is twisted with respect to the BiN_2Si metallacycle, resulting in the Bi-C31 bond length (2.708(3) Å) being shorter than the Bi-C28 length (2.784(3) Å). This twist is not observed with the Cp* ligand of **21** where the Bi-C31 and Bi-C28 bond lengths are identical (within 3σ) and are comparable with the Bi-C31 distance of **19**.

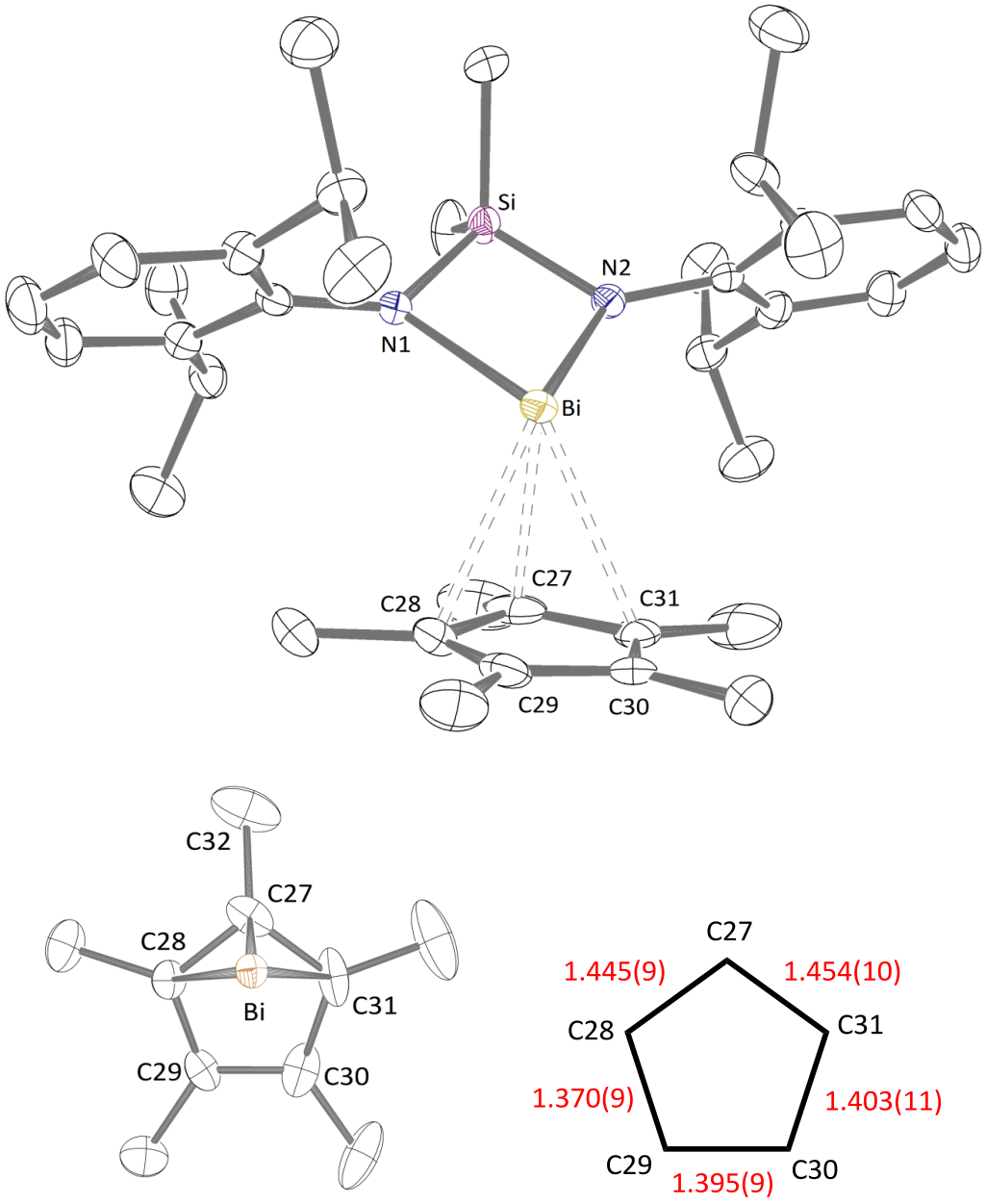

Figure 6.17 – ORTEP representation of Bi({NAr^{iPr}}$_2$$SiMe_2$)Cp* (**21**) and top down view of the Bi-Cp* moiety (with thermal ellipsoids at 30% level), hydrogen atoms omitted for clarity. Selected bond lengths and angles are listed in Table 6.6

Clearly the description of these systems as classic η^1- or η^3-bonding does not fit the data. It appears that the large bismuth centre allows the cyclopentadienyl rings to slip around to adopt the most favorable orientation for efficient crystal packing in the solid state.

Table 6.6 – Selected bond lengths (Å) and angles (°) of 19, 20 and 21

19	**Bi-N1**	2.180(2)	**Bi-C28**	2.784(3)	**N2-Si**	1.729(2)	**C29-C30**	1.385(6)
	Bi-N2	2.176(2)	**Bi-C31**	2.708(3)	**C27-C28**	1.412(5)	**C30-C31**	1.371(6)
	Bi-C27	2.468(3)	**N1-Si**	1.728(2)	**C28-C29**	1.351(5)	**C31-C27**	1.428(6)
	N1-Bi-N2	70.55(8)	**N1-Bi-C31**	136.99(11)	**N2-Bi-C31**	93.18(10)	**Bi-N1-Si**	97.74(10)
	N1-Bi-C27	110.23(11)	**N2-Bi-C27**	99.89(11)	**N1-Si-N2**	93.37(11)	**Bi-N2-Si**	97.85(9)
	N1-Bi-C28	112.91	**N2-Bi-C28**	130.11(10)				
20	**Sb-N**	2.09601(16)	**N-Si**	1.7347(17)	**C16-C17**	1.381(3)	**C17-C17′**	1.424(4)
	Sb-C15	2.281(3)	**C15-C16**	1.463(3)				
	N-Sb-N′	73.36(9)	**Sb-C15-C16**	89.11(14)	**Sb-C15-C18**	113.8(2)	**N-Si-N′**	92.39(11)
	N-Sb-C15	103.22(7)						
21	**Bi-N1**	2.204(4)	**Bi-C28**	2.702(6)	**N2-Si**	1.733(5)	**C29-C30**	1.395(9)
	Bi-N2	2.214(4)	**Bi-C31**	2.707(6)	**C27-C28**	1.445(9)	**C30-C31**	1.403(11)
	Bi-C27	2.397(6)	**N1-Si**	1.729(5)	**C28-C29**	1.370(9)	**C31-C27**	1.454(10)
	N1-Bi-N2	70.11(17)	**N1-Bi-C31**	133.7(2)	**N2-Bi-C31**	104.3(2)	**Bi-N1-Si**	97.1(2)
	N1-Bi-C27	102.9(2)	**N2-Bi-C27**	105.9(2)	**N1-Si-N2**	94.3(2)	**Bi-N2-Si**	96.7(2)
	N1-Bi-C28	100.82(18)	**N2-Bi-C28**	136.15(19)				

6.6 – Summary

The bis(amido) silane complexes Sb({NAr^{iPr}}$_2$SiMe$_2$)Cl (**14**) and Bi({NAr^{iPr}}$_2$SiMe$_2$)Cl (**15**) have been synthesised from the reaction of Me$_2$Si{NAr^{iPr}Li}$_2$ with SbCl$_3$ and BiCl$_3$, respectively. The synthesis of compound **15** is found to be sensitive to light, with a marked increase in the yield of **15** obtained when the reaction is performed in the absence of light. The reaction of **15** with AlCl$_3$ forms the ionic complex [Bi{NAr^{iPr}}$_2$SiMe$_2$][AlCl$_4$] (**16**) which is found to exist a dimeric contact ion pair in the solid state.

The chloride functionality of **14** and **15** enables facile derivitisation using alkali metal salts exemplified by the synthesis of the tris(amido) compound Bi({NAr^{iPr}}$_2$SiMe$_2$)(N{SiMe$_3$}$_2$) (**17**), *via* the reaction of **15** with LiN{SiMe$_3$}$_2$, and the synthesis of the cyclopentadienyl compounds E({NAr^{iPr}}$_2$SiMe$_2$)Cp (E = Sb **18**, Bi **19**) and E({NAr^{iPr}}$_2$SiMe$_2$)Cp* (E = Sb **20**, Bi **21**) *via* the reaction of **14** and **15** with LiCp and KCp* respectively. While the solid state structure of compound **20** unambiguously shows the Cp ligand to bond in an η^1 fashion to antimony, the hapticity of the cyclopentadienyl ligands in bismuth compounds **19** and **21** is much less well defined.

6.7 – Experimental Procedures for Chapter 6

General Information

$BiCl_3$, $SbCl_3$, $AlCl_3$ and $LiN\{SiMe_3\}_2$ were purchased from Sigma Aldrich and were used without any further purification following being transferred in to the glovebox. $Me_2Si(NAr^{iPr}Li)_2$ was prepared following literature procedures.[55] LiCp and KCp*were donated by the Cloke group.

For all other general experimental procedure see Appendix A.

Synthesis of Sb({NAr^{iPr}}$_2$SiMe$_2$)Cl (14)

A thf solution of $Me_2Si(NAr^{iPr}Li)_2$ (500 mg, 1.2 mmol, 1 equiv.) was added dropwise to a thf solution of $SbCl_3$ (224 mg, 1.2 mmol, 1 equiv.) at -78 °C. The resultant solution was left to stir for 3 h while warming to ambient temperature before removal volatiles *in vacuo*, leaving an off white solid from which the product was extracted in hexane. This solution was concentrated and stored at -20 °C for 24 h, resulting in the formation of colourless crystals of **14**. Yield = 0.550 g, 80.1 %.

Anal. calcd. for $C_{26}H_{40}N_2SbCl$ (565.9): C, 55.18 %; H, 7.12 %; N, 4.95 %. Found: C, 55.32; H, 7.16; N, 4.90 %.

^{1}H NMR (D_6-benzene, 500 MHz): δ 7.12 (br, 4H, *m*-C*H*), 7.07 (t, $^3J_{HH}$ = 7.5 Hz, 2H, *p*-C*H*), 4.03 (br, 4H, ^{i}Pr-C*H*), 1.35 (br, 12H, ^{i}Pr-CH_3) 1.16 (br, 12H, ^{i}Pr-CH_3), 0.63 (s, 3H, SiCH_3), 0.01 (s, 3H, SiCH_3)

^{13}C {^{1}H} NMR (D_6-benzene, 125 MHz): δ *,138.1 (*i*-*C*), 125.6 (*p*-*C*H), 124.1 (br, *m*-*C*H), 28.2 (^{i}Pr-*C*H), 26.2 (br, ^{i}Pr-*C*H_3), 7.9 (Si*C*H_3), 2.6 (Si*C*H_3)

* *o*-C not observed

Synthesis of Bi({NAr^{iPr}}$_2$SiMe$_2$)Cl (15)

A thf solution of $Me_2Si(NAr^{iPr}Li)_2$ (750 mg, 1.8 mmol, 1 equiv.) was added dropwise to a thf solution of $BiCl_3$ (568 mg, 1.8 mmol, 1 equiv.) in the absence of light at -78 °C. The resultant

solution was left to stir for 18 h while warming to ambient temperature. Removal of volatiles *in vacuo* followed by washing with toluene resulted in an orange solution. Concentration of this solution followed by storage at -20 °C resulted in the formation of orange crystals of **15**. Yield = 0.800 g, 68.0 %.

Anal. calcd. for $C_{26}H_{40}N_2BiCl$ (653.1): C, 47.81 %; H, 6.17 %; N, 4.29 %. Found: C, 47.69; H, 6.27; N, 4.17 %.

^{1}H NMR (D_6-benzene, 500 MHz): *δ* 7.23 (br, 4H, *m*-C*H*), 6.86 (t, $^3J_{HH}$ = 7.6 Hz, 2H, *p*-C*H*), 4.41 (br, 2H, ^{i}Pr-C*H*), 3.79 (br, 2H, ^{i}Pr-C*H*), 1.65-0.90 (br, 24H, ^{i}Pr-CH_3), 0.60 (s, 3H, Si*Me*), 0.07 (s, 3H, Si*Me*)

^{13}C {^{1}H} NMR (D_6-benzene, 100 MHz): *δ* *, 137.7 (*i*-*C*), 126.3 (*p*-*C*H), 27.4 (^{i}Pr-*C*H_3), 12.23 (Si*Me*), 7.15 (Si*Me*)

* *o*-*C*, *m*-*C*H and ^{i}Pr-*C*H not observed

Synthesis of [Bi{NAr^{iPr}}$_2$SiMe$_2$][AlCl$_4$] (16)

A toluene solution of **15** (250 mg, 0.38 mmol, 1 equiv.) was added rapidly to a suspension of $AlCl_3$ (51 mg, 0.38 mmol, 1 equiv.) in toluene. The resultant dark red solution was left to stir for 4 h after which time the solution was then filtered and concentrated. A small number of tiny red crystals of **16** were deposited following storage at -20 °C for 7 days.

Synthesis of Bi({NAr^{iPr}}$_2$SiMe$_2$)(N{SiMe$_3$}$_2$) (17)

A solution of LiN{$SiMe_3$}$_2$ (100 mg, 0.60 mmol, 1 equiv.) in toluene was added dropwise to a toluene solution of **15** (395 mg, 0.60 mmol, 1 equiv.) cooled to -78 °C. The resultant yellow solution was allowed to warm slowly to ambient temperature and left to stir for 24 h, by which time the solution had turned orange and a white precipitate had formed. The solution was filtered and concentrated until small amounts of an orange solid precipitated out of solution.

The solution was then warmed to redissolve the solid and slow cooling to ambient temperature yielded orange crystals of **17**. Yield = 0.312 g, 66.8 %.

Anal. calcd. for $C_{32}H_{58}N_3SiBi$ (778.1): C, 49.40 %; H, 7.51 %; N, 5.40 %. Found: C, 49.25 %; H, 7.60 %; N, 5.31 %.

^{1}H NMR (D_6-benzene, 400 MHz): δ 7.19 (br, 4H, *m*-C*H*), 6.90 (t, $^3J_{HH}$ = 7.4 Hz, 2H, *p*-C*H*), 4.00 (br, 4H, ^{i}Pr-C*H*), 1.36 (br, 12H, ^{i}Pr-C*H*$_3$), 1.24 (d, $^3J_{HH}$ = 6.5 Hz, 12H, ^{i}Pr-C*H*$_3$), 0.54 (s, 3H, Si*Me*), 0.14 (s, 18H, N{Si*Me*$_3$}$_2$, 0.10 (s, 3H, Si*Me*)

^{13}C {^{1}H} NMR (D_6-benzene, 100 MHz): δ 139.9 (*i-C*), 124.7 (*p-C*H), 123.7 (*m-C*H), 27.4 (^{i}Pr-*C*H$_3$), 25.7 (^{i}Pr-*C*H$_3$), 16.2 (Si*Me*), 5.9 (N{Si*Me*$_3$}$_2$), 3.0 (Si*Me*) *

* ^{i}Pr-*C*H not observed

Synthesis of Sb({NAr^{iPr}}$_2$SiMe$_2$)Cp (18)

A D_6-benzene solution of **14** (112 mg, 0.21 mmol, 1 equiv.) was added to a suspension of LiCp (15 mg, 0.21 mmol, 1 equiv.) in D_6-benzene. The resultant solution was stirred for 5 h before being filtered. Analysis of the filtrate by ^{1}H NMR spectroscopy indicated complete consumption of **14** with proton resonances consistent with the formation of **18**.

^{1}H NMR (D_6-benzene, 400 MHz): δ 7.17 (*,4H, *m*-C*H*), 7.08 (t, $^3J_{HH}$ = 7.5 Hz, 2H, *p*-C*H*), 6.26 (s, 5H, C_5H_5), 3.93 (sept, $^3J_{HH}$ = 6.9 Hz, 4H, ^{i}Pr-C*H*), 1.32 (d, $^3J_{HH}$ = 6.8 Hz, 12H, ^{i}Pr-C*H*$_3$), 1.29 (d, $^3J_{HH}$ = 6.8 Hz, 12H, ^{i}Pr-C*H*$_3$), 0.30 (s, 6H, Si*Me*$_2$)

* partially obscured by solvent peak

^{13}C {^{1}H} NMR (D_6-benzene, 100 MHz): δ 146.4 (*o-C*), 138.8 (*i-C*), 124.3 (*p-C*H), 123.7 (*m-C*H), 114.3 (C_5H_5), 27.7 (^{i}Pr-*C*H), 25.8 (^{i}Pr-*C*H$_3$), 25.0 (^{i}Pr-*C*H$_3$), *

* Si*Me*$_2$ not observed

Synthesis of Bi({NAr^{iPr}}$_2$SiMe$_2$)Cp (19)

As for compound **18** using **15** (130 mg, 0.21 mmol, 1 equiv.) and LiCp (15 mg, 0.21 mmol, 1 equiv.) in D_6-benzene. The solvent was allowed to slowly evaporate from the filtrate in a glovebox resulting in the isolation of **19** as a red crystalline solid.

^{1}H NMR (D_6-benzene, 400 MHz): δ 7.28 (d, $^3J_{HH}$ = 7.7 Hz, 4H, *m*-C*H*), 6.85 (t, $^3J_{HH}$ = 7.7 Hz, 2H, *p*-C*H*), 6.26 (s, 5H, C_5H_5), 3.94 (sept, $^3J_{HH}$ = 6.9 Hz, 4H, ^{i}Pr-C*H*), 1.29 (br, 24H, ^{i}Pr-CH_3), 0.24 (s, 6H, SiCH_3)

^{13}C {^{1}H} NMR (D_6-benzene, 100 MHz): δ 148.1 (*o*-C), 138.2 (*i-C*), 125.3 (*p-C*H), 123.0 (*m-C*H), 113.6 (C_5H_5), 27.5 (^{i}Pr-*C*H_3), 27.2 (^{i}Pr-*C*H), 25.3 (^{i}Pr-*C*H_3), 9.4 (Si*C*H_3)

Synthesis of Sb({NAr^{iPr}}$_2$SiMe$_2$)Cp* (20)

As for compound **18** using **14** (150 mg, 0.28 mmol, 1 equiv.) and KCp* (49 mg, 0.28 mmol, 1 equiv.) in D_6-benzene. The solvent was allowed to slowly evaporate from the filtrate in a glovebox resulting in the isolation of **19** as colourless crystals.

Anal. calcd. for $C_{36}H_{55}N_2SiSb$ (665.7): C, 65.00 %; H, 8.33 %; N, 4.21 %. Found: C, 64.92 %; H, 8.48 %; N, 4.12 %.

^{1}H NMR (D_6-benzene, 400 MHz): δ 7.15 (d, $^3J_{HH}$ = 7.5 Hz, 4H, *m*-C*H*), 7.05 (t, $^3J_{HH}$ = 7.5 Hz, 2H, *p*-C*H*), 4.05 ((br, 4H, ^{i}Pr-C*H*), 1.80 (s, 15H, $C_5\{CH_3\}_5$), 1.41 (d, $^3J_{HH}$ = 6.6 Hz, 12H, ^{i}Pr-CH_3), 1.29 (d, $^3J_{HH}$ = 6.6 Hz, 12H, ^{i}Pr-CH_3), 0.41 (br, 6H, SiCH_3)

^{13}C {^{1}H} NMR (D_6-benzene, 100 MHz): δ 145.7 (*o*-C), 141.9 (*i-C*), 124.3 (*p-C*H), 123.7 (*m-C*H), 121.3 ($C_5(CH_3)_5$), 28.3 (^{i}Pr-*C*H), 26.8 (^{i}Pr-*C*H_3), 25.8 (^{i}Pr-*C*H_3), 10.7 ($C_5(CH_3)_5$) *

* Si*C*H_3 not observed

Synthesis of Bi({NAr^{iPr}}$_2$SiMe$_2$)Cp* (21)

As for compound **18** using **15** (180 mg, 0.29 mmol, 1 equiv.) and KCp* (50 mg, 0.29 mmol, 1 equiv.) in D_6-benzene. The solvent was allowed to slowly evaporate from the filtrate in a glovebox resulting in the isolation of **19** as a red crystalline solid.

^{1}H NMR (D_6-benzene, 400 MHz): δ 7.25 (d, $^3J_{HH}$ = 7.6 Hz, 4H, *m*-C*H*), 6.86 (t, $^3J_{HH}$ = 7.6 Hz, 2H, *p*-C*H*), 4.02 (sept, $^3J_{HH}$ = 6.8 Hz, 4H, ^{i}Pr-C*H*), 2.08 (s, 15H, $C_5(CH_3)_5$), 1.36 (d, $^3J_{HH}$ = 6.8 Hz, 12H, ^{i}Pr-CH_3), 1.30 (d, $^3J_{HH}$ = 6.8 Hz, 12H, ^{i}Pr-CH_3), 0.35 (s, 6H, SiCH_3)

^{13}C {^{1}H} NMR (D_6-benzene, 100 MHz): δ 147.0 (*o*-C), 141.1 (*i-C*), 123.9 (*p-C*H), 123.3 (*m-C*H), 121.1 ($C_5\{CH_3\}_5$), 27.5 (^{i}Pr-*C*H), 26.8 (^{i}Pr-*C*H_3), 26.8 (^{i}Pr-*C*H_3), 10.6 (Si*C*H_3), 10.3 ($C_5\{CH_3\}_5$)

Appendix A: General Experimental Procedures

All experimental procedures were performed under dry N_2 using either standard Schlenk line techniques or an MBraun MB 150B-G glovebox. All glassware, cannulae and glass fibre filter papers were stored in an oven at ≥100 °C for a minimum of 24 h before use.

Solvents

Prior to use, all bulk solvents were pre-dried over sodium wire before being refluxed over an appropriate drying agent and under an atmosphere of N_2 for a minimum of 72 h. Dry solvents were degassed and stored in ampoules under an atmosphere of N_2 over either molecular sieves or a potassium mirror (Table A1). Deuterated solvents were dried by freeze-pump-thaw degassing before refluxing over potassium. Dry deuterated solvents were stored over molecular sieves ampoules in the glovebox.

Table A1

Solvent	Refluxed Over	Stored Over
thf	K	Molecular Sieves
Et_2O	NaK_3	Potassium mirror
Hexane	NaK_3	Potassium mirror
Pentane	NaK_3	Potassium mirror
Toluene	Na	Potassium mirror

Intrumentation

All NMR spectra were recorded using either Varian VNMR400 of VNMR500 spectrometers. GC-MS were recorded on a Perkin Elmer Autosystem XL Chromatograph attached to a Perkin Elmer TurboMass mass spectrometer. Elemental analyses were performed by Stephen Boyer (London Metropolitan University) and mass spectra were obtained by Dr. Alaa Abdul-Sada (University of Sussex). Single crystal X-ray diffraction data were collected by Dr. Martyn Coles

(formally University of Sussex, now Victoria University of Wellington), Dr. Mark Rowe (University of Sussex) or the UK National Crystallographic Service (University of Southampton). X-ray data were solved by Dr. Martyn Coles.

Appendix B

Plots of [benzaldehyde] vs time for each pre-catalyst are shown in Figure B1 and second order plots, 1/[benzaldehdye] vs time, in Figure B2.*** While straight lines are a obtained in the latter for the consumption of benzaldehyde by 1 mol % of **2**, **4**, **XLVIII** and 10 mol % of **XLVIII**, curves are observed for 1 mol % of **1**, **7**, **XXVIII** and 10 mol % of **4**. There is no obvious reason for the order of reaction with respect to substrate to be differ for these chemically very similar compexes so without further experimentation these data are not sufficient to make any confident kinetic assumptions.

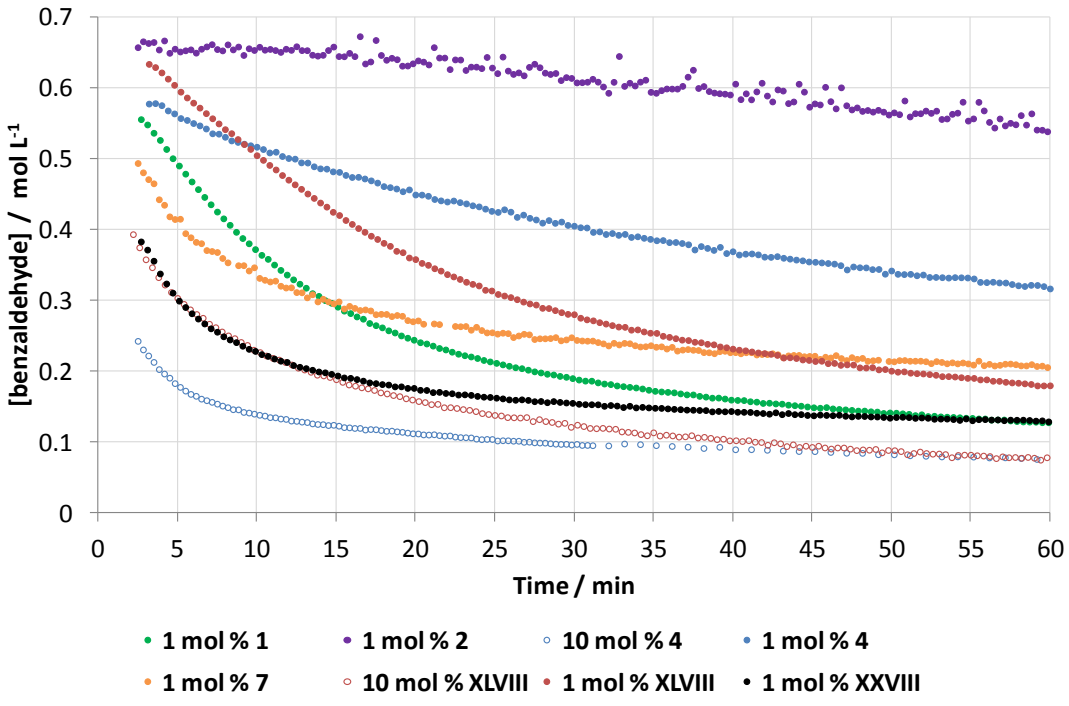

Figure B1 – Plot of concentration of benzaldehyde vs. time for experiments using 1 mol % of **1**, **2**, **4**, **7**, **XXVIII**, **XLVIII** and 10 mol % **4** and **XLVIII.** Values calculated from NMR integrals relative to 1,4-dimethoxybenzene internal standard, monitored for 60 min

*** Attempts to fit this data to a first order plot gave curves for all catalysts

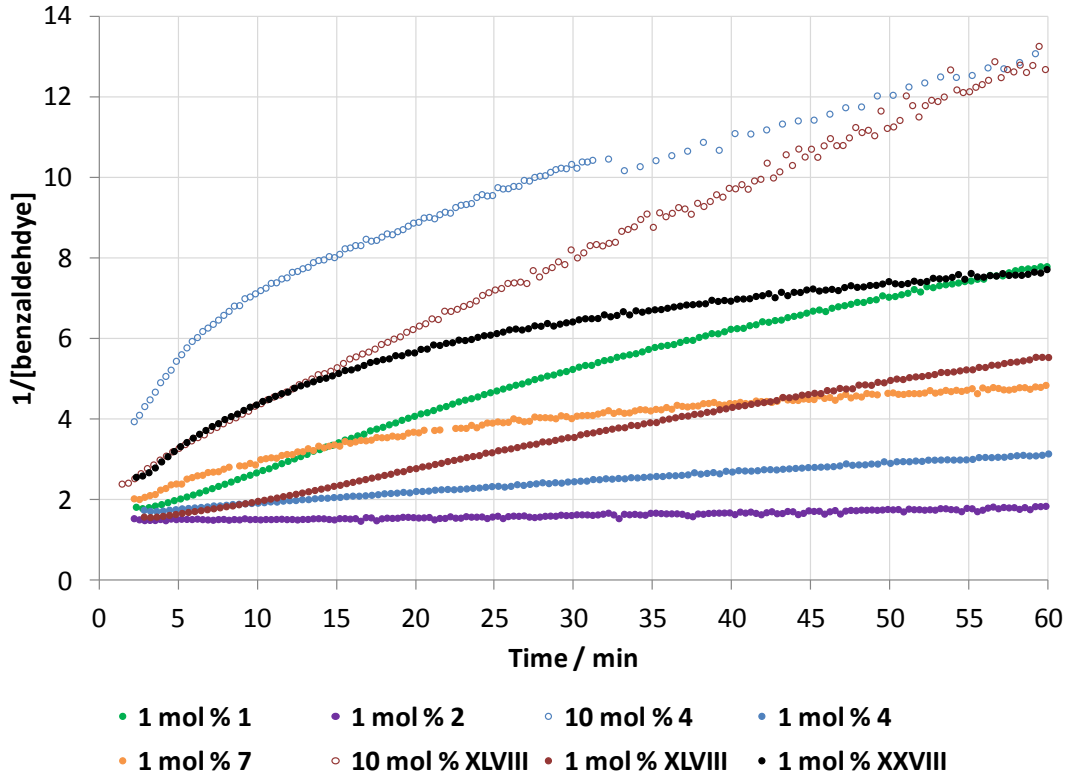

Figure B2 – Plot of 1/[benzaldehyde] vs. time for experiments using 1 mol % of **1**, **2**, **4**, **7**, **XXVIII**, **XLVIII** and 10 mol % **4** and **XLVIII.** Values calculated from NMR integrals relative to 1,4-dimethoxybenzene internal standard, monitored for 60 min

Appendix C

The cause of the relativistic effects originates from the relative velocities of electrons in an atom; the closer an electron gets to the nucleus, the higher its mean velocity. This means that electrons in *s* orbitals will experience the strongest relativistic effects as *s* orbitals have no angular momentum, i.e. they are spherically symmetrical, and therefore have higher electron densities close to the nucleus. The 1s and 2s electrons of heavier elements have velocities that are significant fractions of the speed of light, for example the velocity of 1*s* electrons in bismuth is around 60 % of the speed of light. According to Einstein's special theory of relativity, as the velocity of a body approaches the speed of light, its mass is significantly increased.[186] With respect to the 1*s* electrons of bismuth, this translates to a 26 % increase in mass which in turn results in a 20 % decrease in the Bohr radius of the 1s orbital since the Bohr radius is inversely proportional to mass. Orbital contraction is also observed for *s* orbitals with higher principle quantum numbers as well as *p* orbitals, albeit the latter to a much smaller extent. The net effect of this is that the energy difference between the valence *ns* and *np* orbitals increases as *n* increases, meaning that the *s* orbitals become less readily available for bonding and hybridisation with the *p* orbitals. The effect of this is that *p* orbitals are primarily used for bonding, resulting in bond angles to tend towards 90° for the heavier elements.[187–190]

References

1. P. J. Bailey, K. J. Grant, L. A. Mitchell, S. Pace, A. Parkin, and S. Parsons, *J. Chem. Soc., Dalton Trans.*, 2000, 1887–1891.
2. F. A. Cotton, X. Feng, and M. Matusz, *Inorg. Chem*, 1989, **28**, 594–601.
3. P. J. Bailey, S. F. Bone, L. A. Mitchell, S. Parsons, K. J. Taylor, and L. J. Yellowlees, *Inorg. Chem*, 1997, **36**, 867–871.
4. A. R. Sanger, *Inorg. Nucl. Chem. Letters*, 1973, **9**, 351–354.
5. R. T. Boeré, R. T. Oakley, and R. W. Reed, *J. Organomet. Chem.*, 1987, **331**, 161–167.
6. K. Dehnicke, *Chem.-Zeit.*, 1990, **114**, 295–304.
7. I. Pattison, K. Wade, and B. K. Wyatt, *J. Chem. Soc. A*, 1968, 837–842.
8. E. M. A. Ratilla, B. K. Scott, M. S. Moxness, and N. M. Kostic, *Inorg. Chem*, 1990, **29**, 918–926.
9. P. J. Bailey, L. A. Mitchell, and S. Parsons, *J. Chem. Soc., Dalton Trans.*, 1996, 2839–2841.
10. F. A. Cotton, T. Inglis, M. Kilner, and T. R. Webb, *Inorg. Chem*, 1975, **14**, 2023–2026.
11. F. A. Cotton and L. W. Shive, *Inorg. Chem*, 1975, **14**, 2027–2031.
12. F. A. Cotton, L. M. Daniels, and C. A. Murillo, *Angew. Chem. Int. Ed.*, 1992, **31**, 737–738.
13. F. Albert Cotton, L. M. Daniels, L. R. Falvello, and C. A. Murillo, *Inorg. Chim. Acta*, 1994, **219**, 7–10.
14. F. A. Cotton, L. M. Daniels, D. J. Maloney, and C. A. Murillo, *Inorg. Chim. Acta*, 1996, **249**, 9–11.
15. F. Albert Cotton and R. Poli, *Polyhedron*, 1987, **6**, 1625–1628.
16. F. A. Cotton, L. M. Daniels, J. H. Matonic, X. Wang, and C. A. Murillo, *Polyhedron*, 1997, **16**, 1177–1191.
17. F. A. Cotton, L. M. Daniels, C. A. Murillo, and X. Wang, *Inorg. Chem*, 1997, **36**, 896–901.
18. J. L. Bear, Y. Li, B. Han, and K. M. Kadish, *Inorg. Chem*, 1996, **35**, 1395–1398.
19. F. A. Cotton, J. H. Matonic, and C. A. Murillo, *J. Am. Chem. Soc.*, 1997, **119**, 7889–7890.
20. F. A. Cotton, L. M. Daniels, P. Huang, and C. A. Murillo, *Inorg. Chem*, 2001, **41**, 317–320.
21. K. Issleib, H. schmidt, and H. Meyer, *J. Organomet. Chem.*, 1980, **192**, 33–39.
22. D. H. M. W. Thewissen and H. P. M. M. Ambrosius, *Recl. Trav. Chim. Pays-Bas*, 1980, **99**, 344–345.
23. D. H. M. . Thewissen, H. P. M. M. Ambrosius, H. L. M. Van Gaal, and J. J. Steggerda, *J. Organomet. Chem.*, 1980, **192**, 101–113.
24. E. Hey-Hawkins and F. Lindenberg, *Z. Naturforsch. B*, 1993, **48**, 951–957.
25. F. Lindenberg, J. Sieler, and E. Hey-Hawkins, *Polyhedron*, 1996, **15**, 1459–1464.
26. M. P. Coles and P. B. Hitchcock, *Chem. Commun.*, 2002, 2794–2795.
27. J. Grundy, N. E. Mansfield, M. P. Coles, and P. B. Hitchcock, *Inorg. Chem.*, 2008, **47**, 2258–2260.
28. N. E. Mansfield, M. P. Coles, and P. B. Hitchcock, *Dalton Trans.*, 2006, 2052–2054.
29. M. Westerhausen and H. Hausen, *Z. Anorg. Allg. Chem.*, 1992, **615**, 27–34.
30. D. Walther, P. Gebhardt, R. Fischer, U. Kreher, and H. Görls, *Inorg. Chim. Acta*, 1998, **281**, 181–189.
31. A. R. Sadique, M. J. Heeg, and C. H. Winter, *Inorg. Chem.*, 2001, **40**, 6349–6355.
32. N. Nimitsiriwat, V. C. Gibson, E. L. Marshall, P. Takolpuckdee, A. K. Tomov, A. J. P. White, D. J. Williams, M. R. J. Elsegood, and S. H. Dale, *Inorg. Chem.*, 2007, **46**, 9988–9997.
33. B. Srinivas, C.-C. Chang, C.-H. Chen, M. Y. Chiang, I.-T. Chen, Y. Wang, and G.-H. Lee, *J. Chem. Soc., Dalton Trans.*, 1997, 957–964.
34. M. L. Cole, D. J. Evans, P. C. Junk, and L. M. Louis, *New J. Chem.*, 2002, **26**, 1015–1024.
35. W. Knoweldon, MChem Thesis, University of Sussex, 2007.
36. S. P. Green, C. Jones, and A. Stasch, *Science*, 2007, **318**, 1754 –1757.

37. O. Ciobanu, A. Fuchs, M. Reinmuth, A. Lebkücher, E. Kaifer, H. Wadepohl, and H. Himmel, *Z. Anorg. Allg. Chem.*, 2010, **636**, 543–550.
38. B. M. Day, N. E. Mansfield, M. P. Coles, and P. B. Hitchcock, *Chem. Commun.*, 2011, **47**, 4995.
39. N. E. Mansfield, DPhil Thesis, University of Sussex, 2006.
40. M. Bochmann, *J. Chem. Soc., Dalton Trans.*, 1996, 255–270.
41. L. Resconi, L. Cavallo, A. Fait, and F. Piemontesi, *Chem. Rev.*, 2000, **100**, 1253–1346.
42. H. H. Brintzinger, D. Fischer, R. Mülhaupt, B. Rieger, and R. M. Waymouth, *Angew. Chem. Int. Ed.*, 1995, **34**, 1143–1170.
43. M. Wedler, F. Knösel, U. Pieper, D. Stalke, F. T. Edelmann, and H. Amberger, *Chem. Ber.*, 1992, **125**, 2171–2181.
44. T. V. Lubben, P. T. Wolczanski, and G. D. Van Duyne, *Organometallics*, 1984, **3**, 977–983.
45. A. N. Chernega, R. Gomez, and M. L. H. Green, *J. Chem. Soc., Chem. Commun.*, 1993, 1415.
46. S. Collins, *Coordination Chemistry Reviews*, 2011, **255**, 118–138.
47. Y. Luo, Y. Yao, Q. Shen, J. Sun, and L. Weng, *J. Organomet. Chem.*, 2002, **662**, 144–149.
48. F. T. Edelmann, *Chem. Soc. Rev.*, 2009, **38**, 2253.
49. H. Nagashima, M. Gondo, S. Masuda, H. Kondo, Y. Yamaguchi, and K. Matsubara, *Chem. Commun.*, 2003, 442–443.
50. S. Ge, A. Meetsma, and B. Hessen, *Organometallics*, 2008, **27**, 3131–3135.
51. P. Benndorf, J. Jenter, L. Zielke, and P. W. Roesky, *Chem. Commun.*, 2011, **47**, 2574.
52. D. J. Brauer, H. Bürger, and G. R. Liewald, *J. Organomet. Chem.*, 1986, **308**, 119–130.
53. A. Mommertz, R. Leo, W. Massa, K. Harms, and K. Dehnicke, *Z. Anorg. Allg. Chem.*, 1998, **624**, 1647–1652.
54. H. Chen, R. A. Bartlett, H. V. R. Dias, M. M. Olmstead, and P. P. Power, *Inorg. Chem*, 1991, **30**, 2487–2494.
55. M. S. Hill and P. B. Hitchcock, *Organometallics*, 2002, **21**, 3258–3262.
56. M. Veith, *Angew. Chem. Int. Ed.*, 1975, **14**, 263–264.
57. M. Mantina, A. C. Chamberlin, R. Valero, C. J. Cramer, and D. G. Truhlar, *J. Phys. Chem. A*, 2009, **113**, 5806–5812.
58. S. M. Mansell, C. A. Russell, and D. F. Wass, *Inorg. Chem.*, 2008, **47**, 11367–11375.
59. M. Veith, H. Lange, K. Bräuer, and R. Bachmann, *J. Organomet. Chem.*, 1981, **216**, 377–381.
60. M. Veith, L. Stahl, and V. Huch, *Inorg. Chem*, 1989, **28**, 3278–3280.
61. M. Veith, L. Stahl, and V. Huch, *J. Chem. Soc., Chem. Commun.*, 1990, 359–361.
62. M. Veith and L. Stahl, *Angew. Chem. Int. Ed.*, 2003, **32**, 106–107.
63. H. Werner, *Angew. Chem. Int. Ed.*, 1977, **16**, 1–9.
64. M. Veith, A. Müller, L. Stahl, M. Nötzel, M. Jarczyk, and V. Huch, *Inorg. Chem.*, 1996, **35**, 3848–3855.
65. D. Yang, Y. Ding, H. Wu, and W. Zheng, *Inorg. Chem.*, 2011, **50**, 7698–7706.
66. D. Yang, J. Guo, H. Wu, Y. Ding, and W. Zheng, *Dalton Trans.*, 2012, **41**, 2187.
67. M. Veith, V. Huch, J.-P. Majoral, G. Bertrand, and G. Manuel, *Tetrahedron Lett.*, 1983, **24**, 4219–4222.
68. M. Veith, M. Gouygou, and A. Detemple, *Phosphorus, Sulfur Silicon Relat. Elem.*, 1993, **75**, 183–186.
69. J. K. West and L. Stahl, *Organometallics*, 2012, **31**, 2042–2052.
70. D. A. Fletcher, R. F. McMeeking, and D. Parkin, *J. Chem. Inf. Comput. Sci.*, 1996, **36**, 746–749.
71. I. J. Bruno, J. C. Cole, P. R. Edgington, M. Kessler, C. F. Macrae, P. McCabe, J. Pearson, and R. Taylor, *Acta Crystallogr. Sect. B-Struct. Sci.*, 2002, **58**, 389–397.
72. C.-C. Chang, T.-Y. Her, M.-D. Li, R. Williamson, G.-H. Lee, S.-M. Peng, and Y. Wang, *Inorg. Chem.*, 1995, **34**, 4296–4298.
73. J. D. Monegan and S. D. Bunge, *Inorg. Chem.*, 2009, **48**, 3248–3256.
74. A. W. Addison, T. N. Rao, J. Reedijk, J. van Rijn, and G. C. Verschoor, *J. Chem. Soc., Dalton Trans.*, 1984, 1349–1356.
75. N. C. Mösch-Zanetti, M. Ferbinteanu, and J. Magull, *Eur. J. Inorg. Chem.*, 2002, **2002**, 950–956.

76. G. Stucky and R. E. Rundle, *J. Am. Chem. Soc.*, 1964, **86**, 4821–4825.
77. H. Vitze, H.-W. Lerner, and M. Bolte, *Acta Crystallogr. Sect. E: Struct. Rep. Online*, 2011, **67**, m1614–m1614.
78. N. E. Mansfield, J. Grundy, M. P. Coles, A. G. Avent, and P. B. Hitchcock, *J. Am. Chem. Soc.*, 2006, **128**, 13879–13893.
79. R. A'Court, .
80. L. Claisen, *Ber. Dtsch. Chem. Ges.*, 1887, **20**, 655–657.
81. W. C. Child and H. Adkins, *J. Am. Chem. Soc.*, 1925, **47**, 798–807.
82. W. C. Child and H. Adkins, *J. Am. Chem. Soc.*, 1923, **45**, 3013–3023.
83. I. Lin and A. R. Day, *J. Am. Chem. Soc.*, 1952, **74**, 5133–5135.
84. Y. Ogata, A. Kawasaki, and I. Kishi, *Tetrahedron*, 1967, **23**, 825–830.
85. K. Weissermel and H.-J. Arpe, in *Industrial organic chemistry*, Wiley-VCH, 4th Edition., 2003, pp. 145–192.
86. T. Seki, T. Nakajo, and M. Onaka, *Chem. Lett.*, 2006, **35**, 824–829.
87. A. Hester and K. Himmler, *Ind. Eng. Chem.*, 1959, **51**, 1424–1430.
88. C. Tejel, M. A. Ciriano, and V. Passarelli, *Chem. Eur. J.*, 2011, **17**, 91–95.
89. S. Ogoshi, Y. Hoshimoto, and M. Ohashi, *Chem. Commun.*, 2010, **46**, 3354.
90. Y. Hoshimoto, M. Ohashi, and S. Ogoshi, *J. Am. Chem. Soc.*, 2011, **133**, 4668–4671.
91. H. Berberich and P. W. Roesky, *Angew. Chem. Int. Ed.*, 1998, **37**, 1569–1571.
92. M. R. Bürgstein, H. Berberich, and P. W. Roesky, *Chem. Eur. J.*, 2001, **7**, 3078–3085.
93. A. Zuyls, P. W. Roesky, G. B. Deacon, K. Konstas, and P. C. Junk, *Eur. J. Inorg. Chem.*, 2008, **2008**, 693–697.
94. T. Andrea, E. Barnea, and M. S. Eisen, *J. Am. Chem. Soc.*, 2008, **130**, 2454–2455.
95. M. Sharma, T. Andrea, N. J. Brookes, B. F. Yates, and M. S. Eisen, *J. Am. Chem. Soc.*, 2011, **133**, 1341–1356.
96. M. R. Crimmin, A. G. M. Barrett, M. S. Hill, and P. A. Procopiou, *Org. Lett.*, 2006, **9**, 331–333.
97. L. Cronin, F. Manoni, C. J. O' Connor, and S. J. Connon, *Angew. Chem. Int. Ed.*, 2010, **49**, 3045–3048.
98. K. Tanabe and K. Saito, *J. Catal.*, 1974, **35**, 247–255.
99. T. Seki, H. Kabashima, K. Akutsu, H. Tachikawa, and H. Hattori, *J. Catal.*, 2001, **204**, 393–401.
100. Beachley and J. D. Maloney, *Organometallics*, 1997, **16**, 4016–4019.
101. N. E. Mansfield, M. P. Coles, and P. B. Hitchcock, *Polyhedron*.
102. J. Grundy, M. P. Coles, and P. B. Hitchcock, *Dalton Trans.*, 2003, 2573–2577.
103. G. R. Fulmer, A. J. M. Miller, N. H. Sherden, H. E. Gottlieb, A. Nudelman, B. M. Stoltz, J. E. Bercaw, and K. I. Goldberg, *Organometallics*, 2010, **29**, 2176–2179.
104. J. F. Allan, K. W. Henderson, and A. R. Kennedy, *Chem. Commun.*, 1999, 1325–1326.
105. P. P. Power and Pauer, in *Lithium chemistry: a theoretical and experimental overview*, eds. A.-M. Sapse and P. von R. Schleyer, Wiley, New York, 1995, p. 361.
106. P. C. Blake, E. Hey, M. F. Lappert, J. L. Atwood, and H. Zhang, *J. Organomet. Chem.*, 1988, **353**, 307–314.
107. K. Issleib and H. Deylig, *Chem. Ber.*, 1964, **97**, 946–951.
108. E. Hey, L. M. Engelhardt, C. L. Raston, and A. H. White, *Angew. Chem. Int. Ed.*, 1987, **26**, 81–82.
109. M. Westerhausen, M. H. Digeser, B. Wieneke, H. Nöth, and J. Knizek, *Eur. J. Inorg. Chem.*, 1998, **1998**, 517–521.
110. M. Gärtner, H. Görls, and M. Westerhausen, *Inorg. Chem*, 2008, **47**, 1397–1405.
111. M. Westerhausen, M. H. Digeser, H. Nöth, T. Seifert, and A. Pfitzner, *J. Am. Chem. Soc.*, 1998, **120**, 6722–6725.
112. S. Blair, K. Izod, W. Clegg, and R. W. Harrington, *Eur. J. Inorg. Chem.*, 2003, **2003**, 3319–3324.
113. R. I. Yousef, B. Walfort, T. Rüffer, C. Wagner, H. Schmidt, R. Herzog, and D. Steinborn, *J. Organomet. Chem.*, 2005, **690**, 1178 – 1191.
114. W. Schlenk and W. Schlenk, *Ber. Dtsch. Chem. Ges*, 1929, **62**, 920–924.
115. A. C. Cope, *J. Am. Chem. Soc.*, 1935, **57**, 2238–2240.

116. H. Schäfer, D. Binder, and D. Fenske, *Angew. Chem. Int. Ed.*, 1985, **24**, 522–524.
117. E. Hey, M. F. Lappert, J. L. Atwood, and S. G. Bott, *Polyhedron*, 1988, **7**, 2083–2086.
118. L. Weber, G. Meine, R. Boese, and N. Augart, *Organometallics*, 1987, **6**, 2484–2488.
119. H. Schumann and R. Fischer, *J. Organomet. Chem.*, 1975, **88**, C13–C16.
120. D. W. Stephan, *Organometallics*, 1992, **11**, 996–999.
121. L. B. Kool, M. D. Rausch, H. G. Alt, M. Herberhold, U. Thewalt, and B. Wolf, *Angew. Chem. Int. Ed.*, 1985, **24**, 394–401.
122. L. B. Kool, M. D. Rausch, H. G. Alt, M. Herberhold, B. Wolf, and U. Thewalt, *J. Organomet. Chem.*, 1985, **297**, 159 – 169.
123. P. Sobota, *Chem. Eur. J.*, 2003, **9**, 4854–4860.
124. P. Sobota, J. Utko, and T. Lis, *J. Chem. Soc., Dalton Trans.*, 1984, 2077–2084.
125. P. Sobota, *Coord. Chem. Rev.*, 2004, **248**, 1047–1060.
126. C.-Y. Hsu and M. Orchin, *J. Am. Chem. Soc.*, 1975, **97**, 3553.
127. I. Schwager and J. F. Knifton, *J. Catal.*, 1976, **45**, 256–267.
128. Y. Kawabata, T. Hayashi, and I. Ogata, *J. Chem. Soc., Chem. Commun.*, 1979, 462–463.
129. H. C. Clark, C. Billard, and C. S. Wong, *J. Organomet. Chem.*, 1980, **190**, C105–C107.
130. P. Haelg, G. Consiglio, and P. Pino, *J. Organomet. Chem.*, 1985, **296**, 281–290.
131. M. Gomez, G. Muller, D. Sainz, J. Sales, and X. Solans, *Organometallics*, 1991, **10**, 4036–4045.
132. J. K. Stille, H. Su, P. Brechot, G. Parrinello, and L. S. Hegedus, *Organometallics*, 1991, **10**, 1183–1189.
133. R. van Duren, J. I. van der Vlugt, H. Kooijman, A. L. Spek, and D. Vogt, *Dalton Trans.*, 2007, 1053–1059.
134. J. D. Cotton, P. J. Davison, D. E. Goldberg, M. F. Lappert, and K. M. Thomas, *J. Chem. Soc., Chem. Commun.*, 1974, 893–895.
135. J. D. Cotton, P. J. Davidson, and M. F. Lappert, *J. Chem. Soc., Dalton Trans.*, 1976, 2275–2286.
136. J. D. Cotton, P. J. Davidson, M. F. Lappert, J. D. Donaldson, and J. Silvet, *J. Chem. Soc., Dalton Trans.*, 1976, 2286–2290.
137. S. M. Hawkins, P. B. Hitchcock, and M. F. Lappert, *J. Chem. Soc., Chem. Commun.*, 1985, 1592–1593.
138. M. F. Lappert and P. P. Power, *J. Chem. Soc., Dalton Trans.*, 1985, 51–57.
139. A. V. Zabula, T. Pape, A. Hepp, and F. E. Hahn, *Dalton Trans.*, 2008, 5886–5890.
140. B. M. Donovan, MChem Thesis, University of Sussex, 2011.
141. G. K. Anderson, H. C. Clark, J. A. Davies, G. Ferguson, and M. Parvez, *J. Cryst. Spectrosc. Res.*, 1982, **12**, 449–458.
142. A. Al-Fawaz, S. Aldridge, D. L. Coombs, A. A. Dickinson, D. J. Willock, L. Ooi, M. E. Light, S. J. Coles, and M. B. Hursthouse, *Dalton Trans.*, 2004, 4030–4037.
143. J. Miao, C. Hu, X. Feng, H. Chen, and Y. Nie, *Acta Crystallogr. Sect. E: Struct. Rep. Online*, 2009, **65**, m1025–m1025.
144. M. Veith, O. Schütt, J. Blin, S. Becker, J. Frères, and V. Huch, *Z. Anorg. Allg. Chem.*, 2002, **628**, 138–146.
145. M. Veith, J. Frères, P. König, O. Schütt, V. Huch, and J. Blin, *Eur. J. Inorg. Chem.*, 2005, **2005**, 3699–3710.
146. H. E. Bryndza, W. C. Fultz, and W. Tam, *Organometallics*, 1985, **4**, 939–940.
147. I. Toth, T. Kegl, C. J. Elsevier, and L. Kollar, *Inorg. Chem.*, 1994, **33**, 5708–5712.
148. W. R. Rocha and W. B. De Almeida, *Organometallics*, 1998, **17**, 1961–1967.
149. A. Bedekovits, L. Kollár, and T. Kégl, *Inorg. Chim. Acta*, 2010, **363**, 2029–2045.
150. R. P. Dias and W. R. Rocha, *Organometallics*, 2011, **30**, 4257–4268.
151. A. Scrivanti, S. Paganelli, U. Matteoli, and C. Botteghi, *J. Organomet. Chem.*, 1990, **385**, 439–446.
152. K. A. Ostoja Starzewski, H. Ruegger, and P. S. Pregosin, *Inorg. Chim. Acta*, 1979, **36**, L445.
153. F. J. Ramos-Lima, A. G. Quiroga, J. M. Pérez, M. Font-Bardía, X. Solans, and C. Navarro-Ranninger, *Eur. J. Inorg. Chem.*, 2003, **2003**, 1591–1598.

154. J. X. McDermott, J. F. White, and G. M. Whitesides, *J. Am. Chem. Soc.*, 1976, **98**, 6521–6528.
155. K. B. Dillon, A. E. Goeta, P. K. Monks, and H. J. Shepherd, *Polyhedron*, 2010, **29**, 606–612.
156. H. Suzuki, *Organobismuth chemistry*, Elsevier, 2001.
157. N. M. Leonard, L. C. Wieland, and R. S. Mohan, *Tetrahedron*, 2002, **58**, 8373–8397.
158. P. Majewski, *Advanced Materials*, 1994, **6**, 460–469.
159. R. K. Grasselli, in *Handbook of Heterogeneous Catalysis*, eds. G. Ertl, H. Knozinger, and J. Weitkamp, VCH Verlagsgesellschaft mbH: Weinheim, 1997, p. 2302−2326.
160. F. Cavani, G. Centi, and P. Marion, in *Metal Oxide Catalysis*, eds. S. D. Jackson and J. S. J. Hargreaves, Wiley-VCH, 2009, vol. 1, pp. 771–818.
161. T. A. Hanna, A. L. Rieger, P. H. Rieger, and X. Wang, *Inorg. Chem.*, 2002, **41**, 3590–3592.
162. I. J. Casely, J. W. Ziller, M. Fang, F. Furche, and W. J. Evans, *J. Am. Chem. Soc.*, 2011, **133**, 5244–5247.
163. B. Nekoueishahraki, S. P. Sarish, H. W. Roesky, D. Stern, C. Schulzke, and D. Stalke, *Angew. Chem. Int. Ed.*, 2009, **48**, 4517–4520.
164. C. Knispel and C. Limberg, *Organometallics*, 2011, **30**, 3701–3703.
165. O. J. Scherer, P. Hornig, and M. Schmidt, *J. Organomet. Chem.*, 1966, **6**, 259–264.
166. F. Ando, T. Hayashi, K. Ohashi, and J. Koketsu, *J. Inorg. Nucl. Chem*, 1975, **37**, 2011–2013.
167. W. Clegg, N. A. Compton, R. J. Errington, G. A. Fisher, M. E. Green, D. C. R. Hockless, and N. C. Norman, *Inorg. Chem*, 1991, **30**, 4680–4682.
168. M. Vehkamäki, T. Hatanpää, M. Ritala, and M. Leskelä, *J. Mater. Chem.*, 2004, **14**, 3191.
169. W. Clegg, N. A. Compton, R. J. Errington, N. C. Norman, and N. Wishart, *Polyhedron*, 1989, **8**, 1579–1580.
170. N. Burford, C. L. B. Macdonald, K. N. Robertson, and T. S. Cameron, *Inorg. Chem.*, 1996, **35**, 4013–4016.
171. W. J. Evans, D. B. Rego, and J. W. Ziller, *Inorg. Chim. Acta*, 2007, **360**, 1349–1353.
172. U. Wirringa, H. W. Roesky, M. Noltemeyer, and H.-G. Schmidt, *Inorg. Chem.*, 1994, **33**, 4607–4608.
173. G. G. Briand, T. Chivers, and M. Parvez, *Can. J. Chem.*, 2003, **81**, 169–174.
174. M. Veith and B. Bertsch, *Z. Anorg. Allg. Chem.*, 1988, **557**, 7–22.
175. M. Veith, B. Bertsch, and V. Huch, *Z. Anorg. Allg. Chem.*, 1988, **559**, 73–88.
176. A. M. Caminade, M. Veith, V. Huch, and W. Malisch, *Organometallics*, 1990, **9**, 1798–1802.
177. E. O. Fischer and S. Schreiner, *Chem. Ber.*, 1960, **93**, 1417–1424.
178. B. Deubzer, M. Elian, E. O. F. Und, and H. P. Fritz, *Chem. Ber.*, 1970, **103**, 799–804.
179. W. Frank, *J. Organomet. Chem.*, 1990, **386**, 177–186.
180. J. Lorberth, W. Massa, S. Wocadlo, I. Sarraje, S.-H. Shin, and X.-W. Li, *J. Organomet. Chem.*, 1995, **485**, 149–152.
181. H. Sitzmann and G. Wolmershäuser, *Chem. Ber.*, 1994, **127**, 1335–1342.
182. R. J. Wiacek, J. N. Jones, C. L. Macdonald, and A. H. Cowley, *Can. J. Chem.*, 2002, **80**, 1518–1523.
183. K. Y. Monakhov and G. Linti, *Inorg. Chem.*, 2009, **48**, 6986–6996.
184. Y. Ehleiter, G. Wolmershäuser, H. Sitzmann, and R. Boese, *Z. Anorg. Allg. Chem.*, 1996, **622**, 923–930.
185. P. Jutzi, *Chem. Rev.*, 1986, **86**, 983–996.
186. A. Einstein, *Ann. der Physik*, 1905, **322**, 891–921.
187. N. Burford, Y. Carpenter, E. Conrad, and C. D. L. Saunders, in *Biological Chemistry of Arsenic, Antimony and Bismuth*, ed. H. Sun, John Wiley and Sons, pp. 1–17.
188. C. J. Carmalt and N. C. Norman, in *Chemistry of arsenic, antimony, and bismuth*, ed. N. C. Norman, Springer, 1998, pp. 1–38.
189. K. S. Pitzer, *Acc. Chem. Res.*, 1979, **12**, 271–276.
190. P. Pyykko, *Chem. Rev.*, 1988, **88**, 563–594.